Alpha-2-delta subunits of Voltage-gated calcium channels

Janek K. Hendrich

UCL

2008

Laboratory of Cellular and Molecular Neuroscience

Dept. Pharmacology

Andrew Huxley Building

UCL

Gower St.

London WC1E 6BT

ProQuest LLC
789 East Eisenhower Parkway
P.O. Box 1346
Ann Arbor, MI 48106-1346

I, Janek Hendrich, confirm that the work presented in this thesis is my own. Where information has been derived from other sources, I confirm that this has been indicated in the thesis.

Janek Hendrich

Abstract

The calcium channel alpha-2-delta ($\alpha_2\delta$) subunit is an auxiliary subunit associated with voltage-dependent calcium channels. It is implicated in the trafficking and functional expression of the calcium channel complex. This study expands the functional role of the VWA domain and the RRR motif of the $\alpha_2\delta$ subunit, and the interaction between this subunit and the anti-epileptic drug, gabapentin

The VWA domain is normally found in integrins, where it mediates binding to extracellular proteins. A mutation in the $\alpha_2\delta$-2 subunit VWA domain (μMIDAS) did not produce the increase in current amplitude elicited by the wildtype (WT) $\alpha_2\delta$-2 control. Co-immunoprecipitation studies using tsA-201 cells (stably expressing $\alpha_2\delta$-2 containing a mid-HA tag) co-cultured with cerebellar granule cells identified potential proteins from the cerebellar cultures that co-immunoprecipitate with the $\alpha_2\delta$-2 protein. This suggests that protein from cerebellar cultures may bind the $\alpha_2\delta$-2 subunit.

Secondly, an RRR motif found in $\alpha_2\delta$-1 subunit has been implicated as important for binding of the anticonvulsant drug gabapentin (Wang et al., 1999). The electrophysiological properties of the RRA mutant $\alpha_2\delta$ proteins were examined, and found not to enhance current amplitude to the full extent seen by WT $\alpha_2\delta$–1 and $\alpha_2\delta$–2 coexpression. Binding studies using both membrane and lipid raft of tsA-201 cells expressing $\alpha_2\delta$–1 confirmed a lack of ^{3}H-gabapentin in the R217A mutant condition.

Chronic exposure of tsA-201 cells expressing $Ca_V2.1$, β4, $\alpha_2\delta$-2 or $Ca_V2.2$, β1b, $\alpha_2\delta$-1 to gabapentin resulted in a reduction in size of the resultant currents. The inhibitory action of gabapentin was prevented by pre-incubation of cells with the system-L amino-acid transport inhibitor, suggesting gabapentin acts intracellularly after uptake via this transport mechanism. The inhibitory effects of gabapentin exposure were not replicated using co-expression of $\alpha_2\delta$-3, or the non gabapentin-binding mutant $\alpha_2\delta$-1 R217A or

$\alpha_2\delta$-2 R282A proteins. This indicated the inhibitory effect was mediated through gabapentin-binding calcium channel $\alpha_2\delta$ subunits.

Publications

To date, work detailed in this thesis has contributed to the following publications:

Hendrich, J., A.T.Van Minh, F.Heblich, M.Nieto-Rostro, J.Wratten, A.Davies, and A.C.Dolphin. 2008. Pharmacological disruption of calcium channel trafficking by the alpha-2-delta ligand Gabapentin. *Proc. Natl. Acad. Sci. U. S. A.* 105(9):3628-33.

Davies, A., J.Hendrich, A.T.Van Minh, J.Wratten, L.Douglas, and A.C.Dolphin. 2007. Functional biology of the alpha(2)delta subunits of voltage-gated calcium channels. *Trends Pharmacol. Sci.* 28:220-228.

Field, M.J., P.J.Cox, E.Stott, H.Melrose, J.Offord, T.Z.Su, S.Bramwell, L.Corradini, S.England, J.Winks, R.A.Kinloch, J.Hendrich, A.C.Dolphin, T.Webb, and D.Williams. 2006. Identification of the alpha2-delta-1 subunit of voltage-dependent calcium channels as a molecular target for pain mediating the analgesic actions of pregabalin. *Proc. Natl. Acad. Sci. U. S. A* 103:17537-17542.

Hendrich.J., A.Davies., L.Douglas, J.Wratten, V.M.Tran, I.Foucault, D.Koch, W.S.Pratt, H.R.Saibil, and A.C.Dolphin. 2006. The calcium channel alpha2delta-2 subunit partitions with CaV2.1 into lipid rafts in cerebellum: implications for localization and function. *J. Neurosci.* 26:8748-8757.

Canti, C., M.Nieto-Rostro, I.Foucault, F.Heblich, J.Wratten, M.W.Richards, J.Hendrich, L.Douglas, K.M.Page, A.Davies, and A.C.Dolphin. 2005. The metal-ion-dependent adhesion site in the Von Willebrand factor-A domain of alpha2delta subunits is key to trafficking voltage-gated Ca2+ channels. *Proc. Natl. Acad. Sci. U. S. A* 102:11230-11235.

Contents

Abbreviations

$\alpha_2\delta$	Voltage-gated calcium channel alpha-2-delta subunit
AID	α interaction domain
AMP	Adenosine mono-phosphate
AMPA	Alpha-amino-3-hydroxy-5-methyl-4-isoxazole propionic acid
β	Voltage-gated calcium channel beta subunit
BCH	2-Aminobicyclo(2,2,1)heptane-2-carboxylic acid
BME	Basal medium Eagle
BZP	Benzothiazepine
$Ca_v\alpha_1$	Voltage-gated calcium channel alpha$_1$ subunit
cDNA	Complementary deoxyribonucleic acid
CDS	Cell dissociation solution
CNS	Central nervous system
DHP	1,4 dihydropyridine
DMEM	Dulbeco's modified Eagle's medium
DRG	Dorsal root ganglion
DRM	Detergent-resistant membrane
DTT	Dithiothreitol
EA2	Episodic ataxia type 2
ECC	Excitation-contraction coupling
ECL	Enhanced chemiluminescence
EDTA	Ethylene diamine tetra-acetic acid
EPSC	Excitatory postsynaptic current
ER	Endoplasmic reticulum
FHM	Familial hemiplegic migraine
FTX	Funnel-web spider toxin
γ	Voltage-gated calcium channel gamma subunit
GABA	Gamma-aminobutyric acid
GBP	Gabapentin

GFP	Green fluorescent protein
GC	Granule cell
HA	Haemagglutinin
HBSS	Hank's balanced salt solution
HRP	Horseradish peroxidase
HVA	High-voltage activated
LVA	Low-voltage activated
MBCD	Methyl-β-cyclodextrin
MIDAS	Metal ion-dependent adhesion site
mRNA	Messenger ribonucleic acid
PAA	Phenylalkylamine
PBS	Phosphate-buffered saline
PGB	Pregabalin
PVDF	Polyvinylidene difluoride
SCA6	Spinocerebellar ataxia type-6
SDS-PAGE	Sodium dodecyl sulphate polyacrylamide gel-electrophoresis
SEM	Standard error of the mean
SH3	*src*-homology 3
SNARE	Soluble *N*-ethylmaleimide-sensitive factor attachment protein receptor
SNAP	Synaptosomal-associated protein
SV40	Simian virus 40
t-tubule	Transverse tubule
TARP	Transmembrane AMPA receptor regulatory protein
TBS	Tris-buffered saline
tsA	Temperature-sensitive A
TTX	Tetrodotoxin
UV	Ultraviolet
VGCC	Voltage-gated calcium channel
VWA	Von-Willebrand factor-A

List of Figures and Tables

Chapter 1

Figures:

Chapter 2

Figures:

Chapter 4

Figures:

Chapter 5

Figures:

Chapter 6

Figures:

Appendices

Tables:

Chapter 1: Introduction

1.1 The physiological relevance of Ca^{2+}

1.1.1 The action potential

The nervous system fulfils the need within a physiological system for a mechanism of fast information transfer, with the capacity for complex encoding of signals. The action potential is the fundamental mechanism for this information transfer along neurons. It was originally characterised in squid axon, and led to the ionic hypothesis (Hodgkin and Huxley, 1952). The action potential relies on ion flux across a membrane, and therefore requires an electrostatic potential to be present across the membrane in order for ions to flow. Initiation of the action potential is caused by membrane depolarisation, usually by influx of Na^+ ions.

Figure 1.1. The phases of the action potential in a typical nerve cell. Membrane depolarisation by Na^+ ion influx passes the activation threshold, and results in the steep rising phase. This ceases at the peak (with channel inactivation), followed by repolarisation and hyperpolarisation phases. Figure reproduced from http://library.thinkquest.org/C003758/Function/UnderstandingActionPotential.htm.

The phases of the action potential are shown in Figure 1.1. The resting membrane potential is determined by the number and type of ion channels present in the membrane. The sodium / potassium pump is important in maintaining resting potential. Using ATP, it exchanges three intracellular sodium ions for two extracellular potassium ions. Membrane depolarisation causes opening of sodium channels, followed by Na^+ ion influx down the electrochemical gradient (towards the reversal potential for Na^+ ions, roughly +50 mV depending on the cell). Depolarisation must be sufficient for the membrane potential to reach a threshold (the activation threshold), in order for action potential generation. Above the activation threshold, opening of voltage-gated sodium channels begins a positive feedback loop, culminating in a sharp influx of Na^+ ions (rising phase). With the peak of the action potential, Na^+ influx diminishes and K^+ efflux through potassium channels (opened by depolarisation) causes a repolarisation of the membrane. This proceeds past the original membrane potential, leading to a brief hyperpolarisation. A refractory period (lasting milliseconds) follows, during which time further action potentials cannot be initiated due to Na channel inactivation.

The depolarisation of surrounding membrane causes the action potential to propagate along the nerve. This occurs in only the forward direction however, as the refractory period ensures action potentials do not propagate backwards. The propagating action potential maintains a constant speed and amplitude (Hille, 2001).

The initial characterisation in squid axon found the action potential to be composed of Na^+ and K^+ conductances. This contrasts with action potentials in mammalian neurons, which are typically formed of multiple components of sodium, potassium and calcium current (reviewed in Bean, 2007). This extra layer of complexity present in mammalian neurons is necessary for encoding information into action potentials, subtle differences in the trains of action potentials can alter the pattern of Ca^{2+} entry at presynaptic terminals, and by extension the release pattern of neurotransmitter quanta.

1.1.2 The physiological roles of Ca^{2+}

With the accepted structural function of calcium in the human body (a constituent of bones and teeth), the discovery that it had a role as a biological signal was perhaps a surprise, and accordingly came as result of using tap water in the laboratory (Ringer, 1883). Sydney Ringer had been using the London supply of piped water in his experiments as opposed to using distilled water. When he came to repeat previous work demonstrating rat heart contraction using distilled water, the contractions became weaker, before stopping altogether. Using a mixture of different salts (as a result of calculating the constituent salts of water "supplied by the New River Water Company"), he deduced that it was the calcium salts that led to the continued contraction of the heart tissue.

Ca^{2+} ions are now acknowledged as one of the major signalling ions, indeed Ca^{2+} ions act as "the most widespread, versatile and promiscuous signaling molecule within intracellular compartments" (Nilius et al., 2006). Entry of Ca^{2+} ions into cells involves its translocation across membranes. Ca^{2+} ions release from intracellular stores (such as endoplasmic reticulum (ER) or sarcoplasmic reticulum) is mediated by store-operated calcium channels. Movement across the plasma membrane is mediated by voltage-gated calcium channels (VGCCs), as well as other Ca^{2+}-permeable channels, and leads to a number of essential cellular functions (reviewed in Hille, 2001), such as: initiation of gene expression; muscle contraction; secretion (of neurotransmitters, hormones and enzymes among others), as well as initiation of other secondary cellular processes, some of which are shown in Figure 1.2.

The typical intracellular concentration of Ca^{2+} ions is kept very low (~30 nM to ~200 nM depending on the cell type), by a combination of ATP-dependent Ca^{2+} pumps and Na^{+}-Ca^{2+} exchangers (Hille, 2001). Entry of Ca^{2+} ions through VGCCs allows the local Ca^{2+} concentration to rise up to ~100 μM (for review see Bregestovski and Spitzer, 2005). These large changes in $[Ca^{2+}]$ as a result of Ca^{2+} entry are possible due the steep electrochemical gradient favouring Ca^{2+} influx- for example the Nernst potential is given

as +129 mV (when $[Ca^{2+}]_o$ = 1.5 mM and $[Ca^{2+}]_i$ = 100 nM; Hille (2001)). Ca^{2+} influx results only in a very localized $[Ca^{2+}]$ change however, producing regions of high $[Ca^{2+}]$ known as calcium microdomains (Augustine and Neher, 1992; reviewed in Berridge, 2006).

Figure 1.2. Intracellular processes arising from Ca^{2+} influx. Calcium mobilizing signals are shown in blue (such as the generation of iositol- 1,4,5- triphosphate), and refer to those mechanisms producing Ca^{2+} in cells (for example as a result of receptor activation). Activating signals are shown in green, and activate those processes shown by pink arrows. Cessation of calcium signaling is carried out by processes shown in red (such as transport mechanisms to remove calcium from the cell). Figure taken from Berridge et al., (2000).

1.2 The identification and characterisation of VGCCs

1.2.1 Electrophysiology and pharmacology

The first evidence for Ca^{2+} acting as a permeant ion was shown in the muscle fibres of crab legs (Fatt and Katz, 1953). Substitution of Na^{+} ions (thought to be essential for excitability) with choline or TEA ions resulted in increased excitability, and an increased action potential duration. Choline and TEA act to block potassium channels, preventing their repolarisation of the membrane (Hille, 2001). Coupled with the more positive Nernst potential for Ca^{2+} ions with respect to Na^{+} ions, the cells became substantially more excitable than before, with a corresponding increase in muscle contraction force and duration. The permeant ion responsible was subsequently found to be Ca^{2+} (Fatt and Ginsborg, 1958), in agreement with the observation that radiolabelled Ca^{2+} ions move into the cell during the action potential of the squid axon (Hodgkin and Keynes, 1957).

After the discovery of VGCCs in crustacean muscle, they were then found to be present in other invertebrate muscle preparations. A number of criteria had to be met before the inward current could be denoted a calcium spike (reviewed in Hagiwara & Byerly, 1981). These included: an overshoot that correlates with external $[Ca^{2+}]$; a sufficiently large measurable movement of radioactive calcium to be tied to the observation of a spike; block of spikes with ions such as Mn^{2+} or verapamil, but an absence of block with the sodium channel blocker tetrodotoxin (TTX); and a continuation of spikes by replacing extracellular Ca^{2+} ions with Ba^{2+} or Sr^{2+} ions.

The same omnipresence of calcium channels in invertebrate twitch muscle fibres was not observed in vertebrate twitch muscle fibres, where the action potential is almost entirely Na^{+} ion-mediated (Hagiwara and Byerly, 1981). There were exceptions, such as in the twitch muscle fibres of embryonic chick and rat, however these findings were absent in adult subjects. It was a different story in vertebrate smooth muscle and cardiac muscle however, where influx of Ca^{2+} appeared to be essential for muscle contraction (Reuter, 1973). Work carried out in Purkinje fibres of sheep and calf heart led to the

discovery that it was Ca^{2+} ions rather than Na^{+} ions that made up the current flow upon depolarisation of the fibre (Reuter, 1967). This demonstrated the heart as the first vertebrate tissue in which Ca^{2+} ions initiated the action potential (and therefore muscle contraction).

The first evidence for multiple subtypes of calcium current came with experiments in starfish (Hagiwara et al., 1975), where two distinct Ca^{2+} conductances were found. One required the expected voltage step to about -7 mV, whilst the other required a lesser voltage-step (to about -55 mV). This identified another calcium channel activated at low-voltage, later termed "low-voltage activated" (LVA) current or T-type (T for "transient") due to its fast rate of inactivation. "High-voltage activated" (HVA) current on the other hand had a slowly inactivating current in comparison, and was named "L-type" (for "long-lasting") accordingly. The LVA current was speculated to be a pace-making mechanism due to its inactivation at normal resting potential (Carbone and Lux, 1984).

In addition to electrophysiological classification, pharmacological classification was possible to distinguish L- and T-type channels. L-type channels are activated by the agonist Bay K 8644 and blocked by dihydropyridines (DHPs; such as nitrendipine), phenylalkylamines (PAAs) and benzothiazepines (BZPs). These modulatory effects are brought about by changes in the gating behaviour of the L-type channels (Hess et al., 1984).

With the advent of the patch-clamp technique (Hamill et al., 1981) came the ability to record from smaller cells, in particular vertebrate neurons. One such experiment identified a new type of current in chick dorsal root ganglion (DRG) neurons (Nowycky et al., 1985). Application of DHP antagonists (or agonists such as Bay K 8644) had no effect. The current was named N-type, as it was "neither" L- nor T-type current. This channel still required a stronger depolarisation to activate, but the rate of inactivation was significantly faster (between 40 and 110 ms) than L-type currents which did not seem to inactivate in response to a 200 ms step (Fox et al., 1987). Whilst N-type current

is unaffected by DHPs, it been found to be specifically and irreversibly blocked by the sea snail (*Conus geographus*) toxin ω-conotoxin GVIA (Sher and Clementi, 1991).

The use of toxins also helped identify another neuronal calcium current, this time in cerebellar Purkinje cells (Llinas et al., 1989). The use of the funnel-web spider venom blocked Ca^{2+}-dependent spikes in Purkinje cells. These channels were unaffected by ω-conotoxin GVIA. The current was named P-type after the Purkinje cells in which they were found. Later, ω-agatoxin IVA was purified (from *Agelenopsis aperta*) as a more specific blocker of P-type current (Mintz et al., 1992). A similar current type (named Q-type due to it similarity) was found in cerebellar granule cells (GCs; Randall and Tsien, 1995), this current inactivated more rapidly than P-type current, and was less sensitive to block by ω-agatoxin IVA.

Finally, an HVA current "resistant" to DHPs, ω-conotoxin GVIA (except in the millimolar range) and ω-agatoxin IVA was found, and consequently named R-type current (Ellinor et al., 1993; Soong et al., 1993). R-type current inactivated more quickly than the other HVA currents, though not to the same extent as T-type current (Randall and Tsien, 1997). In addition R-type current was blocked by application of Ni^{2+} ions.

1.2.2 Purification and molecular structure

Purification of calcium channels involved the extensive use of DHPs to bind "DHP receptors" in skeletal muscle, due to the much higher (50 – 100 times) abundance of DHP receptor here than in any other tissue (Hess, 1990b). DHP receptors were speculated to be linked to calcium channels (Borsotto et al., 1985) due to the observed block of calcium currents by DHPs, as well as the lack of labelling of DHP-receptors in the muscle sarcolemma compared to the t-tubule membranes (which correlated with the occurrence of calcium currents).

Using the radiolabelled DHP ^{3}H-nitrendipine in guinea pig ileum smooth muscle membrane preparations, a molecular weight of 270,000 was deduced for the calcium channel (Venter et al., 1983), and provided an initial estimate for the size of the DHP-receptor complex. The first purification of calcium channel subunits followed (Curtis and Catterall, 1984). Three polypeptides were purified, and were named α (160 kDa), β (50 kDa) and γ (33 kDa) subunits. The α subunit was reduced to form a 130 kDa subunit by the reducing agent dithiothreitol (DTT). Reconstitution of these subunits into an artificial membrane produced functional (L-type) calcium channel currents, suggesting that the DHP-receptor was not only linked to a calcium channel, but was the channel itself (Flockerzi et al., 1986).

Another α subunit was subsequently found as a subunit of equivalent size and equimolar stoichiometry which was not reduced in mass under reducing conditions, suggesting it did not contain disulphide bonds (Vaghy et al., 1987; Leung et al., 1987). The non-reducing subunit was termed α_1 (termed $Ca_v\alpha_1$ here), and the reducing subunit termed α_2 (Vaghy et al., 1987).

Identification of the amino-acid sequence of the $Ca_v\alpha_1$ ($Ca_v1.1$ from rabbit skeletal muscle) subunit (Tanabe et al., 1987) showed it to be a 4 transmembrane (TM) structure which contained the binding site for DHPs and also formed the channel pore. This structure was analogous to that of the voltage-gated sodium channel (Noda et al., 1984). Similar functional residues were identified as compared to those located in sodium channels. These included charged residues at every third position in the S4 segment, responsible for voltage sensing.

The purification of L-type channels from skeletal muscle was followed by purification of other channel types as they were identified by their electrophysiology in other tissues.

1.3 The VGCC $Ca_v\alpha_1$ subunit

1.3.1 Topology of the $Ca_v\alpha_1$ subunit

The structure of the VGCC $Ca_v\alpha_1$ subunit is similar to that of the pore-forming subunits of voltage-gated potassium and sodium channels (reviewed in Catterall, 2000), and therefore the studies of one type of channel may generalise for the others. VGCC α_1 subunits are composed of 4 TM domains, each containing 6 segments (S1 to S6). A representation of VGCC channel structure (with associated auxiliary subunits) is shown in Figure 1.3.

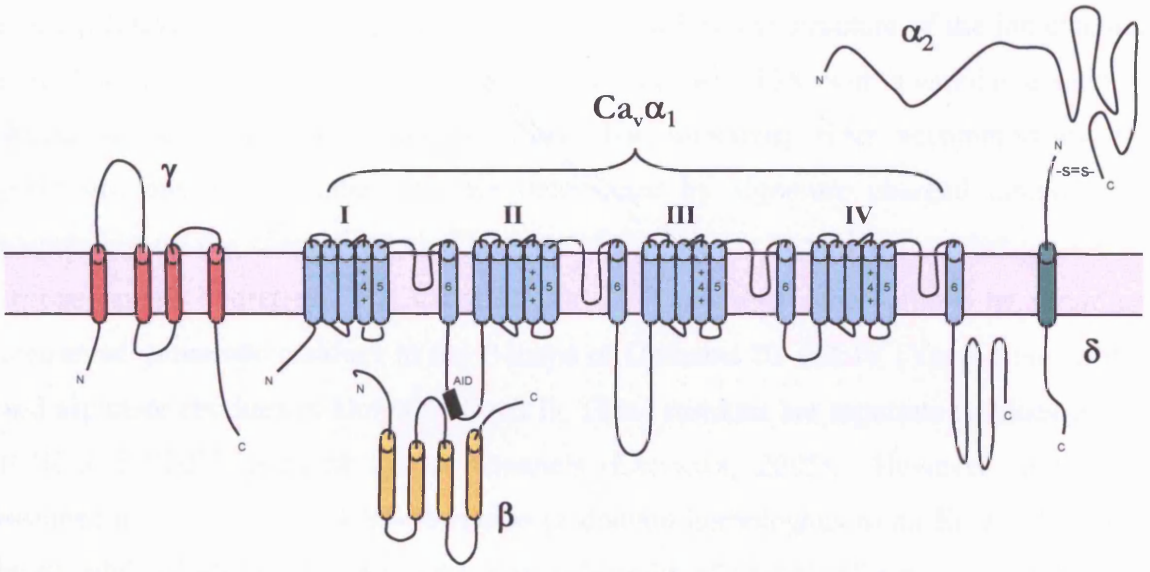

Figure 1.3. Schematic representation of VGCC topology. The $Ca_v\alpha_1$ subunit is represented as a 24 TM protein structure, arranged into four domains (I-IV) with each domain containing six TM segments (1-6). The voltage-sensing S4 segments are shown, as well as the S5 and S6 segments (between which lie the membrane re-entrant loops which make up the channel pore). The intracellular β, membrane-bound γ and extracellular α_2 (associated with the membrane-bound δ) auxiliary subunits are shown.

"C" and "N" refer to carboxyl and amino terminal sequences respectively. S=S represents one or more disulphide bonds between the α_2 and δ polypeptide sequences.

1.3.2 The channel pore and selectivity filter

The $Ca_v\alpha_1$ subunit forms the channel pore (which can function as a calcium channel in the absence of auxiliary subunits), and therefore must be able to selectively distinguish between ions. The channel pore itself is formed by the membrane re-entrant pore-loop ("P-loop") between segments S5 and S6 (Yellen et al., 1991). The P-loop is about 20 amino-acids long and forms the narrow extracellular end of the channel pore (Yellen, 1998). The solution of the structure of the KcsA potassium channel from *Streptomyces lividans* (Doyle et al., 1998) provided much insight into the structure of the ion channel pore. For this channel the length of the channel pore was 45Å, with a variable diameter. Within the pore lies the selectivity filter. The selectivity filter accommodates the permeant ions at a number of sites determined by signature charged amino-acids (depending on the channel type). This part of the pore is constricted so that the ion is stripped of its hydration. VGCCs select for Ca^{2+} ions over other cations by virtue of conserved glutamate residues in the P-loops of Domains III and IV (Yang et al., 1993) and aspartate residues in Domains I and II. These residues are aspartate residues in the II-III and III-IV loops of $Ca_v3.x$ channels (Lacinova, 2005). However, additional residues in the Domain III S5-S6 region (a domain homologous to an EF hand, which binds calcium) also contribute to the ionic selectivity of VGCCs (Feng et al., 2001). The EF hand is shown in Figure 1.7.

1.3.3 The voltage-sensor

Voltage-gated channels need to open and close in response to changes in potential across the cell membrane. This is achieved by the movement of charged residues within the channel structure which couple to gating machinery. These residues are located in the

$Ca_v\alpha_1$ subunit of VGCCs (Tanabe et al., 1987). Repeats of arginine and lysine residues within the S4 segments suggested the cloned skeletal muscle calcium channel was indeed a voltage-gated channel, as the same motifs had been found previously for voltage-gated sodium channels (Noda et al., 1982; Noda et al., 1984). The movement of these charged residues can be observed by removing permeant ions from the external solution, whereby a small "gating" current remains in the absence of ion flow (Armstrong and Bezanilla, 1974). The contribution of each S4 charged residue to the gating current can be calculated by its removal (Aggarwal and MacKinnon, 1996). A number of models exist for how the S4 segment moves in response to a depolarisation to enable channel opening (Catterall, 1988; Cuello et al., 2004; Jiang et al., 2003).

The gating of voltage-gated channels allows another means by which channels can be modulated. Inhibition of channels is possible either by a physical block of the channel pore, or by preventing the movement of the gating machinery (for review see Catterall et al., 2007). As with pore-blocking drugs, it is possible to influence channel function by interfering with the voltage sensor, as is the case with DHPs (Doering and Zamponi, 2003).

1.4 Current classification of VGCC $Ca_v\alpha_1$ subunits

Originally divided into HVA and LVA families, and then according to their electrophysiological characteristics (L, P/Q, N, R, T-type), VGCCs are now classified according to gene homology (Ertel et al., 2000). A total of 10 genes for different α_1 subunits have been identified and the resulting channels are arranged into three families: $Ca_v1.x$; $Ca_v2.x$; and $Ca_v3.x$. The sequence similarity between members of the different VGCC families is shown in Figure 1.4.

Figure 1.4. Phylogeny of VGCCs. The 10 human VGCC genes (and the channels they produce) are shown, as is their similarity in amino acid sequence to one another. Adapted from Ertel et al., (2000).

1.4.1 The $Ca_v1.x$ subfamily (L-type)

Members of the $Ca_v1.x$ gene family give rise to channels with L-type current (see Section 1.2.1). They are also characterized pharmacologically by their sensitivity to DHPs. These can have an antagonistic action on the channels (such as isradipine) or agonistic effect (such as Bay K 8644; reviewed in Catterall., 2005). DHPs bind at the S5-S6 regions in Domains III and IV, and influence the gating machinery so that channels enter a more or less "willing" state (Doering and Zamponi, 2003). PAAs bind a different site (albeit one with overlapping residues), but cause channel block rather than altering gating properties. BZPs also bind $Ca_v1.x$ channels at another distinct site involving many of the same residues.

A number of studies have attempted to produce images of VGCCs by electron microscopy in an attempt to further elucidate their structure (reviewed in Wang et al., 2004), as shown in Figure 1.5. These studies used VGCCs purified from skeletal or cardiac muscle tissue due to VGCC abundance there, and as a result examine $Ca_v1.x$ channel structure.

Figure 1.5. Representations of VGCC structure using purified $Ca_v1.x$ channels from skeletal muscle. The studies are relatively consistent in showing a membrane-bound $Ca_v\alpha_1$ subunit, intracellular β subunit (although shown to be located in the membrane in (D)), and an extracellular α_2 subunit that extends into the extracellular space. Figure adapted from Wang et al., (2004).

1.4.1.1 $Ca_v1.1$ (α_{1S})

Due to it high occurrence in skeletal muscle, $Ca_v1.1$ was the first VGCC subunit to be purified. Its main location is in the t-tubules of skeletal muscle fibres, where it is involved in excitation-contraction coupling and Ca^{2+} homeostasis (Catterall et al., 2005). $Ca_v1.1$ associates with the auxiliary subunits $\alpha_2\delta$, β and γ (Takahashi et al., 1987), Blockers include DHP antagonists such as verapamil and isradipine), whilst activators include BayK8644 and DHP agonists (Catterall et al., 2005). $Ca_v1.1$ channels open with characteristically slow kinetics, and therefore allow negligible Ca^{2+} entry with a single muscle action potential.

$Ca_v1.1$ in skeletal muscle is implicated in excitation-contraction coupling (ECC), but this is dependent on the gating charge movement of the L-type channel in response to depolarisation, rather than by entry of calcium ions (Rios and Brum, 1987). This charge movement makes an interaction with ryanodine receptors in the sarcoplasmic reticulum, triggering Ca^{2+} release (Catterall, 2000). Accordingly, mutations of the $Ca_v1.1$ subunit result in a number of skeletal muscle-related pathologies. The absence of $Ca_v1.1$ causes muscular dysgenesis, a lethal condition arising from a failure of ECC (Adams and Beam, 1990).

Regulation of skeletal $Ca_v1.1$ channels occurs via phosphorylation of both the α_1 and associated β subunits, as reviewed in Catterall (2000). The α_1 subunit is regulated by cAMP-dependent protein phosphoylation, with cAMP-dependent protein kinase causing an increase in the mean open-time of single channels (Flockerzi et al., 1986). Phosphorylation sites have been identified in both the α_1 and β subunits, as reviewed in Catterall (2000).

1.4.1.2 $Ca_v1.2$ (α_{1C})

$Ca_v1.2$ (α_1c) was originally purified from chick cardiac muscle (Chang and Hosey, 1988; Cooper et al., 1987), however it is also found in smooth muscle and central nervous system (CNS; Snutch et al., 1991). The $\alpha1$ subunit is larger (185 kDa) than the $Ca_v1.1$ α_1 subunit (~170 kDa), and was poorly recognised by antibodies against $Ca_v1.1$ (Chang and Hosey, 1988). $Ca_v1.2$ undergoes significant phosphorylation by cAMP-dependent protein kinase (reviewed in Kamp and Hell, 2000). It is involved in excitation-contraction coupling in cardiac muscle, as well as propagating the action potential in the sino-atrial and atrio-ventricular nodes of the heart (reviewed in Catterall et al., 2005). In cardiac muscle tissue, the $Ca_v1.2$ channel makes a functional interaction to ryanodine receptors which does involve the influx of calcium, rather than a mechanical interaction resulting in the release of Ca^{2+} from the sarcoplasmic reticulum,

as in skeletal muscle (Avila and Dirksen, 2000). In neurons, $Ca_v1.2$ channels form clusters, and have been shown to localize in the extrasynaptic space in hippocampal neurons (Obermair et al., 2004). As with $Ca_v1.1$, $Ca_v1.2$ is subject to alternative splicing (Snutch et al., 1991).

1.4.1.3 $Ca_v1.3$ (α_{1D}) and $Ca_v1.4$ (α_{1F})

The existence of $Ca_v1.3$ and $Ca_v1.4$ subunits occurred at the same time as alternative splice variants of $Ca_v1.1$ and $Ca_v1.2$ were being discovered (Snutch et al., 1991; Perez-Reyes et al., 1990; Seino et al., 1992; Tomlinson et al., 1993). $Ca_v1.3$ was considered a "neuroendocrine" channel due to its location in endocrine cells (such as pancreatic β cells) as well as neurons, sensory receptor cells, vascular smooth muscle and nodes of the heart (reviewed in Catterall et al., 2005). $Ca_v1.3$ knockout mice displayed deafness, due to a lack of sound-evoked depolarization in cochlear inner hair cells. These mice also displayed bradycardia and arrhythmia, as a result of sinoatrial node dysfunction (Platzer et al., 2000).

$Ca_v1.4$ is located in retinal photoreceptors, where mutations can lead to congenital stationary night-blindness (Strom et al., 1998), as well as localizing in spinal cord and lymphoid tissue (Catterall et al., 2005).

1.4.2 The $Ca_v2.x$ subfamily

The $Ca_v2.x$ family makes up the predominantly neuronal family of VGCCs. These channels typically give rise to currents intermediate in their rate of inactivation between $Ca_v1.x$ and $Ca_v3.x$ families. $Ca_v2.x$ VGCCs are classically blocked by various peptide neurotoxins, which enabled their pharmacological dissection from one another.

1.4.2.1 $Ca_v2.1$ (α_{1A}, P/Q type)

The initial identification (Llinas et al., 1989) and characterization (Mintz et al., 1992; Usowicz et al., 1992) of P-type channels found them to possess HVA currents with little inactivation over a 1 second depolarization. Currents were inhibited rather than activated by Bay K 8644, although the inhibition was slight (Usowicz et al., 1992). $Ca_v2.1$ channels are implicated in neurotransmitter release at central synapses (Turner et al., 1992; Takahashi and Momiyama, 1993).

Purification of the α_{1A} ($Ca_v2.1$) protein (Mori et al., 1991; Starr et al., 1991) identified a calcium channel subtype expressed throughout the nervous system (Hillman et al., 1991). As well as being located on the dendrites and cell bodies of Purkinje cells, a high incidence of $Ca_v2.1$ protein was found at presynaptic terminals, of many neurons (Westenbroek et al., 1995). P-type channels encoded by the $Ca_v2.1$ subunit are highly sensitive to block by ω-agatoxin IVA with an IC_{50} in the region of 1-3 nM (Mintz et al., 1992) and ω-conotoxin MVIIC with an IC50 of 18 nM (Hillyard et al., 1992; McDonough et al., 1996), whilst being insensitive to ω-conotoxin GVIA block. Application of funnel-web spider venom showed a block of muscle contraction and evoked neurotransmitter release (Uchitel et al., 1992), implicating $Ca_v2.1$ in these functions. ω-agatoxin IVA is thought to bind the S3-S4 linker in Domain IV and shift activation kinetics, whilst w-conotoxin MVIIC is thought to occlude the channel pore (reviewed in McDonough et al., 2002).

Q-type current was subsequently identified in cerebellar granule cells. When the $Ca_v2.1$ gene (expected to produce P-type channels) was expressed in *Xenopus oocytes*, it was found to be less sensitive to ω-agatoxin IVA and possess faster activation and inactivation kinetics (Sather et al., 1993). The sensitivity to ω-agatoxin IVA block was lower than that of P-type channels with an IC_{50} of 100-200 nM (Catterall, 2000). Alternative splicing of $Ca_v2.1$ appears to be responsible for the production of both P and Q channel types (Bourinet et al., 1999). A valine insertion (V_{421}) in the I-II linker region (near to the β binding site), as well as the insertion of Asp and Pro (N_{1605}-P_{1606}) residues

in domain IV caused the production of an α_{1A} subunit with properties such as a reduced inactivation rate. A mutation in the S5-SS1 linker region (E1740R) produced a threefold increase in peak current (Hans et al., 1999). Therefore, alterations in the Domain IV structure can induce significant changes on the biophysical properties of the resultant channels.

Mouse *Cacna1a* mutants give rise to a number of phenotypes displaying ataxia and dyskinesias. *Tottering*, *leaner* and *rolling* phenotypes all result in a decrease in Pukinje cell current density (reviewed in Zwingman et al., 2001). Other phenotypes include *tottering-3J* and *rocker*. These phenotypes all result in ataxia, with *tottering* also causing dyskinesia (Zwingman et al., 2001) and *tottering*, *leaner*, *rocker* and *tottering-3J* resulting in absence seizures.

Mutations in human $Ca_v2.1$ have also been found to result in a number of pathological phenotypes such as familial hemiplegic migraine (FHM), episodic ataxia type 2 (EA2), and spinocerebellar ataxia type 6 (SCA6; Pietrobon, 2002). SCA6 is caused by a polyglutamine expansion in the carboxy terminal region of the *CACNA1A* gene, whilst FHM is caused by various mutations throughout the coding region, and EA2 is most usually caused by mutations that result in truncations of $Ca_v2.1$ (Ducros et al., 1999).

The knock-out of $Ca_v2.1$ in mice results in ataxia and dystonia, and proves fatal within two to three weeks (Fletcher et al., 2001; Jun et al., 1999). P/Q type currents were found to be absent from dissociated Purkinje cells and GCs. However, there was evidence for a compensatory contribution from N and R type current, although this was not sufficient to recover the quantal release of neurotransmitter (Urbano et al., 2003).

The contribution of individual domains to channel properties has been investigated, following the identification of what may be a two-domain form of $Ca_v2.1$ (or a breakdown product) which interacts with the channel complex (Scott et al., 1998). This 95 kDa glycoprotein is comprised of Domains I and II of $Ca_v2.1$ (as well as part of the II-III linker region), and interacts with both the $Ca_v2.1$ and β subunits. It is found to be

enriched in the cerebellum (Arikkath et al., 2002). When a Domain I-II construct of $Ca_v2.1$ was expressed with a Domain III-IV construct of $Ca_v1.1$, the hybrid subunit showed an ability to recover voltage sensing (Ahern et al., 2001), suggesting this protein may provide a functional voltage sensing contribution to its associated $Ca_v2.1$ subunit in neurons. Co-expression with the $Ca_v2.1$ subunit was also found to inhibit currents via competition for β subunit binding (Arikkath et al., 2002).

1.4.2.2 $Ca_v2.2$ (α_{1B}, N-type)

N-type channels were the first additional calcium channel to be identified by electrophysiology after L-type channels (Nowycky et al., 1985), and α_{1B} protein shown to be present in neurons (Dubel et al., 1992). Following the cloning of $Ca_v2.2$ by homology with other calcium channels, it was identified as the molecular counterpart of N-type channels. $Ca_v2.2$ plays a role in neurotransmitter release from motor nerve terminals. This is mainly at early times during development however, with $Ca_v2.1$ channels replacing them in the adult (Urbano et al., 2003), except at some synapses (such as sensory neurons in the peripheral nervous system). The role in neurotransmitter release comes from the association of $Ca_v2.2$ with soluble *N*-ethylmaleimide-sensitive factor attachment protein receptor (SNARE) proteins (see Section 1.9). These include syntaxin 1A, synaptotagmin and synaptosomal-associated protein 25 (SNAP-25), which can inhibit $Ca_v2.2$ function (Bezprozvanny et al., 2000; Wiser et al., 1996a; Sheng et al., 1997). $Ca_v2.2$ is also important in synaptogenesis and regulation of gene expression (Gray et al., 2007). As is the case for other $Ca_v2.x$ VGCCs, $Ca_v2.2$ channels are modulated by G proteins (Dolphin, 2003b). They are also selectively blocked by ω-conotoxin GVIA. Unlike ω-agatoxin IVA, ω-conotoxin GVIA appears to act as a pore-blocker, binding residues in the S5-S6 linker region of Domain III (Ellinor et al., 1994).

$Ca_v2.2$ associates with auxiliary subunits $\alpha_2\delta$ and β (McEnery et al., 1991; Scott et al., 1996). Its localization and organization in the developing synapse is regulated by laminin β3 (Nishimune et al., 2004).

$Ca_v2.2$ (for example in dorsal root ganglion cells) is important for mediating nociceptive information from the periphery to the central nervous system (Altier et al., 2007). $Ca_v2.2$ is subject to alternative splicing (Stea et al., 1999), and different isoforms of the channel can alter the excitability of nociceptive neurons (Raingo et al., 2007). A peptide blocker of $Ca_v2.2$ channels based on ω-conotoxin MVIIC (Ziconotide), has shown efficacy in treating hyperalgesia, allodynia and inflammatory pain (reviewed in Catterall et al., 2005).

1.4.2.3 $Ca_v2.3$ (α_{1E}, R-type)

The R-type current was originally classified according to its "resistant" or "residual" nature, when applying toxins to block L, N and P/Q type currents. R-type current inactivated more rapidly than either N or P/Q type, as well as activating at lower potentials. It was initially considered both an HVA and an LVA channel (Ellinor et al., 1993; Soong et al., 1993). Following the cloning of $Ca_v2.3$, it was found to have properties in common with channels giving rise to R-type current. A number of $Ca_v2.3$ isoforms are produced, each with differing sensitivity to the tarantula toxin SNX-482, selectivity for Ca^{2+} ions and Ba^{2+} ions, as well as having differences in voltage-dependence of current activation (Tottene et al., 2000).

The VGCCs which gave rise to R-type current are now recognized as HVA channels. These currents are not affected by DHPs, ω-agatoxin IVA or ω-conotoxin GVIA, although studies have shown a sensitivity to ω-agatoxin IVA (Stephens et al., 1997). They are blocked by Ni^{2+} ions, unlike other VGCC subtypes (Soong et al., 1993) and also SNX-482, with an IC_{50} of 15-30 nM (Newcomb et al., 1998). SNX-482 inhibits $Ca_v2.3$ channels irreversibly, by preventing normal activation gating of the channels rather than by blocking them. This depolarises the voltage-dependence of channel opening, an effect reliant on Domains III and IV (Bourinet et al., 2001). Additional

modulation comes from activated G proteins, which bind to the I-II linker of $Ca_v2.3$ channels (Dolphin, 2003b).

$Ca_v2.3$ knockout mice have increased the confusion surrounding $Ca_v2.3$ and R-type current (Wilson et al., 2000). A small component of the "residual" current in cerebellar GCs and dorsal root ganglion was ablated in $Ca_v2.3$ -/- mice, which corresponded to that blocked by application of SNX-482. In both cases however, a significant proportion of the current remained, suggesting $Ca_v2.3$ channels make up only part of this residual current.

1.4.3 The $Ca_v3.x$ subfamily (α_{1G} / α_{1H} / α_{1I}, T-type)

Channels of the $Ca_v3.x$ family pass T-type current, characterized by a transient influx of calcium with a fast rate of inactivation. These currents were first observed in starfish (Hagiwara et al., 1975) and chick sensory neurons (Carbone and Lux, 1984). These currents activate at lower potentials than members of the $Ca_v1.x$ and $Ca_v2.x$ families (HVA channels), and are known as low-voltage activated (LVA) channels. LVA VGCCs are roughly equally selective for Ba^{2+} ions and Ca^{2+} ions, unlike the HVA channels.

Three $Ca_v3.x$ channels have been described (Catterall, 2000). $Ca_v3.1$ is found predominantly in the brain, as well as heart, placenta and ovary (Catterall et al., 2005). $Ca_v3.2$ is found in kidney, smooth muscle and heart. $Ca_v3.3$ is found exclusively in brain tissue (Catterall et al., 2005). Due to their characteristic current-voltage relationship, Cav3.x channels are important for producing low-voltage spikes in neurons, as well as being involved in hormone secretion from the adrenal gland (Lacinova, 2005). Expression of $Ca_v3.1$ and $Ca_v3.2$ subunits produces calcium currents similar to those seen in native cells, and $Ca_v3.x$ amino acid sequences do not contain an AID sequence, suggesting they do not associate with auxiliary subunits (Lacinova, 2005).

No specific T-type current blockers were identified initially, ruling out pharmacological classification of the currents. However newer agents such as the gating modifier kurtoxin (from scorpion) have since been identified (Chuang et al., 1998), although their absolute specificity for $Ca_v3.x$ channels is not assured, with block of $Ca_v2.x$ channels (and also voltage-gated sodium channels) observed. Ni^{2+} ions also block $Ca_v3.x$ channels, with greatest affinity block for $Ca_v3.2$ (reviewed in Catterall et al., 2005) However, Ni^{2+} ions also block $Ca_v2.x$ channels with a lower affinity (reviewed in Doering and Zamponi, 2003).

1.5 Function and modulation of VGCCs

1.5.1 Channel inactivation

One of the important characteristics of channel function is the kinetics of activation and inactivation. This imposes a degree of control over the amount of Ca^{2+} that will enter the cell for a given duration of depolarization. Three mechanisms of inactivation exist: calcium-dependent and voltage-dependent: of which there are fast and slow forms (reviewed in Hering et al., 2000).

Figure 1.6. Inactivation states of VGCCs. Open, closed and the three inactivated states of VGCCs, represented as single protein structures (black) embedded in the membrane (blue). Channels may move between states as indicated by the arrows. Figure adapted from Hering et al., (2000).

1.5.1.1 Calcium-dependent inactivation

Another inactivation mechanism for VGCCs (specifically $Ca_v1.2$ and $Ca_v2.1$) involves the entry of Ca^{2+} itself. Replacing Ca^{2+} ions with Sr^{2+} or Ba^{2+} ions resulted in a change in the time-course of inactivation, suggesting Ca^{2+} ions were involved in switching off the current (Lee et al., 1985). The underlying cause of this inactivation was indeed the entry of Ca^{2+} ions, and their association with calmodulin. Calmodulin binds to an IQ domain on the C-terminal of VGCCs (Zuhlke and Reuter, 1998). Residues within this domain are responsible for binding calmodulin/Ca^{2+} and mediating this inactivation (Zuhlke et al., 2000b). It is thought that calmodulin binds to the IQ domain

constitutively, but only has an effect upon inactivation kinetics when Ca^{2+} binds to it (Catterall, 2000).

The IQ domain is responsible for mediating calcium-dependent facilitation in addition (Zuhlke et al., 2000a), and is thought to be mediated by binding of calmodulin/Ca^{2+} to the IQ domain. Facilitation can be observed by applying double or multiple pulses. Demonstrating the facilitation effect with a pre-pulse, a larger peak current was obtained in the presence of Ca^{2+} ions, but not Ba^{2+} ions (Xiao et al., 1994). The facilitation could also be blocked by application of the Ca^{2+} chelator BAPTA, as well as the CaMKII blocker ICK. The same inhibitory and facilitatory effects have been observed in $Ca_v2.1$ currents (Lee et al., 1999), and involve Ca^{2+}-calmodulin binding to the C-terminal end of the $Ca_v2.1$ α_1 subunit at a novel site (Catterall, 2000).

1.5.1.2 Voltage-dependent inactivation

Voltage-dependent inactivation confers a level of control over VGCC activity in relation to excitability. VGCCs inactivate in response to a long depolarisiation, from members of the $Ca_v1.x$ family which show little or no inactivation, to members of the $Ca_v3.x$ family which inactivate in the order of tens of milliseconds (reviewed in Catterall et al., 2005). $Ca_v2.3$ inactivates only marginally more slowly than $Ca_v3.x$ channels, and $Ca_v2.2$ and $Ca_v2.1$ inactivate more slowly. It was found that Ba^{2+} flux through VGCCs decayed in a bi-exponential manner in a number of cases, suggesting the presence of two (fast and slow) voltage-dependent phases of inactivation (reviewed in Hering et al., 2000).

A number of mutation studies (involved in disease phenotypes) have been demonstrated to have an effect on voltage-dependent channel inactivation, such as $Ca_v2.1$ mutations in S6 segments and their involvement in familial hemiplegic migraine (FHM; Kraus et al., 1998; Kraus et al., 2000). $Ca_v2.1$ mutations associated with FHM patients were introduced into rabbit $Ca_v2.1$. A total of six mutations were found to alter the rate of inactivation (and recovery from inactivation). Additionally, chimeric studies using the

S6 segment of Domain I (in $Ca_v2.1$) as a replacement for that of the faster-inactivating $Ca_v2.3$ caused a slowing of inactivation (Zhang et al., 1994). Mutation of residues in the I-II linker (Herlitze et al., 1997), as well as regions in the S3-S4 and S5-S6 linker regions in Domain IV of $Ca_v2.1$ (Hans et al., 1999) also alter inactivation.

The slow-phase of voltage-dependent inactivation is not well dissected from the fast-phase and have a time constant of several seconds in $Ca_v1.x$ channels, as reviewed in Lacinova, (2005). In many instances decay curves can be fitted adequately using a single exponential (see Materials and Methods).

Membrane potential is therefore an important factor in VGCC inactivation. A given potential will result in a certain proportion of the channel population that is in the inactivated state, the rest being in open, closed or calcium-inactivated states (see Figure 1.6). The proportion of channels that are voltage-inactivated will vary with membrane potential, and can be described by a Boltzmann function (see Materials and Methods). This is referred to as steady-state inactivation.

1.5.2 G protein modulation

For $Ca_v2.x$ channels (especially $Ca_v2.1$ and $Ca_v2.2$ type channels), modulation by G proteins represents a significant mechanism for modulation (Scott and Dolphin, 1986; Dolphin, 2003b), with calcium currents in many neurons such as dorsal root ganglion and superior cervical ganglion being inhibited by G proteins. Studies trying to identify the type of G protein involved found that a number of $G\alpha$ subunits caused G protein-mediated inhibition. It was subsequently found that the $G\beta\gamma$ subunit rather than the $G\alpha$ subunit was responsible for inhibition (Herlitze et al., 1996). The required $G\beta\gamma$ subunits are provided by activation of a number of receptor types- such as α_2-adrenoceptors, δ and μ opioid receptors, $GABA_B$ receptors and adenosine A1 receptors (Dolphin, 2003b).

G proteins bind to the I-II linker of the $Ca_v\alpha_1$ subunit in $Ca_v2.x$ channels (Dolphin, 2003b), to a site which overlaps with the binding site of the $Ca_v\beta$ subunit. Binding of the β subunit facilitates voltage-dependent G protein modulation, rather than preventing it (Canti et al., 2000; Meir et al., 2000). The same site in $Ca_v1.x$ channels will bind the $Ca_v\beta$ subunit, but not $G\beta\gamma$ (Bell et al., 2001; Herlitze et al., 1997).

G protein-mediated inhibition of calcium channels is characterized by a shift in voltage-dependence to more depolarized potentials (Bean, 1989), rather than a reduction in single-channel conductance or a reduction in the number of channels present. The shift in voltage-dependence is due to a shift of the channel population to the "reluctant" mode (with $G\beta\gamma$ bound) rather than the "willing" mode (with no $G\beta\gamma$ bound). A prolonged depolarisation of the channels by pre-pulse (Bean, 1989; Ikeda, 1991) offers a means of relief from G protein modulation, and suggests the importance of action-potential frequency in the modulation of presynaptic inhibition.

1.5.3 Channel phosphorylation

The $Ca_v\alpha_1$ (and β) subunits are subject to phosphorylation, which results in an increased expression of both subunits in skeletal muscle (reviewed in Catterall, 2000). This occurs via the cAMP-dependent protein kinases (A and C). Phosphorylation also enhances current amplitude and shifts channels towards the "willing" mode, and can reverse G protein modulated inhibition in $Ca_v2.2$ channels (Swartz, 1993).

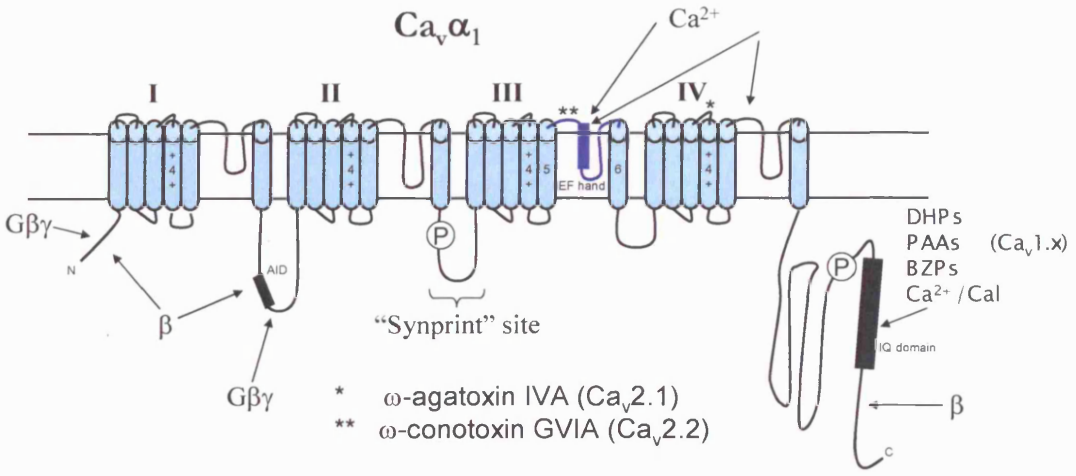

Figure 1.7. Sites of modulation and functional importance in the $Ca_v\alpha_1$ subunit. Sites shown are: the AID sequence and N- / C- termini, which bind β subunits (depending on the $Ca_v\alpha_1$ subunit and β isoform); the synprint site, involved in binding SNARE proteins; the IQ domain (in $Ca_v1.x$ channels), which binds the Ca^{2+} / calmodulin complex; the main Gβγ binding site, overlapping with the AID sequence; and the EF hand involved in Ca^{2+} selectivity, located within the S5-S6 linker of Domain III. Binding regions for ω-agatoxin IVA (in $Ca_v2.1$) in the S3-S4 region of Domain IV, and for ω-conotoxin GVIA (in $Ca_v2.2$) in the S5-S6 region of Domain III are shown. Multiple sites of importance (such as individual residues implicated in inactivation, or the binding of DHPs in $Ca_v1.x$ channels) are omitted for simplicity, and referred to in the text.

1.6 The beta (β) subunit

The β subunit was originally purified as one peptide of the DHP receptor complex (Curtis and Catterall, 1984). It was found to contain α-helices, but no TM domains, suggesting it was an intracellular protein (Ruth et al., 1989) associated to the $Ca_v\alpha_1$ subunit via a protein-protein interaction. Four β subunit genes (*cacnb* 1-4, each with additional splice variants) have been identified (Ruth et al., 1989; Castellano et al., 1993a; Castellano et al., 1993b; Hullin et al., 1992; Perez-Reyes et al., 1992; Birnbaumer et al., 1998). A schematic of the β subunit structure is shown in Figure 1.3.

One of the primary effects of the β subunit is to increase the observed current amplitude through the $Ca_v\alpha_1$ subunit, as seen when β1 was co-expressed with $Ca_v1.2$ (Perez-Reyes et al., 1992). Additional biophysical effects include a hyperpolarizing shift in current-voltage relationship with co-expression of β1 or β3 subunits, but a depolarization with co-expression of β2 (Birnbaumer et al., 1998), as well as acceleration of inactivation kinetics (Singer et al., 1991) and hyperpolarisation of the steady-state inactivation (Leroy et al., 2005). The co-expression of different β subunits affects the rate of inactivation differently, with β1 accelerating inactivation rate, and β2a slowing it (Birnbaumer et al., 1998).

The increase in peak-current amplitude with co-expression of β subunits is attributed to an enhancement of trafficking of the $Ca_v\alpha_1$ subunit (Brice et al., 1997). The ability of β subunits to enhance expression is controversial however, with some studies finding a lack of increase in the gating charge movement (for review see Richards et al., 2004). The interaction site between the α_1 and β subunits has been shown to be in the I-II linker region of the $Ca_v\alpha_1$ subunit (Pragnell et al., 1994). The I-II linker was subsequently found to contain an ER retention signal, which prevents full expression of produced $Ca_v\alpha_1$ protein (Bichet et al., 2000). Binding of β subunits to the I-II linker prevents the function of this retention signal, and allows enhanced membrane expression of $Ca_v\alpha_1$ subunits. The site at which the β subunit binds is the "alpha interaction domain" (AID), an 18 amino acid sequence (QQxExxLxGYxxWIxxxE in HVA channels, where x can be any amino acid) within the I-II linker sequence (Dolphin, 2003a). A tryptophan residue within this is essential for the β subunit binding. However this is not the case in the palmitoylated β2a subunit, suggesting the presence of another binding site, and / or the additional role of palmitoylation in increasing juxta-membrane concentration (Berrou et al., 2002; Leroy et al., 2005). The AID is not the sole binding site within $Ca_v\alpha_1$ subunits for β subunit binding, as there are also thought to be sites in the C and N termini (reviewed in Dolphin, 2003a).

As with the calcium channels they modulate, β subunits are located throughout the body. The β1a subunit is found in skeletal muscle where it is vital for excitation-contraction coupling (Schredelseker et al., 2005), whilst the β1b subunit is distributed throughout the brain and heart tissue (reviewed in Dolphin, 2003a). β2 is present in some neurons (such as Purkinje cells), as well as smooth muscle. β3 and β4 subunits are preferentially expressed in brain tissue, such as the cerebellum in the case of β4 (Ludwig et al., 1997).

Structural analysis of the β1b subunit has shown it to be a five-domained structure (Hanlon et al., 1999), similar to membrane associated guanylate kinases (MAGUKs), important for correct arrangement of ion channels and adhesion molecules at the synapse (Helton and Horne, 2002). The domain structure of β subunits includes a PDZ-like domain, *src*-homology 3 (SH3) domain and a guanylate kinase-like (GK) domain (Hanlon et al., 1999). The SH3 and GK domains are linked by a HOOK region important for causing β-mediated effects on voltage-dependent inactivation of channels (Richards et al., 2007).

Alternative splicing of β subunits affects their interaction with and influence over the $Ca_v\alpha_1$ subunit. An example of this is the alternately spliced β4 subunit (Helton and Horne, 2002), found with both a short and a long-form of the N-terminal domain. Co-expression of the short form results in more pronounced effects on voltage-dependent inactivation.

1.7 The gamma (γ) subunit

The γ subunit (now γ1) was initially purified as a 32 kDa constituent protein of the skeletal muscle DHP-R complex (Curtis and Catterall, 1984). The γ subunit is shown in Figure 1.3. Sequencing of the subunit (Jay et al., 1990) revealed it to be a 25 kDa 4 TM structure with two glycosylation sites. Stargazin, a second gamma subunit (γ2) was found solely in the brain, as opposed to γ1 being found in muscle (Letts et al., 1998). The γ2 knockout mouse (*stargazer*) displays unusual gait as well as frequent head elevations, implicating γ proteins in the regulation of neuronal excitability. A further 6 γ proteins have been found (Chu et al., 2001; Klugbauer et al., 2000): γ3 and γ4 are localized exclusively in brain (Klugbauer et al., 2000; Moss et al., 2003); γ5 is also found in various tissues outside the brain (Klugbauer et al., 2000); γ6 is found in skeletal and cardiac muscle; γ7 in most tissues (although concentrated in the brain), and γ8 in brain and testis (Chu et al., 2001). All γ subunits contain a 4 TM structure, although the number of exons present varies between subunits.

Co-expression of γ subunits causes different effects on the resultant VGCC complex, depending on the γ subunit expressed. γ1 has been found to cause a decrease in current amplitude, although studies also suggest an acceleration of inactivation kinetics (Black, III, 2003). The status of most other putative γ subunits as VGCC "subunits" is questionable, it is not clear whether these γ homologues are actually associated with, or influence VGCC activity. The γ2 subunit hyperpolarizes steady-state inactivation of $Ca_v2.1$ channels (Letts et al., 1998), although γ2 (and γ4) were found to have no effect on peak current density, steady state inactivation or voltage dependence of activation of $Ca_v2.2$-mediated currents (Moss et al., 2003). γ4 and γ5 co-expressed with $Ca_v2.1$ channels caused a hyperpolarisation in steady-state inactivation (Klugbauer et al., 2000). Co-expression of γ7 with $Ca_v2.2$ channels resulted in a significant reduction in $Ca_v2.2$ expression (Moss et al., 2002).

A significant overlap exists between the calcium channel γ subunits and the alpha-amino-3-hydroxy-5-methyl-4-isoxazole propionic acid receptor (AMPA-R) transmembrane AMPA-R regulatory proteins (TARPs). γ2 is known to modulate AMPA receptor activity- enhancing trafficking and regulating channel gating (Tomita et al., 2007; Bats et al., 2007). Therefore the role of γ subunits in regulating synaptic efficacy is not limited to action at VGCCs.

1.8 The alpha-2-delta ($\alpha_2\delta$) subunit

1.8.1 Topology of the $\alpha_2\delta$ subunit

The initial purification of the DHP-receptor complex from rabbit skeletal muscle (Curtis and Catterall, 1984) isolated the $\alpha_2\delta$ subunit as a large 160 kDa polypeptide subunit of the channel, non-covalently associated with smaller β and γ subunits. The 160 kDa subunit was reduced to 130 kDa by di-sulfide bond reduction, another study showing this reduction (from 170 to 142 kDa) also produced a 32 kDa subunit (Schmid et al., 1986). The reduction of this subunit allowed it to be recognized as separate from the 175 kDa subunit (Cooper et al., 1987; Leung et al., 1987), and was termed the α_2 subunit (Vaghy et al., 1987). The other subunit product of the α_2 reduction reaction was named the δ subunit (Takahashi et al., 1987).

The initial model of the $\alpha_2\delta$ subunit was a 3 TM structure, with three hydrophobic regions proposed at amino acids 422-444, 882-906 and 1043-1062 (Ellis et al., 1988). However, the structure has since been revised, as shown in Figure 1.3. α_2 can be removed from membranes by reduction, whereas the δ subunit remains membrane-associated (Jay et al., 1991), suggesting α_2 is extracellular. Antibody targeting of TM regions in permeabilised and non-permeabilised cells (Brickley et al., 1995), as well as improper processing of a TM III truncation (Wiser et al., 1996b) provide extra evidence that $\alpha_2\delta$ is a single TM protein. The N-terminus of the δ subunit, as well as the N-

terminus of α_2 and the sequence between previously proposed TM segments were all found to be extracellular, suggesting the α_2 subunit was located extracellularly and anchored to the cell membrane via the δ subunit (Brickley et al., 1995). A number of studies have provided structural representations of L-type calcium channel complexes (Wang et al., 2004). These reported structures share a common feature in that the α_2 subunit is proposed to be a large extracellular protrusion (see Figure 1.5).

The $\alpha_2\delta$ protein is extensively glycosylated (Ellis et al., 1988). Deglycosylation (using peptide-N-glycosydase F) causes a reduction in mass from 150 kDa to 106 kDa in $\alpha_2\delta$-1, and co-expression of this deglycosylated form of $\alpha_2\delta$-1 with $Ca_v2.1$ / $\beta4$ subunits caused a 67% reduction in current amplitude (compared to co-expression of fully-glycosylated $\alpha_2\delta$-1) when expressed in oocytes (Gurnett et al., 1996). Deglycosylated $\alpha_2\delta$-1 still associates with the $Ca_v\alpha_1$ subunit, but significantly reduces the amount of $Ca_v\alpha_1$ expression (Gurnett et al., 1997). Deglycosylated $\alpha_2\delta$ also fails to enhance currents to the same extent as fully glycosylated $\alpha_2\delta$ (Sandoval et al., 2004).

The $\alpha_2\delta$ subunit is the protein product of a single gene (De Jongh et al., 1990). It is post-translationally cleaved to produce α_2 and δ, which remain joined by one or more disulphide bonds (Jay et al., 1991). The disulphide bond is formed between cysteine residues within the $\alpha_2\delta$ sequence, however the exact residues involved are not yet identified.

Recent work has further probed the processing and cleavage of $\alpha_2\delta$. Non-cleaved forms of $\alpha_2\delta$ exist are present when $\alpha_2\delta$ is heterologously expressed in cell-lines, however it appears to retain its functionality (Douglas et al., 2006), suggesting either that cleavage is not essential, or that the small proportion of cleaved $\alpha_2\delta$ is sufficient for function on a cellular level.

The processing of $\alpha_2\delta$ is reviewed in Douglas et al. (2006), and shown in Figure 1.8. This involves production of a pro-form of the $\alpha_2\delta$ protein. The N-terminal signal

sequence is removed, and glycosylation and disulphide bind formation occur, followed by cleavage and expression. The site of cleavage has not been mapped to a specific site, but multiple mutations between Arg-941 and Val-946 in rat $\alpha_2\delta$-1 steadily reduce its effect on current amplitude without affecting its biophysical modulation of the resultant currents (Andrade et al., 2007).

Figure 1.8. Processing of the $\alpha_2\delta$ subunit, including cleavage and disulphide formation steps to produce the "mature" form of the protein. Taken from Douglas et al. (2006).

A total of four $\alpha_2\delta$ genes have now been described (*CACNA2D1-4*), which encode the $\alpha_2\delta$-1-4 subunits (Klugbauer et al., 1999; Qin et al., 2002). All $\alpha_2\delta$ subunits show several structural similarities including: hydrophobicity profiles; conserved glycosylation sites and cysteine residues involved in disulphide bond formation (Arikkath and Campbell, 2003). The $\alpha_2\delta$-2, $\alpha_2\delta$-3 and $\alpha_2\delta$-4 subunits show 56%, 30% and 30% homology to $\alpha_2\delta$-1 respectively. Differences in structure arise in structures such as the VWA domain (see Section 1.8.6). $\alpha_2\delta$-1 is located primarily in skeletal muscle, but also expresses in the brain and heart (Arikkath and Campbell, 2003). Expression in the brain is most pronounced in the cerebral cortex, hippocampus, cerebellum and olfactory bulb (Klugbauer et al., 1999). The $\alpha_2\delta$-2 subunit shows a more diverse localization- including the brain, heart, pancreas and liver (Hobom et al., 2000). Within the brain, $\alpha_2\delta$-2 is localized strongly in the cerebellum, in particular Purkinje cells (Barclay et al., 2001). $\alpha_2\delta$-3 is present in the heart and skeletal muscle, as well as showing strong expression in the hippocampus, cortex and caudate putamen (Klugbauer

et al., 1999). $\alpha_2\delta$-4 is not found in the brain, but found in heart, skeletal muscle and endocrine tissues such as the adrenal glands and pituitary (Qin et al., 2002).

1.8.2 Effect of $\alpha_2\delta$ co-expression on VGCC electrophysiology

The most apparent feature of $\alpha_2\delta$ co-expression is a significant enhancement of macroscopic current size when expressed with numerous $Ca_v\alpha_1$ subunits (Mori et al., 1991; Singer et al., 1991; Gurnett et al., 1996; Walker and De Waard, 1998; Catterall, 2000; Bangalore et al., 1996). Radioligand binding studies suggested this increase in current amplitude to be linked to an increase in $Ca_v\alpha_1$ subunit cell-surface expression (Shistik et al., 1995), as have studies examining the extra gating charge when $\alpha_2\delta$ is co-expressed (Bangalore et al., 1996; Jones et al., 1998). Enhancement of current amplitude was not found when the δ subunit was expressed alone (Felix et al., 1997; Gurnett et al., 1997), suggesting the importance of the α_2 subunit in this function. It has since been found that $\alpha_2\delta$ makes an intracellular interaction with the $Ca_v\alpha_1$ subunit by means of a von Willebrand Factor-A (VWA) domain (see Section 1.8.6.1) which leads to an enhancement of $Ca_v\alpha_1$ trafficking and subsequent cell-surface expression (Canti et al., 2005), although this has only been demonstrated for $\alpha_2\delta$-1 and $\alpha_2\delta$-2 so far.

It is clear that the β subunit is also important (perhaps more so than $\alpha_2\delta$) in mediating an increase in $Ca_v\alpha_1$ cell-surface expression, and the presence of the β subunit is often required for the effects of $\alpha_2\delta$ to be manifested (De Waard and Campbell, 1995; Arikkath and Campbell, 2003). In addition to enhancing trafficking of the VGCC channel complex, $\alpha_2\delta$ appears to play a role in maintaining the expressed channels at the cell-surface for longer, by delaying their internalization and subsequent degradation (Bernstein and Jones, 2007).

The $\alpha_2\delta$ subunit elicits changes in the biophysical properties of channels with which they associate. These properties include channel activation and inactivation rates, as well

as the voltage-dependence of current activation and maximal whole-cell conductance (Welling et al., 1993; Singer et al., 1991; Bangalore et al., 1996; Shirokov et al., 1998; Felix et al., 1997; Qin et al., 1998). These biophysical effects appear to be mediated by the δ subunit. Co-expression of the δ subunit (of $\alpha_2\delta$-1) alone caused an equivalent acceleration of inactivation as intact $\alpha_2\delta$ (Felix et al., 1997). The same study found co-expression of the δ subunit alone also caused a hyperpolarisation of steady-state inactivation. Therefore, the association of the δ subunit with the $Ca_v\alpha_1$ subunit is sufficient to influence voltage-dependent inactivation.

Unlike the gamma subunit, where interactions with the VGCC complex are often not to be found, $\alpha_2\delta$ associates and makes a functional interaction with all members of the $Ca_v1.x$ and $Ca_v2.x$ families. However, their association with $Ca_v3.x$ channels is not clear (see Section 1.4.3).

1.8.3 The $\alpha_2\delta$ subunit and disease

1.8.3.1 Epilepsy

A number of mutations in the $\alpha_2\delta$-2 subunit give rise to epileptic phenotypes (Barclay et al., 2001; Brill et al., 2004; Ivanov et al., 2004). Mutation of the mouse $\alpha_2\delta$-2 gene (*Cacna2d2*), by a duplication and inversion within exon 3, results in a loss of full-length $\alpha_2\delta$ protein and production of a truncated form of the protein (Barclay et al., 2001). The mutant mouse strain was termed "ducky" (*du*) due to their wide-based gait. *du/du* mice also displayed ataxia and absence epilepsy, as well as an inability to survive beyond 35 days. Another mutation (du^{2J}), caused by a deletion in exon 9, also results in loss of full-length $\alpha_2\delta$-2 (Barclay et al., 2001). Both *du/du* and du^{2J}/du^{2J} mice display reductions in the size of the dendritic arbor of their Purkinje cells, and the amplitude of calcium currents recorded from them.

Another mutation in the *Cacna2d2* gene produces the *entla* phenotype (Brill et al., 2004). The *Cacna2d2*^{entla} allele contains a duplication (in exon 3), which results in the production of a membrane-expressed $\alpha_2\delta$-2 protein which is cleaved, but not subsequently disulphide linked. This produced a phenotype of absence epilepsy and dyskinesia, as well as reduced calcium current amplitude from Purkinje cells.

1.8.3.2 Neuropathic pain

The role of $\alpha_2\delta$ in enhancing Ca^{2+} influx has been implicated as a factor in the establishment of neuropathic pain. Neuropathic pain refers to a collection of conditions including allodynia (in which non-noxious stimuli cause pain) and hyperalgesia (exaggerated pain response to mild noxious stimulus). Traditional analgesics (opiates and non-steroidal anti-inflammatory drugs) are less effective in these conditions, and other drugs such as anti-epileptic drugs (carbamazepine (a sodium channel blocker) and gabapentin (GBP)) have proven more useful (reviewed in Backonja, 2000). Although carbamazepine and GBP act upon different channels, their clinical efficacy may be due to control of neuronal over-excitability. GBP binds $\alpha_2\delta$-1 and $\alpha_2\delta$-2 subunits, and is discussed in more detail below.

Recent studies have implicated $\alpha_2\delta$-1 upregulation in central sensitisation, a mechanism involving alterations in neuronal excitability as a result of changes in channel expression, which is a cause of neuropathic pain. $\alpha_2\delta$-1 is upregulated in dorsal horn (Xiao et al., 2007) and DRGs of nerve-injured rats (Luo et al., 2001), which corresponds to onset of allodynia. This up-regulation of $\alpha_2\delta$-1 diminishes in rats recovering from allodynia, and corresponds to sensitivity to the anti-allodynic effects of GBP (Luo et al., 2002).

1.8.3.3 Tumour suppression

The human $\alpha_2\delta$-2 gene (*CACNA2D2*) is located in a tumour suppressor gene region in chromosome 3p21.3 (Gao et al., 2000). This allele is frequently deleted or mutated in many lung and breast cancers (among others), suggesting a possible additional function of $\alpha_2\delta$-2.

1.8.3.4 Role in photoreceptors

The $\alpha_2\delta$-4 subunit has a physiological role in photoreceptors, as determined by spontaneously arising $\alpha_2\delta$-4 mutant mice (Wycisk et al., 2006a). The mutation causes the expression of a truncated $\alpha_2\delta$-4 protein, and results in rod-cone photoreceptor dysfunction. This mutation correlates with one found in exon 25 of the human *CACNA2D4* gene, which underlies autosomal recessive cone dystrophy, leading to night blindness (Wycisk et al., 2006b).

1.8.4 Localisation of $\alpha_2\delta$ to cholesterol-rich microdomains

Cholesterol-rich microdomains (or lipid rafts) are cholesterol-containing regions of plasma membrane, thought to represent regions of order within the comparatively disordered plasma membrane (Brown, 2006). They were isolated as detergent-resistant membranes (DRMs) across a sucrose gradient (Brown and Rose, 1992), although these may not correspond directly to the lipid rafts that are thought to exist in native cells, due to the cold temperatures required for their purification (Brown, 2006). Along with purification of DRMs, disruption of lipid rafts (using agents such as methyl-β-cyclodextrin (MBCD), filipin or nystatin) has been used to demonstrate the importance of lipid rafts in a number of cellular functions.

Lipid rafts consist of certain lipids (such as sterols and sphingolipids) that spontaneously form crystalline structures within the otherwise disordered membrane structure. A number of trans-membrane proteins are thought to associate with lipid rafts, and their association may represent either a form of membrane specialization or a targeting

mechanism. The $\alpha_2\delta$ subunit, along with the $Ca_v2.1$ and $Ca_v2.2$ subunits have been shown to be such proteins (Toselli et al., 2005). These associations are discussed further in Chapter 4.

1.8.5 Gabapentin binding to the $\alpha_2\delta$ subunit

GBP has been demonstrated to be clinically useful in a number of conditions. It shows efficacy in a number of epilespy models, such as maximal electroshock; DBA/2 audiogenic seizure and genetic absence (reviewed in Taylor et al., 2007). Its original role as an anti-epileptic agent has been expanded to include a number of other conditions (Bialer et al., 2007). There is evidence for anti-nociceptive effects in neuropathic pain, and efficacy in generalized anxiety disorder, as well as other conditions such as SCA6, migraine headaches and bipolar disorder (Maneuf et al., 2003).

The effective doses of GBP used to treat epileptic conditions have been high compared to other drugs. Doses range from 300 mg to 900 mg, with an approved maximum of 3600 mg per day (reviewed in Wang and Ketter, 2002). The average daily dose of GBP is 1500 mg / day, 1424 mg / day resulted in a plasma concentration of 8.54 μg / ml (reviewed in Bialer et al., 2007). GBP is not metabolized by humans, and its maximal bioavailability before saturation is in the region of 65-70% (Stewart et al., 1993). However, subsequent studies have questioned the saturation of GBP absorption (attributed to saturation of System-L amino acid transport) in dose escalation studies (reviewed in Bialer et al., 2007). In recent years, the focus of GBP treatment has shifted from epilepsy to neuropathic pain, (Bialer et al., 2007).

GBP was initially synthesized in 1977 in an attempt to produce an analogue of gamma-aminobutyric acid (GABA) with better CNS penetrating properties. However, whilst GBP acted to reduce evoked neurotransmitter release (Reimann, 1983; Schlicker et al., 1985), this was not altered by the presence of baclofen (a $GABA_B$ receptor antagonist)

or high concentrations of GABA, suggesting GBP did not act through GABA receptors (Martin et al., 2002).

The identification of calcium channel $\alpha_2\delta$ subunit as the binding site for GBP (Gee et al., 1996) led to the proposal that modulation of calcium currents through voltage-gated calcium channels was the mechanism of effect of the drug. However, a direct inhibitory effect of GBP upon calcium channels has proven hard to demonstrate. Several studies have concluded a direct inhibitory effect of acute application of GBP on calcium channel currents. An inhibition of up to 34% was observed when 10 mM GBP was applied to pyramidal neocortical cells (Stefani et al., 1998), along with smaller inhibitions seen in other cells types. Incubation of DRG neurons with 10 μM GBP for 60 min caused a reduction in HVA VGCC current amplitude, after application of a pre-pulse (Alden and Garcia, 2001). Similar results were observed in skeletal myotubes. A small inhibition of VGCC current amplitude in cultured DRG neurons and F-11 cell cultures was observed with 2.5 μM GBP application by Martin et al (2002), which correlated with the amount of $\alpha_2\delta$ protein present in cells.

Other studies have provided evidence against such an inhibitory effect: Brown and Randall (2005) found only a small reduction (~10%) in amplitude of EPSCs in hippocampal slices in the presence of 10 μM GBP; Rock et al (1993) failed to find any inhibitory effect of GBP (up to 100 μM) upon VGCC current amplitude in a variety of cultured neurons; as was the case with 10 μM application to cultured Purkinje cells (Davies et al., 2006).

Rather than a direct inhibition of VGCC currents, some studies have observed reductions in either the amplitude of frequency of excitatory postsynaptic potentials (EPSCs) in the presence of GBP, and concluded that a reduction of neurotransmitter release comes as a result of GBP-mediated VGCC inhibition. K^+-evoked release of noradrenaline from rat neocortical slices was reduced by both GBP and pregabalin (PGB) in the low micromolar range (Dooley et al., 2000a). Glutamate release from rat neocortical or hippocampal slice preparations was reduced (by 10 - 25%) in the presence of 100 mM

GBP (Dooley et al., 2000b). Cunningham et al (2004) looked at evoked and spontaneous release of glutamate from layer V neurons of rat entorhinal cortex, and found a reduction in evoked EPSC amplitude, as well as a reduction in spontaneous EPSC frequency in the presence of 20 μM GBP. In addition, release of capsaicin-evoked release of sensory neuropeptides in spinal cord sensory neurons is reduced by 10 μM GBP (Fehrenbacher et al., 2003).

A number of factors have been suggested to be important in GBP-mediated action at VGCCs, and that may explain the discrepancies in results. The culture conditions for DRG neurons (in particular the type of nerve growth factor used) proved important in the GBP-mediated inhibition of VGCC currents (Cunningham et al., 2004), this may be explained by a difference in the VGCC abundance in these cells. Also, long-term incubation of GBP has been found to be vital for the reported GBP-mediated inhibition in several studies (Alden and Garcia, 2001; Fox et al., 2003).

Gabapentin represents the first of an emergent class of compounds to bind to the $\alpha_2\delta$ subunit (Belliotti et al., 2005). Both the α_2 and the δ parts of the protein are required for GBP binding (Brown and Gee, 1998). The concept of $\alpha_2\delta$ ligands has come to light with the finding that many amino acids and related compounds will bind $\alpha_2\delta$, and some of these have proven to be efficacious in neuropathic pain treatment, such as (L)-phenylglycine (Lynch, III et al., 2006). However, other $\alpha_2\delta$ binding compounds fail to have such an effect (Lynch, III et al., 2006), suggesting $\alpha_2\delta$ binding is not a simple route to therapeutic effect.

The importance of interruption of $\alpha_2\delta$ function was at first not apparent. However, recent studies have implicated $\alpha_2\delta$-1 upregulation in central sensitization, a condition where nociceptive neurons are more susceptible to firing following peripheral tissue damage. $\alpha_2\delta$-1 protein production is upregulated in dorsal horn (Xiao et al., 2007) and mRNA production in DRGs is also increased in nerve-injured rats (Luo et al., 2001), which corresponds to the onset of allodynia. This up-regulation of $\alpha_2\delta$-1 diminishes in

rats recovering from allodynia, and corresponds to sensitivity to the anti-allodynic effects of GBP (Luo et al., 2002).

The importance of $\alpha_2\delta$ up-regulation is another compounding factor that may explain the lack of GBP-mediated inhibition of calcium currents in some cases. Evidence has shown that $\alpha_2\delta$ ligands such as GBP act to block activity of $\alpha_2\delta$ in the sensitized state, but not the normal state (Li et al., 2006). Different culture conditions (such as time spent in culture for cells that have had axons / dendrites cut) may influence the regulation of $\alpha_2\delta$ in cultured cells, and the ability of GBP to inhibit its function.

1.8.6 Adhesion domains in the $\alpha_2\delta$ subunit

1.8.6.1 The VWA domain

The von-Willabrand Factor A (VWA) domain is found in a variety of proteins (such as integrins and extracellular matrix proteins) and is involved in making adhesion interactions (Whittaker and Hynes, 2002). The discovery of a VWA domain within the α_2 portion of the $\alpha_2\delta$ subunit (Bork and Rohde, 1991) suggested that $\alpha_2\delta$ might make functional adhesion interactions via this domain in a divalent cation-dependent process, much in the same way integrins and other VWA domain-containing proteins. The $\alpha_2\delta$-2 VWA is located in the α_2 portion of the subunit, and is therefore situated extracellularly when the subunit is expressed at the cell surface.

Figure 1.9. Structure of the $\alpha_2\delta$-2 VWA domain. The approximate location of the VWA domain within the α_2 structure is shown. In the enlarged view is the β sheet, as well as α helices containing the residues required for co-ordinating binding of a divalent cation with the MIDAS motif. A divalent cation is included (shown in purple). Model of VWA structure adapted from Canti et al. (2005).

The VWA domain does not consist of a completely conserved amino acid sequence across the range of proteins in which it is found (Bork and Rohde, 1991). It consists of a single β sheet, with amphipathic α helices at each face of the β sheet (reviewed in Springer, 2006). An important sequence within the VWA domain is the metal ion dependent adhesion site (MIDAS). This is a five amino acid sequence (DVSGS) which binds a divalent cation. The divalent cation (e.g. Mg^{2+}) coordinates to aspartate and threonine residues in "MIDAS loops", and with the MIDAS itself. The binding of a divalent cation to these sites triggers a conformational change in the VWA domain, which allows binding of a protein ligand. The protein ligand contributes a final co-ordinating amino acid (glutamate or aspartate) to bind the divalent cation with high affinity. A VWA domain model is shown in Figure 1.9.

1.8.6.2 Cache domains

The $\alpha_2\delta$ subunit contains two cache domains (Anantharaman and Aravind, 2000). These domains (derived from their occurrence in $\underline{Ca}^{2+}$ channels and chemotaxis receptors) are located adjacent to the VWA domain. The first cache domain is situated from amino acid 446 to 540 in human $\alpha_2\delta$-1 and the second from 764 to 869. Cache domains are involved in the binding and recognition of small-molecule ligands (Anantharaman and Aravind, 2000), although the exact ligand (if any) for the $\alpha_2\delta$ subunit has not yet been described. Multiple point mutations in the first cache domain (of porcine $\alpha_2\delta$-1) resulted in an abolition of GBP binding (Wang et al., 1999). However, mutation of a non-cache domain amino acid (residue 217 in porcine $\alpha_2\delta$-1) in the same study also abolished GBP binding, suggesting the cache domain is not the sole binding site involved.

1.8.7 Splice variants of $\alpha_2\delta$

$\alpha_2\delta$ subunit RNA is subject to alternative splicing. Three areas of alternative splicing have been identified in $\alpha_2\delta$-1: two consecutive upstream regions spanning 19 and five amino acids, and a downstream region spanning eight amino acids (Angelotti and Hofmann, 1996). These variants have been observed in murine and human $\alpha_2\delta$-1. The different splice variants are distributed across different tissues, suggesting physiological significance for localization of different splice variants. For example, skeletal muscle and brain tissue each express only one splice variant of $\alpha_2\delta$-1, whereas cardiovascular tissue expresses all five (Angelotti and Hofmann, 1996).

$\alpha_2\delta$-2 possesses two regions across the 39 exon subunit which show alternative splicing in the human and murine $\alpha_2\delta$-2 subunits described (Hobom et al., 2000; Barclay and Rees, 2000). The first of these is exon 13, which is only present in 13% of the total expressed $\alpha_2\delta$-2 protein (Barclay and Rees, 2000). In addition, a variation in the 3' acceptor region within intron 38 leads to the insertion of CP residues. This is the case for

25% of expressed $\alpha_2\delta$-2 protein (Barclay and Rees, 2000). These splice variants have been observed in human $\alpha_2\delta$-2 (Hobom et al., 2000) and do not correspond to changes in electrophysiology.

The $\alpha_2\delta$-4 subunit has also been found to display alternative splicing (Qin et al., 2002), leading to four potential variants. The protein is composed from 39 exons, and both the N- and C-termini display two variants.

1.9 VGCCs at the synapse

Ca^{2+} ions have long been implicated in mediating neurotransmitter (NT) release. NT release at the neuromuscular junction was calculated to be proportional to the fourth power of Ca^{2+} concentration (Dodge, Jr. and Rahamimoff, 1967). The influx of Ca^{2+} required for this enters the cell via presynaptic VGCCs, i.e. $Ca_v2.1$ and $Ca_v2.2$ channels (Dunlap et al., 1995). This transduction of presynaptic membrane depolarisation into Ca^{2+} influx drives the synaptic machinery, which couple Ca^{2+} to docking of vesicles to the presynaptic membrane, and release of the neurotransmitter they contain.

SNARE proteins make up the machinery required for neurotransmitter release. Several SNARE proteins make functional interactions with VGCCs, specifically $Ca_v2.1$ and $Ca_v2.2$ (Sheng et al., 1994; Catterall, 1999), although interactions with $Ca_v1.2$ have been observed (Wiser et al., 1999). These interactions are made via a site in the II-III linker on the VGCC (the "synprint" site, see Figure 1.7), to which syntaxin 1A, SNAP-25 and synaptotagmin bind (Rettig et al., 1996; Sheng et al., 1997) and have an inhibitory effect on VGCCs. This may represent a means of negative feedback to avoid excessive neurotransmitter release during periods of increased activity (Pozzi et al., 2007). Synprint peptides prevent the binding of these proteins (Sheng et al., 1994).

Syntaxin 1A is important for bringing the synaptic vesicle into contact with the plasma membrane (Jarvis and Zamponi, 2005). It also regulates the activity of the VGCCs to

which it binds. These interactions lead to a reduction in the level of VGCC expression, as well as hyperpolarizing the steady-state inactivation of the expressed channels (Catterall, 2000; Sutton et al., 1999). Syntaxin 1A also enhances the G protein-mediated inhibition of $Ca_v2.2$ (Jarvis et al., 2000).

SNAP-25 inhibits $Ca_v2.2$ (although not through an enhancement of G protein-mediated inhibition). In addition, it also inhibits the syntaxin 1A-mediated inhibition of $Ca_v2.2$ (Wiser et al., 1996a). This has led to the notion that incomplete SNARE complexes will inhibit Ca^{2+} influx, but complete (and functional) SNARE complexes will not (Jarvis and Zamponi, 2005).

A number of interactions with proteins at the synapse are also mediated by VGCCs, such as the association with synaptic adaptor proteins such as CASK and Mint1 (Maximov et al., 1999). Laminin β3 binds to VGCCs, preferentially $Ca_v2.1$ and $Ca_v2.2$ (Nishimune et al., 2004). Here, the association promotes clustering of VGCCs, which is proposed to be required for correct synaptic development. Another adhesion molecule family, the α-neurexins, couple VGCC-mediated Ca^{2+} influx at the synapse to neurotransmitter release (Missler et al., 2003). In addition, the RIM1 protein is required for making interactions with other components of the presynaptic active zone (Kiyonaka et al., 2007). One of these components is the VGCC β subunit (β4 and β2a were tested in the study), which binds RIM1 via the SH3 and GK domains. This association decelerates inactivation kinetics (and depolarises the voltage-dependence of inactivation) and leads to an overall increase in neurotransmitter release.

1.10 Aims of the study

At the beginning of the study, several key pieces of information regarding the $\alpha_2\delta$ subunit were unknown. The $\alpha_2\delta$ subunit had been found in most studies to enhance current amplitude in many expressed VGCC complexes (see Section 1.8.2). This had been proposed to be due to an increase in the number of available channels at the cell-

surface, whether by an increase in forward trafficking (Shistik et al., 1995) or a reduction in channel turnover when at the membrane. The presence of a number of potential binding domains within the $\alpha_2\delta$ subunits (see Section 1.8.6) alluded to the possibility that $\alpha_2\delta$ functionality involved binding ligands. The presence of a VWA domain within the α_2 portion of the subunit suggested that α_2 may play an additional role in the function of the subunit, given that the δ portion is responsible for many of the biophysical effects of $\alpha_2\delta$ co-expression (Felix et al., 1997).

Therefore, two sites implicated in potential ligand interactions (the VWA domain, found on integrins) and the RRR motif essential for GBP binding were investigated in this study. Interruption of these sites by mutating amino acids within them would allow their physiological function to be assessed, and allow the importance of any ligand binding to be established. In the case of the VWA domain, the identification and location of binding of a potential ligand could be established. In the case of the RRR motif, where the exogenous ligand is known to be GBP / PGB, the possibility of an endogonous ligand could be investigated.

Chapter 2: Materials and Methods

2.1.1 Suppliers

All chemicals were supplied by Sigma Aldrich Chemicals Ltd. (UK) unless stated otherwise. All water used was obtained from a water purification system (Millipore), unless stated otherwise.

2.1.2 cDNAs and expression vectors.

Most of the complementary deoxyribonucleic acids (cDNAs) used in this investigation were subcloned into the pMT-2 mammalian expression vector. pMT-2 is a plasmid expression vector displaying a relatively high level of expression of heterologous proteins, which have proven to be both functional and stable over the course of a transient transfection (Swick et al., 1992). pMT-2 contains the simian virus 40 (SV40) promoter.

Mouse $\alpha_2\delta$-2 (Genbank accession number AF247139) was used (Barclay and Rees, 2000), from which a number of constructs were produced. Mouse brain $\alpha_2\delta$-2 RNA displays alternative splicing in exons 23 and 38 (Barclay and Rees, 2000). The mouse $\alpha_2\delta$-2 was the common splice variant form, which lacked exon 23 and 6 base pairs of exon 38 (see Section 1.8.7). This $\alpha_2\delta$-2 was used to produce both the stable $\alpha_2\delta$-2 mid-HA and $\alpha_2\delta$-2 R282A constructs (Davies et al., 2006). An internal hemagglutinin (HA) tag was inserted between amino acids 652 and 653 to produce the mid-HA construct, and the R282A construct was produced by site-directed mutagenesis. A similar mutation (R217A) was introduced into rat brain $\alpha_2\delta$-1 (M86621) in the lab. All $\alpha_2\delta$-2 constructs were subcloned into pMT-2.

Additional cDNAs used that were subcloned into pMT-2 included: rabbit $Ca_v2.2$ (D14157, lacking the 3'-untranslated region); rat β1b (Tomlinson et al., 1993); rat β4 (LO2315) and rat $Ca_v2.1$ E1686R (M64373). The E1686R mutation in rat $Ca_v2.1$ is the equivalent mutation as that used in human $Ca_v2.1$ E1740R (Hans et al., 1999), an

engineered gain-of-function mutation in the S5-SS1 extracellular loop (in Domain IV). This mutation results in an elevation in expressed $Ca_v2.1$ protein and a corresponding three-fold increase in current amplitude, as well as a hyperpolarised $V_{50,\ inact}$ (see Introduction). No significant changes in activation or inactivation kinetics were observed compared to WT $Ca_v2.1$.

Mut-3 green fluorescent protein (GFP; M2653) was used as a reporter gene for successful heterologous protein expression, due to the green fluorescence observed when exposed to ultraviolet light. Mut-3 GFP contains mutated amino acids in the chromophore sequence, resulting in a greatly enhanced fluorescence intensity compared to GFP (Cormack et al., 1996).

Two cDNAs used in the study (porcine brain $\alpha_2\delta$-1 (WT) and $\alpha_2\delta$-1 R217A, both gifts from Pfizer) were subcloned into the mammalian expression vector pcDNA3 (Invitrogen). α_2 and δ were subcloned into pcDNA separately from full-length porcine brain $\alpha_2\delta$ cDNA (Wang et al., 1999). The porcine and rat brain splice variants used are 96% homologous to one-another, and are identical in the three regions of alternative splicing for $\alpha_2\delta$-1 (Angelotti and Hofmann, 1996; Wang et al., 1999).

2.1.3 Antibodies

A list of the primary and secondary antibodies used is provided in Table 2.1.

Name	Antigen	Species	Supplier	Dilution
Anti-HA	HA peptide sequence (YPYDVPDYA)	Rat	Roche	1:1000
Anti-α_2-1	Residues 27 – 41 of rat α_2	Rabbit	Alomone	1:500
Anti-$\alpha_2\delta$-1 (chicken)	Unknown (generated in-house @ Pfizer)	Chicken	Pfizer	1:500
Anti-$Ca_v2.2$	Peptides in the II – III loop	Rabbit	Generated in lab	1:500
Anti-Flotillin	Whole molecule	Mouse	BD Biosciences	1:1000
Anti-Rabbit IgG	Whole molecule	Goat	Sigma	1:1000
Anti-Rat IgG	Whole molecule	Mouse	Abcam	1:1000
Anti-Chicken IgG	Whole molecule	Rabbit	Sigma	1:500

Table 2.1 Antibodies used in the study.

2.2 Cell Culture

All cell-cultures were maintained at 37°C in an atmosphere containing 5% CO_2. All culture solutions were filter-sterilised before used.

2.2.1 tsA-201 cells

The temperature-sensitive A (tsA-201) cell-line (European Collection of Cell-Cultures number 96121229) is a modified form of the HEK293 (human embryonic kidney) cell-line, stably expressing a simian virus 40 (SV40) temperature-sensitive T antigen. This allows a higher expression of recombinant proteins from plasmids containing the SV40 promoter.

tsA-201 cells were maintained as adherent monolayers, cultured in Dulbeco's modified Eagle's medium (D-MEM; GIBCO) plus: 10% (v/v) Foetal bovine serum (FBS; GIBCO), 1% (v/v) Penicillin-Streptomycin (5 Kunits/ml penicillin and 5 mg/ml streptomycin stock), and 2 mM glutamine. Cells were maintained in either flasks (175 cm^2 or 75 cm^2) or dishes (35 mm diameter). The cells were passaged twice weekly when they reached a confluency of approx. 80-90%, and split to a confluency of approximately 20%.

Passaging of cells proceeded as follows. The density of the cell monolayer was estimated using a light microscope. The D-MEM culture medium was then removed from the adherent cells by means of 2 gentle washes with warm phosphate-buffered saline (PBS). Having removed the PBS, cells were then washed in either 1 ml (for a 75 cm^2 flask) or 3 ml (for a 175 cm^2 flask) trypsin (500 units/ml). The flask was moved and swirled gently, to allow trypsin to cover all cells in the flask and to gently encourage the lifting-off of cells. After one minute of trypsin application, a volume of the D-MEM was added (~10 ml, depending on the estimated density of the monolayer). Gentle trituration of the cell-trypsin-medium mixture then followed, and 1 ml volumes of this mixture then used to seed cells in a fresh flask.

Seeding of 35 mm (~10 cm^2) dishes with tsA-201 cells for transfection was often carried out concurrently with passaging, and achieved by further diluting the mixture as was deemed necessary to allow them to grow up to a confluency of 100% after 2 days. At this point, they were re-plated for use in electrophysiological recording (see Section 2.7).

Cell cultures were maintained for approximately eight weeks before being discarded. They were replaced with a newly grown up culture (from frozen stocks). The majority of tsA-201 cell-culture work was carried out routinely by a tissue-culture technician.

2.2.2 DRG cell-culture

All DRG cell culture was carried out by a colleague in the lab (Fay Heblich). Adult Sprague-Dawley rats (21 days) were used, within a weight range of 300-400 grams.

2.2.3 GC cell-culture

Initial steps in this protocol were carried out using dissection medium (DM). DM consisted of: Hanks balanced salt-solution (HBSS; GIBCO) and gentamycin (100 μg/ml; Sigma-Aldrich). Seeding of GCs onto poly-lysine-coated coverslips was carried out in seeding medium (SM). This consisted of: Basal medium Eagle (BME; GIBCO) and foetal calf serum (10% v/v; GIBCO). GC medium was used for maintainng GC cultures. A 50 ml stock solution of GC medium consisted of: BME (42 ml); glucose (2.4 ml of a 10% (w/v) solution); penecillin-streptomycin (100 μl of a 5 Kunits/ml penicillin and 5 mg/ml streptomycin stock); glutamine (1 mM); NaCl (20 μM); growth cocktail (500 μl; Sigma-Aldrich); KCl (20 μM); horse serum (5 ml; GIBCO).

Four rats (aged postnatal day 1 (P1)) were killed by decapitation. Cerebella were removed with forceps and placed in a dish on ice, containing DM. Meninges and blood vessels were removed using forceps and a dissection microscope. Cerebella were transferred to warm DM and inverted gently to remove small pieces of tissue, then centrifuged (1000 RPM) for 2 min. The DM was replaced with fresh warm DM (10 ml) and inverted again. This was removed, and replaced with 2 ml 0.1% (w/v) Trypsin (GIBCO). Cells were left to trypsinize in a shaking waterbath for 10 min. Following this,

two DM wash / two minute 1000 RPM centrifugation cycles were carried out, and then cells were removed to a 1 ml volume of D-MEM containing 2000 units / ml deoxyribonuclease I (DNAse). DNAse cuts DNA released by cells lysed in the dissection procedure, and thus helps prevent clumping. Cells were triturated in this volume, first using a large-bore pipette, followed by a small-bore pipette and finally with a 200 µl Gilson pipette. This ensured that the cells were reduced to a single-cell suspension. Following this, 9 ml DM was added, and cells were inverted. Cells were centrifuged for five min (1500 RPM), and all medium / DNAse was removed. Cells were then re-suspended in 1 ml SM. A 100 µl sample of this suspension was taken, and an estimate of the cell density made using a haemocytometer. Having done this, the volume of SM added to the cells was increased to attain a cell density of roughly 10^6 cells / ml.

90 µl of cells in SM were pipetted onto each poly-lysine-coated coverslip. These coverslips were kept in 35 mm dishes in an incubator (37°C) for 3 h, to allow the cells to adhere to the coverslips. After 3 h, 2 ml GC medium was added to each dish, and cells left until required. Cells were fed by replacing the GC medium every two days. Figure 2.1 shows CG cultures after two (Figure 2.1 A) and seven (Figure 2.1 B) days.

2.2.4 GC / tsA-201 cell co-cultures

Co-cultures made use of already-established GC and tsA-201 cell-cultures. tsA-201 cells were transfected (see Section 2.3) and left for 3 h. The following evening, cells were replated. tsA-201 cells were washed in warm PBS and then resuspended in cell dissociation solution (CDS). The cell / CDS mixture was added straight to 35 mm dishes containing coverslips of GCs. tsA-201 cells were plated at a lower density than would be the case for tsA-201 cells alone, as they were left in culture with GCs overnight before being used in the morning. An example GC / tsA-201 cell co-culture is shown in Figure 2.1 C.

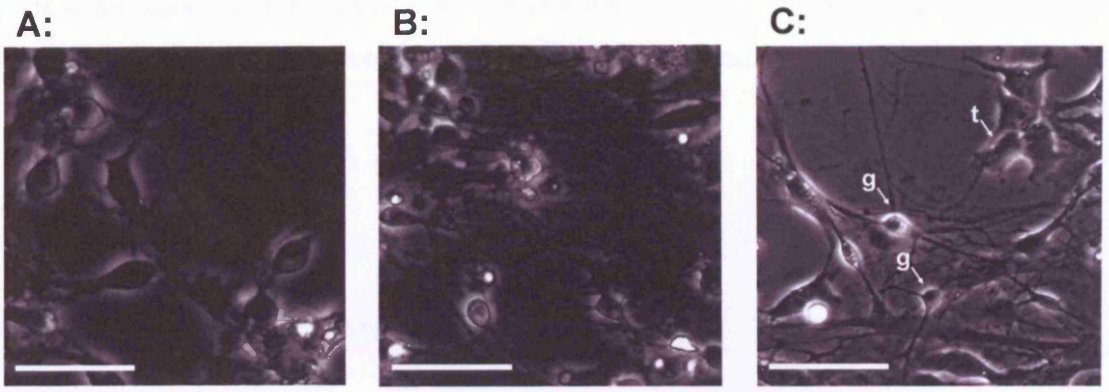

Figure 2.1. GC and GC / tsA-201 cell co-cultures. (**A**), GCs, two days in culture. (**B**), GCs, seven days in culture. The neurite network is significantly more established than that of the two day old culture. (**C**), GC / tsA-201 cell co-culture. Photo is taken of a seven day GC culture, 14 h after the addition of tsA-201 cells. (t = tsA-201 cell; g = GC). GCs were identified by size and morphology, and were phase-bright compared to tsA-201 cells. Scale = 50 μm.

2.3 Transfection of cells

For transfection of tsA-201 cells in 25 mm dishes, a cDNA mix (containing all cDNAs necessary for a particular experiment) was prepared in advance. This allowed a more reproducible and uniform method of heterologous transfection than transfecting individual subunit cDNAs. The mix contained VGCC subunit cDNAs for $Ca_v\alpha_1$, β, α2δ and mut-3 GFP in a 3:2:2:0.2 ratio.

tsA-201 cells were transfected using the Fugene 6 reagent (Roche). The transfection procedure involved mixing 3% Fugene 6 (in serum-free medium) with cDNA (1 μg/μl) in a 3:2 ratio (Fugene 6 : cDNA). The quantities used depended on the flask being transfected (ratios shown are Fugene 6 : cDNA in μl): 45:30 (in 5 ml serum-free medium) for a 175 cm^2 flask; 30:20 (in 2 ml serum-free medium) for a 75 cm^2 flask, and 3:2 (in 100 μl serum-free medium) for a 35 mm dish. Transfection involved diluting the Fugene 6 reagent in serum-free medium, before mixing with cDNA. After being left for

15 min, the mixture was added to cells. A confluency of 20 – 30% was selected for cells at the point of transfection in order to allow 2 days for protein expression.

2.4 Treatments

2.4.1 Cholesterol depletion

A stock of methyl-β-cyclodextrin (MBCD) was produced on a daily basis. MBCD does not have an exact molecular mass, due to variable methylation, and hence it was assumed to be 1300. 50 mM MBCD (in serum-free medium) was sterile-filtered to remove small clumps of un-dissolved material, and kept for no longer than 10 h. The treatment of cells on 35 mm dishes with MBCD caused them to lift of the bottom of the dishes. For this reason, cells to be treated with MBCD (and as well as the control condition) were re-plated onto collagen-coated dishes. Re-plated cells were exposed to 5 mM MBCD for 1 h at 37°C, immediately before electropysiological experiments (as in Christian et al., 1997). Control cells were treated with serum-free medium for the same length of time.

2.4.2 Cholesterol addition

Cells were cultured in the same way for experiments involving cholesterol addition as for those involving cholesterol depletion. 10 mM cholesterol was dissolved in serum-free medium and left overnight at 4°C on a rotator in order to facilitate its entry into solution. 50 mM MBCD was then added to complete the stock solution, as above. Exposure to a final concentration of 5 mM MBCD / 1 mM cholesterol was then carried out at 37°C for 1 h before recording.

2.4.3 Application of GBP / PGB

GBP (Sigma-Aldrich or VWR) and PGB (a gift from Pfizer) were applied to cells chronically, from shortly after the point of transfection, up to the point of re-plating (a total of 40 h).

GBP / PGB were obtained as powder. This powder was dissolved in water to make a 100 mM stock solution. The stock solution was kept at 4°C. GBP / PGB were applied to cells 1 h after adding the (Fugene 6 / cDNA) transfection mixture, to prevent any interruption of transfection. GBP was added to the culture medium to obtain a final concentration of either 100 μM or 1 mM in the 2 ml culture medium. PGB was applied to make a final concentration of either 200 μM or 1 mM in the culture medium. In all cases the equivalent volume of water was added to the control condition. This application would last roughly 40 h, until the point at which cells were re-plated for electrophysiology (Section 2.7). GBP / PGB application was effectively stopped at this point, as GBP / PGB were omitted from the media used for re-plating.

2.5 Biochemistry

All steps were carried out at 4°C unless stated otherwise. PBS solutions were made up from tablets left to dissolve in water. Protease inhibitor (Roche) was added to PBS solution in tablet form. This produced a PBS / protease inhibitor (PI) solution used in most experiments.

2.5.1 Sample preparation

2.5.1.1 Cell harvesting and preparation of whole-cell lysate

tsA-201 cells were harvested from either 75 cm^2 or 175 cm^2 flasks, both using the same method. First, cells were washed twice in ice-cold PBS, before being left in an ice-cold PBS solution containing 5 mM ethylenediamine tetraacetic acid (EDTA) for five min. After this, cells could be gently washed off the bottom of the flask. Cells were then pelleted at 3000 x g for 5 min, the supernatant removed, and stored at -20°C until required.

Whole-cell lysate was prepared for Western blotting experiments (Section 2.5.3). Harvested cell-pellets were left to thaw on ice, and made up to 200 µl volumes with PBS / PI. Samples then underwent three rounds of low-intensity sonication, each round lasting 5 seconds. 50 µl Igepal (5% v/v) was added before the last round of sonication. Samples were left to solubilise for 30 min on ice, and then spun at 1300 RPM in a bench-top centrifuge for 15 min to pellet non-lysed cells. After this, a sample of the supernatant was removed for a protein assay (see Section 2.5.2).

2.5.1.2 Preparation of membrane samples

In order to harvest sufficient material for ^{3}H-GBP binding to membranes, six 175 cm^2 flasks containing transfected tsA-201 cells were grown up. The resultant pellet (after cell-harvesting) was re-suspended in a final volume of 25 ml PBS / PI containing 10 mM HEPES.

Cells were sonicated for three rounds of 15 seconds each (and left on ice for a minute between each round), before being left to solubilise on ice for a further 30 min. Cell debris and non-lysed cells were pelleted using a Beckman desktop centrifuge for 15 min at 1000 x g. The resulting supernatant was removed to a 30 ml thick-walled

ultracentrifuge tube (Beckman-Coulter). Membranes were pelleted in an ultracentrifuge (Beckman-Coulter) for 1 h at 100,000 x g.

After ultracentrifugation, the supernatant was removed by aspiration. Samples were re-suspended in a 4 ml of the PBS / PI / HEPES buffer, and two 20 µl samples taken for protein assay. Having completed the protein assay, a volume of buffer equating to 50 mg sample was aliquoted into storage tubes for subsequent use in binding assays (50 mg being the required amount of sample for a single binding assay).

2.5.1.3 Preparation of lipid raft samples

As with membrane samples, six 175 cm^2 of tsA-201 cells were required for binding assays involving lipid rafts. After harvesting (and storage at -20°C in some cases) pellets were kept on ice (and thawed if they had not been harvested immediately beforehand).

A number of sucrose solutions and buffer solutions were prepared. See Appendix I for the composition of Buffers 1 and 2. Sucrose solutions (5%, 35% and 90% w/v) were prepared in 50 ml volumes. Whilst the 5% and 35% sucrose solutions dissolved easily in PBS, it was necessary to heat the 90% sucrose solution in a waterbath (~90°C) until it dissolved fully.

Cell pellets of each 175 cm^2 flask were re-suspended in 1 ml Buffer 1. 1 ml Buffer 2 was added, before incubating on ice for 40 min (to lyse and solubilise the sample). The volume was doubled again to 4 ml using the 90% sucrose solution. This 4 ml sucrose / cell mixture was then added to a 13 ml ultracentrifuge tube (Beckman), followed by the addition of 4 ml 35% sucrose and 5 ml 5% sucrose solutions. All additions were made using a 1 ml Gilson pipette, taking care not to allow sucrose solutions to touch the sides of the tube. For the 5% sucrose additions the narrow tip of the plastic pipette was cut off to reduce the speed at which solution was added to the tube and reduce the risk of 5% sucrose solution mixing with 35% sucrose solution. For one experiment (the western

blot of which is shown in Figure 4.1C), 5 ml 90 % sucrose, 4 ml 35% sucrose and 5 ml 5% sucrose were added to each ultracentrifuge tube, due to an excess of sample. The resultant six ultracentrifuge tubes were then paired, and the mass of each pair equaled by the addition of 5% sucrose solution. Samples were then centrifuged at 70,000 x g for 18 h.

After centrifugation, fractions were removed from each of the six tubes 1 ml at a time. Detergent-resistant membranes were observed at the boundary between the 5% and 35% sucrose solutions, these "peak-fractions" were usually fractions 4 & 5 or fractions 5 & 6. 100 µl of each 1 ml fraction were removed from one of the ultracentrifuge tubes in order to determine the presence of $\alpha_2\delta$ protein by western blot analysis. Sodium dodecyl sulphate polyacrylamide gel-electrophoresis (SDS-PAGE) and western blot analysis were performed as described in Section 2.5.3. However, a 15-well Tris-acetate gel (Invitrogen) was used instead of the 10-well gel described.

The peak-fractions of the six ultracentrifuge tubes were then pooled and a 20 µl sample taken for protein assay. From the result of the protein assay it was possible to make aliquots from the pooled lipid raft samples, each one containing 120 µg lipid rafts for use in a binding assay.

2.5.2 Assay of protein concentration

A modified Bradford assay (Bio-Rad protein assay; Bio-Rad) was used to assess protein concentration in biochemical experiments. These steps were performed at room temperature. The Bradford protein assay involves binding of Coomassie blue dye to (primarily basic and aromatic) amino-acids in order to provide quantification of protein. Bio-Rad reagent concentrate (Bio-Rad) was used for the protein assay, and consisted of dye, phosphoric acid and methanol. It was diluted with water to obtain the correct concentration. Protein concentrations of a known standard (bovine serum albumin) were measured initially in order to provide a conversion factor between the absorbance and

the protein concentration of the sample. Absorbance was measured using a DU800 spectrophotometer and associated software (Beckman-Coulter).

Assessment of protein concentration was carried out using small volumes of Bio-Rad reagent, mixed with a range of concentrations of the protein sample. At least three concentrations were selected, within the linear range of the assay (0.2 to 0.9 mg/ml). Duplicates of each protein concentration were prepared. Absorbance was measured at 595 nm, and the conversion factor applied in order to obtain a value of protein concentration. Assuming no significant outliers from the straight line, the mean value of protein concentration was taken from the various concentrations and duplicates.

2.5.3 Gel-running and western-blotting

2.5.3.1 SDS-PAGE

Before being subjected to electrophoresis, 4x loading sample buffer (Invitrogen) was added to solubilised cell samples (this produced a 1x final concentration of buffer). The composition of 4x loading sample buffer is given in Appendix II. Loading sample buffer also contained 200 μM DTT which was included in order to reduce disulphide-bonded protein structures. Solubilised cell samples then were denatured in a heating block (90°C) for 10 min. After the denaturing step, sample tubes were centrifuged using a bench-top centrifuge to reclaim any evaporated content stuck to the lid of the tubes.

SDS is an anionic detergent which denatures protein (although not disulphide bonds) and confers effectively a uniform negative charge to protein according to its mass. Therefore, the subsequent charge separation by PAGE equates to separation by size of the proteins. Separation by SDS-PAGE was carried out using NuPAGE 3-8% Tris-acetate gel kits (Invitrogen) in a NuPAGE electrophoresis chamber (Invitrogen). The outer chamber was filled with gel running buffer (see Table 2.2 for composition), and the central chamber was also filled with gel running buffer, plus thioglycolic acid

(0.01% v/v). The purpose of this was to prevent disulphide bond formation during the running of the gel. The inner chamber was filled to above the level of the wells, and the wells were then washed in the running buffer / thioglycolic acid solution using a P1000 Gilson pipette.

Gels were routinely loaded with 25 µl sample, which contained between 10 and 30 µg protein, depending on the antibody being used for detection. Full-range Rainbow molecular weight marker (Amersham) was used to provide a measure of protein size. Gels were run for approximately 1 h at 150 mV, 50 mA.

After electrophoresis, the gel was removed from its plastic case and immersed in gel equilibration buffer solution for 10 min (see Table 2.2). The SDS in the buffer solution inhibited protein binding to the gel, thus facilitating movement of protein during the electro-transfer step.

Buffer solution	Component reagent	Quantity
Gel running buffer (800 ml w/ water)	(20X) NuPAGE Tris-acetate running buffer or (20X) NuPAGE MOPS running buffer (see Appendix II)	40 ml
Gel equilibration buffer (50 ml w/ water)	(20X) NuPAGE transfer buffer	5 ml
	20% SDS (v/v)	80 µl
Gel transfer buffer (50 ml w/ water)	(20X) NuPAGE Transfer Buffer	10 ml
	Methanol	10 ml
	2% (v/v) Thioglycolic acid	100 µl
Blocking buffer (50 ml w/ water)	(10X) TBS	10 ml
	10 % (v/v) Tween 20	100 µl
	Bovine serum albumin	1.5 g
Antibody diluent (1 l w/ water)	TBS	100 ml
	Tween 20	500 µl
	Bovine serum albumin	30 g
	Goat serum	100 ml
	Ovalbumin chicken egg	5 g

Table 2.2. Composition of solutions used for SDS-PAGE and subsequent electro-transfer.

2.5.3.2 Electro-transfer

Protein transfer was carried out from the gel to a polyvinylidene difluoride (PVDF) membrane (Bio-Rad). The PVDF membrane binds protein as it is moved from the gel by the voltage difference. The PVDF membrane (with an area of 7.5 cm x 8.5 cm to approximate the dimensions of the gel) was soaked in methanol for 5 min, followed by water, followed by gel transfer buffer (see Table 2.2 for composition). Similarly, two sets of three blotting paper squares (each 7 cm x 5 cm; Whatman) were soaked in gel transfer buffer. The presence of methanol in the gel transfer buffer prevents SDS binding to the protein, thus removing SDS from the PVDF membrane.

Electro-transfer took place in a semi-dry electophoretic transfer cell (Bio-Rad). Transfer is possible by direct contact of the electrodes with the gel / membrane stack. The arrangement of the PVDF membrane, blotting paper and gel within the cell is shown in Figure 2.2. Layers of the stack were placed in succession, with a small volume of transfer buffer applied in between each layer. A tube was rolled across the top of the stack to remove any bubbles of air left between layers. The lid / cathode was secured and the protein transferred over a 30 - 35 min period at 10 V, 400 mA.

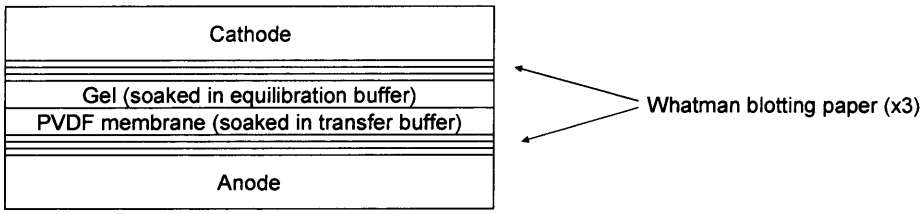

Figure 2.2. Arrangement of the electro-transfer apparatus. Transfer buffer was applied to all layers, and air bubbles removed to allow optimal electrical contact between the electrodes and through the stack.

2.5.3.3 Antibody step

After electro-transfer, PVDF membranes were subjected to a blocking step in blocking buffer (see Appendix III for composition) for 1 h. This step took place at room temperature on a rotator. After this, blocking solution was removed, and replaced with a small volume (3 ml) of antibody diluent (see Table 2.2 for composition) containing the appropriate dilution of antibody (see Section 2.1.3 for a complete list of antibodies used). The PVDF membrane was left submerged in antibody / antibody diluent overnight at 4°C.

Following overnight exposure to primary antibody, three washes in a 1 M Tris-buffered saline (TBS) solution were carried out, each wash lasting 10 min. The purpose of this was to remove any primary antibody not bound to the target protein on the PVDF membrane and therefore reduce non-specific binding. The three TBS washes were followed by exposure to secondary antibody (see Section 2.1.3 for a complete list), an antibody specific to the species of the primary antibody (IgG). This secondary antibody was conjugated to the horseradish-peroxidase (HRP) enzyme in order to allow visualisation in the following imaging step.

2.5.3.4 Imaging

Imaging of the labelled protein on the PVDF membrane was carried out using the ECL-plus Western Blotting detection system (Amersham). Enhanced chemiluminescence (ECL) arises in the ECL-plus system due to oxidation of a Lumigen PS-3 Acridan substrate, by the combined presence of HRP and peroxide.

Three washes (in TBS) of the PVDF membrane were carried out, to remove any non-bound secondary antibody. The PVDF membrane was then immersed in ~2 ml detection mixture for at least five min. Detection solutions A and B (from the ECL-plus kit) were

mixed at a ratio of 40:1 to produce the detection mixture. Imaging was the carried out using a Typhoon 9410 variable mode imager (Molecular Dynamics).

The majority of western blot analysis was carried out in order to demonstrate simply the presence of a particular protein. When quantitative comparison was required, the ImageQuant program (Amersham) was used. Areas of interest (i.e. boxes surrounding an imaged protein band) were selected. Corresponding areas containing no protein were subtracted in order to provide a correction for the background immunoreactivity. Immunoreactivity was then calculated as a function of intensity of the band, and normalised to the peak value of the WT condition. Values are presented as mean ± standard error of the mean (SEM).

2.5.4 Immunoprecipitation assay

Freshly harvested cell pellets were made up to 250 µl with lysis buffer. Lysis buffer contained (in PBS / PI): 50 mM tris-HCl; 100 mM NaCl; 1% Igepal. Samples were left on ice to solubilise for 60 min. Following this the lysate was sonicated for five seconds. Samples were then left to bind primary antibody (anti-HA) on an end-to-end mixer for 2 h.

Sepharose beads conjugated to IgG (Invitrogen) were used for precipitation of the HA immunoreactive protein. Following antibody binding, 30 µl Protein G-sepharose beads (50% slurry in lysis buffer) were added to the lysate / antibody samples and left to incubate for a further 60 min. The protein G-sepharose beads were then pelleted using a bench-top centrifuge (1000 x g for two min), before three further cycles of washing with 1 ml lysis buffer and centrifugation.

Bound protein was eluted with the addition of 40 µl loading sample buffer, followed by incubation for 20 min and subsequent centrifugation of the protein G-sepharose beads. Samples of the supernatant were taken for SDS-PAGE, and run on a 4 – 12% Bis-Tris

gel kit (Invitrogen). This step was essentially the same as the gel-running step described previously (Section 2.5.3.1), except that NuPage MOPS running buffer (Invitrogen; see Appendix II for composition) was used instead of Tris-acetate running buffer.

Solution	Component reagent	Quantity
Fixing solution (250 ml w/ water)	Ethanol	100 ml
	Acetic acid (glacial)	25 ml
Sensitizing solution (250 ml w/ water)	Ethanol	75 ml
	Glutardialdehyde (25% w/v)	1.25 ml
	Sodium thiosulphate (5% w/v)	10 ml
	Sodium acetate	17 g
Silver reaction solution (250 ml w/ water)	Silver nitrate (2% w/v)	25 ml
	Formaldehyde (37% w/v)	0.1 ml
Developing solution (250 ml w/ water)	Sodium carbonate	6.25 g
	Formaldehyde (37% w/v)	0.05 ml
Stopping solution (250 ml w/ water)	EDTA-Na_2-$2H_2O$	3.65 g
Preserving solution (250 ml w/ water)	Glycerol (87% w/v)	25 ml

Table 2.3. Component reagents of the solutions used in silver-staining of gels.

Silver staining was carried out to detect protein. Solutions used are described in Table 2.3. An initial fixation step was carried out by immersion in fixing solution for 30 min. This was followed by immersion in sensitizing solution for 30 min, to prime the gel for the following silver reaction. Three washes of the sensitized gel were carried out in water (each one lasting 5 min), before immersion in the silver reaction solution for 20 min. Two washes with water (each 1 min) were then carried out, followed by development of the silver-stained gel. Developing the gel involved immersion in developing solution, and over the course of a few minutes, bands (corresponding to the occurrence of protein in the gel) appeared. At a suitable point, this process was halted by exposure to stopping solution ceased. Silver-stained gels were then immersed in preserving solution (for 20 min), coated in plastic film, and imaged using a scanner.

2.6 Radioligand binding

2.6.1 Binding assay

^{3}H-GBP was stored at -80°C until use. All solutions and reagents were prepared and maintained on ice unless stated otherwise. Tubes were prepared containing: cell sample (3 μg cholesterol-rich microdomains or 50 μg membranes) in 10 mM HEPES buffer; various concentrations of ^{3}H-GBP (in 10 mM HEPES/KOH, pH 7.4); GBP (in water). Volumes were made up to 250 μl with 10 mM HEPES buffer (containing PI). Binding was carried out in a final volume of 250 μl at room temperature over the course of 2 h. Each replicate experiment was carried out in triplicate, and the mean value used for subsequent analysis. Total counts per minute were determined (also in triplicate) to give an estimate of the activity of the ^{3}H-GBP. Non-specific binding was determined using 10 μM unlabelled PGB.

Transferring the membrane samples or Triton X-insoluble membrane fractions to scintillant vials was carried out using a Brandel Harvester (Brandel). The GF/B filter

paper used to recover material was soaked in 0.3% polyetheleneimine briefly before harvesting in order to reduce non-specific binding to the filter paper. Samples were transferred by Tris-HCl (10 mM, pH 7.4) washes of the tubes, and then GF/B cut-outs were removed to vials containing 5 ml scintillant.

Detection for chemiluminescence arising from ^{3}H decay was carried out on a scintillantion counter (Beckman Coulter) for a period of 10 min per scintillant vial. A ^{14}C count was performed in conjunction in order to detect luminescence arising from auto-fluorescing entities, such as detergent / scintillant vials etc.

2.6.2 Data analysis

Data were fitted with a hyperbola function (see Equation 1) using the Origin 7.0 program (Microcal), in order to obtain estimate values for the dissociation constant (K_D) and maximum number of binding sites (B_{max}). All data are presented as mean ± SEM. An example curve is shown in Figure 2.3.

$$y = B_{max}.x/(K_D + x) \qquad \text{(Eq. 1)}$$

Where:

x = [GBP] (nM)

y = GBP bound (pmol / mg protein)

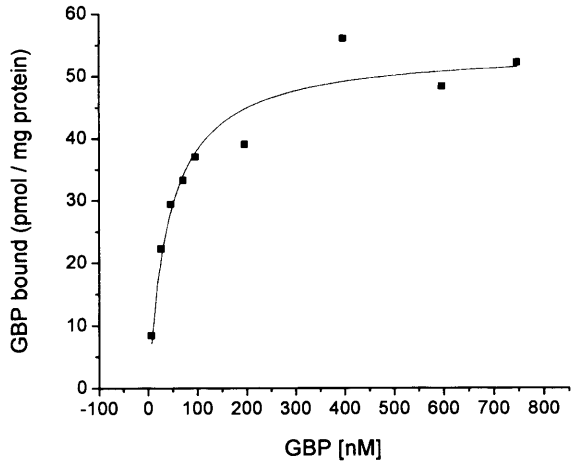

Figure 2.3. Sample radioligand binding assay curve. The mean data are fitted with the hyperbola function.

2.7 Whole-cell electrophysiology

2.7.1 Preparation of cells

For experiments using solely tsA-201 cells (as opposed to tsA-201 / GC co-cultures) it was necessary to re-plate the transfected cells before they were utilised for electrophysiological recordings. This ensured cells were isolated, rather than being in clumps. 35 mm dishes were seeded so that they were confluent on the morning of recording, either 2 or 3 days after seeding / transfection. Re-plating of co-cultures was not possible because this would disrupt the presence of GC projections.

tsA-201 cells were re-plated as follows. 35 mm dishes with a confluent monolayer of cells were taken and immersed in CDS for two min. This prevented adherence of the cells to the dish and caused them to lift off. Cells were then removed into 10 ml warm culture medium and gently triturated using a graduated pipette, before being split across

a further five 35 mm dishes. These dishes were left at 37°C for at least 30 min before experimental use, to ensure adherence to the bottom of the dish.

For the experiments using GC / tsA-201 co-cultures, cells did not need replating, having been seeded the evening before recording took place. They were therefore used immediately.

As with tsA-201 cells, re-plating DRGs before use was necessary prior to electrophysiology, in order to reduce the cell density achieved in cell culture. Cells were re-suspended by a mixture of washing in culture medium (using a Pasteur pipette) or scraping (with a cell-scraper). They were then triturated gently before being added drop-wise to coverslips. Coverslips were then left for at least 1 h before further use.

2.7.2. Equipment

2.7.2.1 Microscope and recording chamber

The recording set-up consisted of a Nikon Diaphot 200 inverted microscope (Nikon) and the recording chamber arranged around it, as illustrated in Figure 2.4. Phase contrast was employed to improve visibility. Cells (in a 35 mm dish) were held in a Perspex recording chamber. The recording chamber was separated from KCl solution (3 M) by an agar bridge. This KCl solution made contact with a Ag:AgCl pellet, which was then connected by wire to the headstage.

The entire recording set-up was maintained on an airtable (Technical Manufacturing Corporation) in order to minimise the impact of vibrations. The microscope, Faraday cage and airtable were connected to the signal grounding point of the amplifier.

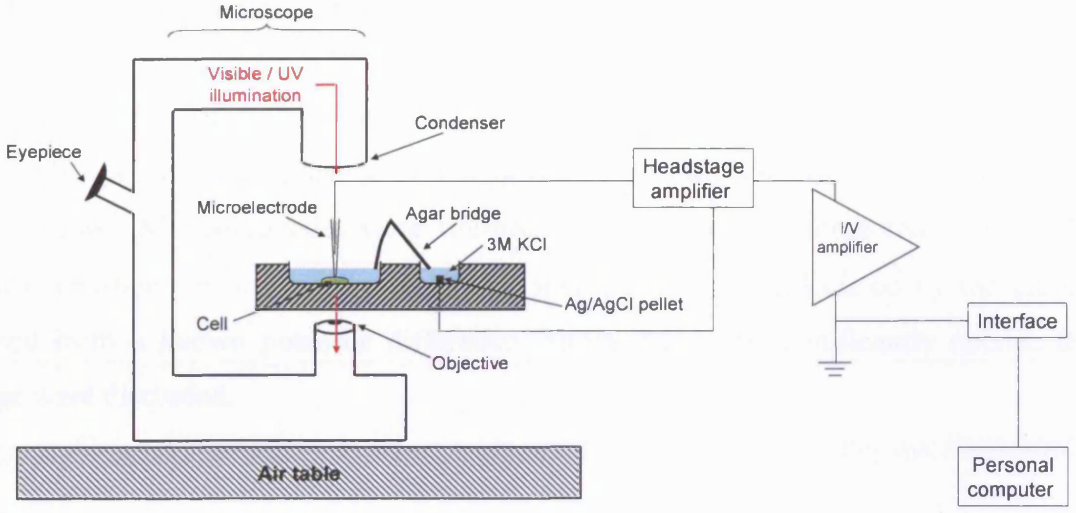

Figure 2.4. Microscope and microelectrode set-up. The cell-containing dish and KCl solution are connected by an agar bridge, and secured within a platform on the microscope. The recording apparatus and microscope were enclosed within a Faraday cage.

2.7.2.2 Amplifier and acquisition apparatus

Two set-ups were used for making electrophysiological recordings, both of which made use of an Axopatch 1-D amplifier (Molecular Devices). The associated head-stage had a gain of 1 (see Figure 2.5). Initially, recordings were made using an Intel 80486 personal computer running Clampex program of the pClamp 6 suite of programs (Molecular Devices), using a Digidata 1200 (Molecular Devices) These recordings make up the data presented in Chapter 3. The data presented in Chapters 4 & 5 were produced from recordings obtained using a Digidata 1322A interface and a Pentium III personal computer running Clampex in the pClamp9 suite (Molecular Devices). In both cases, Clampex was used both to produce voltage pulses and record current. Currents were sampled at 10 kHz and filtered at 2 kHz.

2.7.3.3 Microelectrodes

Electrodes were composed of borosilicate glass capillary. Capillary glass was pulled by the double-pull procedure, using a Flaming-Brown Model P-90 horizontal puller (Sutter Instruments). Microelectrodes were fire-polished using a microforge (Narishige). The typical resistance of these microelectrodes was 2-3 MΩ, as calculated by the current passed from a known potential difference. Those that were significantly outside this range were discarded.

2.7.4 Solutions

A 10 mM Ba^{2+}-containing external solution was used for experiments on tsA-201 cells, as has been described previously (Campbell et al., 1995). The external solution contained (in mM): $BaCl_2$ (10); tetraethylammonium Br (150); D-glucose (4); $MgCl_2$ (1); $NaHCO_3$ (1); HEPES (10); KCl (3). The pH of the solution was adjusted to pH 7.4 with NaOH and the osmolarity was adjusted to 320 mOsm with sucrose. The internal solution contained (in mM): Cs-aspartate (140); EGTA (5); $MgCl_2$ (2); $CaCl_2$ (0.1); K_2ATP (2); HEPES (10).

In the case of recordings made from DRGs, an internal solution of the same composition was used, with the exception that the external solution contained 1 mM $BaCl_2$ (instead of 10 mM $BaCl_2$) due to the larger size of DRGs compared to tsA-201 cells. The external solution contained 500 nM TTX to block sodium currents.

External solutions were adjusted to pH 7.4 and internal solutions adjusted to pH 7.2. The osmolarity of the solutions was also adjusted, to prevent swelling or shrinking of cells during the whole-cell configuration as a result of a difference in osmotic pressure. A vapour-pressure osmometer (Wescor) was used. The external solution was adjusted to 320 mOsm and the internal solution was adjusted to 310 mOsm, by adding sucrose solution in both cases.

tsA-201 cells do not express many channel types endogenously, hence their selection for use as an expression system. An exception to this is the expression of K^+ channels (Yu and Kerchner, 1998). These channels were blocked by including Cs^+ ions in the internal solution and Ba^{2+} ions in the external solution.

2.7.4.1 Using Ba^{2+} ions as charge carrier

1 mM or 10 mM Ba^{2+} was used as the charge carrier in patch clamp experiments. The use of Ba^{2+} ions rather than Ca^{2+} ions in calcium channel recordings has an impact on the data obtained. $Ca_v2.1$ and $Ca_v2.2$ channels are more selective for Ba^{2+} ions than Ca^{2+} ions. Therefore more ions pass through the channel per unit time that the channels are open, and hence larger currents were obtained for the equivalent test-pulse.

In addition, the use of Ba^{2+} ions reduces the extent of calcium-dependent inactivation of currents, allowing voltage-dependent inactivation to be isolated. However, it has been suggested that some calcium-dependent inactivation still occurs even when using Ba^{2+} ions, and that monovalent ions should be used to completely prevent it (reviewed in Lacinova, 2005).

2.7.5 Data acquisition: whole-cell voltage-clamp

All experiments were carried out at room temperature (21-24°C). Green cells were selected by illumination with ultraviolet (UV) light. A typical tsA-201 cell had a capacitance of roughly 5 pF. Having found a suitable target cell, UV illumination was switched off and a pipette was back-filled with internal solution using a non-metallic syringe needle. Any bubbles were removed by gentle tapping of the side of the pipette. The pipette tip was dipped in Sigmacote solution (Sigma-Aldrich) in order to reduce the

capacitive transient caused by water creeping up the shank of the pipette. The pipette was then fastened into the holder on the headstage.

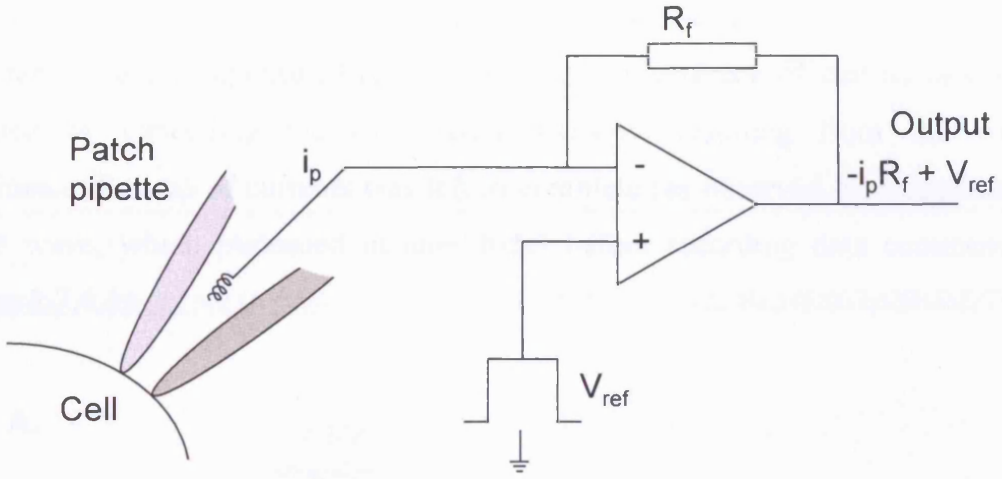

Figure 2.5 Schematic representation of the headstage circuit. The current response to the applied potential difference is fed into the headstage amplifier and subsequently to the output (Axopatch amplifier).

Approaching the cell with the pipette proceeded as follows. The pipette was attached to the microelectrode holder, and the holder orientated towards the cell. Positive pressure was applied to the internal solution in the pipette using a syringe. The current was zeroed using the over-ride control on the amplifier. Then pipette was then manoeuvred towards the cell, and into the bath solution using a macro-manipulator (Narishige).

Having placed the pipette over the cell (~10 - 20 μm), control was switched to the micro-manipulator (Narishige). The electrode potential between the pipette and bath solution was adjusted to zero, and a 5 mV square-wave test potential applied in the "Sealtest" function of Clampex. This was used to provide an estimate of pipette resistance. The positive pressure in the pipette was removed, and the cell approached slowly until the current response to the square-wave reduced. This was due to increased resistance as a result of pipette contact with the cell (see Figure 2.6). At this point, gentle negative pressure was applied to encourage gigaseal formation. With gigaseal formation

obtained, negative pressure was removed, and a holding potential of -90 mV applied to the cell. Fast capacitative transients (relating to the pipette capacitance) were cancelled. Short, sharp bursts of suction were then applied to cause the membrane seal to break, and for the cell to enter the whole-cell configuration. Series resistance and whole-cell capacitance were compensated (up to 80-90%). An estimate of cell surface area was provided by cancelling the capacitative transient resulting from the whole-cell capacitance. Run-up of currents was left to complete (as observed by a application of a square wave, which plateaued in amplitude) before recording data commenced (see Section 2.7.4.1).

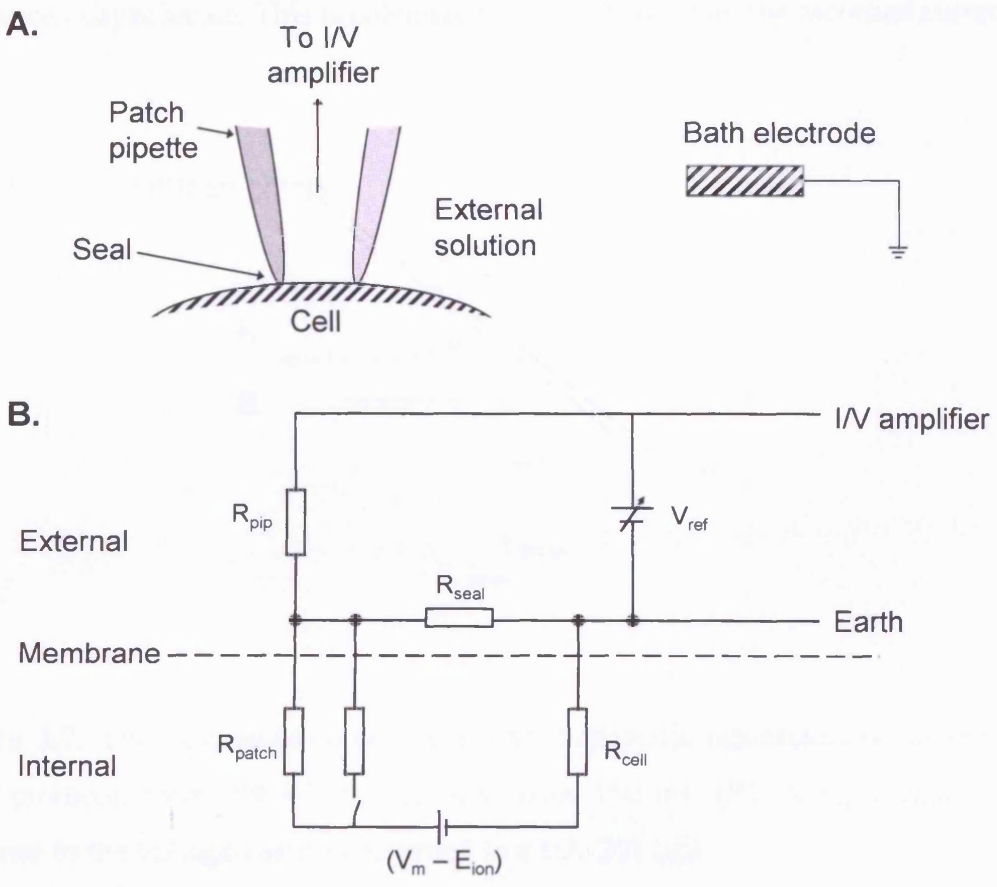

Figure 2.6. Schematic representation of the circuit produced when forming a seal. (A), Diagram of the microelectrode tip making contact with the cell membrane. (B), The cell (R_{cell}), patch (R_{patch}), seal (R_{seal}) and pipette walls (R_{pip}) all have a resistance. The bath electrode completes the circuit through the external solution, and is earthed. The pipette

electrode feeds to the I/V amplifier (via the headstage amplifier). Figure adapted from Ogden (1994).

2.7.6 Voltage-clamp protocols and analysis

A number of protocols were produced in Clampex, these are listed below. All protocols included a P/4 leak subtraction protocol, before the test pulse. The P/4 protocol applies four waveforms (each ¼ the amplitude of the test pulse) of opposite polarity to measure the linear passive current that represents the leak current passing through the membrane resistance / capacitance. This is calculated and removed from the recorded current trace.

2.7.6.1 Voltage-ramp

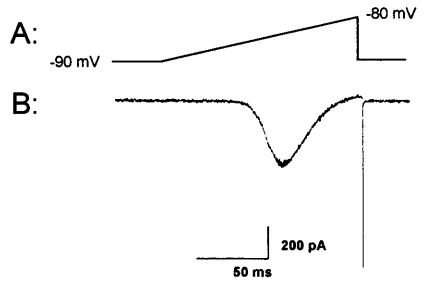

Figure 2.7. The voltage-ramp protocol. (**A**), Schematic representation of the voltage-ramp protocol, from -90 mV to +80 mV, over 150 ms. (**B**), A representative current response to the voltage-ramp as recorded in a tsA-201 cell.

Having broken the membrane upon the addition of suction from the syringe, a ramp protocol was applied to give an estimate as to the size of the current, as shown in Figure 2.7. In addition, it was then applied repeatedly at 10 second intervals for each cell, until

"run-up" of current size had reached completion. This lasted from 30 to 90 seconds on average. Run-up is an ATP- and GTP-dependent process, and is less pronounced in the presence of Ba^{2+} ions compared to Ca^{2+} ions (Wagner and Alger, 1994).

By convention, the inward flow of divalent cations into cells is represented as a negative current, and a downward deflection on the current trace.

2.7.6.2 Current-Voltage relationship

The current-voltage (I-V) relationship is an important measure of calcium channel activity. The shift in the curve ($V_{50,\ act}$) to different potentials or an increase in current sizes obtained gives a measure of factors such as the number of active channels present in the membrane, or the biophysical properties they possess.

The I-V curve was obtained using a holding potential of -90 mV. Test potential steps were applied for 200 ms at potentials of -30 mV to +80 mV, before returning to the holding potential. The period between each sweep was 10 s.

Analysis of the I-V data was carried out using the Clampfit program within the Clampex package. The mean current over a 2 ms period, 20 ms after the onset of each test potential was used for analysis. The observed current at each point was then divided by the estimate of whole-cell capacitance (obtained when cancelling capacitive transients after obtaining the whole-cell configuration, as in Section 2.7.5). This value for current/capacitance was termed current density (in pA/pF), and plotted against the test potential in order to obtain an I-V curve (see Figure 2.8).

The section of the I-V plot between -30 mV and +50 mV was used for analysis. The Origin 7.0 program (Microcal) was used. The use of potentials up to +50 mV removed the rectifying component of the I-V graph, so that the resulting line could be treated with

the combination of a Boltzmann single exponential function and a straight line component (termed IVFIT):

$$I = G_{max}(V - V_{rev})/(1 + \exp(- (V - V_{50,act}) / k))$$

(Eq. 2)

Where:

I = current density (pA/pF)

G_{max} = maximal whole-cell conductance, normalised to cell capacitance (nS/pF)

V_{rev} = an estimate of apparent reversal potential (mV)

$V_{50, act}$ = mid-point of maximal current density (mV)

k = maximal gradient of the Boltzmann function fitted to activation

From Equation 2, it is possible to obtain estimates for the maximal conductance of the cell (G_{max}), the mid-point of current activation ($V_{50, act}$), the maximal downward slope (k), and from the intercept of the straight line component with the x-axis- the apparent reversal potential (V_{rev}). The value obtained for V_{rev} was an underestimate in the majority of cases, due to the inwardly rectifying nature of the I-V component near the true V_{rev}. Therefore the estimates of V_{rev} obtained from applications of IVFIT have been omitted. All data are presented as mean ± SEM.

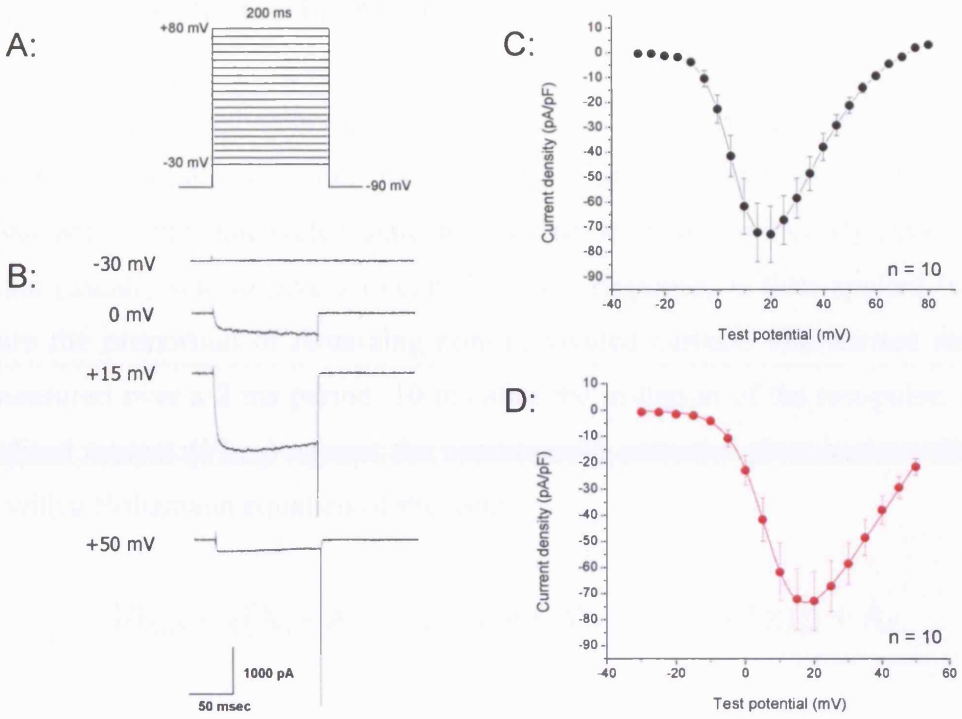

Figure 2.8. The current-voltage protocol, shown in a tsA-201 cell expressing $Ca_v2.1$, β4, $\alpha_2\delta$-2. (**A**), Schematic representation of the I-V protocol, depolarising voltage-steps are applied from the holding potential of -90 mM to -30 mV to +80 mV (in 5 mV increments). (**B**), Representative current responses to the I-V protocol- example current responses at -30, 0, +15 and +50 mV are shown. (**C**), The mean current response (normalised to capacitance) over a 2 ms period 10 ms after the initiation of the test-pulse is shown. (**D**), -30 mV to +50 mV section of the I-V relationship, fitted with the IVFIT function.

Complete I-V curves are presented in the results chapters. These include test potentials ranging from -30 mV to +80 mV. The mean (± SEM) values are plotted, and joined by a smooth line. Values for mean peak-current density are obtained by this method, rather than using the IVFIT function.

2.7.6.3 Steady-state inactivation.

The steady-state inactivation curve is produced by applying varying conditioning potentials for a sustained period (five seconds), until the proportion of channels in the cell that are in the inactivated state reaches equilibrium (or "steady-state"). A test-potential (usually one to give a maximal current response) is then applied in order to measure the proportion of remaining non-inactivated current. The current response is that measured over a 2 ms period, 10 ms after the initiation of the test-pulse. A plot of normalised current (I/I_{max}) against the conditioning potential gives a curve that can be fitted with a Boltzmann equation of the form:

$$I/I_{max} = ((A_1 - A_2) / [1 + \exp((V - V_{50,inact}) / k)]) + A_2 \quad \text{(Eq. 3)}$$

Where:

I_{max}	= maximal overall current
I	= measured current of the test potential
$V_{50, inact}$	= the half-maximal voltage for current inactivation.
A_1	= proportion of inactivating current
A_2	= proportion non-inactivating current

An example of a steady-state inactivation trace (and subsequent fit with Equation 3) is shown in Figure 2.9.

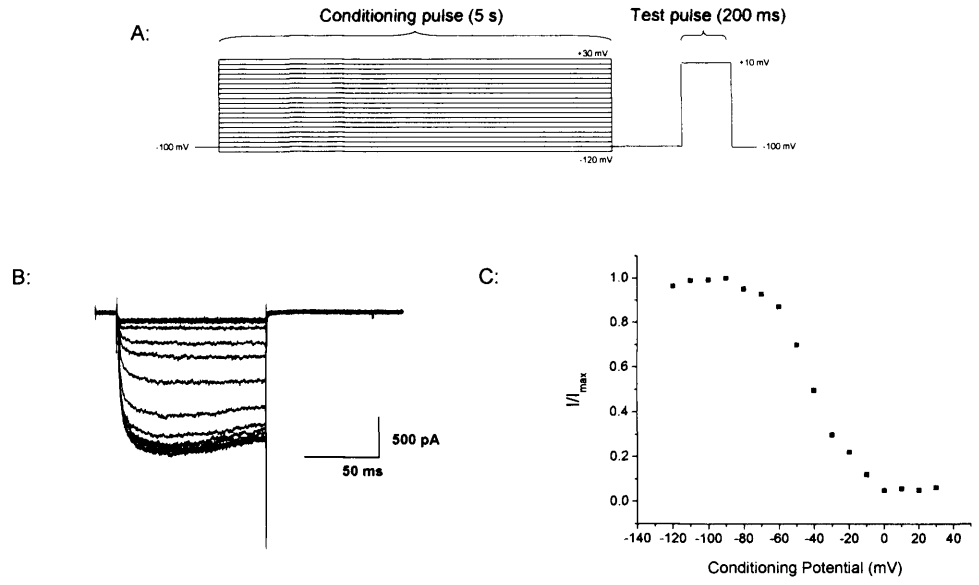

Figure 2.9. The steady-state inactivation protocol, shown in a tsA-201 cell expressing $Ca_v2.1$, β4, $\alpha_2\delta$-2 subunits. (**A**), Schematic representation of the steady-state inactivation protocol. (**B**), Current response to the +10 mV test potential following conditioning potentials of -120 mV to +30 mV. The mean current response over a 2 ms period 10 ms after the initiation of the test-pulse is shown, and fitted with the Boltzmann function (Equation 3).

2.7.6.4 Fit of inactivation kinetics

Inactivation kinetics were measured as a response to a long depolarising pulse (see Figure 2.10), applied for 900 ms (usually to +10 mV). The decay component of the current response was fitted with a single exponential curve. Inactivation data have previously been fitted with either a single exponential (Felix et al., 1997) or double exponential (Sokolov et al., 1999), however in this study a single exponential was sufficient for a satisfactory fit of the current decay:

$$y = A_1 e^{-(x-y0)/\tau} + C$$

Where:

x	=	Time (msec)
y	=	Current (pA)
y^0	=	Initial current (pA)
τ	=	Time-constant of inactivation (termed τ_{inact}; ms)
C	=	Non-inactivating current (pA)

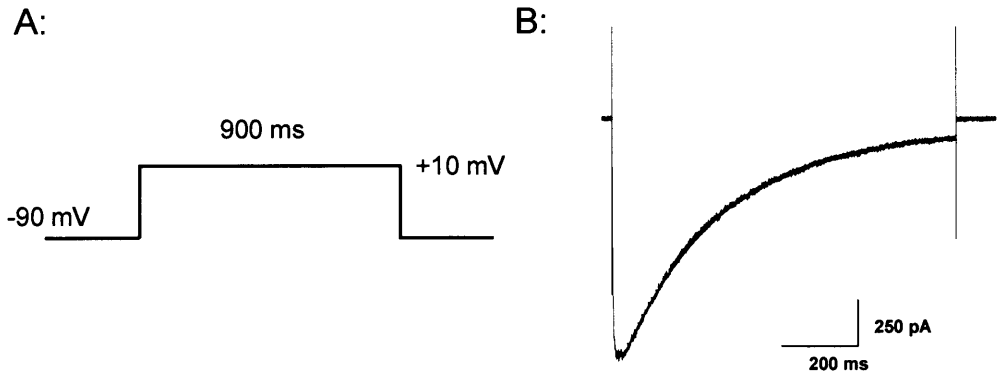

Figure 2.10. The long-pulse protocol. (A), Representation of the long-pulse protocol (B), Sample current trace in response to a 900 ms voltage step to +10 mV, in a tsA-201 cell expressing $Ca_v2.1$, β4, $\alpha_2\delta$-2. The current trace has been fitted with an exponential function (shown in red) to calculate τ_{inact}.

2.7.6 Sources of error

A number of potential errors are present in the recordings made, which must be accounted for.

One such error is that introduced by the series resistance (R_S) of the cell membrane and the pipette. R_S produces a discrepancy between the current flowing across the membrane and the true potential difference. The voltage-drop across R_S was compensated to between 80-90 % in order to avoid the injected current causing oscillations. R_S was of

the order of 5 – 10 MΩ for tsA-201 cells and 10 – 15 MΩ for DRGs. Passing a 1 nA current across a cell with a R_S of 5 MΩ will produce an error of 5 mV when 80% compensated. It is possible to minimize this error by reducing the concentration of Ba^{2+} in the external solution (thus reducing the current flow). 10 mM Ba^{2+} was selected for use in external solutions for patching tsA-201 cells (1 mM Ba^{2+} for DRGs owing to their larger size) to allow large currents without introducing excessive error from uncompensated R_S.

The junction potential between the internal and external solutions is another source of error. This is caused by the differing mobilities of the different ions comprising each solution. The junction potential between the Ag/AgCl pellet and the external solution was nulled between entering the bath solution and making contact with the cell. The junction potential between the internal and external solutions was not compensated. It was calculated as ~6 mV.

2.8 Statistical analysis

Differences between mean values (e.g. peak-current density) were assessed for statistical significance using either a Student's t-test or a one-way analysis of variance (ANOVA) followed by a Dunnett's test. The threshold for statistical significance was $P<0.05$.

Chapter 3: Results

Investigation of the function of the $\alpha_2\delta$ VWA domain

3.1 Introduction

As discussed in the Introduction, $\alpha_2\delta$ subunits contain a VWA domain, which are also found in a number of adhesion proteins such as integrins (Whittaker and Hynes, 2002). This chapter explores the functional contribution of the VWA domain to functionality of the $\alpha_2\delta$ subunit. As a potential binding domain, it was thought possible that the $\alpha_2\delta$ subunit might be able to bind a small protein ligand through the VWA domain. As the $\alpha_2\delta$ subunit plays an intracellular role in enhancing expression of the $Ca_v\alpha1$ subunit (Shistik et al., 1995; De Waard and Campbell, 1995), this interaction could be intracellular. However, as the VWA domain lies within the entirely extracellular α_2 portion of the $\alpha_2\delta$ subunit when expressed at the cell-surface, an interaction through the VWA domain may also be extracellular. VWA domain-mediated protein interactions made by integrins are primarily extracellular, and often involve binding to extracellular matrix proteins.

Therefore experiments were carried out to look at the effect of disrupting the VWA domain by mutating the MIDAS motif (see Introduction), with the aim of preventing the $\alpha_2\delta$-mediated enhancement of $Ca_v\alpha_1$ subunit expression. This would identify either an intracellular function of the $\alpha_2\delta$ VWA domain (upon enhancement of $Ca_v\alpha_1$ subunit cell-surface expression) or a cell-surface function (for instance upon the $\alpha_2\delta$-mediated changes in biophysical properties of expressed VGCCs). Additionally, co-cultures of tsA-201 cells (expressing VGCC subunits) and cerebellar granule cells (GCs) were used to look for evidence of an interaction between the two cell-types that might be mediated by protin binding at the VWA domain. GCs were used due to their synaptic contact with cerebellar Purkinje cells. The work involved whole-cell patch clamp performed on tsA-201 cells, expressing $Ca_v\alpha1$, β and $\alpha_2\delta$ subunits. γ subunits were omitted from the transfection in all cases. 10 mM Ba^{2+} ions were used as charge carrier.

3.2 Results

3.2.1 Characterisation of the function of $\alpha_2\delta$-2

The $\alpha_2\delta$-2 μMIDAS construct was used to assess the importance of the $\alpha_2\delta$-2 VWA domain (Canti et al., 2005), as is described in Section 3.2.2. However before examining the effects of a mutated VWA domain in the $\alpha_2\delta$-2 subunit, an initial investigation into the function of $\alpha_2\delta$-2 itself was carried out. $\alpha_2\delta$ subunits are known for their ability to increase the number of DHP binding-sites at the channel membrane, an effect thought to be mediated by a enhancing effect on $Ca_v\alpha_1$ subunit cell-surface expression (Shistik et al., 1995). An enhancement of current density agrees with the view that more channels are present at the membrane. In addition, $\alpha_2\delta$ effects on the channel properties include a hyperpolarisation of the voltage of current activation, steady-state inactivation, as well as effects on macroscopic current activation and inactivation kinetics (see Introduction). This section examines some of the effects of $\alpha_2\delta$-2 co-expression with the $Ca_v2.1$, β4 subunit combination.

The data in this section are not taken from an individual experiment, rather they are comprised of the pooled results of a number of experiments, always directly pairing control (no $\alpha_2\delta$-2) data with co-expressed $\alpha_2\delta$-2 data. Where $\alpha_2\delta$-2 cDNA is omitted from the transfection mixture, the equivalent volume is made up with empty vector (pMT-2) cDNA (see Materials and Methods).

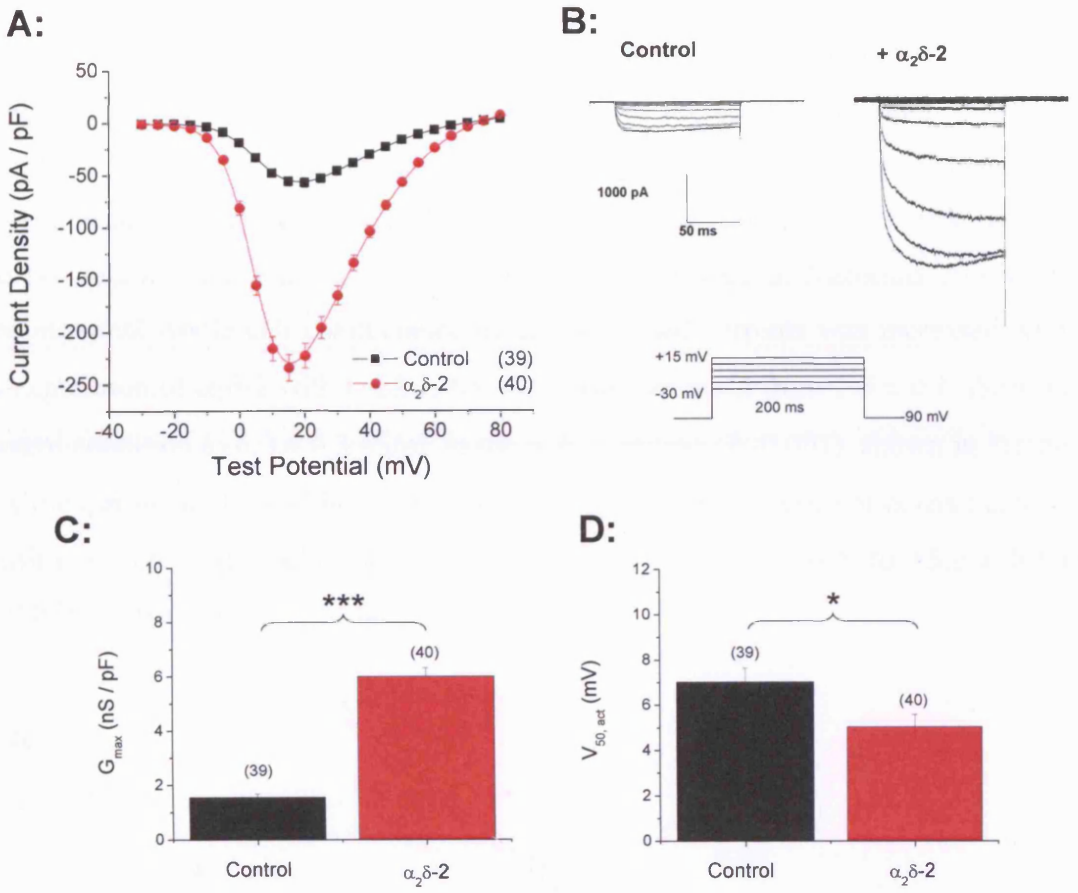

Figure 3.1. Co-expression of $\alpha_2\delta$-2 enhances I_{Ba} in channels composed of $Ca_v2.1$ and β4 subunits. (**A**), Current-voltage relationships for I_{Ba} in the $Ca_v2.1$, β4, (black squares, n=39) and $Ca_v2.1$, β4, $\alpha_2\delta$-2 (red circles, n=40). Current amplitude was normalised to whole-cell capacitance and plotted against membrane potential. Holding potential was -90 mV. (**B**), Representative current traces for the two conditions in response to -30 to +15 mV voltage steps. A schematic of the I-V protocol is shown. Mean values for G_{max} (**C**) and $V_{50,\ act}$ (**D**) were obtained from fits of individual I-V relationships using the IVFIT function. * denotes $P<0.05$, *** denotes $P>0.001$ (Student's t test).

Figure 3.1 shows how the co-expression of $\alpha_2\delta$-2 affects current amplitude of the heterologously expressed $Ca_v2.1$, β4 subunit combination. Control data was obtained using a $Ca_v2.1$, β4, pMT-2 cDNA mix. Control data is shown in black, and the condition including heterologous expression of $\alpha_2\delta$-2 is shown in red. $\alpha_2\delta$-2 co-expression results

in a significant increase in current amplitude and peak current-density (Figures 3.1 A & B respectively). Mean peak current-density was enhanced significantly with the presence of $\alpha_2\delta$-2 (-234.6 ± 12.6 pA/pF), in comparison to the control condition (-57.1 ± 4.4 pA/pF, $P<0.001$). Whole-cell conductance (G_{max}) and the voltage-dependence of activation of currents ($V_{50,\ act}$) were measured by fitting -30 mV to +50 mV portions of the I-V relationship with the IVFIT function, as described in Materials and Methods. The maximal whole-cell conductance of the expressed currents was increased with the co-expression of $\alpha_2\delta$-2 with $Ca_v2.1$, $\beta4$. G_{max} was increased from 1.6 ± 0.1 nS/pF in the control condition to 6.0 ± 0.3 nS/pF in the $\alpha_2\delta$ condition ($P<0.001$), shown in Figure 3.1 C. Co-expression of $\alpha_2\delta$-2 has an effect on the voltage-dependence of current activation, causing a slight hyperpolarisation in $V_{50,\ act}$ (from +7.0 ± 0.6 mV to +5.0 ± 0.5 mV, $P<0.05$), shown in Figure 3.1 D.

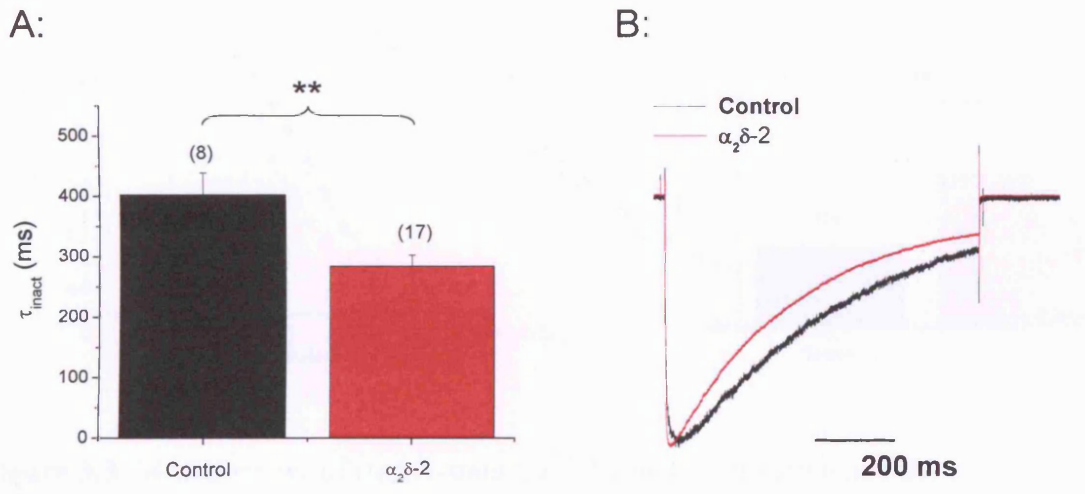

Figure 3.2. Co-expression of $\alpha_2\delta$-2 causes an increase in inactivation kinetics of channels composed of $Ca_v2.1$ and $\beta4$ subunits. (**A**), Mean time-constant of inactivation (τ_{inact}) data is shown for the $Ca_v2.1$, β_4, (black, n=8) and $Ca_v2.1$, β_4, $\alpha_2\delta$-2 (red, n=17). The decay phase of individual current traces at +10 mV was fitted with a single exponential function. Holding potential was -90 mV. (**B**), Representative current traces

in response to a long depolarising voltage step to +10 mV, traces are normalised to peak. ** denotes P<0.01, (Student's t test).

Inactivation kinetics were hastened by the co-expression of $\alpha_2\delta$-2 (Figure 3.2). A single exponential function was fitted to the decaying portion of currents through expressed channels in response to a voltage step to +10 mV for 800 ms. τ_{inact} was reduced from 402.7 ± 36.2 ms in the control condition to 283.8 ± 18.8 ms with the co-expression of $\alpha_2\delta$-2 (P<0.01), as shown in Figure 3.2 A. Sample current traces are shown in Figure 3.2 B.

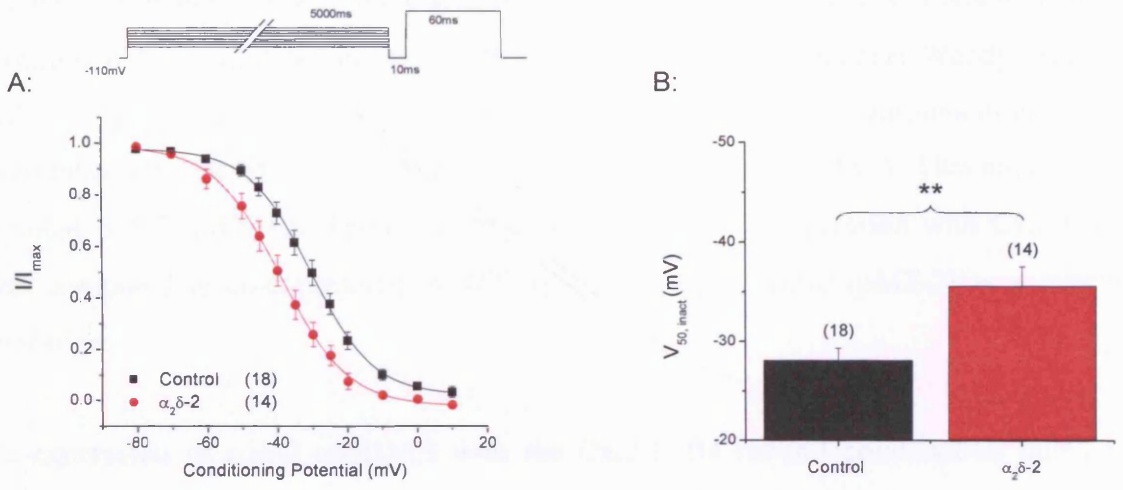

Figure 3.3. Measurement of steady-state Ca^{2+} channel inactivation and the effect of $\alpha_2\delta$-2 co-expression. (**A**), Steady-state inactivation curves for $Ca_v2.1$, β4, (black squares, n=18) and $Ca_v2.1$, β4, $\alpha_2\delta$-2 (red circles, n=14) conditions. (**B**), Mean $V_{50,\ inact}$ data were obtained by fitting a Boltzmann function to individual steady-state inactivation curves. ** denotes P<0.01, (Student's t test).

The presence of $\alpha_2\delta$-2 also causes a hyperpolarisation in the steady-state inactivation of currents, obtained in response to a constant voltage step following a conditioning potential of varying voltage (Figure 3.3 A). $V_{50,\ inact}$ in the $\alpha_2\delta$ condition (-35.6 ± 2.0

mV) was significantly more negative than the control condition (-28.1 ± 1.2 mV, P<0.01), as shown in Figure 3.3 B.

Therefore the co-expression of $\alpha_2\delta$-2 with $Ca_v\alpha_1$ and β4 subunits has significant effects on various channel properties, in agreement with previous studies (see Introduction).

3.2.2 $\alpha_2\delta$-2 μMIDAS

The identification of a VWA domain in $\alpha_2\delta$ subunits hinted at an additional role for the subunit in terms of extracellular ligand binding, or at least a site by which its intracellular interaction with the $Ca_v\alpha_1$ subunit might be mediated. The VWA domain of mouse $\alpha_2\delta$-2 was mutated in the lab (by molecular biology technician Wendy Pratt) in order to probe its function (see Canti et al., 2005). Three point-mutations were introduced into the MIDAS, to convert the DVSGS motif to AVAGA. This mutant was denoted $\alpha_2\delta$-2 μMIDAS. The effect of $\alpha_2\delta$-2 μMIDAS co-expression with $Ca_v2.1$, β4 was compared to co-expression of WT $\alpha_2\delta$-2, or empty vector (pMT-2) as a control condition.

Co-expression of $\alpha_2\delta$-2 μMIDAS with the $Ca_v2.1$, β4 subunit combination failed to enhance current amplitude over those of the control condition (Figure 3.4 A). The current response to a range of potentials (Figure 3.4 A), as well as the I-V curve (Figure 3.4 B) suggest that $\alpha_2\delta$-2 μMIDAS is non-functional as an $\alpha_2\delta$-2 subunit in terms of its ability to enhance current size. The peak current density of the $\alpha_2\delta$-2 μMIDAS condition was similar to that of the control condition (-40.2 ± 5.1 pA/pF and -43.1 ± 5.3 pA/pF respectively), both of which were significantly lower than the WT $\alpha_2\delta$-2 condition (-222.7 ± 18.2 pA/pF, P<0.001 for both). There was no significant increase in the whole cell conductance measured for the $\alpha_2\delta$-2 μMIDAS condition (1.1 ± 0.1 nS/pF) over control (1.1 ± 0.1 nS/pF), both of which were significantly smaller than the WT $\alpha_2\delta$-2 condition (5.7 ± 0.5 nS/pF, P<0.001 for both), as shown in Figure 3.4 C. Similar values

were obtained for $V_{50,\ act}$ (+5.0 ± 0.7 mV for control, +4.1 ± 0.2 mV for WT $\alpha_2\delta$-2, +5.1 ± 0.1 mV for $\alpha_2\delta$-2 μMIDAS conditions, see Figure 3.4 D), which were not significantly different.

Insufficient data were obtained to establish mean values for either $V_{50,\ inact}$ or τ_{inact}, although similar work (using $\alpha_2\delta$-2 μMIDAS co-expressed with $Ca_v2.2$, β1b) found a failure of $\alpha_2\delta$-2 μMIDAS to hyperpolarise the $V_{50,\ inact}$ in a similar manner to WT $\alpha_2\delta$-2 (Canti et al., 2005).

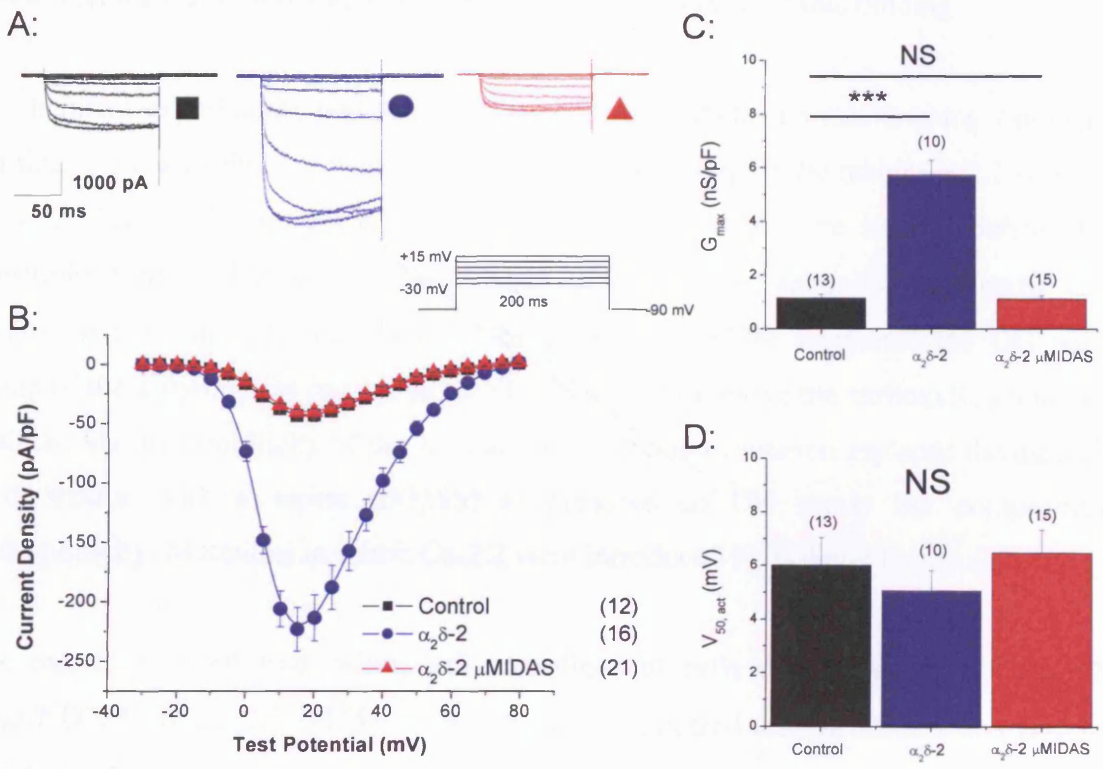

Figure 3.4. Failure of $\alpha_2\delta$-2 μMIDAS co-expression to enhance I_{Ba} through $Ca_v2.1$, β4 channels. (**A**), Representative current traces for the three conditions in response to -30 to +15 mV voltage steps. (**B**), Current-voltage relationships for $Ca_v2.1$, β4, (black, n=12), $Ca_v2.1$, β4, $\alpha_2\delta$-2 (blue, n=16) and $Ca_v2.1$, β4, $\alpha_2\delta$-2 μMIDAS (red, n=21) conditions. All currents are normalised to whole-cell capacitance and plotted against membrane potential. Holding potential was -90 mV. G_{max} in the $\alpha_2\delta$-2 condition was significantly

increased (P<0.001, ANOVA) over control, whereas there was no significant increase in the $\alpha_2\delta$-2 μMIDAS condition. No significant difference was observed between $V_{50,\,act}$ of the three conditions (P>0.05, ANOVA).

3.2.3 Mutations of a putative VWA binding site on the $Ca_v\alpha_1$ subunit

Given the importance of the VWA domain in the interaction between the $\alpha_2\delta$ and $Ca_v\alpha_1$ subunits, the next step was to determine whether the VWA domain was binding to a domain on the $Ca_v\alpha_1$ subunit, and if so, to which amino acids it was binding.

Biochemical experiments performed in the lab (by Isabelle Foucault) using candidate peptides suggested the involvement of an extracellular loop of the rabbit $Ca_v2.2$ subunit. This residue would possess a negatively charged side-chain, be located outside the selectivity filter, and would be conserved in all HVA $Ca_v\alpha_1$ subunits. An aspartic acid residue at position 325, was chosen. One mutation, D325N, converted the OH polar group of the aspartic acid residue to an NH_2 in order to remove the carboxylic group but maintain the hydrophilicity of the residue. Another point mutation replaced the aspartic acid residue with a serine (D325S) to preserve an OH group but compromise hydrophilicity. Mutations in rabbit $Ca_v2.2$ were introduced by Isabelle Foucault.

The results obtained from whole-cell recordings of cells co-expressing WT $Ca_v2.2$, $Ca_v2.2$ D325S or $Ca_v2.2$ D325N with β1b, $\alpha_2\delta$-1 indicated that the D325S and D325N mutations did not prevent the association of the $Ca_v\alpha_1$ subunit with $\alpha_2\delta$-1. The mean peak-current densities were similar in the D325N (-337.3 ± 143.4 pA/pF) and D325S (-452.9 ± 101.7 pA/pF) conditions to that of the control condition (413.0 ± 83.0 pA/pF), as shown in Figure 3.5 A. Whole-cell conductance was not significantly impaired by either the D325N or D325S mutations. G_{max} values of 9.9 ± 3.8 nS/pF for the D325N condition and 14.8 ± 3.1 nS/pF were similar to that of the control condition (12.6 ± 2.6 nS/pF), as shown in Figure 3.5 B. Similarly, no change in the voltage-dependence of current activation was observed. $V_{50,\,act}$ values for the D325N and D325S conditions

(+7.4 ± 2.4 mV and +12.3 ± 1.3 mV respectively) were similar to the $V_{50,\,act}$ observed for the control condition (+7.7 ± 2.3 mV), shown in Figure 3.5 C. No negative control condition in the absence of the $\alpha_2\delta$-1 subunit was included. However, the similar values for peak-current density and G_{max} among the D325N, D325S and control suggest that an interaction between the $Ca_v2.2$ and $\alpha_2\delta$-1 subunits still occurs.

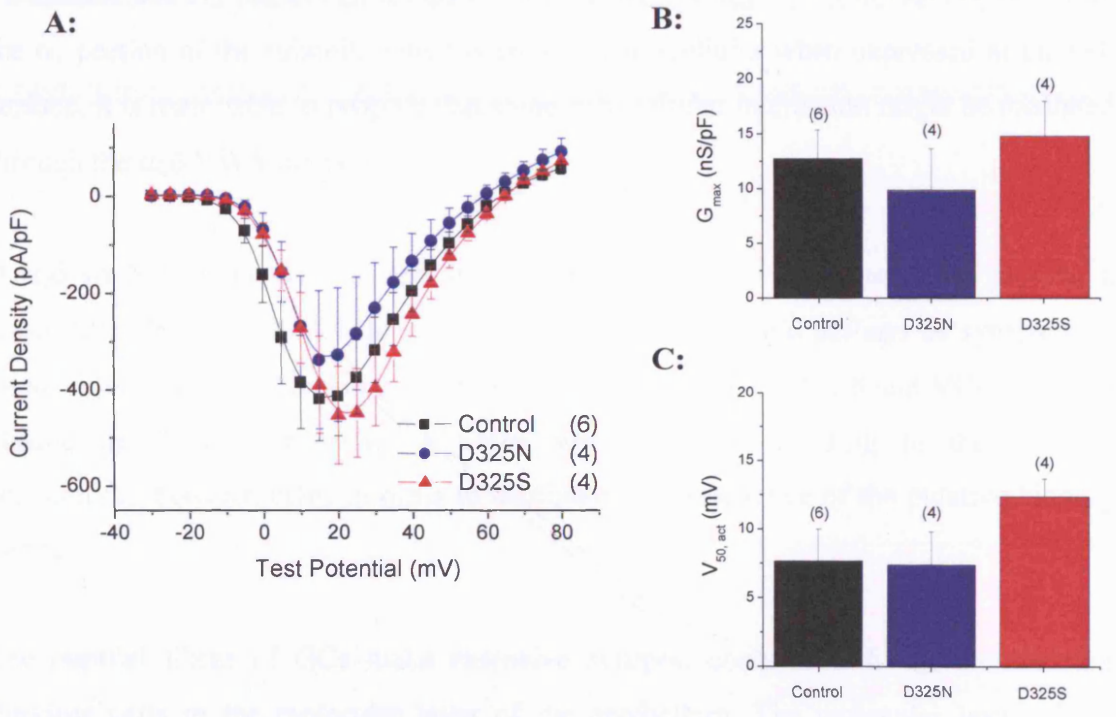

Figure 3.5. I-V relationships of channels including $Ca_v2.2$ D325N or $Ca_v2.2$ D325S subunits are not significantly different from those including WT $Ca_v2.2$. (**A**), Current-voltage relationships for β1b, $\alpha_2\delta$-1, co-expressed with: WT $Ca_v2.2$ (black squares); $Ca_v2.2$ D325N (blue circles) and $Ca_v2.2$ D325S (red triangles). All currents are normalised to whole-cell capacitance and plotted against membrane potential. Holding potential was -90 mV. Mean values for G_{max} (**B**) and $V_{50,\,act}$ (**C**) were obtained from fits of individual I-V relationships using the IVFIT function. In all cases, the D325N and D325S conditions were not significantly different from the control condition (ANOVA).

3.2.5 The use of GC cultures as a source of the putative binding partner of the $\alpha_2\delta$-2 VWA domain

The $\alpha_2\delta$ VWA domain is important for enhancing trafficking of the calcium channel complex to the membrane. However, the vast majority of VWA domain interactions are extracellular, such as those involving integrins and extracellular matrix proteins (Whittaker and Hynes, 2002). Coupled with the fact the $\alpha_2\delta$ VWA domain is located in the α_2 portion of the subunit, which is entirely extracellular when expressed at the cell surface, it is reasonable to propose that some extracellular interaction might be mediated through the $\alpha_2\delta$ VWA domain.

If $\alpha_2\delta$ ($\alpha_2\delta$-2 in the case of the study) were to bind to an extracellular protein, a reasonable place to look for this binding partner protein would perhaps be synapses on nerve cells, given the functional importance of the presence of $\alpha_2\delta$ and VGCCs at the plasma membrane. Therefore, a tissue was selected according to the synaptic connectivity between cells, in order to maximise the occurrence of the putative binding partner.

The parallel fibres of GCs make extensive synaptic contacts with $\alpha_2\delta$-2-containing Purkinje cells in the molecular layer of the cerebellum. The molecular layer of the cerebellum contains the parallel fibres of the GCs and the dendrites of Purkinje cells, and displays significant ^{3}H-PGB binding (Bian et al., 2006). Therefore, cerebellar GC cultures were selected as a potential source of binding partner for the $\alpha_2\delta$ VWA domain.

3.2.5.1 Assessment of culture media

When cultured separately, tsA-201 cells and GCs are grown in different media (D-MEM and BME respectively). Therefore an initial assay was set up to determine which medium to select for co-cultures. This was attempted with 2 separate cultures for GCs (cultured in D-MEM), and 2 separate flasks of tsA-201 cells (cultured in BME). Whilst

no striking differences were observed in either the appearance or number of tsA-201 cells cultured in BME compared to D-MEM, a large proportion of the GCs failed to adhere / survive in D-MEM. Therefore, co-cultures proceeded to use BME as a culture medium. Cells of the control condition (tsA-201 cells "alone") were also cultured in BME, despite the absence of GCs. Images of tsA-201 / GC co-cultures are shown in Figure 2.1).

3.2.5.2 Testing a mid HA-tagged $\alpha_2\delta$-2 stable-cell line

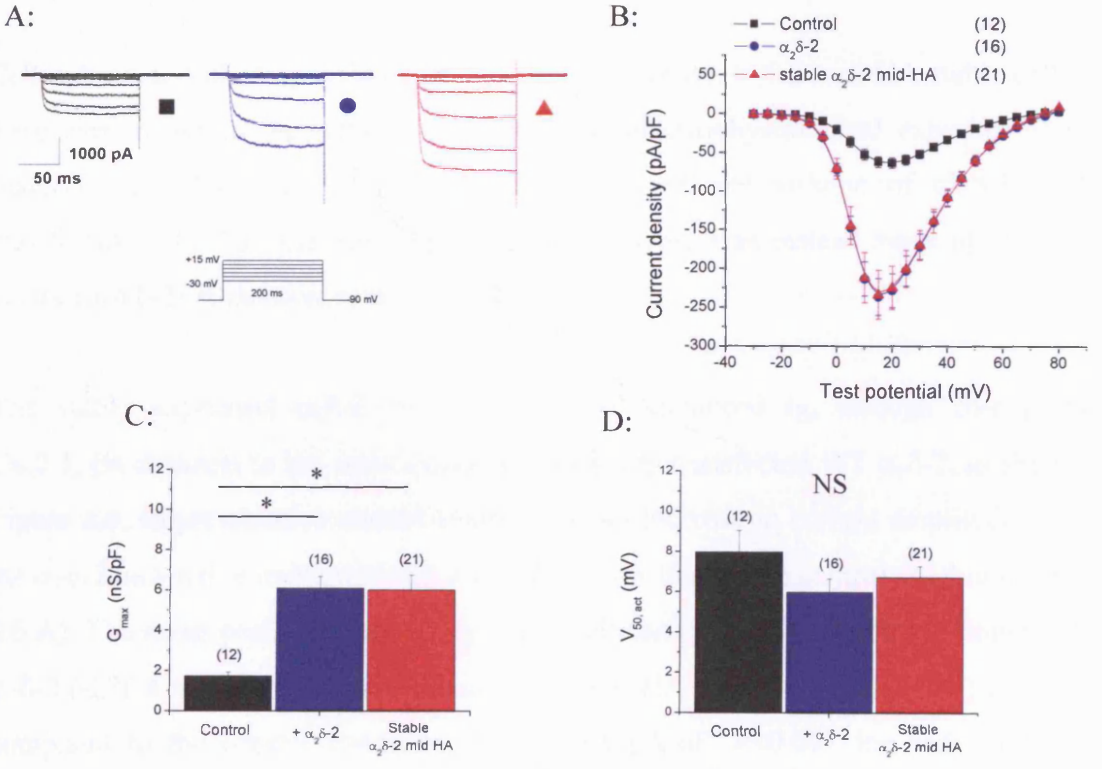

Figure 3.6. Functionality of the stable $\alpha_2\delta$-2 mid-HA construct. (**A**), Representative current traces for $Ca_v2.1$, β4, (control, black), $Ca_v2.1$, β4, $\alpha_2\delta$-2 (blue) and $Ca_v2.1$, β4, $\alpha_2\delta$-2 stable mid-HA (red) conditions in response to -30 to +15 mV voltage steps. (**B**), Current-voltage relationships for the three conditions. All currents are normalised to whole-cell capacitance and plotted against membrane potential. Holding potential was -90 mV. (**C**) Mean G_{max} values of $Ca_v2.1$, β4, $\alpha_2\delta$-2 $Ca_v2.1$, β4, $\alpha_2\delta$-2 stable mid-HA

were significantly different from control (ANOVA). (**D**) Mean values for $V_{50,\ act}$ were different among the three conditions. Values for (**C**) and (**D**) were obtained from fits of individual I-V relationships using the IVFIT function.

One route of investigation that was followed up was the possibility that the $\alpha_2\delta$ VWA domain bound an extracellular protein ligand. This would involve co-immunoprecipitation experiments, and therefore a stable tsA-201 cell-line expressing an HA-tagged $\alpha_2\delta$-2 was produced in the lab (by Jack Wratten). Before use in experiments, it was necessary to demonstrate the construct was expressed as a functional tagged $\alpha_2\delta$-2 protein ($\alpha_2\delta$-2 mid-HA).

Cell culture and electrophysiological recording using the $\alpha_2\delta$-2 mid-HA stable cell-line were carried out in the same way as previous electrophysiological experiments (see Materials and Methods for more detail). However, the volume of cDNA in the transfection mix that was normally made up by $\alpha_2\delta$-2 was instead made up by empty vector (pMT-2) in the case of this experiment.

The stably expressed $\alpha_2\delta$-2 mid-HA construct enhanced I_{Ba} through co-expressed $Ca_v2.1$, $\beta4$ channels to the same extent as transiently transfected WT $\alpha_2\delta$-2, as shown in Figure 3.6. Representative current traces show an increase in current amplitude in both the $\alpha_2\delta$-2 and stable $\alpha_2\delta$-2 mid-HA conditions over that of the control condition (Figure 3.6 A). The mean peak-current density was significantly larger (3.8-fold) in both the WT $\alpha_2\delta$-2 (-236.4 ± 23.7 pA/pF) and stable $\alpha_2\delta$-2 mid-HA (-234.0 ± 31.6 pA/pF) conditions compared to the control condition (63.5 ± 6.8 pA/pF, $P<0.001$ for both, ANOVA), shown in Figure 3.6 B. Maximal whole-cell conductance was also increased to the same extent by the stable $\alpha_2\delta$-2 mid-HA condition (6.0 ± 0.7 nS/pF) as by WT $\alpha_2\delta$-2 condition (6.1 ± 0.6 nS/pF) over the control condition (1.7 ± 0.2 nS/pF, $P<0.05$ for both, ANOVA), as shown in Figure 3.6 C. In contrast to data shown in Figure 3.1 D, mean values of $V_{50,\ act}$ of transient WT $\alpha_2\delta$-2 (and stable $\alpha_2\delta$-2 mid-HA) conditions were not significantly different to that of the control condition (Figure 3.6 D). The ability of $\alpha_2\delta$

to hyperpolarise $V_{50,\ act}$ is not certain, with some studies not finding $\alpha_2\delta$ ($\alpha_2\delta$-1) expression to alter $V_{50,\ act}$ (Shirokov et al., 1998), whilst another study found it to hyperpolarise $V_{50,\ act}$ (Felix et al., 1997).

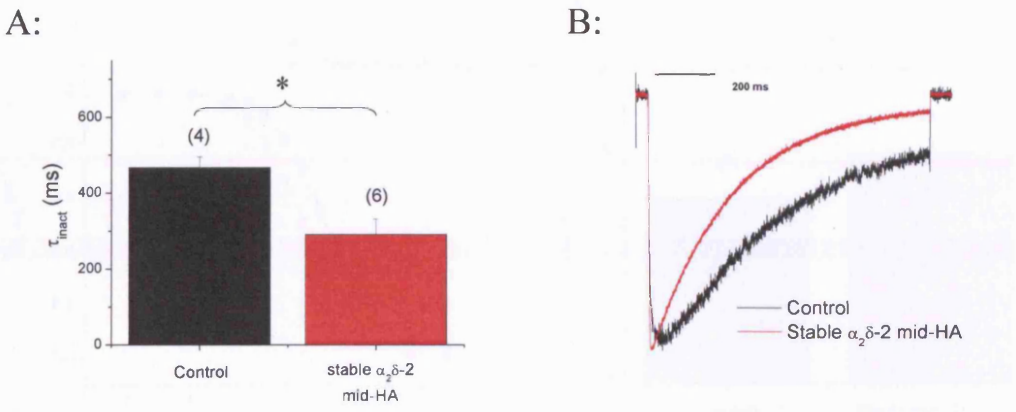

Figure 3.7. Stably transfected $\alpha_2\delta$-2 mid-HA affects inactivation kinetics of $Ca_v2.1$, $\beta4$ channels. (**A**), Mean time-constant of inactivation (τ_{inact}) data is shown for the control $Ca_v2.1$, $\beta4$, (black, n=4) and $Ca_v2.1$, $\beta4$, stable $\alpha_2\delta$-2 mid-HA (red, n=6) conditions. Holding potential was -90 mV. The decay phase of individual current traces at +10 mV was fitted with a single exponential function. (**B**) Representative current traces in response to a long depolarising voltage step to +10 mV, traces are normalised to peak. * denotes $P<0.05$, (Student's t test).

In addition, the time-constant of inactivation of currents was significantly reduced by co-expression of the stable $\alpha_2\delta$-2 mid-HA construct (291.0 ± 40.7 ms) compared to the control condition (467.0 ± 28.0 ms, $P<0.05$), as shown in Figures 3.7 A & B. Unfortunately, insufficient data were obtained for the transiently-transfected WT $\alpha_2\delta$-2 condition. However, equivalent data are presented in Figure 3.2 for transiently-transfected WT $\alpha_2\delta$-2. The stable $\alpha_2\delta$-2 mid-HA construct also had the same effect on steady-state inactivation of the currents as the WT $\alpha_2\delta$-2 (Figure 3.8 A). The $V_{50,\ inact}$ values for stable $\alpha_2\delta$-2 mid-HA (-29.5 ± 1.9 mV) was hyperpolarised compared to that

of the control condition (-23.9 ± 1.3 mV, P<0.05, Student's t test), as shown in Figure 3.8 B. Unfortunately, insufficient WT $\alpha_2\delta$-2 data were obtained for analysis.

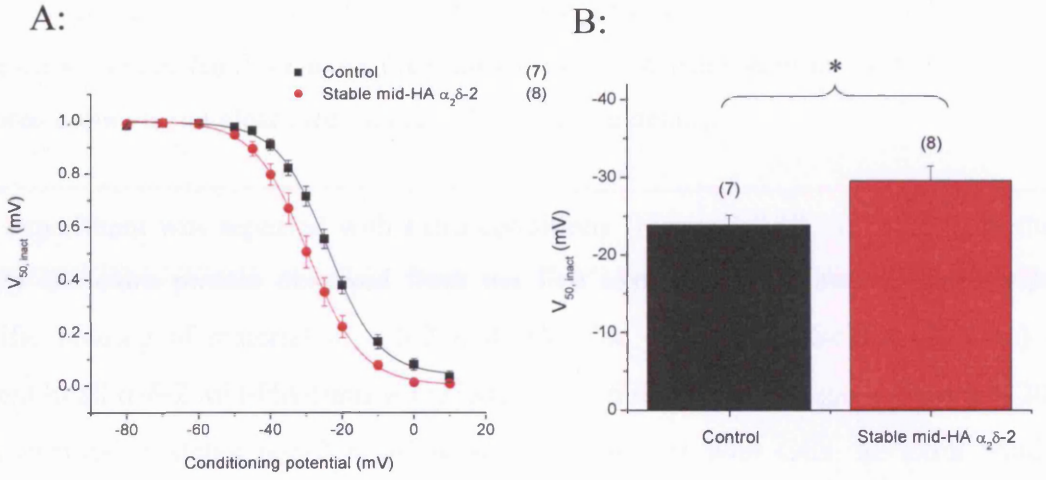

Figure 3.8. Effect of stable $\alpha_2\delta$-2 mid-HA expression on the steady-state inactivation of $Ca_v2.1$, β4 currents. (**A**), Steady-state inactivation curves for control $Ca_v2.1$, β4 (black squares, n=7) and $Ca_v2.1$, β4, stable $\alpha_2\delta$-2 mid-HA (red circles, n=8) conditions. (**B**), Mean $V_{50,\ inact}$ data were obtained by fitting a Boltzmann function to individual steady-state inactivation curves. Individual values for $V_{50,\ inact}$ in the $\alpha_2\delta$-2 condition are shown. * denotes P<0.05, (Student's t test).

3.2.5.3 Protein from the GC cultures binds to $\alpha_2\delta$–2 mid-HA

Initially, it was important to ascertain whether of not any proteins from the GC cultures bound to $\alpha_2\delta$-2. In order to do this, co-immunoprecipitation experiments were carried out using co-cultures of tsA-201 cells (stably expressing $\alpha_2\delta$-2 mid-HA) and GC cultures.

Two co-immunoprecipitation experiments were carried out (Figure 3.9). These involved lysis and solubilisation of cells in tsA-201 / GC co-cultures, and binding of $\alpha_2\delta$-2 mid-HA protein to protein G / sepharose beads. This was followed by SDS-PAGE separation

and silver-staining of the gel in order to detect protein (see Materials and Methods). The first experiment (Figure 3.9 A) compared tsA-201 transfected with $Ca_v2.1$, β4, stable $\alpha_2\delta$-2 mid-HA cultured either alone, or with GCs to see if any extra protein would be bound to the $\alpha_2\delta$-2 mid-HA. Extra protein was observed at ~70 kDa. Whether this represents another band, or extra material (of the same band seen in the tsA-201 cells cultured alone) is not clear (see Figure 3.9 B for more detail).

The experiment was repeated with extra conditions (Figure 3.9 C), in order to further clarify the extra protein observed from the first experiment. Column 5 shows non-specific binding of material to $\alpha_2\delta$-2 mid-HA. The $\alpha_2\delta$ protein itself (~170 kDa) is present in all $\alpha_2\delta$-2 mid-HA-transfected lanes (3, 4, 6 and 7). Once again, when tsA-201 cells expressing stable $\alpha_2\delta$-2 mid-HA were co-cultured with GCs, an extra band / additional protein was observed at ~70 kDa (black arrow in Figures 3.9 C & D). This material was not observed in co-cultures which did not express stable $\alpha_2\delta$-2 mid-HA (lane 5). In addition to the extra material observed at ~70 kDa, two further bands of ~75 kDa (red arrow) and ~65 kDa (green arrow) were observed (Figures 3.9 C & D).

This result suggested that protein from the GC cultures bound to the mid-HA $\alpha_2\delta$-2 expressed on tsA-201 cells. At this point, there was no way of distinguishing any difference as being an effect of ligand binding to the VWA domain rather than some other effect elicited by the GCs. For a VWA domain ligand to be detected by co-immunoprecipitation, it had to remain bound to the VWA domain for the entirety of the immunoprecipitation process. The switching of the VWA to the inactive state in the absence of divalent cations also had to be considered. However, although the likelihood of one of the identified extra proteins being a VWA domain ligand was negligible, it was still investigated by electrophysiology. This involved examining the currents formed by $Ca_v2.1$, β4, stable mid-HA $\alpha_2\delta$-2 expressed in tsA-201 cells, according to their proximity to GC projections.

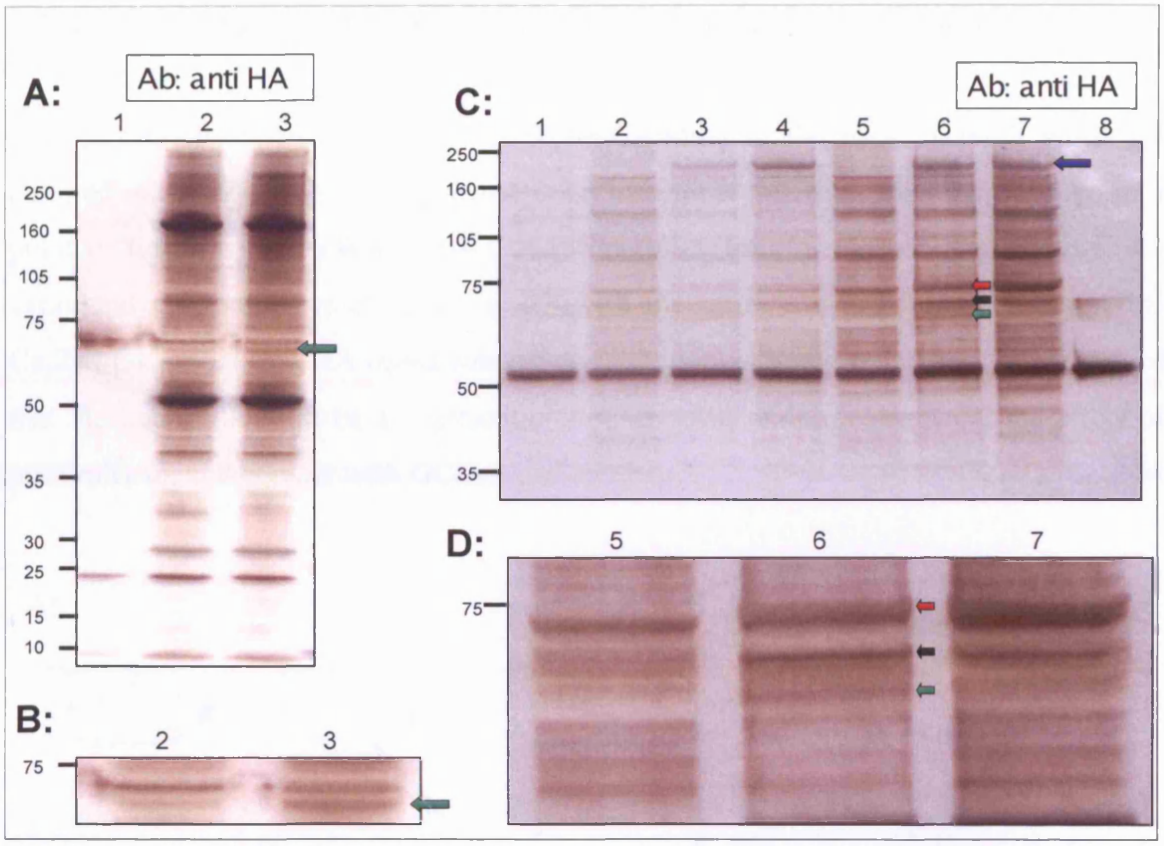

Figure 3.9. Co-immunoprecipitation of tsA-201 / GC co-cultures. (**A**), Silver-stained 3-8% tris-acetate gel of protein pulldown using Protein G / sepharose beads and anti-HA antibody. Lane 1- Protein G; lane 2- tsA-201 expressing $Ca_v2.1$, β4 stable $\alpha_2\delta$-2 mid-HA; lane 3- tsA-201 expressing $Ca_v2.1$, β4 stable $\alpha_2\delta$-2 mid-HA + GC. Green arrow refers to an additional protein band at ~70 kDa in co-cultures. (**B**), Enlarged section of lanes 2 and 3 in the region of 75 kDa. (**C**), Silver-stained 3-8% tris-acetate gel of protein pulldown using Protein G / sepharose beads and anti-HA antibody. Lane 1- GC; lane 2- untransfected tsA-201 + GC; lane 3- tsA-201 expressing stable $\alpha_2\delta$-2 mid-HA; lane 4- tsA-201 expressing $Ca_v2.1$, β4 stable $\alpha_2\delta$-2 mid-HA; lane 5- untransfected tsA-201 + GC; lane 6- tsA-201 expressing stable $\alpha_2\delta$-2 + GC; lane 7- tsA-201 expressing $Ca_v2.1$, β4 stable $\alpha_2\delta$-2 mid-HA +GC. Additional protein bands in co-cultures were observed at ~75 kDa (red arrow), ~70 kDa (black arrow) and ~65 kDa (green arrow). The blue arrow refers to $\alpha_2\delta$-2 mid-Ha protein. (**D**), Enlarged section of lanes 5-7 in the region of 75 kDa. Arrows refer to additional protein in co-cultures.

3.2.5.4 Whole-cell electrophysiology using tsA-201 / GC co-cultures

Having established the possibility of protein binding to the $\alpha_2\delta$-2 subunit when co-cultured with GCs, cells were patched in an attempt to see the effect that binding of a putative ligand to the VWA domain might have on the currents obtained through co-expressed calcium channel subunits. As with the co-immunoprecipitation assay, the $Ca_v2.1$, β4, stable mid-HA $\alpha_2\delta$-2 subunit combination was selected. It was hypothesised that the ligand likely to be an extracellular or secreted protein. Therefore, the effect of proximity to, and contact with GCs was investigated.

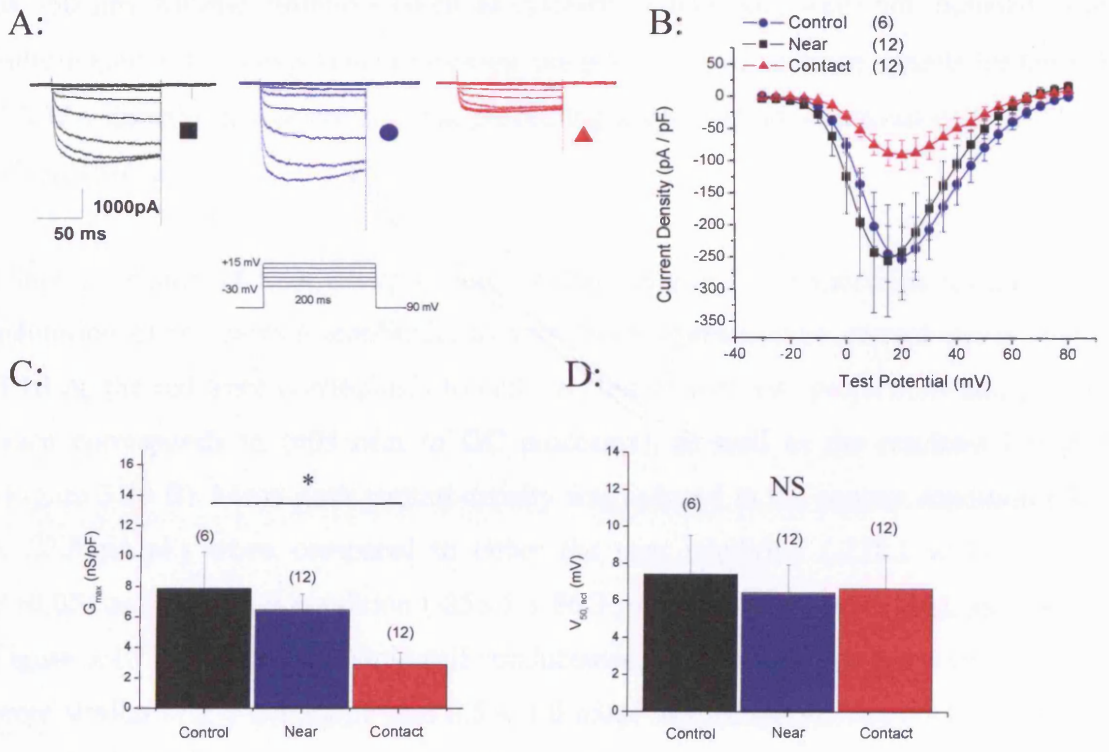

Figure 3.10. GC contact inhibits I_{Ba} in cells expressing $Ca_v2.1$, β4, stable $\alpha_2\delta$-2 mid-HA. (**A**), Representative current traces for the three conditions in response to -30 to +15 mV voltage steps. (**B**), Current-voltage relationships for $Ca_v2.1$, β4, stable $\alpha_2\delta$-2 mid-HA cultured alone (control condition; black, n=6), near to GC projections (blue, n=12) and in contact with GC projections (red, n=12) conditions ($P<0.05$, ANOVA). All currents are normalised to whole-cell capacitance and plotted against membrane

potential. Holding potential was -90 mV. Mean values for G_{max} (**C**) and $V_{50,\,act}$ (**D**) were obtained from fits of individual I-V relationships using the IVFIT function. Mean G_{max} of the control condition was significantly higher than the contact condition ($P<0.05$, ANOVA), this was not the case for the near condition. No significant difference in $V_{50,\,act}$ of the three conditions was observed ($P>0.05$, ANOVA)

The conditions were defined as follows. tsA-201 cells seen touching or laying on top of a GC projection were defined as "in contact". tsA-201 cells which appeared in the same field of view as a GC was defined as "near". This distance could feasibly have been up to ~50 μm. Mitotic inhibitors (such as cytosine arabinoside) were not included in the culture media. In an experiment assessing the possibility of secreted ligands for the $\alpha_2\delta$-2 VWA domain, it was not felt that preventing growth of non-neuronal cells would be advantageous.

Close proximity of VGCC-expressing tsA-201 cells to GC projections resulted in an inhibition of the current amplitude, as seen from representative current traces (Figure 3.10 A, the red trace corresponds to cells in contact with GC projections and the blue trace corresponds to cells near to GC processes), as well as the resultant I-V plots (Figure 3.10 B). Mean peak current-density was reduced in the contact condition (-91.3 ± 22.8 pA/pF) when compared to either the near condition (-228.1 ± 39.2 pA/pF, $P>0.05$) or the control condition (-255.5 ± 86.3 pA/pF, $P>0.05$, ANOVA), as shown in Figure 3.10 B. Regarding whole-cell conductance, both the control and near conditions were similar (7.9 ± 2.4 nS/pF and 6.5 ± 1.0 nS/pF respectively). The control condition was significantly larger than that of the contact condition (2.9 ± 0.8 nS/pF, $P>0.05$ ANOVA), shown in Figure 3.10 C. Despite the reduction in mean peak-current density seen in the contact condition, no change was observed in the voltage-dependence of current activation, with the $V_{50,\,act}$ similar in all three conditions (+7.4 ± 2.1 mV in the control condition, +6.4 ± 1.5 mV in the near condition, +6.6 ± 1.8 mV in the contact condition), shown in Figure 3.10 D.

Steady-state inactivation was also affected by proximity to GC projections (Figure 3.11). Shown in Figure 3.11 A are the three experimental conditions (along with a green dotted line corresponding to previous data obtained for the $Ca_v2.1$, β4 subunit combination, in order to illustrate the steady-state inactivation in the absence of $\alpha_2\delta$-2). Whilst no significant change was observed in $V_{50,\ inact}$ of the near condition compared to control condition ($V_{50,\ inact}$ values of -32.7 ± 1.4 mV and -30.7 ± 1.1 mV respectively, ANOVA), a significant hyperpolarisation in $V_{50,\ inact}$ was observed in the contact condition (-37.9 ± 1.6 mV) compared to mean $V_{50,\ act}$ for the control condition ($P<0.05$, ANOVA). This is shown in Figure 3.11 B.

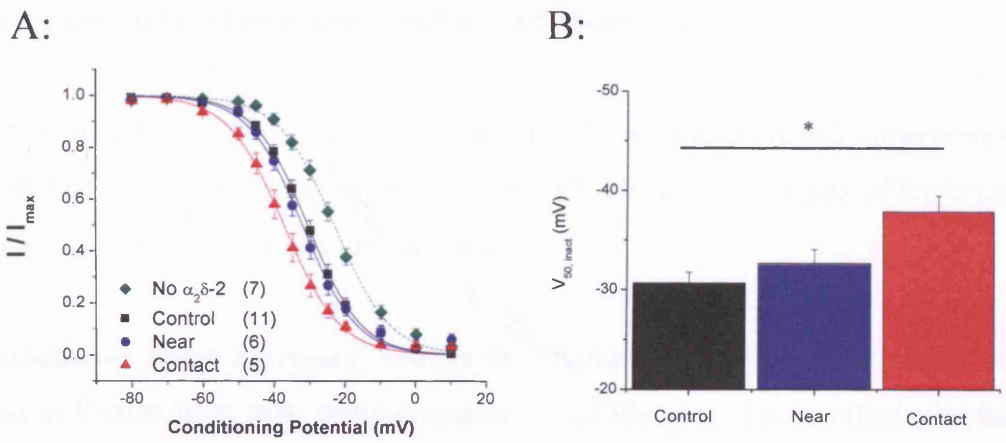

Figure 3.11. Effect of GC projection contact on the steady-state inactivation of $Ca_v2.1$, β4, stable $\alpha_2\delta$-2 mid-HA currents. (**A**), Steady-state inactivation curves for control (black, n=11), near to (blue, n=6) and in contact with GC projection (red, n=5) conditions ($P<0.05$), also displayed is a representative mean curve for $Ca_v2.1$, β4 currents from unpaired data (green, n=7). (**B**), Mean $V_{50,\ inact}$ data were obtained by fitting a Boltzmann function to individual steady-state inactivation curves. * denotes $P<0.05$ between mean $V_{50,\ inact}$ of the contact condition and control condition (ANOVA).

3.3 Discussion

The co-expression of $\alpha_2\delta$-2 as a VGCC auxiliary subunit

The discovery of a VWA domain (Whittaker and Hynes, 2002) within the $\alpha_2\delta$ subunit (see Introduction) suggested that $\alpha_2\delta$ might make functional adhesion interactions via this domain in a divalent cation dependent process, much in the same way as integrins and other VWA domain-containing proteins. Experiments using an $\alpha_2\delta$-2 subunit containing a mutated MIDAS motif (Canti et al., 2005) also suggested that the $\alpha_2\delta$-2 VWA domain was important in the intracellular interaction the $\alpha_2\delta$ makes with the $Ca_v\alpha_1$ subunit to enhance its cell-surface expression.

Before using the $\alpha_2\delta$-2 μMIDAS construct, the effects of $\alpha_2\delta$-2 co-expression were examined, when transiently expressed in the tsA-201 cell-line as part of the heterologous $Ca_v2.1$, β4, $\alpha_2\delta$-2 subunit combination.

$\alpha_2\delta$ subunits affect expressed VGCCs in a number of ways (see Introduction). From what is known from their characterisation so far, the modulatory effects are fairly well conserved amongst the 4 isoforms of $\alpha_2\delta$. Co-expression of $\alpha_2\delta$ subunits causes an increase in observed current amplitude through VGCCs (Qin et al., 2002; Klugbauer et al., 1999; Singer et al., 1991). However, the importance of a β subunit (and more specifically the exact isoform of β subunit) must also be taken into account (Walker and De Waard, 1998). The most well characterised $\alpha_2\delta$ subunit, $\alpha_2\delta$-1, is known to increase activation and inactivation kinetics, as well as hyperpolarising both the steady-state inactivation and I-V curves (Singer et al., 1991; Welling et al., 1993; Bangalore et al., 1996). The results of the $\alpha_2\delta$-2 co-expression experiment (Figures 3.1 – 3.3) agree with previous studies which have reported these effects.

Non-functionality of the $\alpha_2\delta$-2 μMIDAS construct

The use of the $\alpha_2\delta$-2 μMIDAS construct illustrates the importance of the $\alpha_2\delta$-2 VWA domain. In this study, the lack of a functional VWA domain resulted in an inability of $\alpha_2\delta$-2 to enhance current density when co-expressed with $Ca_v2.1$, β4 subunits. These data are in agreement with data (obtained in the lab at the same time as this study was carried out), which demonstrates this lack of function as resulting from the failure of $\alpha_2\delta$-2 μMIDAS to enhance $Ca_v2.2$ trafficking and subsequent cell-surface expression (Canti et al., 2005).

The $\alpha_2\delta$-2 μMIDAS mutation was further characterised by Canti et al., (2005). $\alpha_2\delta$-2 μMIDAS was expressed to the same extent as WT $\alpha_2\delta$-2 when expressed alone (i.e. in the absence of $Ca_v2.2$). It also bound GBP with the same affinity (Canti et al., 2005), suggesting that the $\alpha_2\delta$-2 μMIDAS is functionally expressed and properly folded when expressed alone, but retained intracellularly when co-expressed with $Ca_v2.2$ (and β1b), hence the lack of enhanced current amplitude and failure to hyperpolarize $V_{50,\ inact}$ of expressed currents.

The binding of divalent cations to the $\alpha_2\delta$ MIDAS motif is also important, given that it is an auxiliary subunit of a calcium channel. Replacing Ba^{2+} ions with Na^+ ions as the charge carrier (calcium channels also permit Na^+ ion permeation, but only in the complete absence of divalent cations) still did not cause an $\alpha_2\delta$-mediated enhancement of current amplitude in the $\alpha_2\delta$-2 μMIDAS condition (Canti et al., 2005), suggesting the μMIDAS did not affect the ability of ions to permeate through the channels.

Membrane protein processing (after the assembly of an amino acid chain at the ribosome) involves the ribosome / nascent peptide / translocon complex. The nascent peptide is fed from the ribosome, through the translocon- and is arranged across the ER membrane (Deutsch, 2003). When $\alpha_2\delta$-2 μMIDAS is co-expressed with $Ca_v2.2$, it appears that both subunits are "trapped" in an intracellular compartment- most likely the

ER (Canti et al., 2005). Therefore the interaction between $\alpha_2\delta$ and $Ca_v\alpha_1$ subunits is likely to be during their time in the ER, although the exact mechanism is not clear.

It is not known whether the VWA-mediated interaction between the $\alpha_2\delta$ and $Ca_v\alpha_1$ subunits involves an immature $\alpha_2\delta$ protein, or a fully processed one. However, the $\alpha_2\delta$ subunit undergoes glycosylation and cleavage steps before its functional expression (Douglas et al., 2006). $\alpha_2\delta$ subunits that are not fully glycosylated fail to enhance current amplitude to the same extent as fully glycosylated $\alpha_2\delta$ (Sandoval et al., 2004). It has been shown that the vast majority of $\alpha_2\delta$ remains un-cleaved following heterologous expression (Douglas et al., 2006). The $\alpha_2\delta$ subunits in these cells still produce an enhancement of current amplitude, although it is not clear whether this effect is mediated by un-cleaved $\alpha_2\delta$, or by the small proportion of cleaved $\alpha_2\delta$. Therefore, it is feasible that the $\alpha_2\delta$ VWA domain-mediated enhancement of trafficking occurs in the ER after glycosylation, and could occur before or after cleavage into α_2 and δ.

The function of $\alpha_2\delta$ as an auxiliary subunit aiding the trafficking of the pore-forming subunit is not unique. The calcium channel β subunit binds to the I-II loop of the $Ca_v\alpha_1$ subunit in the ER and blocks an ER retention signal located on the $Ca_v\alpha_1$ subunit (Bichet et al., 2000). This $Ca_v\alpha_1$ retention signal acts as both a quality control mechanism and an expression "brake", with the result that control over $Ca_v\beta$ subunit expression leads to control over the functional expression of $Ca_v\alpha_1$ subunits. Facilitating ER transport is a major activity of many ion channel subunits, preventing ER retention and helping subunit proteins enter the ER exit pathway.

Ligands of the $\alpha_2\delta$-2 VWA domain

The importance of the $\alpha_2\delta$ VWA domain in the role of trafficking the $Ca_v\alpha_1$ subunit to the membrane is detailed above, and this intracellular action may well be the only role of the VWA domain. An effort to identify the VWA domain binding site on $Ca_v2.2$ (using

the D325N and D325S mutations) proved unsuccessful (Figure 3.5). The experiment was carried out in the absence of a negative control for the $\alpha_2\delta$ subunit, however the peak-current density and whole-cell conductance of currents obtained from both mutants was similar to that of the control condition. Therefore, the putative site on the $Ca_v\alpha_1$ subunit where the $\alpha_2\delta$ VWA domain binds remains unidentified.

The importance of VGCCs at the presynaptic membrane is well established (Dunlap et al., 1995). In addition, it has been shown that association of neuronal VGCCs with laminin is important in the formation and maintenance of active zones in the synaptic cleft (Nishimune et al., 2004). This interaction is just one of many adhesion interactions in the synaptic cleft required to maintain the synapse. The possibility of the VGCC $\alpha_2\delta$ subunit being involved in a trans-synaptic interaction with a post-synaptic protein is plausible, perhaps to maintain positioning of VGCCs within the active zone.

Some of the most widespread proteins to carry the VWA domain are those of the integrin family. These are proteins comprised of an α and a β subunit, both of which span the cell membrane, with the majority of the protein in the extracellular space (Arnaout et al., 2005). 18 α subunits and 8 β subunits have been identified in mammals, which assemble to form 24 different integrins (Hynes, 2002). The VWA domain is found in roughly half of the known integrin α-subunits (Arnaout et al., 2005), where it forms the functional binding site. The presence of the VWA domain in integrins is integral for their role in binding extracellular molecules, for example fibronectin and laminin via an RGD amino acid motif (Arnaout et al., 2005), and linking them across the cell membrane to the cytoskeleton.

Much like integrins, VGCC $\alpha_2\delta$ subunits contain a VWA domain in the extracellular portion of the protein. Whether this confers a physical adhesion or signalling function to the $Ca_v\alpha_1$ subunit is not yet known, neither is the mechanism by which the VWA domain of $\alpha_2\delta$ enhances the cell-surface expression of VGCCs. It is believed that the δ subunit makes an interaction with the $Ca_v\alpha_1$ subunit at the cell-surface, through which

the biophysical effects on $\alpha_2\delta$-channel properties are elicited (Felix et al., 1997). Should the VWA domain-containing α_2 subunit make an additional extracellular interaction with the $Ca_v\alpha_1$ subunit, this is not apparent from changes in channel permeation properties (Canti et al., 2005).

The $\alpha_2\delta$ VWA domain may have an additional role in EC activity

There are other means of investigating the inhibitory effect of GC proximity. These would include using co-expression of the $\alpha_2\delta$-2 μMIDAS construct in an attempt to establish whether the inhibitory effects on I_{Ba} occurred as a result of ligand binding the VWA domain.

The study failed to identify a binding partner for the $\alpha_2\delta$-2 VWA domain. A small number of candidate ligand proteins were identified in the co-immunoprecipitation experiment (for example one at ~70 kDa, Section 3.2.5.3). However the amount of cerebellar material required in order to produce sufficient protein for identification of these bands proved prohibitive. In addition, the lack of a tagged $\alpha_2\delta$-2 μMIDAS meant that the extra protein bands observed in co-cultures could not necessarily be attributed to material binding to the VWA domain. Other means of purifying a putative ligand (such as the use of antibody columns) would encounter the same problems, and therefore this work remains within the scope for future experimentation.

Contact with GC projections resulted in an inhibition of current amplitude in $Ca_v2.1$, β4, stable $\alpha_2\delta$-2 mid-HA (expressed in tsA-201 cells). Once again, it was not possible to determine if this inhibitory effect was absent from an $\alpha_2\delta$-2 μMIDAS condition as a stable mid-HA tagged cell-line was not produced. Therefore the inhibitory effect cannot be attributed to an adhesion interaction at the VWA domain, rather it may be a non-specific effect. In addition to the use of a stable $\alpha_2\delta$-2 μMIDAS cell-line, a control

condition measuring currents through expressed potassium or sodium channels would be able to determine whether this is the case.

Conclusion

The $\alpha_2\delta$ VWA domain has been shown to be important in the intracellular interaction between the $Ca_v\alpha_1$ and $\alpha_2\delta$ subunits which allows enhancement of $Ca_v\alpha_1$ cell-surface expression. Mutation of amino acids in the MIDAS motif of the $\alpha_2\delta$-2 subunit prevents enhancement of cell-surface expression of the VGCC complex (Canti et al., 2005). This may be the result of inability of the VWA to function (in terms of ligand binding) This study provides evidence that the $\alpha_2\delta$-2 subunit binds (an as-tey unidentified) protein when stably expressed in tsA-201 cells and co-cultured with GCs, and demonstrates an inhibitory effect of GC contact upon $Ca_v2.1$, $\beta4$, stable $\alpha_2\delta$-2 mid-HA currents. The study does not however attribute these observed effects directly to involvement of the $\alpha_2\delta$-2 VWA domain.

Chapter 4: Results

Effects of mutation of an RRR motif on the $\alpha_2\delta$ subunit necessary for gabapentin binding.

4.1 Introduction

The mutation of an RRR motif in the $\alpha_2\delta$ subunit (RRA) results in an $\alpha_2\delta$ protein that displays negligible GBP binding (Wang et al., 1999). This mutation has been previously engineered into $\alpha_2\delta$-1 (R217A) and $\alpha_2\delta$-2 (R282A) subunits (Wang et al., 1999; Davies et al., 2006). This chapter details some experiments carried out to examine the effect of the RRA mutation on the function of $\alpha_2\delta$ at the cellular level.

Once the VGCC $\alpha_2\delta$ subunit was established as the binding protein for GBP, it was proposed that the anti-epileptic effects of GBP might be mediated through the $\alpha_2\delta$ subunit, resulting in an inhibitory effect on the VGCCs with which they associate (Gee et al., 1996). A subsequent study (Wang et al., 1999) located a number of regions within the α_2 portion of the subunit that were important for GBP binding. These included residues 206-222, 516-537 and 583-603 (in porcine $\alpha_2\delta$-1). In addition, a single-point arginine to alanine mutation at residue 217 resulted in an $\alpha_2\delta$-1 protein that displayed negligible GBP binding.

$\alpha_2\delta$-1 null mutant mice die during embryonic development, making it difficult to examine the importance of $\alpha_2\delta$-1 in terms of physiological function and drug-binding (Joshi and Taylor, 2006). However, a transgenic knock-in mouse-line containing the $\alpha_2\delta$-1 R217A mutation was produced, in order to determine the location and importance of GBP binding to the $\alpha_2\delta$-1 subunit (Bian et al., 2006). Autoradiographic binding studies using this transgenic mouse strain found a loss of binding of both ^{3}H-GBP and ^{3}H-PGB in areas of the brain and spinal cord which express $\alpha_2\delta$-1, compared to significant binding in the wildtype mice. Binding of these ligands was still present in areas such as Purkinje cells in the Purkinje cell layer and the molecular layer of the cerebellum, due to the presence of $\alpha_2\delta$-2.

However, the protein expression of $\alpha_2\delta$-1 R217A (in neocortex brain samples taken for western blot analysis) was similar to that of WT $\alpha_2\delta$-1, as was the level of expressed

$\alpha_2\delta$-1 R217A mRNA (Field et al., 2006). $\alpha_2\delta$-1 R217A mice displayed no grossly abnormal phenotype (Field et al., 2006; Bian et al., 2006), and exhibited much the same normal behaviour as WT mice such as the nocifensive response to formalin injection. Whole-cell recording of DRG neurons cultured from $\alpha_2\delta$-1 R217A mice found a similar current amplitude to those of WT mice (Field et al., 2006), suggesting the $\alpha_2\delta$-1 R217A mutation did not impair the current amplitude in native neurons. However, $\alpha_2\delta$-1 R217A mice were non-responsive to PGB or GBP in a chronic constriction injury model of neuropathic pain, but responsive to opiates and to the tricyclic antidepressant amitriptyline (Field et al., 2006). An additional study showed (100 μM) PGB to reduce the strength of muscle contractions, through presynaptic action at the neuromuscular junction (rather than an effect on excitation-contraction coupling). This effect was seen in WT , but not $\alpha_2\delta$-1 R217A mice (Joshi and Taylor, 2006).

Given the importance of the RRR motif on $\alpha_2\delta$-1 and $\alpha_2\delta$-2 subunits for binding GBP, it was of interest to know the implications of disrupting this motif. Therefore, effects of RRR motif disruption were investigated in this study. The $\alpha_2\delta$-1 R217A and $\alpha_2\delta$-2 R282A mutant subunits were co-expressed in tsA-201 cells along with $Ca_v\alpha_1$ and β subunits to determine what the implications would be on the observed effects of $\alpha_2\delta$ co-expression (see Chapter 3). The function of the RRR motif had already been established (Wang et al., 1999), however the normal functionality of RRA mutant $\alpha_2\delta$ subunits (i.e. in the absence of GBP) had not been tested. This was therefore the aim of the study.

A previous study has shown that dilaysis of membrane preparations (expressing $\alpha_2\delta$-1) results in the removal of a bound ligand (< 12 kDa in size) from the $\alpha_2\delta$-1 protein, and that removal of this ligand results in an increase in affinity in $\alpha_2\delta$-1 ^{3}H-GBP binding (Dissanayake et al., 1997). This raises the possibility that GBP binding to $\alpha_2\delta$ subunits may interfere with the binding of a ligand normally bound to $\alpha_2\delta$ subunits. As non GBP-binding proteins, the RRA mutant $\alpha_2\delta$ proteins might also not bind this ligand. The inability of RRA mutant $\alpha_2\delta$ subunits to bind this ligand might potentially explain any differences seen when compared to WT $\alpha_2\delta$ subunits.

Two $\alpha_2\delta$-1 R217A subunits were used in this the study: porcine and rat $\alpha_2\delta$-1 R217A (see Section 2.1.2). The porcine $\alpha_2\delta$-1 R217A has been described previously (Wang et al., 1999). The rat $\alpha_2\delta$-1 R217A (as well as the rat $\alpha_2\delta$-2 R282A) was produced in the lab (by Wendy Pratt).

4.2 Results

4.2.1 Radioligand binding

GBP binding to the $\alpha_2\delta$ subunit has been previously demonstrated for both $\alpha_2\delta$-1 and $\alpha_2\delta$-2, but not $\alpha_2\delta$-3 or $\alpha_2\delta$-4 (Marais et al., 2001; Qin et al., 2002; Gong et al., 2001). These subunits do not possess the RRR motif necessary for GBP binding (Wang et al., 1999). Previous studies have demonstrated a lack of PGB binding to the $\alpha_2\delta$-1 R217A protein in comparison to WT $\alpha_2\delta$-1, both in autoradiographic studies on brain and spinal cord (Bian et al., 2006) as well as in GBP binding assays using porcine $\alpha_2\delta$-1 R217A transiently expressed in HEK293 cells (Field et al., 2006).

In this study, radioligand binding assays were carried out to determine the amount of GBP-binding to (the previously untested) rat $\alpha_2\delta$-1 R217A relative to rat WT $\alpha_2\delta$-1. ^{3}H-GBP was used as the radioligand (see Materials and Methods, Section 2.6). $\alpha_2\delta$ was transfected alone (i.e. in the absence of other VGCC subunits). Co-expression of other VGCC subunits was not expected to cause a significant increase in cell-surface $\alpha_2\delta$ subunit expression (altering binding) to warrant their presence.

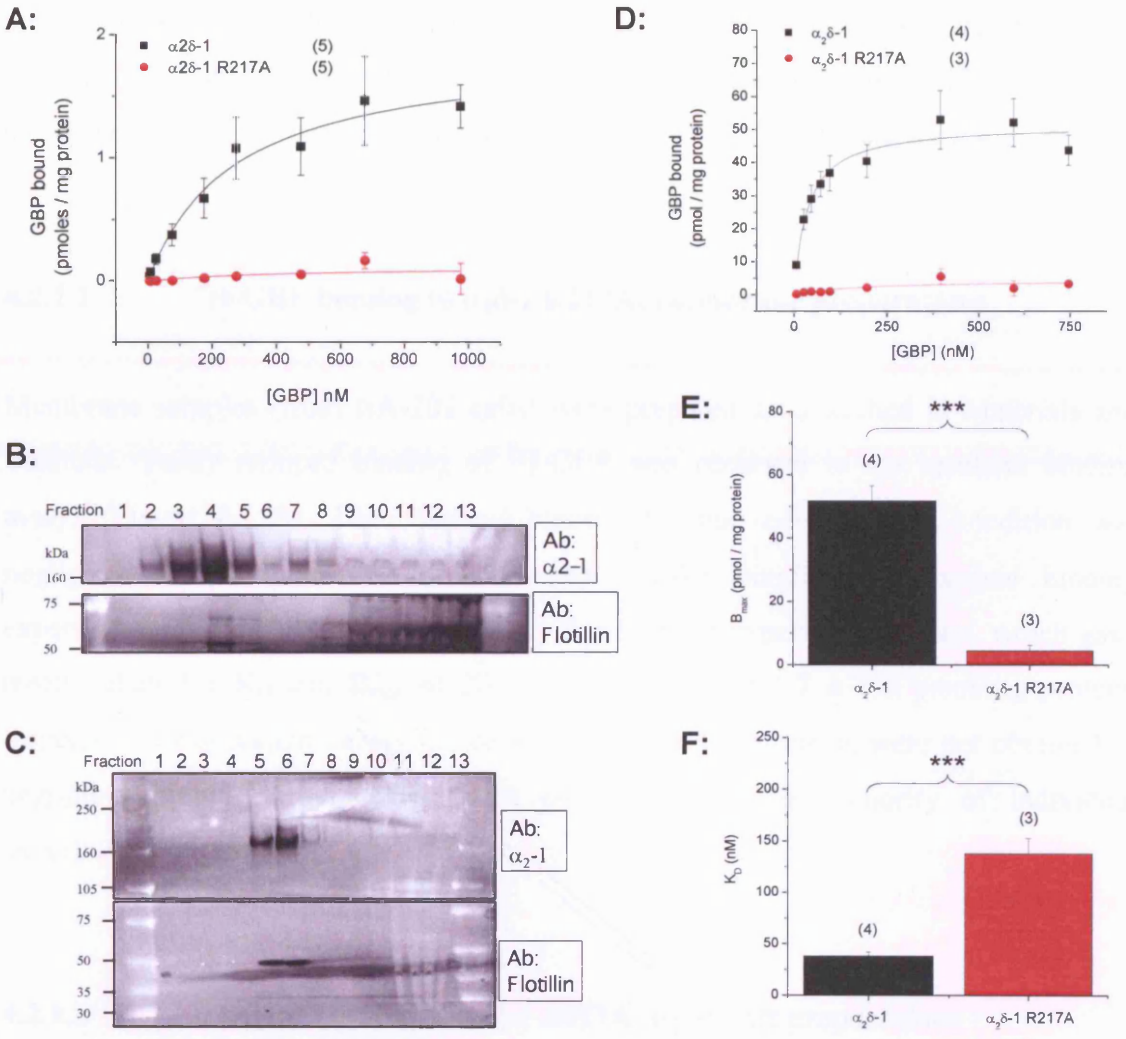

Figure 4.1. The $\alpha_2\delta$-1 R217A mutation results in impaired ^{3}H-GBP binding. (**A**), Specific binding of ^{3}H-GBP to membranes from cells expressing WT $\alpha_2\delta$-1 (black squares, n=5) or $\alpha_2\delta$-1 R217A (red circles, n=5). The curves are hyperbolae fitted to the mean data. (**B**), $\alpha_2\delta$-1 is present in lipid raft peak-fractions. An anti $\alpha_2\delta$-1 immunoreactive band at ~170 kDa is present in a number of lipid-raft fractions (top panel), but mainly in the peak-fractions (4 & 5), corresponding to the presence of an anti-flotillin-1 immunoreactive band at 50 kDa (lower panel). (**C**), $\alpha_2\delta$-1 R217A was present in lipid-raft fractions. Anti-$\alpha_2\delta$-1 immunoreactivity was detected in the peak-fractions (5 & 6), which corresponded to immunoreactivity for anti-flotillin-1. (**D**), Specific binding of ^{3}H-GBP to lipid rafts from cells expressing WT $\alpha_2\delta$-1 (black

squares, n=4) or $\alpha_2\delta$-1 R217A (red circles, n=3). The curves are hyperbolae fitted to the mean data. Mean values for B_{max} (**E**) and K_D (**F**) were calculated from fitting individual experiments with a hyperbola function. *** denotes P<0.001 (Student's t-test).

4.2.1.1 ^{3}H-GBP binding to $\alpha_2\delta$-1 R217A: membrane preparations

Membrane samples (from tsA-201 cells) were prepared as described in Materials and Methods. Vastly reduced binding of ^{3}H-GBP was observed in the resultant binding assays (Figure 4.1 A). The observed binding for the $\alpha_2\delta$-1 R217A condition was negligible compared to that of the control $\alpha_2\delta$-1 condition. Individual binding experiments of the control condition were fitted with a hyperbola function, which gave mean values for K_D and B_{max} of 231.5 ± 33.8 nM and 1.7 ± 0.4 pmol/mg protein, respectively. Equivalent values for the $\alpha_2\delta$-1 R217A experiments were not obtained as negligible binding observed rendered curve-fitting to the majority of individual experiments impossible.

4.2.1.2 ^{3}H-GBP binding to $\alpha_2\delta$-1 R217A: lipid-raft preparations

Detergent-insoluble membrane fractions were prepared from WT $\alpha_2\delta$-1 and $\alpha_2\delta$-1 R217A-transfected cells, as these proteins localise in lipid-rafts, as discussed in the Introduction (Section 1.8.4). This allowed further characterisation of ^{3}H-GBP binding to $\alpha_2\delta$-1, as shown in Figure 4.1.

As shown in Figures 4.1 B and 4.1 C, both WT $\alpha_2\delta$-1 and $\alpha_2\delta$-1 R217A were found to be present in the Triton X-100-insoluble membrane fractions when separated across a sucrose gradient (see Materials and Methods). This indicated they localised to lipid rafts. ^{3}H-GBP binding to $\alpha_2\delta$-1 R217A in lipid raft fractions displayed the same significant reduction in binding (~100-fold decrease in B_{max}) when compared to WT $\alpha_2\delta$-1, as

shown in Figure 4.1 D. Despite the low amount of binding, it was possible to fit individual binding curves to $\alpha_2\delta$-1 R217A binding data, suggesting that binding still occurred. The observed B_{max} was reduced from 51.8 ± 4.8 pmol/mg protein in the control condition to 4.5 ± 1.8 pmol/mg protein in the $\alpha_2\delta$-1 R217A condition ($P<0.001$), as shown in Figure 4.1 E. The mean K_D (137.9 ± 14.8 nM) was significantly higher than the control condition (37.9 ± 4.1 nM, $P<0.001$), as shown in Figure 4.1 F. Additionally, ^{3}H-GBP binding to WT $\alpha_2\delta$-1 resulted in a significantly increased (6.1-fold) affinity (a K_D of 37.9 ± 4.1 nM in lipid-raft preparations, compared to 231.5 ± 33 nM in membrane samples, $P<0.01$).

4.2.2 Whole-cell electrophysiology

4.2.2.1 $\alpha_2\delta$-1 R217A does not enhance I_{Ba} to the same extent as WT $\alpha_2\delta$-1 when co-expressed with $Ca_v2.2$, β1b

Having confirmed that $\alpha_2\delta$-1 R217A is expressed in tsA-201 cells, but does not bind GBP, it was necessary to examine how it would compare to WT $\alpha_2\delta$-1 in terms of its ability to alter characteristics such as $V_{50,\,inact}$, $V_{50,\,act}$, and G_{max}. Therefore, tsA-201 cells co-expressing $Ca_v2.2$, β1b and either WT $\alpha_2\delta$-1 or $\alpha_2\delta$-1 R217A were subjected to whole-cell patch-clamp electrophysiology, as shown in Figure 4.2.

The immediate difference observed between currents obtained with $Ca_v2.2$, β1b co-expressed with either $\alpha_2\delta$-1 R217A or WT $\alpha_2\delta$-1 was a smaller enhancement of the current size (see sample traces in Figure 4.2 A), as well the mean current density across a range of test-potentials (Figure 4.2 B). The mean peak-current density recorded for the $\alpha_2\delta$-1 R217A condition was -94.1 ± 23.2 pA/pF, a value significantly lower than that recorded for the WT $\alpha_2\delta$-1 condition (-284.1 ± 85.5 pA/pF, $P<0.05$, ANOVA), but significantly increased over control (-39.8 ± 8.7 pA/pF, $P<0.05$, ANOVA). As shown in Figure 4.2 C, the $\alpha_2\delta$-1 R217A condition had an intermediate G_{max} as well, with a mean

value of (2.7 ± 1.0 nS/pF) compared to values of 7.5 ± 5.2 nS/pF for the WT condition (which was not significantly different at P<0.05, ANOVA) and 1.2 ± 1.0 nS/pF in the control condition (P<0.05, ANOVA). No significant differences in $V_{50,\,act}$ were observed between the $\alpha_2\delta$-1 R217A, WT $\alpha_2\delta$-1 and control conditions (Figure 4.2 D).

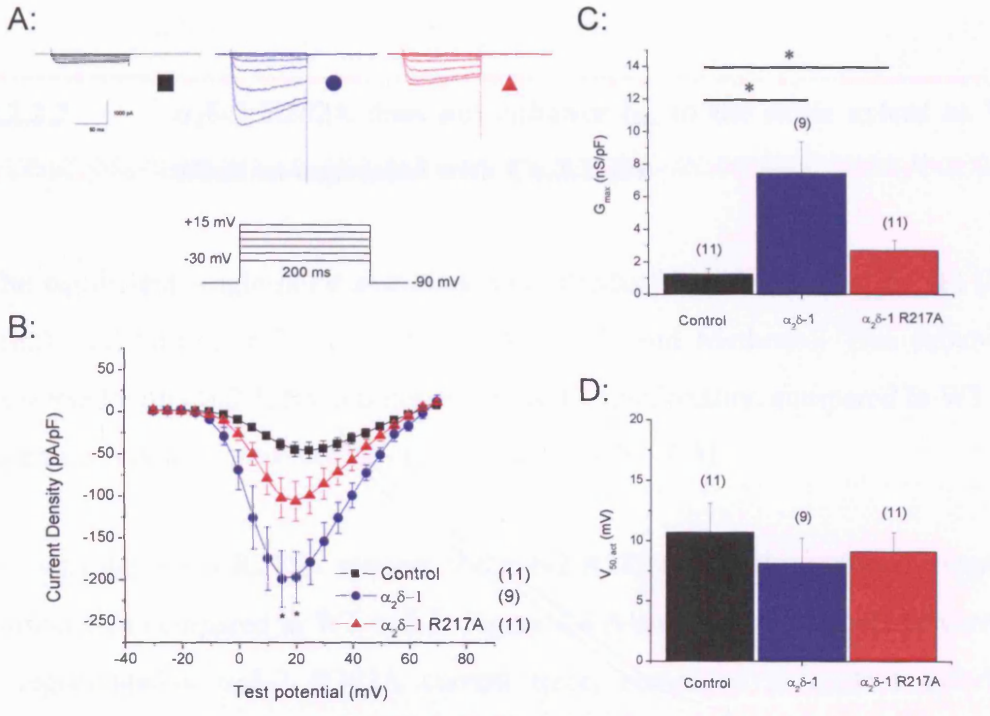

Figure 4.2. Submaximal enhancement of I_{Ba} with co-expression of $\alpha_2\delta$-1 R217A co-expressed with $Ca_v2.2$, β1b subunits. (**A**), Representative current traces for the three conditions in response to -30 to +15 mV voltage steps. A schematic of the I-V protocol is shown. (**B**), I-V relationships for I_{Ba} in the $Ca_v2.2$, β1b control (black squares, n=11), $\alpha_2\delta$-1 (blue circles, n=9) and $\alpha_2\delta$-1 R217A (red triangles, n=11) conditions (P<0.05, ANOVA). Current amplitude was normalised to whole-cell capacitance and plotted against membrane potential. Holding potential was -90 mV. Mean values for G_{max} (**C**) and $V_{50,\,act}$ (**D**) were obtained from fits of individual I-V relationships using the IVFIT function. A significant increase (P<0.05, ANOVA) in G_{max} was observed in the $Ca_v2.2$, β1b, WT $\alpha_2\delta$-1 condition and $\alpha_2\delta$-1 R217A conditions compared to control (P<0.05 for both, ANOVA). No significant diference among means values for $V_{50,\,act}$ was observed (P>0.05, ANOVA).

Unfortunately, due to the fragility of the cells when in the whole-cell configuration (as well as an increase in series resistance and I_{leak}), insufficient steady-state inactivation and long-pulse data were obtained to allow adequate analysis.

4.2.2.2 $\alpha_2\delta$-2 R282A does not enhance I_{Ba} to the same extent as WT $\alpha_2\delta$-2 when co-expressed with $Ca_v2.1$, $\beta4$

The equivalent single-point mutation was introduced into $\alpha_2\delta$-2 in the lab (by Wendy Pratt), and termed $\alpha_2\delta$-2 R282A (see Materials and Methods). This subunit was co-expressed with $Ca_v2.1$, $\beta4$ in order to assess its functionality, compared to WT $\alpha_2\delta$-2 and an empty-vector control condition (see Figures 4.3 – 4.5).

As with the $\alpha_2\delta$-1 R217A subunit, the $\alpha_2\delta$-2 R282A caused a reduced enhancement of current size compared to WT $\alpha_2\delta$-2. Figure 4.3 A shows the intermediate current size of a representative $\alpha_2\delta$-2 R282A current trace, compared to control and WT $\alpha_2\delta$-2 representative traces. The mean I-V curve of the $\alpha_2\delta$-2 R282A (Figure 4.3 B) was also intermediate between control and WT $\alpha_2\delta$-2 conditions, with a mean peak-current density of 162.8 ± 23.0 pA/pF, significantly larger than that of the control condition (-65.1 ± 9.3 pA/pF, $P<0.05$, ANOVA), and significantly lower than that of the WT $\alpha_2\delta$-2 (-241 ± 21.0 pA/pF $P<0.05$, ANOVA). The mean G_{max} of both the $\alpha_2\delta$-2 R282A condition (4.4 ± 0.6 nS/pF) and WT $\alpha_2\delta$-2 (6.1 ± 0.5 nS/pF,) conditions were increased over the value for control (1.8 ± 0.2 nS/pF, $P<0.05$, ANOVA), as shown in Figure 4.3 C. No significant differences were observed in $V_{50,\ act}$, with only a small non-significant hyperpolarisation seen in the WT $\alpha_2\delta$-2 condition (+3.9 ± 1.0 mV) compared to control (+7.2 ± 1.4 mV, $P>0.05$, ANOVA), and an intermediate value for the $\alpha_2\delta$-2 R282A condition (+6.2 ± 0.9 mV, $P>0.05$, ANOVA), shown in Figure 4.3 D.

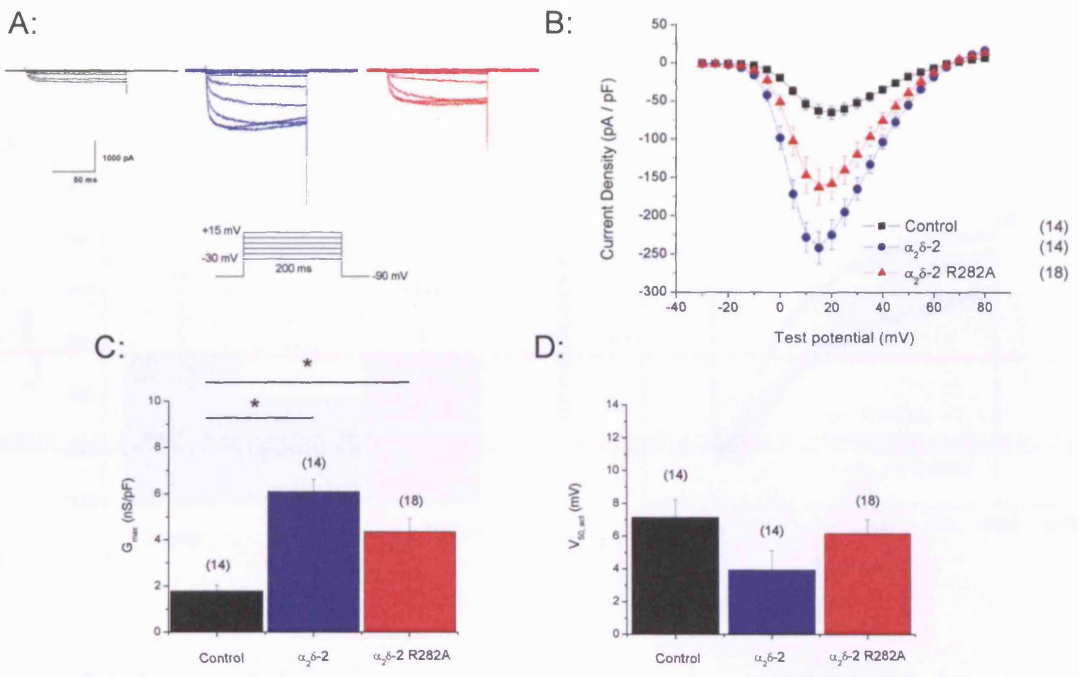

Figure 4.3. Current amplitude in the $\alpha_2\delta$-2 R282A condition is intermediate between the control and WT $\alpha_2\delta$-2 conditions. (**A**), Representative current traces for the three conditions in response to -30 to +15 mV voltage steps. A schematic of the I-V protocol is shown. (**B**), I-V relationships for I_{Ba} in the control (black squares, n=14), $\alpha_2\delta$-2 (blue circles, n=14) and $\alpha_2\delta$-2 R282A (red triangles, n=18) conditions. Current amplitude was normalised to whole-cell capacitance and plotted against membrane potential. Holding potential was -90 mV. Mean values for G_{max} (**C**) and $V_{50,\,act}$ (**D**) were obtained from fits of individual I-V relationships using the IVFIT function. G_{max} of both $\alpha_2\delta$-2 and $\alpha_2\delta$-2 R282A were significantly increased over the control condition ($P<0.05$, ANOVA). No significant difference was observed among values for $V_{50,\,act}$ ($P>0.05$, ANOVA).

No significant change was observed in the inactivation kinetics of the currents. τ_{inact} was similar between the $\alpha_2\delta$-2 and $\alpha_2\delta$-2 R282A conditions (279.9 ± 20.5 ms and 335.5 ± 41.6 ms respectively), although neither of these values were significantly different from control (338.4 ± 51.0 ms), as shown in Figure 4.4 A. Respresentative current traces are shown in Figure 4.5 B.

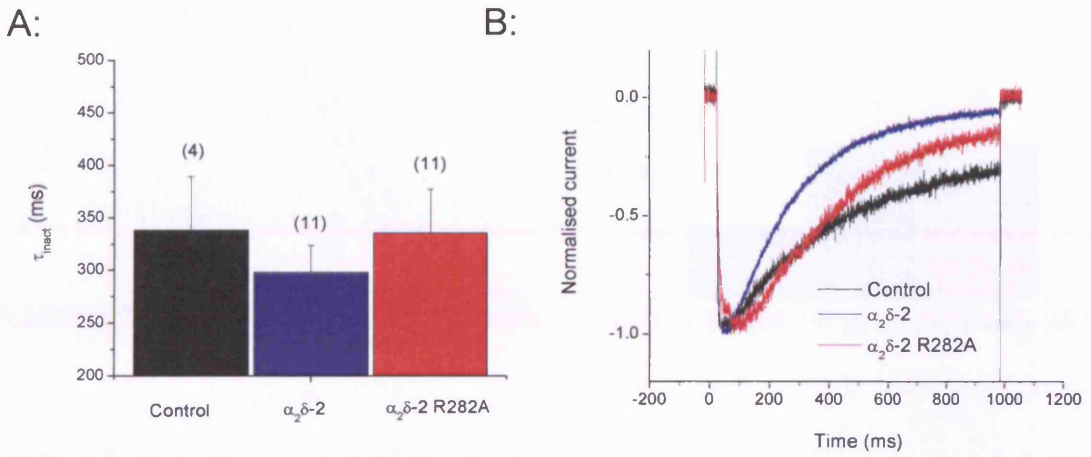

Figure 4.4. Inactivation kinetics of channels containing $\alpha_2\delta$-2 R282A (co-expressed with $Ca_v2.1$, β4 subunits) remain similar to those containing WT $\alpha_2\delta$-2. (**A**), Mean time-constant of inactivation (τ_{inact}) data is shown for control (black, n=4), WT $\alpha_2\delta$-2 (blue, n=11) and $\alpha_2\delta$-2 R282A (red, n=11) conditions. The decay phase of individual current traces at +10 mV was fitted with a single exponential function. Holding potential was -90 mV. (**B**) Representative current traces of control (black, n=4), WT $\alpha_2\delta$-2 (blue, n=11) and $\alpha_2\delta$-2 R282A (red, n=11) conditions in response to a long depolarising voltage step to +10 mV. Traces are normalised to peak. No significant difference among mean values for τ_{inact} was observed (ANOVA).

In addition to a sub-maximal enhancement of current size, the $\alpha_2\delta$-2 R282A condition had a similar mean effect on steady-state inactivation curve to WT $\alpha_2\delta$-2 (Figure 4.5 A). The mean $V_{50,\ inact}$ in the $\alpha_2\delta$-2 R282A condition (-37.3 ± 2 mV) was similar to the WT $\alpha_2\delta$-2 condition (-37.0 ± 2 mV), both of which were significantly more negative than the mean $V_{50,\ inact}$ observed in the control condition (-30.8 ± 1 mV, $P<0.05$ for both, ANOVA), as shown in Figure 4.5 B. This suggested $\alpha_2\delta$-2 R282A maintained its ability to hyperpolarise the steady-state inactivation curve.

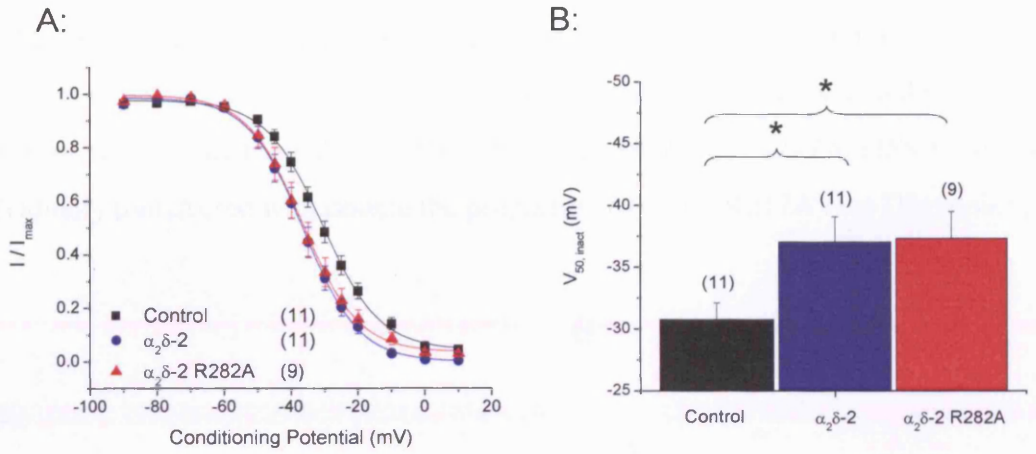

Figure 4.5. Hyperpolarisaton of the steady-state inactivation curve with $\alpha_2\delta$-2 R282A (co-expressed with $Ca_v2.1$, $\beta4$ subunits). (**A**), Steady-state inactivation curves for control (black squares, n=11), $\alpha_2\delta$-2 (blue diamonds, n-11) and $\alpha_2\delta$-2 R282A (red triangles, n=9) conditions. Holding potential was -100 mV. Curves are Boltzmann fits to the mean data. (**B**), Mean $V_{50,\ inact}$ data were obtained by fitting a Boltzmann function to individual steady-state inactivation curves. * denotes $P<0.05$ (ANOVA).

4.2.2.3 Increasing the proportion of $\alpha_2\delta$-1 R217A cDNA present in the transfection mixture did not cause a recovery of current amplitude

Both the $\alpha_2\delta$-1 R217A and $\alpha_2\delta$-2 R282A mutant constructs displayed an ability to enhance I_{Ba} when co-expressed with $Ca_v\alpha_1$ and β subunits, but not to the same extent as WT $\alpha_2\delta$-1 or WT $\alpha_2\delta$-2. However, co-expression of the $\alpha_2\delta$-2 R282A subunit still caused the characteristic hyperpolarisation of $V_{50,\ inact}$. One possible interpretation of this result was that the $\alpha_2\delta$-1 R217A and $\alpha_2\delta$-2 R282A did not facilitate the trafficking of as many $Ca_v\alpha_1$ subunits to the cell-surface (see Discussion). This raised questions as to the mechanism of $\alpha_2\delta$-mediated enhancement of $Ca_v\alpha_1$ expression, and also the efficiency and mechanism of heterologous expression of VGCC subunits.

An experiment was carried out to determine whether a higher proportion of $\alpha_2\delta$-1 R217A in the transfection mixture could result in a recovery of the $\alpha_2\delta$-mediated enhancement of current size. This experiment assumed that cells transfected with a cDNA mixture containing double the proportion of $\alpha_2\delta$-1 R217A cDNA would be individually transfected with double the proportion of $\alpha_2\delta$-1 R217A (see Discussion).

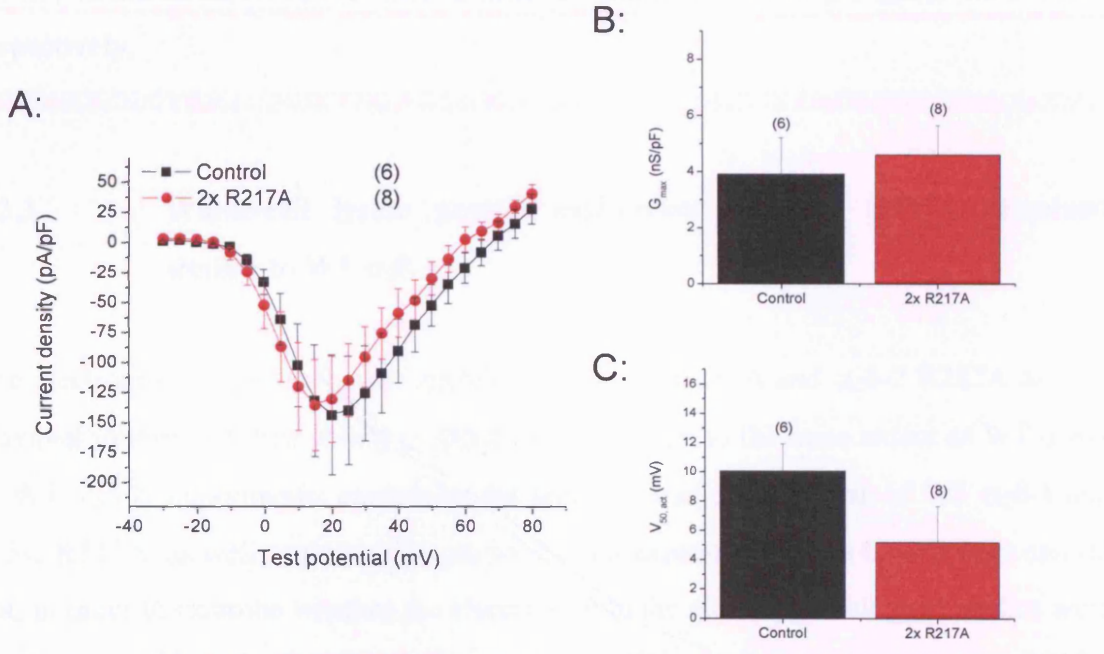

Figure 4.6. Doubling $\alpha_2\delta$-1 R217A cDNA did not cause a recovery of current amplitude. (**A**), I-V relationships for I_{Ba} in the control condition containing $Ca_v2.1$, β1b, $\alpha_2\delta$-1 R217A (black squares, n=6) and the same cDNA composition but with double the volume of R217A cDNA ("2x R217A", red circles, n=8) conditions. Current amplitude was normalised to whole-cell capacitance and plotted against membrane potential. Holding potential was -90 mV. Mean values for G_{max} (**B**) and $V_{50, act}$ (**C**) were obtained from fits of individual I-V relationships using the IVFIT function. No significant difference in either G_{max} or $V_{50, act}$ was observed (Student's t-test).

As shown in Figure 4.6, an increase in the proportion of $\alpha_2\delta$-1 R217A cDNA used in the transfection mixture failed to increase the current amplitude. Mean peak-current densities were similar in both conditions (-162.6 ± 56.7 pA/pF in the control condition, and -161.7 ± 46.1 pA/pF in the 2x R217A condition), as shown in Figure 4.6 A. There was no significant difference observed in the G_{max} (3.9 ± 1.3 nS/pF in control and 4.6 ± 1.1 nS/pF in the 2x R217A condition) or $V_{50,\,act}$ (+10.1 ± 1.9 mV in control and +5.2 ± 2.5 mV in the 2x R217A condition) of either condition, as shown in Figures 4.6 B and C respectively.

4.2.3 Whole-cell lysate protein expression of $\alpha_2\delta$-1 R217A remained similar to WT $\alpha_2\delta$-1

The electrophysiological studies identified the $\alpha_2\delta$-1 R217A and $\alpha_2\delta$-2 R282A as sub-maximal in terms of their ability to enhance current size to the same extent as WT $\alpha_2\delta$-1 or WT $\alpha_2\delta$-2. Experiments examining the relative protein expression of WT $\alpha_2\delta$-1 and $\alpha_2\delta$-1 R217A, as well as their effect on whole-cell expression of the $Ca_v2.2$ were carried out, in order to examine whether the effects seen in the electrophysiological studies were due to a possible reduction in protein expression. The pig WT $\alpha_2\delta$-1 and $\alpha_2\delta$-1 R217A proteins were used for this experiment (see Materials and Methods).

Figure 4.7 shows the whole-cell protein expression from three separate experiments, comparing expression of $\alpha_2\delta$-1 R217A to WT $\alpha_2\delta$-1. As shown in Figure 4.7 A, the immunoreactivity detected using the $\alpha_2\delta$-1 antibody demonstrates the similar expression between the two conditions. Further analysis using ImageQuant software shows the mean normalised immunoreactivity is similar between both $\alpha_2\delta$-1 R217A and WT $\alpha_2\delta$-1 conditions (Figure 4.7 B).

Further experiments were performed to examine how the presence of $\alpha_2\delta$-1 R217A would affect $Ca_v2.2$ expression, compared to the presence of WT $\alpha_2\delta$-1. Unfortunately

only one experiment was successful (see Figure 4.7 C), although it suggested a possible reduction in whole-cell expression of $Ca_v2.2$ in the presence of $\alpha_2\delta$-1 R217A when compared to WT $\alpha_2\delta$-1. However, more work is required to demonstrate this conclusively.

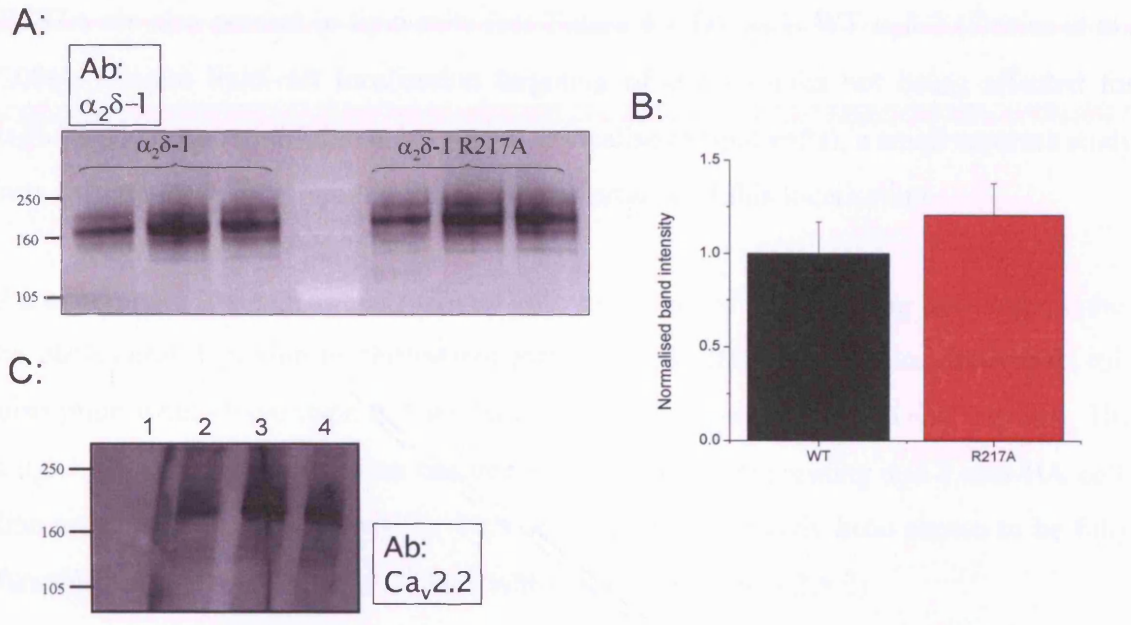

Figure 4.7. Whole-cell lysate protein expression is similar in the $\alpha_2\delta$-1 R217A condition, compared to WT $\alpha_2\delta$-1. (**A**), Immunoreactive bands at ~170 kDa were detected using the anti-$\alpha_2\delta$-2 Ab for WT $\alpha_2\delta$-1 and $\alpha_2\delta$-1 R217A conditions (n = 3 for each). (**B**), No significant difference in mean normalised immunoreactivity of the bands shown in (**A**), following analysis using ImageQuant software. (**C**), Immunoreactive bands at ~190 kDa were detected using an anti-$Ca_v2.2$ Ab. Lanes: *1*, no transfection; *2*, $Ca_v2.2$; *3*, $Ca_v2.2$, β1b, WT $\alpha_2\delta$-1; *4*, $Ca_v2.2$, β1b, $\alpha_2\delta$-1 R217A.

4.2.4 Lipid-raft localisation of $\alpha_2\delta$

The binding-experiments carried out (see Section 4.2.1) involved using $\alpha_2\delta$-1 and $\alpha_2\delta$-1 R217A purified as lipid-raft preparations. This work confirmed the localisation of $\alpha_2\delta$-1 to lipid-rafts, in agreement with previous observations made for the $\alpha_2\delta$-2 subunit (Davies et al., 2006). In addition to their WT counterparts, both $\alpha_2\delta$-1 R217A and $\alpha_2\delta$-2 R282A are also present in lipid-rafts (see Figure 4.1 D), as is WT $\alpha_2\delta$-2 (Davies et al., 2006). Despite lipid-raft localisation targeting of $\alpha_2\delta$ subunits not being affected for $\alpha_2\delta$-1 R217A or $\alpha_2\delta$-2 R282A (as they also localise to lipid-rafts), a small separate study was carried out to look into the functional importance of this localisation.

An experiment was performed to investigate the effect of manipulating lipid-rafts, either by cholesterol depletion or cholesterol enrichment, in order to examine the impact this disruption would have upon $\alpha_2\delta$-mediated effects on co-expressed VGCC currents. The $Ca_v2.1$, $\beta4$ subunit combination transfected into a stably-expressing $\alpha_2\delta$-2 mid-HA cell-line was used for the experiments. This cell-line has previously been shown to be fully functional, in terms of the $\alpha_2\delta$ present within it (see Section 3.2.5.2).

4.2.4.1 Cholesterol depletion

Cholesterol was depleted from the cells as described in Materials and Methods. Whilst no assessment of cholesterol depletion was carried out, the protocol used has been previously demonstrated to cause a reduction in membrane cholesterol (Christian et al., 1997). The results are shown in Figures 4.8 & 4.9.

Application of 5 mM methyl-β-cyclodextrin (MBCD) for 1 h (immediately before experimentation) caused a significant increase in size of currents observed (Figure 4.8 A), as well as the observed mean peak-current density (-387.5 ± 44.9 pA/pF) compared to the control condition (-266.7 ± 34.7 pA/pF, $P<0.05$), as shown in Figure 4.8 B. This

increase in peak current density did not translate to a significant increase (at $P<0.05$) in whole-cell conductance of the MBCD condition (9.5 ± 4.2 nS/pF) over the control condition (6.8 ± 1.6 nS/pF), as shown in Figure 4.8 C. Similarly, no differences in $V_{50,\,act}$ of the two conditions were seen, as shown in Figure 4.8 D.

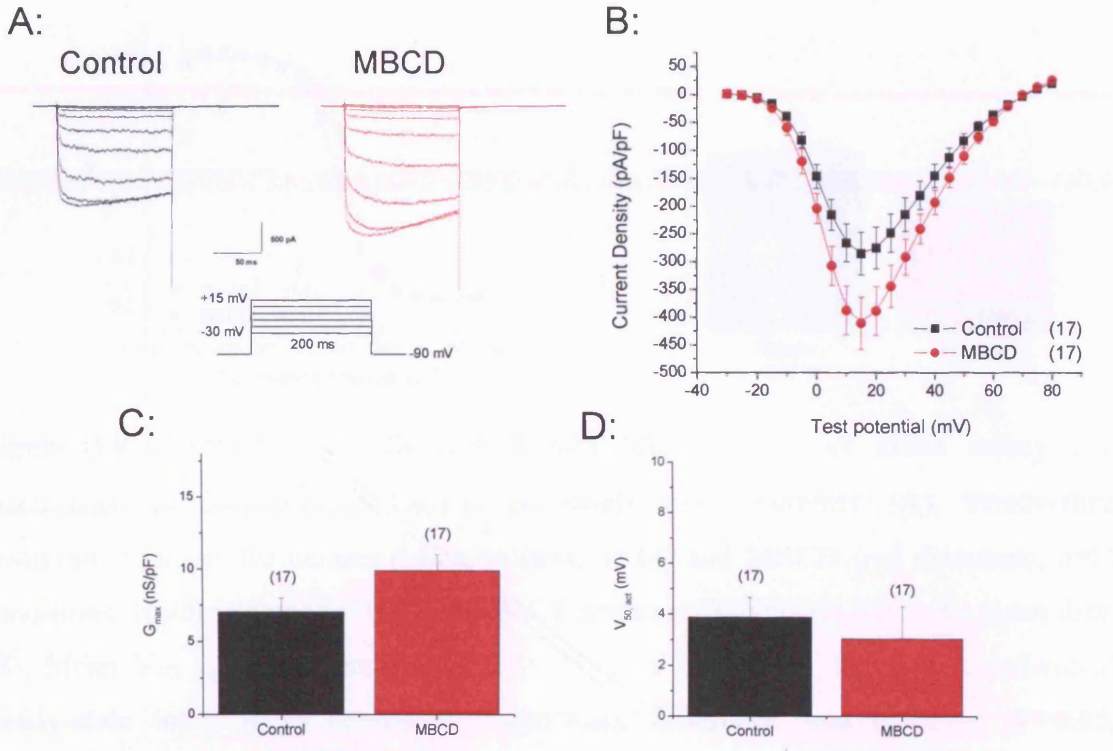

Figure 4.8. Disruption of lipid rafts causes an increase in current amplitude through co-expressed $Ca_v2.1$, $\beta4$, stable $\alpha_2\delta$-2 mid-HA channels. (**A**), Representative current traces show the increase in current amplitude in response to a range of test-potentials (-30 mV to +15 mV). (**B**), I-V relationships of control (black squares, n=17) and 5 mM MBCD (red circles, n=17) conditions. Holding potential was -90 mV. Mean values for whole-cell conductance (**C**) and $V_{50,\,act}$ (**D**) were obtained from fits of individual I-V relationships using the IVFIT function. No significant difference in either G_{max} or $V_{50,\,act}$ was observed.

The mean steady-state inactivation curves were similar (Figure 4.9 A), and the resultant mean $V_{50,\ inact}$ for the 5 mM MBCD condition (-36.3 ± 2.0 mV) was not significantly different from the control condition (-42.4 ± 1.3 mV), as shown in Figure 4.9 B.

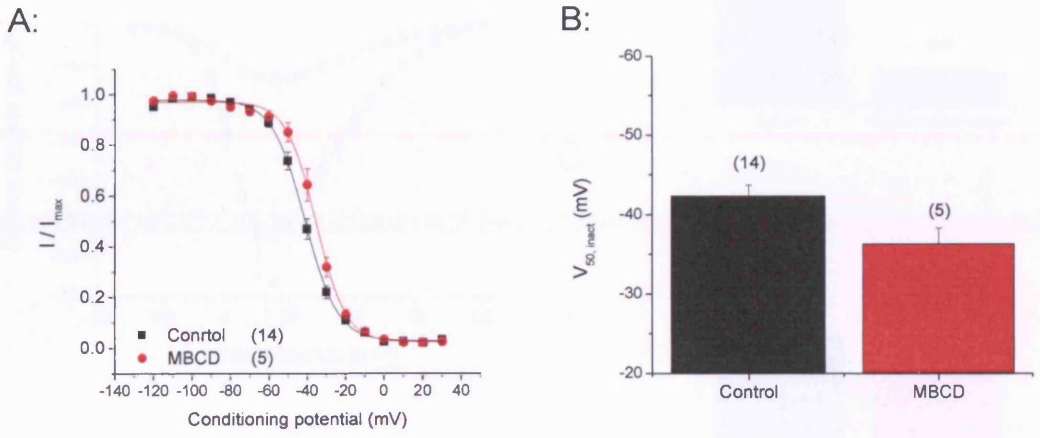

Figure 4.9. Treatment of cells with 5 mM MBCD does not affect steady-state inactivation of co-expressed $Ca_v2.1$, β4, stable $\alpha_2\delta$-2 currents. (**A**), Steady-state inactivation curves for control (black squares, n=14) and MBCD (red diamonds, n=5) conditions. Holding potential was -100 mV. Curves are Boltzmann fits to the mean data. (**B**), Mean $V_{50,\ inact}$ data were obtained by fitting a Boltzmann function to individual steady-state inactivation curves, no significant difference was observed (P>0.05, Student's t test).

4.2.4.2 Cholesterol addition

Since the depletion of cholesterol from tsA-201 cells co-expressing $Ca_v2.1$, β4, stable $\alpha_2\delta$-2 mid-HA caused an unexpected increase in the size of current amplitude, the opposite treatment was applied to see the effect this would have on macroscopic currents. The same subunit combination ($Ca_v2.1$, β4, stable $\alpha_2\delta$-2 mid-HA) was used, and cells were treated with combined 5 mM MBCD / 1 mM cholesterol in order to load the cells with cholesterol.

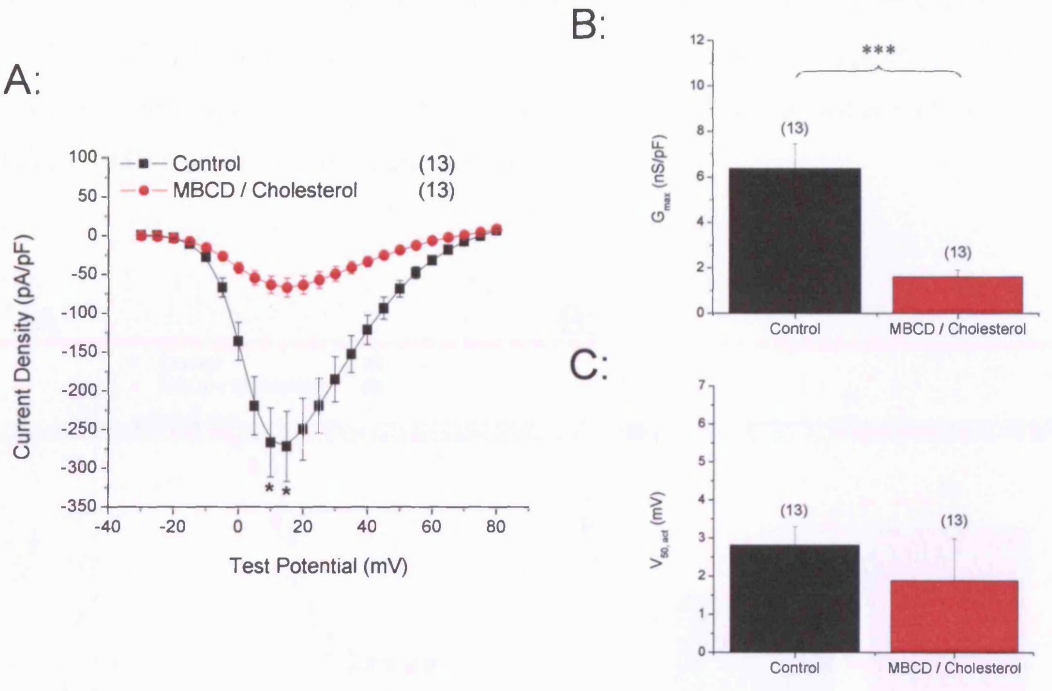

Figure 4.10. Cholesterol enrichment inhibits I_{Ba} through co-expressed $Ca_v2.1$, β4, stable $\alpha_2\delta$-2 mid-HA channels. (**A**), I-V relationships of control (black squares, n=13) and 5 mM MBCD / 1 mM cholesterol (red circles, n=13) conditions. Mean values for whole-cell conductance (**B**) and $V_{50,\,act}$ (**C**; no significant difference) were obtained from fits of individual I-V relationships using the IVFIT function. (*** denotes P<0.001, Student's t-test).

Treatment with 5 mM MBCD / 1 mM cholesterol resulted in an inhibition of I_{Ba} through the co-expressed $Ca_v2.1$, β4, stable $\alpha_2\delta$-2 combination, as shown in Figure 4.10. The mean peak-current density was reduced from -271.7 ± 45.3 pA/pF in the control condition to -67.4 ± 12.3 pA/pF in the MBCD / cholesterol condition (P<0.001), as shown in Figure 4.8A. A similar reduction in whole-cell conductance (6.4 ± 1.1 nS/pF in the control condition, 1.6 ± 0.3 nS/pF in the MBCD / cholesterol condition, P<0.001) was also observed (Figure 4.10 B). No significant changes were observed between conditions for $V_{50,\,act}$ (Figure 4.10 C).

A hyperpolarisation was observed in the mean steady-state inactivation curve (Figure 4.11 A), which equated to a significant hyperpolarisation in $V_{50,\ inact}$ in the MBCD / cholesterol condition (-46.3 ± 2.5 mV) compared to that of the control condition (-39.9 ± 1.4 mV, $P<0.01$), as shown in Figure 4.11 B.

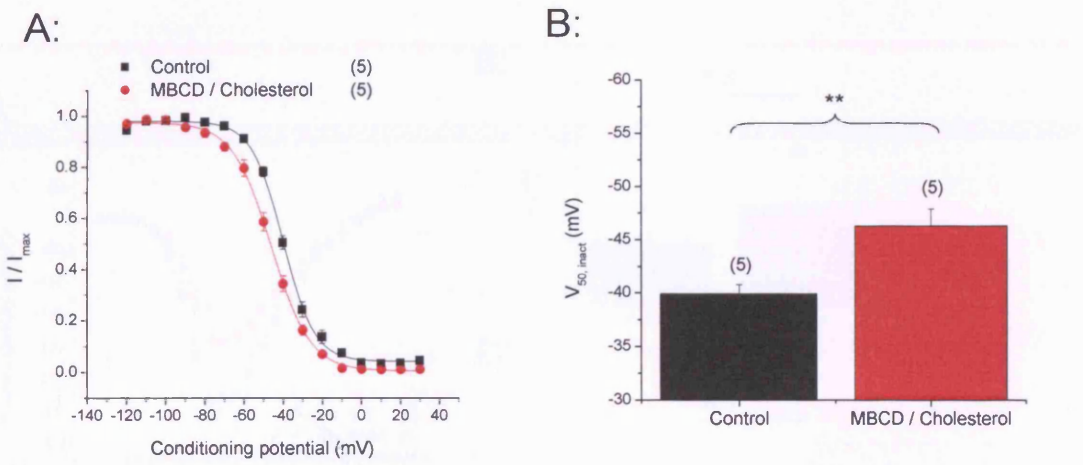

Figure 4.11. Treatment of cells with 5 mM MBCD / 1 mM cholesterol does not affect steady-state inactivation of co-expressed $Ca_v2.1$, β4, stable $\alpha_2\delta$-2 currents. (**A**), Steady-state inactivation curves for control (black squares, n=5) and MBCD / cholesterol (red circles, n=5) conditions. Holding potential was -100 mV. Curves are Boltzmann fits to the mean data. (**B**), Mean $V_{50,\ inact}$ data were obtained by fitting a Boltzmann function to individual steady-state inactivation curves. ** denotes $P<0.01$, (Student's t-test).

4.2.4.3 Co-expression of stomatin with $Ca_v2.1$, β4, stable $\alpha_2\delta$-2 mid-HA

Stomatin is known to co-localise as a constituent protein of lipid-rafts as a member of the SPFH (stomatin/prohibitin/flotillin/HflK) family (Davies et al., 2006). α2δ-2 was found to precipitate with both stomatin-like protein-2 and prohibitin (Davies et al., 2006), suggesting the potential for a physical interaction.

A similar structural protein, caveolin-1, is also concentrated in detergent-resistant membranes. Stable transfection of caveolin-1 into an NG-108 cell-line resulted in an inhibition of N-type current (Toselli et al., 2005). In an effort to examine the effect that proximity to an SPFH-family protein would have on $\alpha_2\delta$, stomatin was over-expressed along with the co-expressed $Ca_v2.1$, $\beta4$, stable $\alpha_2\delta$-2 mid-HA subunit combination.

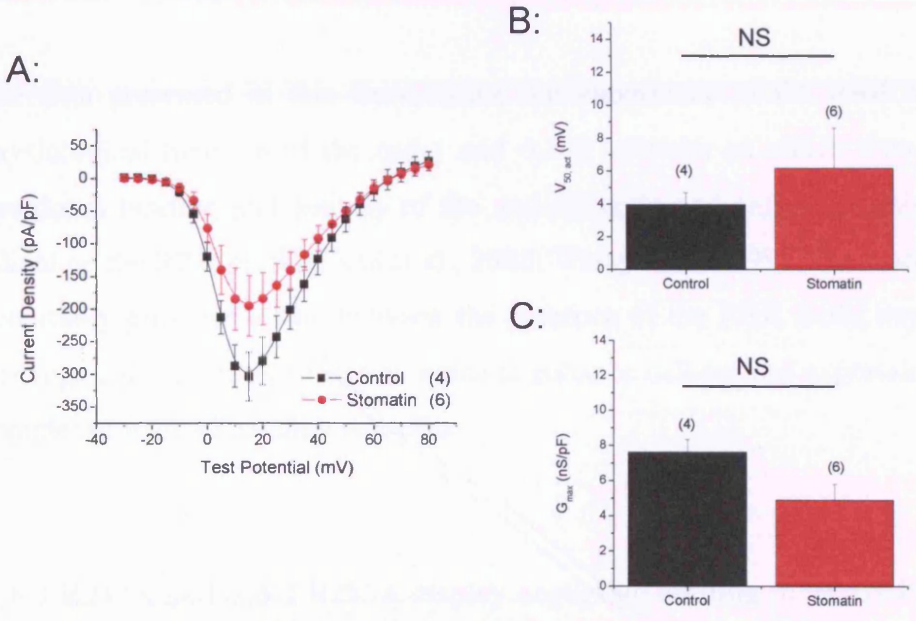

Figure 4.12. Co-expression of stomatin inhibits I_{Ba} through co-expressed $Ca_v2.1$, $\beta4$, stable $\alpha_2\delta$-2 mid-HA channels. (**A**), I-V relationships of control (black squares, n=4) and stomatin (red circles, n=6) conditions. The mean peak current-density is smaller in the stomatin condition, but not significantly smaller (P>0.05, Student's t-test). Mean values for whole-cell conductance (**B**) and $V_{50,\,act}$ (**C**) were obtained from fits of individual I-V relationships using the IVFIT function, no significant difference was observed (Student's t test).

The results are shown in Figure 4.12. A reduction in mean peak-current density (Figure 4.12 A) was observed in the stomatin condition (-195.5 ± 46.3 pA/pF) compared to the

control condition (-303.3 ± 37.6 pA/pF), although this was not statistically significant. A similar non-significant reduction in G_{max} was observed (7.6 ± 0.7 nS/pF in the control condition, and 4.9 ± 0.9 nS/pF in the stomatin condition), as shown in Figure 4.12 B. No significant change in $V_{50, act}$ was observed (Figure 4.12 C).

4.3 Discussion

The data presented in this demonstrate the importance of the RRR motif in normal physiological function of the $\alpha_2\delta$-1 and $\alpha_2\delta$-2 subunits on which they are found. The functional binding and activity of the anti-epileptic and anti-nociceptive drug GBP is reliant on the RRR motif (Field et al., 2006; Wang et al., 1999). The work presented here potentially provides a link between the presence of the RRR motif important for GBP binding, and the ability of $\alpha_2\delta$ subunits to enhance cell-surface expression of the VGCC complexes with which they associate.

$\alpha_2\delta$-1 R217A and $\alpha_2\delta$-2 R282A display negligible binding to ^{3}H-GBP

The binding data confirm that the RRR motif at position 215-217 on $\alpha_2\delta$-1 is essential for GBP binding. The $\alpha_2\delta$-1 R217A mutation resuslts in negligible ^{3}H-GBP binding, as observed in both membrane and lipid raft preparations. An absence of binding has been shown previously in membrane preparations of $\alpha_2\delta$-1 R217A-transfected COS-7 cells (Wang et al., 1999).

Binding of ^{3}H-GBP to $\alpha_2\delta$ has been demonstrated previously in lipid rafts for the $\alpha_2\delta$-2 subunit (Davies et al., 2006). A 4.8-fold increase in affinity was observed in lipid raft preparations over membrane preparations (both made from mouse cerebellum). This corresponds to a 6.1-fold increase in affinity seen for $\alpha_2\delta$-1 in this study. Dialysis of $\alpha_2\delta$-1 has been shown to result in a two-fold increase in affinity (Dissanayake et al., 1997; Brown et al., 1998), attributed to removal of a 12 kDa endogenous ligand.

Whole cell electrophysiology suggests the functionality of the $\alpha_2\delta$-1 R217A and $\alpha_2\delta$-2 R282A subunits is impaired

When co-expressed with $Ca_v\alpha_1$ and β subunits, both the $\alpha_2\delta$-1 R217A and $\alpha_2\delta$-2 R282A subunits fail to enhance current size to the same extent as their WT $\alpha_2\delta$ counterparts. However, a significant enhancement of current size over control conditions was observed in both experiments. This result has also been observed in *Xenopus* oocytes expressing the $Ca_v2.2$, β1b, $\alpha_2\delta$-1 subunit combination (Field et al., 2006).

This intermediate enhancement of current size was observed in conjunction with changes in $V_{50,\ inact}$ as normally elicited by $\alpha_2\delta$ co-expression. The hyperpolarisation of $V_{50,\ inact}$, measured from the steady-state inactivation curves obtained in the $\alpha_2\delta$-2 R282A experiment (see Figure 4.5) was similar between the WT $\alpha_2\delta$-2 and $\alpha_2\delta$-2 R282A conditions. Both of these values were significantly hyperpolarised compared to the control condition.

A number of changes normally elicited by $\alpha_2\delta$ co-expression were seen when co-expressing both $\alpha_2\delta$-1 and $\alpha_2\delta$-2, but were not considered statistically significant. Co-expression of both WT $\alpha_2\delta$-1 and WT $\alpha_2\delta$-2 caused a hyperpolarisation of $V_{50,\ act}$ compared to their respective control conditions, although these changes were not significant. It is worth noting that both the $\alpha_2\delta$-1 R217A and $\alpha_2\delta$-2 R282A elicited the same trend as their WT $\alpha_2\delta$ counterparts (see Figures 4.2 and 4.3 respectively). In addition neither the WT $\alpha_2\delta$-2 or $\alpha_2\delta$-2 R282A τ_{inact} values were significantly different from control (at $P<0.05$), despite being the case for previous experiments. These results differ from those shown in Chapter 3, despite the conditions for the experiments (i.e. $[Ba^{2+}]$, transfection procedure etc.) being the same. Such differences may perhaps highlight a flaw in the reproducibility of the transfection procedure. The ability of $\alpha_2\delta$ to hyperpolarise $V_{50,\ act}$ is not certain, with some studies not finding $\alpha_2\delta$ ($\alpha_2\delta$-1) expression to alter $V_{50,\ act}$ (Shirokov et al., 1998), whilst another study found it to hyperpolarise $V_{50,\ act}$ (Felix et al., 1997).

The only overall difference between the WT $\alpha_2\delta$-1 Vs $\alpha_2\delta$-1 R217A and the WT $\alpha_2\delta$-2 Vs $\alpha_2\delta$-2 R282A in the experiments was the increase in amplitude of currents observed: the R282A subunit produced a 3.8-fold increase over control current density, compared to a 2.3-fold increase over control current density in the case of $\alpha_2\delta$-1 R217A. One interpretation of these results is that the lack of a GBP binding-site on $\alpha_2\delta$-1 and $\alpha_2\delta$-2 impairs the ability of $\alpha_2\delta$ subunits to increase the cell-surface expression of the pore-forming $Ca_v\alpha_1$ subunit, resulting in smaller recorded macroscopic currents.

Whole-cell lysate expression of $\alpha_2\delta$-1 R217A

The observed electrophysiological differences observed when co-expressing $\alpha_2\delta$-1 R217A or WT $\alpha_2\delta$–1 are not a result of impaired expression of the $\alpha_2\delta$ protein. No significant difference was observed in the amount of $\alpha_2\delta$-1 protein present in either WT or R217A conditions. This data corresponds to the finding that $\alpha_2\delta$-1 R217A protein expresses in the cortex (of R217A mice) to the same extent as WT $\alpha_2\delta$–1 protein in WT mice (Field et al., 2006). However, the μMIDAS $\alpha_2\delta$-2 protein (see Chapter 3) expressed to the same extent as WT $\alpha_2\delta$-2 when expressed alone, but intracellular retention occurred when it was co-expressed with $Ca_v2.2$ (Canti et al., 2005). Initial but incomplete evidence (n=1) for a reduction in $Ca_v2.2$ expression is seen when co-expressed with $\alpha_2\delta$-1 R217A compared to WT $\alpha_2\delta$-1 (Figure 4.7 C), although it cannot be concluded that this is due to intracellular retention of $\alpha_2\delta$-1 R217A / $Ca_v2.2$.

Increasing the proportion of $\alpha_2\delta$-1 R217A cDNA in the transfection mix

One effect of co-expression of either the $\alpha_2\delta$-1 R217A or $\alpha_2\delta$-2 R282A mutations was to impair, but not abolish the ability of the $\alpha_2\delta$ subunits to enhance cell-surface expression of $Ca_v\alpha_1$ subunits, compared to WT $\alpha_2\delta$-1 or WT $\alpha_2\delta$-2. These mutant $\alpha_2\delta$ subunits still

retain a partial functionality in the enhancement cell-surface expression of the $Ca_v\alpha_1$ subunits, due to the significant increases in current density over control when co-expressing both the $\alpha_2\delta$-1 R217A and $\alpha_2\delta$-2 R282A subunits.

This raised questions as to the production and processing of $\alpha_2\delta$ subunits, their intracellular interaction with the $Ca_v\alpha_1$ subunit, and the role of the RRR motif. Work carried out using DRGs from an $\alpha_2\delta$-1 R217A knock-in mouse line suggested that these currents were similar in terms of size to those from WT mice (Field et al., 2006). If it was possible that some compensatory mechanism was active in order to produce $\alpha_2\delta$-1 R217A currents the same size as WT $\alpha_2\delta$-1 currents, perhaps this could be reproduced in a cell-line. One possible method of doing this was to increase the proportion of $\alpha_2\delta$-1 R217A cDNA in the transfection mixture, and to look for a "recovery" of current size.

The validity of this experiment rested upon the notion that all VGCC subunits are successfully transfected into each cell. From personal experience, it has been found that cells that are labelled by GFP, but have no detectable macroscopic current are relatively rare, suggesting the co-expression of VGCC subunits is successful the majority of the time.

The failure of increasing the proportion of $\alpha_2\delta$-1 R217A (into the transfection mixture) to increase peak current density suggests that its intermediate enhancement of currents represents a qualitative impairment of an intracellular function of the $\alpha_2\delta$ protein, rather than a quantitative factor such as a reduction of $\alpha_2\delta$-1 R217A expression. A previous study (Sandoval et al., 2004) has found similar a similar intermediate enhancement of current size, using co-expression of (two different) $\alpha_2\delta$-1 subunits with single-point mutations. Each single-point $\alpha_2\delta$-1 mutant failed to fully enhance current size to the same extent as WT $\alpha_2\delta$-1, and an $\alpha_2\delta$-1 subunit with both mutations introduced into it displayed current amplitudes similar to those without co-expressed $\alpha_2\delta$-1. These reductions in current amplitude came in the absence of any observed changes in $V_{50,\ inact}$ in the $\alpha_2\delta$-2 R282A experiment (see Figure 4.5).

The observation that the $\alpha_2\delta$-1 R217A protein has the same level of whole-cell expression as WT $\alpha_2\delta$-1, coupled with the absence of any changes in observed $V_{50,\ inact}$ or $V_{50,\ act}$ seen when co-expressing $\alpha_2\delta$-1 R217A or $\alpha_2\delta$-2 R282A instead of WT $\alpha_2\delta$, suggests that the $\alpha_2\delta$-1 R217A and $\alpha_2\delta$-2 R282A proteins are produced and expressed to the same extent at their WT $\alpha_2\delta$ counterparts, and when co-expressed with $Ca_v\alpha_1$ subunit will still make a functional interaction at the cell surface.

Further work is required to demonstrate that the impaired current amplitude caused when co-expressing an $\alpha_2\delta$-1 R217A or $\alpha_2\delta$-2 R282A subunit arises as a result of impaired expression or stability of the respective $Ca_v\alpha_1$ subunit. Cell-surface biotinylation of, or radioligand binding to expressed $Ca_v\alpha_1$ subunits would be a good way to demonstrate this.

Conclusion: $\alpha_2\delta$-1 R217A and $\alpha_2\delta$-2 R282A

In addition to a cell-surface interaction with the pore-forming $Ca_v\alpha_1$ subunit that changes biophysical properties of the expressed channels (Gurnett et al., 1997; Felix et al., 1997) $\alpha_2\delta$ subunits are implicated in facilitating the trafficking of the $Ca_v\alpha_1$ subunit (Canti et al., 2005). This study demonstrates the importance of RRR motif on $\alpha_2\delta$-1 and $\alpha_2\delta$-2 in facilitating a full increase in current amplitude of co-expressed $Ca_v\alpha_1$ (and β) subunits, potentially by an effect on cell-surface expression of the channels.

4.4 Manipulation of cell-membrane cholesterol

Preparation of fractions of cells transfected with either $\alpha_2\delta$-1 R217A or WT $\alpha_2\delta$-1 across a sucrose gradient (for the binding experiment detailed in Section 4.2.1.2) confirmed that both these proteins are targeted to lipid rafts. This is in agreement with

similar data showing that the mature, cleaved forms of both WT $\alpha_2\delta$-2 and $\alpha_2\delta$-2 R282A are located entirely in lipid-rafts (Davies et al., 2006).

Lipid-rafts are heterogenous sterol- and shphingolipid-enriched structures within membranes that are about 10-200 nm in size (reviewed in Jacobson et al., 2007). Lipid raft targeting may be of importance for neuronal calcium channel subtypes. Cholesterol addition has been previously shown to inhibit calcium currents in NG108-15 and smooth muscle cells (Jennings et al., 1999; Toselli et al., 2005). $Ca_v2.1$ is targeted to lipid-rafts, where it makes functional interactions with SNARE proteins (Taverna et al., 2004). Disruption of these structures (using saponin) led to a reduction in both basal and depolarisation-induced Ca^{2+} influx into synaptosomes through neuronal VGCCs. This suggests the lipid raft localisation of $Ca_v2.1$ and SNARE-complex proteins may be of importance in pre-synaptic neurotransmitter release. Similarly, the presence of caveolin-1, a protein implicated in the delivery of cholesterol from the ER to the plasmalemma, caused an inhibition in N-type current amplitude. This reduction in amplitude occurred in the absence of any changes in $V_{50,\,act}$ or τ_{inact} (Toselli et al., 2005). The inhibition of N-type current was paralleled by the addition of cholesterol to cells. Both these studies hint at the importance of neuronal VGCC localisation and modulation in lipid rafts.

The findings of cholesterol manipulation experiments in this study suggest an important modulatory effect of membrane cholesterol upon $Ca_v2.1$ currents. Depletion of membrane cholesterol (and therefore disruption of the lipid rafts) led to a small but significant increase in the peak-current density of $Ca_v2.1$ currents. Addition of cholesterol to cells resulted in an inhibition of the $Ca_v2.1$, as well as a hyperpolarisation of $V_{50,\,inact}$. Previous work suggests that the exogenous addition of membrane cholesterol affects neuronal calcium channels in a specific manner, as no inhibitory effect was seen on non-neuronal L-type Ca^{2+} or delayed-rectifier K^+ current (Toselli et al., 2005). This inhibition was attributed to a shift in single-channel kinetics to favour the null P_o mode, rather than being attributed to an increase in VGCC turnover.

The cholesterol manipulation experiments leave plenty of scope for future work. It would be interesting to examine whether or not the modulation of $Ca_v2.1$ currents seen with cholesterol manipulation is reversible, either by the opposite treatment with MBCD / cholesterol, or by a recovery of the original membrane cholesterol levels by the cell itself. Additionally, if the inhibition of $Ca_v2.1$ currents seen in this study arises from a shift to the null P_o mode, it remains to be determined whether or not the increase in current amplitude seen upon depletion of membrane cholesterol is due to a shift in the channel population to favour the normal P_o mode. Although the data collected in the stomatin experiment were not sufficient in order to claim an inhibitory effect of co-expressed stomatin, such an inhibition may arise from the same cholesterol-addition mechanism seen previously (Toselli et al., 2005) and the cholesterol addition experiment shown here.

Conclusion: Lipid-raft localisation and modulation of $Ca_v2.1$

The $Ca_v2.1$ and $\alpha_2\delta$-2 subunits used in the experiments both partition into lipid-rafts. The ability of MBCD and MBCD / cholesterol to alter the membrane cholesterol level, results in a modulatory effect on the current amplitude through the expressed channels. This raises questions as to the localisation of VGCCs at the cell-surface, and the subsequent implications for their functionality.

Chapter 5: Results

Chronic inhibition of VGCCs by gabapentin

5.1 Introduction

The results from the study examining the single-point mutations made in $\alpha_2\delta$-1 (R217A and $\alpha_2\delta$-2 (R282A) (see Chapter 4) showed an inability of the mutant $\alpha_2\delta$ to fully enhance current size of co-expressed VGCC subunits. However, the mutant $\alpha_2\delta$ subunuts still elicit changes in biophysical characteristics (such as $V_{50,\,act}$, $V_{50\,inact}$) seen with WT $\alpha_2\delta$. A possible explanataion for this is that the RRR site is required for the $\alpha_2\delta$-mediated enhancement of cell-surface expression of $Ca_v\alpha_1$ subunits (see Chapter 4).

The importance of the RRR site for enhancing currents through co-expressed VGCC complexes (potentially by enhancing cell surface expression), coupled with the importance of the site in binding GBP led to the idea that GBP might act chronically rather than acutely. Evidence for a long-term action of GBP rather than acute has been put forward before (Alden and Garcia, 2001).

Therefore, the mechanism of GBP action could be tested with the hypothesis that it acts chronically, perhaps to interfere with VGCC cell-surface expression. It is feasible that GBP is able to bind $\alpha_2\delta$ either at the cell surface (the GBP-binding α_2 subunit being extracellular (reviewed in Davies et al., 2007)) or intracellularly (GBP is taken into cells via the System-L amino acid transport system (Su et al., 1995)). It was therefore hypothesised that GBP acts intracellularly (via uptake into cells) in binding $\alpha_2\delta$ subunits and prevents the $\alpha_2\delta$-mediated enhancement of VGCC cell-surface expression.

A number of ligands for $\alpha_2\delta$ exist (see Introduction), some of which are amino acids such as leucine and isoleucine (Lynch, III et al., 2006). An endogenous ligand was proposed to be removed from the $\alpha_2\delta$ protein during lipid-raft preparations, as a large decrease in K_D of ^{3}H-GBP binding was observed (Dissanayake et al., 1997). If GBP acts to displace this ligand, this interaction may also occur inside the cell. GBP-treated cells

(expressing $\alpha_2\delta$) might be expected to have similar impairments in current density as seen in the RRA $\alpha_2\delta$ mutants (see Chapter 4).

5.2 Results

As mentioned above, GBP is not the only ligand of $\alpha_2\delta$ subunits. Several amino acids also bind $\alpha_2\delta$ and compete with GBP for binding (Thurlow et al., 1993), some of which were present in the culture medium (leucine and isoleucine (both at 800 μM) and valine (400 μM)). Coupled with the idea that GBP is to be taken up into cells, and the lack of clear electrophysiological evidence for an action of GBP at lower doses, two concentrations of GBP were selected for initial experiments- these were 100 μM and 1 mM. Drug was present from 1 h after the point of transfection to avoid any interference in the transfection procedure (see Materials and Methods), up to the point of re-plating cell cultures for recording. As the hypothesis supports an inhibitory effect on the trafficking function of $\alpha_2\delta$ rather than channel-block, GBP was omitted from the cultures after re-plating.

5.2.1 Inhibition of VGCCs by chronic exposure to GBP

5.2.1.1 Calcium channel currents resulting from the $Ca_v2.1$, β4, $\alpha_2\delta$-2 subunit combination are affected by chronic 100 μM GBP application

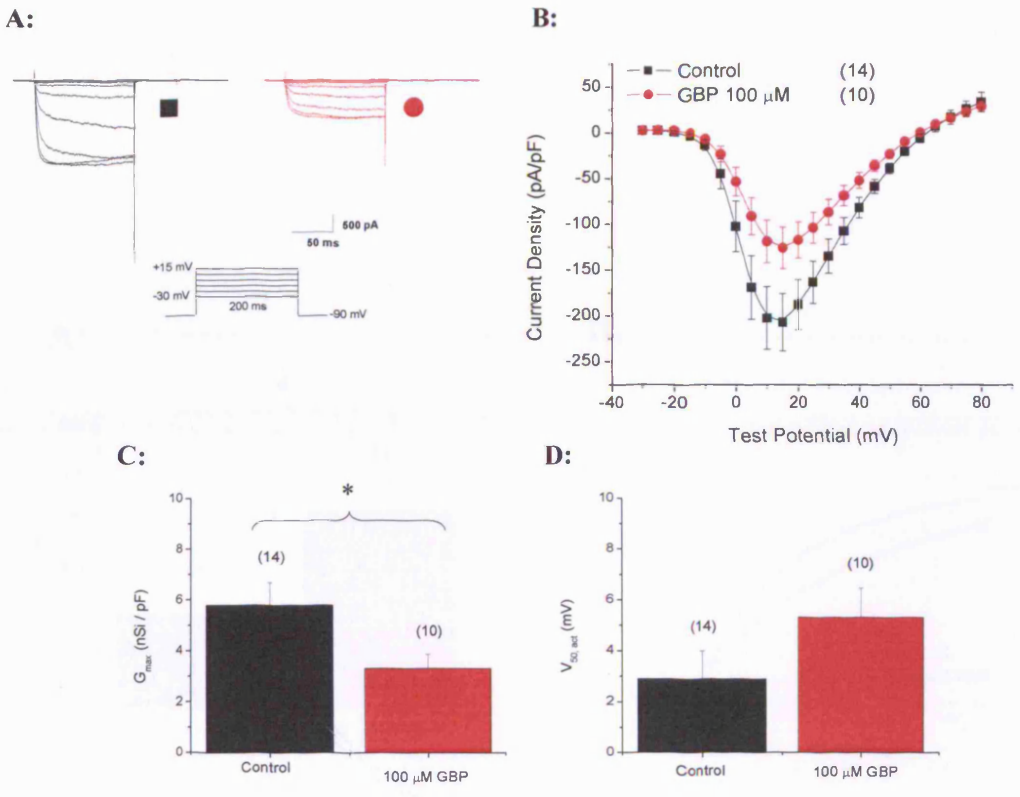

Figure 5.1. Chronic application of 100 µM GBP inhibits I_{Ba} through co-expressed $Ca_v2.1$, β4, $\alpha_2\delta$-2 channels. (**A**), Representative current traces for the two conditions in response to -30 to +15 mV voltage steps. A schematic of the I-V protocol is shown. (**B**), I-V relationships for I_{Ba} in the control (black squares, n=14) and 100 µM GBP (red circles, n=10) conditions. Current amplitude was normalised to whole-cell capacitance and plotted against membrane potential. Holding potential was -90 mV. Mean values for G_{max} (**C**) and $V_{50,\,act}$ (**D**; no significant difference) were obtained from fits of individual I-V relationships using the IVFIT function. * denotes $P<0.05$ (Student's t test).

The results of chronic application of 100 µM GBP are shown in Figures 5.1 to 5.3. Chronic application of 100 µM GBP produced a significant inhibition of current amplitude, as shown in representative current traces (Figure 5.1 A), which corresponded to a decrease in peak current density of 45.0 % ± 9.9 % (a decrease from -228.5 ± 32.5 pA/pF to -125.7 ± 22.6 pA/pF, $P<0.05$) when applied chronically (Figure 5.1 B). This

inhibition coupled with a decrease in whole-cell conductance (from 5.8 ± 0.9 nS/pF in the absence of GBP to 3.3 ± 0.6 nS/pF in the presence of GBP, P<0.05), as shown in Figure 5.1C. However, chronic application of 100 μM GBP did not elicit a shift in $V_{50,act}$ (Figure 5.1 D).

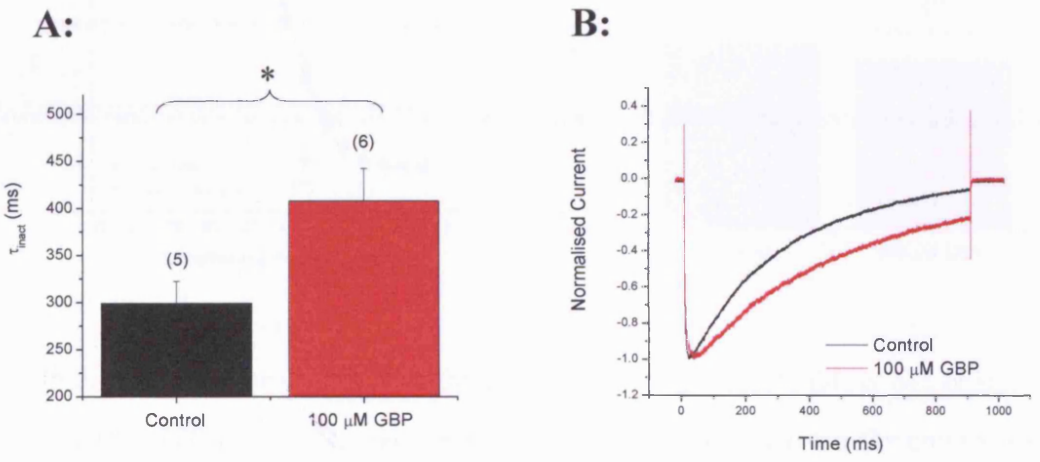

Figure 5.2. Effect of chronic 100 μM GBP application upon inactivation kinetics of I_{Ba} through co-expressed $Ca_v2.1$, β4, $\alpha_2\delta$-2 channels. (**A**), Mean time-constant of inactivation (τ_{inact}) data is shown for control (black, n=5) and 100 μM GBP (red, n=6) conditions. The decay phase of individual current traces at +10 mV was fitted with a single exponential function. Holding potential was -90 mV. (**B**) Representative current traces of control (black) and 100 μM GBP (red) conditions in response to a long depolarising voltage step to +10 mV. Traces are normalised to peak. * denotes P<0.05, (Student's t-test).

Inactivation kinetics of $Ca_v2.1$, β4, $\alpha_2\delta$-2 channels were slowed by chronic application of 100 μM GBP (Figure 5.2 A). τ_{inact} was 450.3 ± 56.7 ms in the 100 μM GBP condition, compared to 296.6 ± 31.3 ms in control (Figure 5.2 B). However, chronic 100 μM GBP application had no impact on steady-state inactivation curves of currents

through these channels (Figure 5.3 A). $V_{50,\ inact}$ was not altered significantly (-33.9 ± 2.5 mV in the absence and -32.2 ± 3.2 mV in the presence of GBP, shown in Figure 5.3 B).

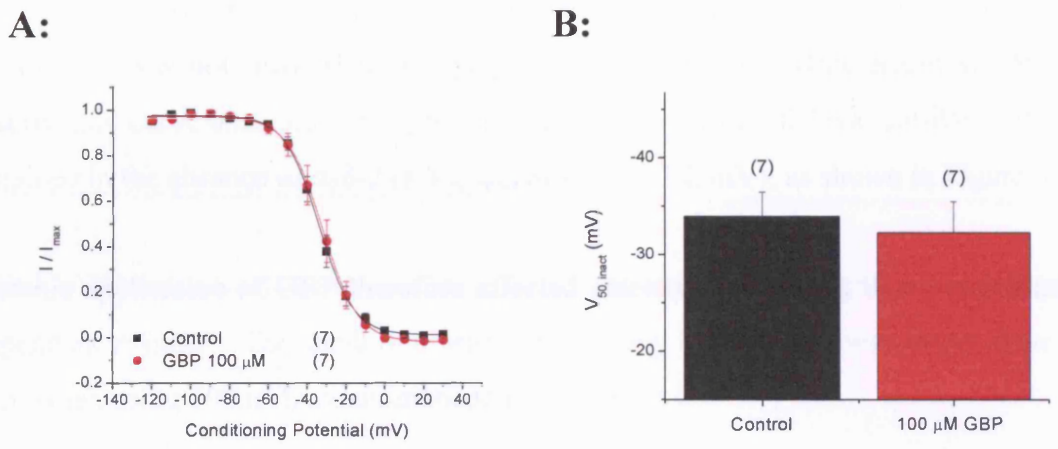

Figure 5.3. Steady-state inactivation in cells expressing $Ca_v2.1$, β4, $\alpha_2\delta$-2 channels is not affected by 100 µM GBP. (**A**), Steady-state inactivation curves for control (black squares, n=7) and 100 µM GBP (red circles, n=7) conditions. Holding potential was -100 mV. Curves are Boltzmann fits to the mean data. (**B**), Mean $V_{50,\ inact}$ data were obtained by fitting a Boltzmann function to individual steady-state inactivation curves, and showed no significant difference between control and 100 µM GBP conditions.

Chronic application of 1 mM GBP affected currents obtained (from $Ca_v2.1$, β4, $\alpha_2\delta$-2 channels) in such a way as to suggest either a partial or total reduction in functionality of $\alpha_2\delta$-2. Sample current traces are shown in Figure 5.4 A, and show the reduction in current size in response to chronic application of GBP. The mean peak current density (-247.8 ± 43.8 pA/pF in the control condition) was inhibited by 72.2 ± 4.2 % (to -68.8 ± 10.5 pA/pF, $P<0.01$) in the 1 mM GBP condition (Figure 5.4 B). This inhibition was greater than that seen with 100 µM GBP, and corresponded to a greater reduction in the whole-cell conductance (from 5.7 ± 0.9 nS/pF in the control condition to 1.7 ± 0.3 nS/pF in the chronic presence of 1 mM GBP, $P<0.01$), as shown in Figure 5.4 C. A significant depolarisation in $V_{50,\ act}$ was observed with chronic GBP application (+5.4 ± 1.2 mV in

the absence and +10.5 ± 0.9 mV in the presence of 1 mM GBP, P<0.05), as shown in Figure 5.4 D. In addition, the steady-state inactivation curve was depolarised by the chronic presence of 1 mM GBP (shown in Figure 5.5 A). $V_{50,\ inact}$ was depolarised from -37.6 ± 2.1 mV to -28.3 ± 2.7 mV (P<0.05) as shown in Figure 5.5 B. This depolarisation of $V_{50,\ inact}$ was not seen when applying 100 μM GBP. The depolarised steady-state inactivation curve obtained in the presence of chronic 1 mM GBP was similar to the one obtained in the absence of $\alpha_2\delta$-2 (a $V_{50,\ inact}$ of -28.1 ± 1.2 mV), as shown in Figure 3.3A.

Chronic application of GBP therefore affected calcium channel I_{Ba} in a concentration-dependent manner. The inhibition seen when using 1 mM GBP was larger than that seen when using 100 μM, as summarised in Figure 5.4 E.

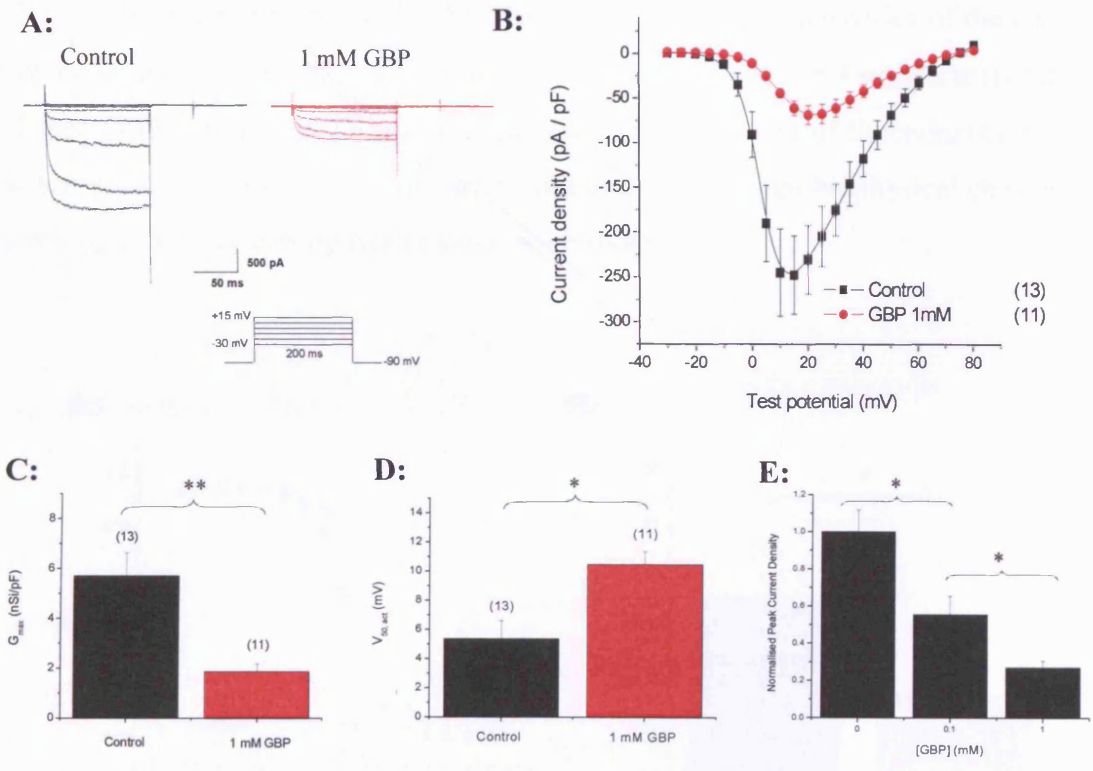

Figure 5.4. Chronic application of 1 mM GBP inhibits I_{Ba} through co-expressed $Ca_v2.1$, β4, $\alpha_2\delta$-2 channels. (**A**), Representative current traces for the two conditions in response to -30 to +15 mV voltage steps. A schematic of the I-V protocol is shown. (**B**), I-V

relationships for I_{Ba} in the control (black squares, n = 13) and 1 mM GBP (red circles, n = 11) conditions, mean peak current density was significantly different ($P<0.01$, Student's t-test). Current amplitude was normalised to whole-cell capacitance and plotted against membrane potential. Holding potential was -90 mV. Mean values for G_{max} (**C**) and $V_{50,\,act}$ (**D**) were obtained from fits of individual I-V relationships using the IVFIT function. (**E**), The mean peak-current density of the 1 mM GBP condition (n=11) is significantly smaller than that of the 100 μM GBP (n=10) and control (n=14) conditions (both from Figure 5.1). * denotes $P<0.05$, ** denotes $P<0.01$ (Student's t test for B, C, D; ANOVA for E).

In summary, the results showed a concentration-dependent inhibition of calcium channel currents (peak-current reductions of 45.0 ± 9.9 % in the presence of 100 μM GBP and 72.2 ± 4.2 % in the presence of 1 mM GBP). Biophysical characteristics of the channel appeared largely unchanged by the application of 100 μM GBP, but significantly altered by 1 mM GBP application. Overall this suggests an impairment of functionality of $\alpha_2\delta$-2, in terms of its ability to enhance current size and also to elicit biophysical changes on macroscopic currents arising from expressed channels.

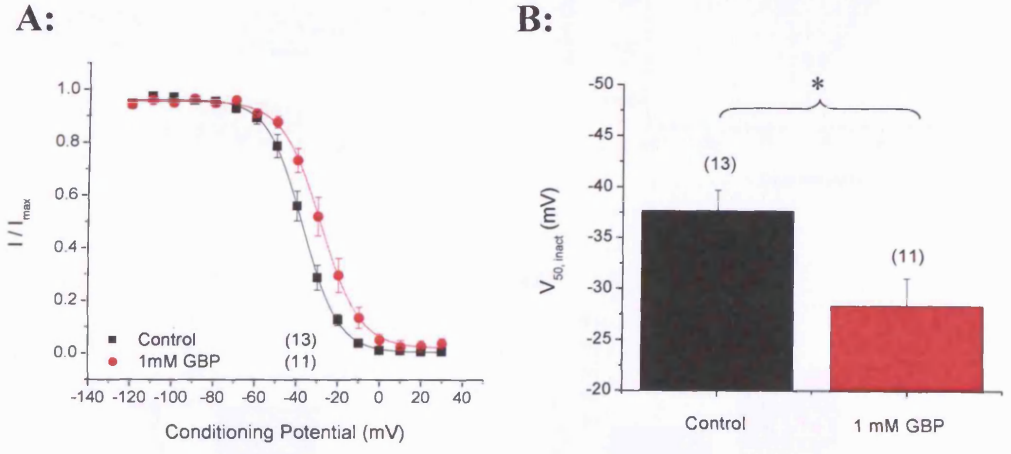

Figure 5.5. Steady-state inactivation of co-expressed $Ca_v2.1$, β4, $\alpha_2\delta$-2 channels is depolarised by 1 mM GBP. (**A**), Steady-state inactivation curves for control (black

squares, n=13) and 1 mM GBP (red circles, n=11) conditions. Curves are Boltzmann fits to the mean data. (**B**), Mean $V_{50,\ inact}$ data were obtained by fitting a Boltzmann function to individual steady-state inactivation curves. * denotes $P<0.05$, (Student's t test).

5.2.1.2 The $Ca_v2.2$, $\beta1b$, $\alpha_2\delta$-1 subunit combination is also inhibited by chronic GBP application

The experiments detailed in Section 5.2.1 imply that 1 mM GBP is a more appropriate concentration to use in order to see significant changes in the electrophysiological properties of expressed calcium channels. Having established inhibitory effects of GBP using the $Ca_v2.1$, $\beta4$, $\alpha_2\delta$-2 subunit combination, it was necessary to correlate these with the other GBP-binding $\alpha_2\delta$ subunit, $\alpha_2\delta$-1.

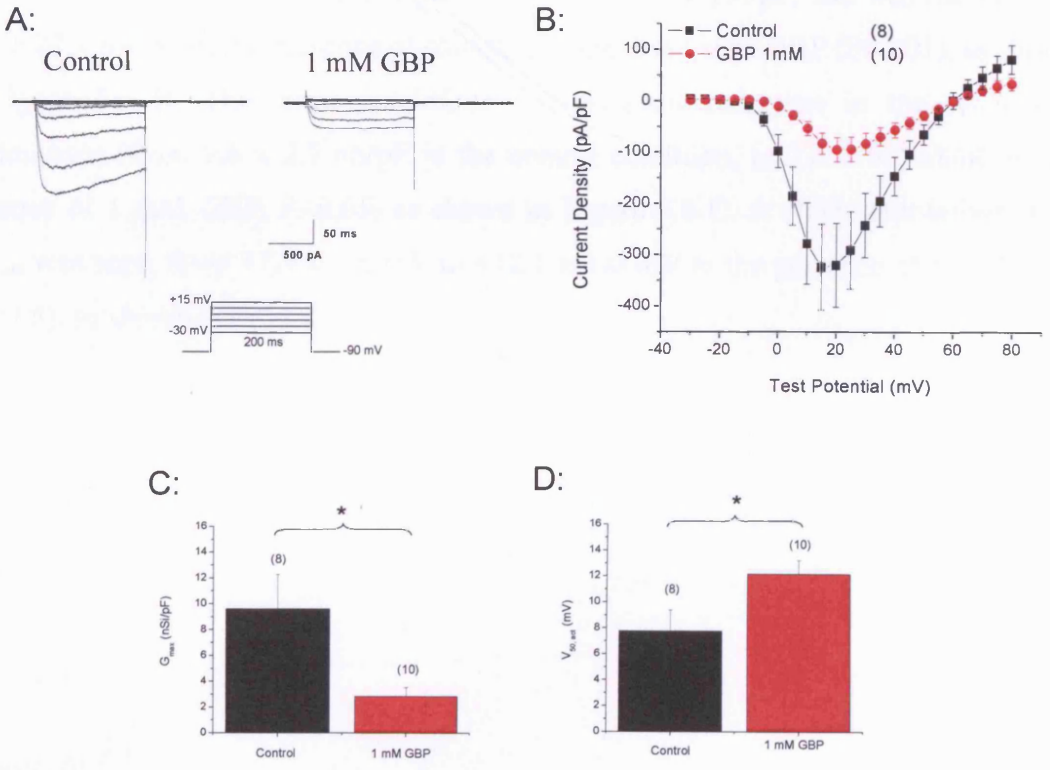

Figure 5.6. Chronic application of 1 mM GBP inhibits I_{Ba} through co-expressed $Ca_v2.2$, β1b, $\alpha_2\delta$-1 channels. (**A**), Representative current traces for the two conditions in response to -30 to +15 mV voltage steps. A schematic of the I-V protocol is shown. (**B**), I-V relationships for I_{Ba} in the control (black squares, n = 8) and 1 mM GBP (red circles, n = 10) conditions. Current amplitude was normalised to whole-cell capacitance and plotted against membrane potential. Holding potential was -90 mV. Mean values for G_{max} (**C**) and $V_{50,\,act}$ (**D**) were obtained from fits of individual I-V relationships using the IVFIT function. * denotes $P<0.05$ (Student's t test).

The same experiment (i.e. using 1 mM GBP) was carried out, this time using the $Ca_v2.2$, β1b, $\alpha_2\delta$-1 subunit configuration (Figures 5.6 to 5.8). The $\alpha_2\delta$-1 subunit has been more extensively studied as a pharmaceutical target for GBP treatment of neuropathic pain (Bian et al., 2006; Field et al., 2006). The same result was obtained, namely an inhibition of currents when cells were chronically exposed to 1 mM GBP. Sample current traces for the control and 1 mM GBP conditions are shown in Figure 5.6 A. The mean peak-current density in the control condition was -340.9 ± 95.0 pA/pF, and was reduced to -94.5 ± 27.7 pA/pF in the presence of chronically applied 1 mM GBP ($P<0.01$), as shown in Figure 5.6 B. This corresponded to a significant reduction in the whole-cell conductance (from 9.6 ± 2.7 nS/pF in the control condition, to 2.8 ± 0.7 nS/pF in the presence of 1 mM GBP, $P<0.05$) as shown in Figure 5.6 C. A slight depolarisation in $V_{50,\,act}$ was seen, from +7.8 ± 1.6 mV to +12.1 ± 1.0 mV in the presence of 1 mM GBP ($P<0.05$), as shown in Figure 5.6 D.

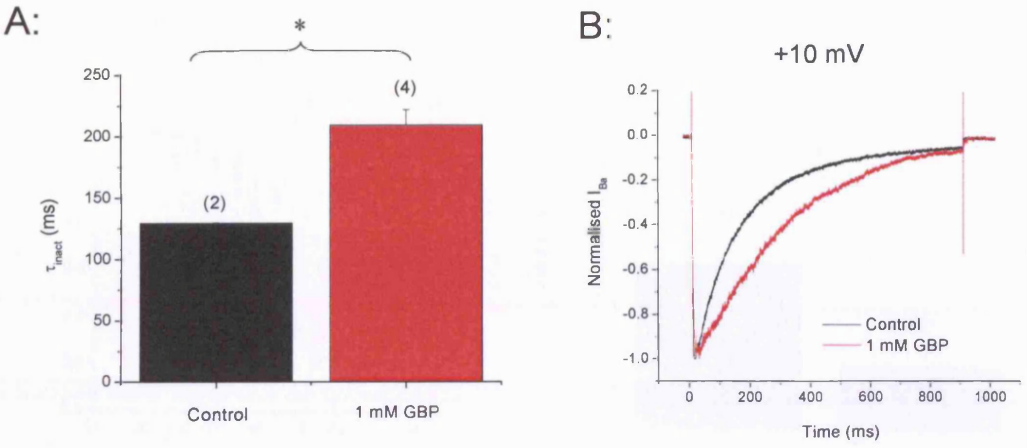

Figure 5.7. Effect of chronic 1 mM GBP application upon inactivation kinetics of I_{Ba} through co-expressed $Ca_v2.2$, β1b, $\alpha_2\delta$-1 channels. (**A**), Mean time-constant of inactivation (τ_{inact}) data is shown for control (black, n=2) and 1 mM GBP (red, n=4) conditions. The decay phase of individual current traces (at +10 mV) was fitted with a single exponential function. Holding potential was -90 mV. (**B**), Representative current traces of control (black) and 1 mM GBP (red) conditions in response to a long depolarising voltage step to +10 mV. Traces are normalised to peak. * denotes $P<0.05$, (Student's t test).

As with the previous experiment, a significant ($P<0.05$) reduction in the rate of current inactivation was observed with chronic application of 1 mM GBP (as shown in Figure 5.7 A). The mean τ_{inact} in the control condition (129.4 ± 0.3 ms) was slowed in the 1 mM GBP condition (209.2 ± 12.6 ms), as shown in Figure 5.7 B. Finally, a depolarising shift in the steady-state inactivation curve was also observed using $\alpha_2\delta$-1 (shown in Figure 5.8 A). $V_{50,\ inact}$ was shifted from -55.5 ± 3.4 mV in the control condition, to -39.7 ± 2.6 mV in the presence of 1 mM GBP ($P<0.05$), as shown in Figure 5.8 B.

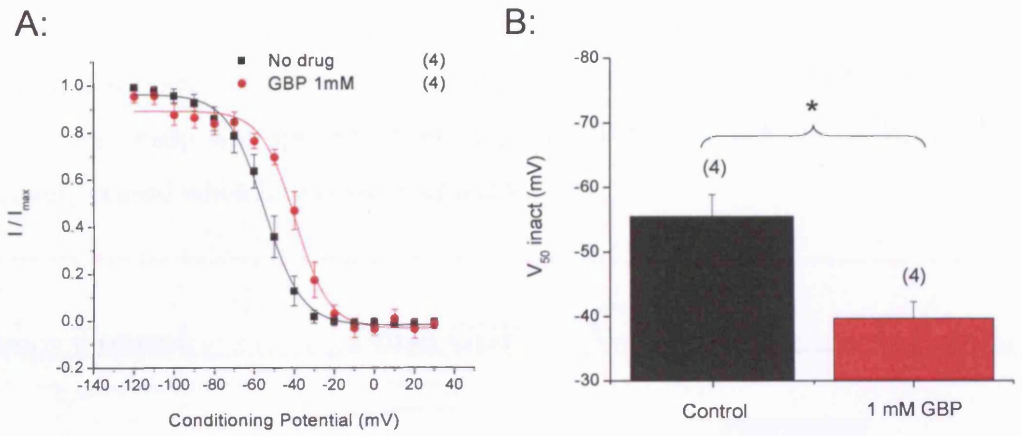

Figure 5.8. Steady-state inactivation of co-expressed $Ca_v2.2$, β1b, $\alpha_2\delta$-1 channels is depolarised by 1 mM GBP. (**A**), Steady-state inactivation curves for control (black squares, n=4) and 1 mM GBP (red circles, n=4) conditions. Holding potential was -100 mV. Curves are Boltzmann fits to the mean data. (**B**), Mean $V_{50,\ inact}$ data were obtained by fitting a Boltzmann function to individual steady-state inactivation curves. * denotes $P<0.05$, (Student's t test).

Therefore, the same inhibition of calcium channel currents observed using the $Ca_v2.1$, β4, $\alpha_2\delta$-2 subunit combination was observed using the $Ca_v2.2$, β1b, $\alpha_2\delta$-1 subunit combination.

5.2.1.3 I_{Ba} in cultured neurons is inhibited by chronic exposure to 1mM GBP

It was important to demonstrate that the effects seen thus far could be replicated in a neuronal system. DRGs have been identified as a site where $\alpha_2\delta$-1 is up-regulated after nerve injury (Luo et al., 2001). If GBP were to act in these circumstances to have therapeutic effect, it is important to demonstrate that GBP could elicit an inhibitory effect on calcium channels in DRGs. DRGs were taken from Sprague-Dawley rats (see Materials and Methods). Culture of DRGs was performed by a Fay Hebich, and the

following results from DRGs were obtained jointly with her (roughly haf-half). The internal and external solutions used for whole-cell patch clamp were the same as for patching tsA-201 cells, however the external solution contained 1 mM BaCl as opposed to 10 mM BaCl (see Materials and Methods) due to the larger size of DRGs compared to tsA-201 cells. GBp was applied chronically (for 40 h as in tsA-201 cells), application effectively ceased when DRGs were replated.

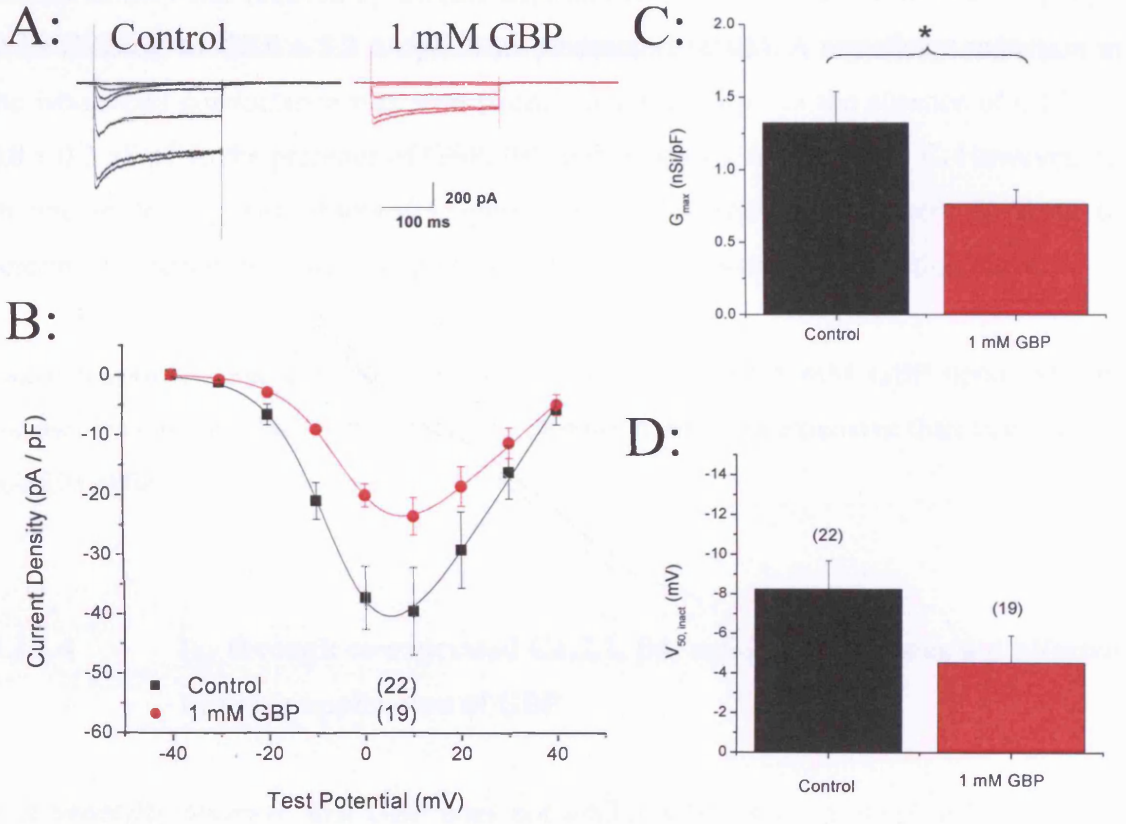

Figure 5.9. Chronic exposure to 1 mM GBP inhibits I_{Ba} in cultured DRGs. (**A**), Representative current traces for control and 1 mM GBP conditions, in response to test potentials from -40 mV to +10 mV. Holding potential was -40 mV. (**B**). I-V relationships for the control (black squares, n=22) and 1 mM GBP (red circles, n=19) conditions. The mean data are fitted with the IVFIT function. Mean data for G_{max} (**C**) and $V_{50,\ act}$ (**D**; no significant difference) were obtained by fitting individual I-V traces with the IVFIT function. * denotes $P<0.05$ (Student's t test).

DRGs express a number of VGCC types, including N-type, P/Q type and T-type (Varadi et al., 1999). T-type current was inactivated by holding cells at -40 mV, and sodium currents blocked using 500 nM TTX (see Materials and Methods).

As shown in Figure 5.9, the inhibition observed in DRGs was in line with that seen using tsA-201 cells. These included a significant inhibition of current amplitude (Figure 5.9 A), as well as the corresponding peak-current density (Figure 5.9 B). Mean peak-current density was reduced by chronic exposure to 1 mM GBP from -39.6 ± 7.4 pA/pF in its absence, to -23.6 ± 3.2 pA/pF in its presence ($P<0.05$). A significant reduction in the whole-cell conductance was seen (from 1.3 ± 0.2 nS/pF in the absence of GBP, to 0.8 ± 0.1 nS/pF in the presence of GBP, $P<0.05$), as shown in Figure 5.9 C. However, no change in $V_{50,\ act}$ was observed (Figure 5.9 D). Insufficient data were obtained to determine whether there was a depolarisation of the steady-state inactivation curve.

Taken together, these data suggest an inhibitory effect of 1 mM GBP upon calcium channel currents in DRGs. However, the inhibition was less extensive than that seen in tsA-201 cells.

5.2.1.4 I_{Ba} through co-expressed $Ca_v2.1$, β4, $\alpha_2\delta$-2 channels was not affected by acute application of GBP

It is generally accepted that GBP does not inhibit VGCCs via a physical binding and immediate block of the channels. Currents in tsA-201 cells (expressing the same $Ca_v2.1$, β4, $\alpha_2\delta$-2 as used in previous experiments) were recorded as usual, and run-up of currents allowed to proceed to completion. A test potential of +10 mV was then applied every 30 seconds (Figure 4.10 A). Acute application of GBP for 10 min (via a gravity feed) did not cause a significant inhibition of current amplitude, as shown in representative current traces comparing zero (black) and 10 min (blue) after application of GBP (or external solution in the control condition), as shown in Figure 5.10 B. The

mean data showed no significant inhibition of 1 mM GBP applied for 10 min both over the 10 minute period (Figure 5.10 C), or afterwards (Figure 5.10 D).

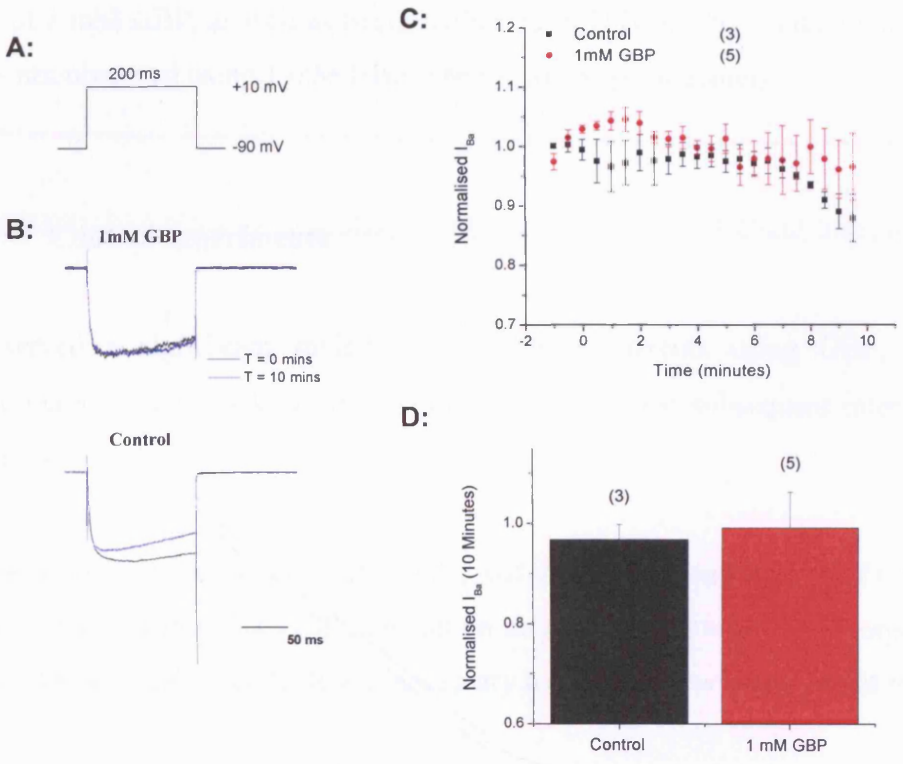

Figure 5.10. Acutely applied 1 mM GBP does not inhibit calcium channels. (**A**), A test potential of +10 mV was applied to cells (holding potential was -90 mV). (**B**), Representative current traces before (black) and after (blue) a 10 minute application of external solution (control) or external solution containing 1 mM GBP. (**C**), Time-course of drug-application. Currents are normalised to the mean value of three time-points immediately preceding the initiation of drug application. (**D**), Bar-chart showing the mean normalised I_{Ba} after 10 min of drug application. No significant difference was observed between the means.

The findings of these initial experiments describe the inhibitory effects of chronic application of GBP. The inhibition is concentration-dependent, and the results are consistent with an impairment of $\alpha_2\delta$ functionality. The same results were obtained for subunit combinations containing both the $\alpha_2\delta$-1 and $\alpha_2\delta$-2 subunits with the chronic application of 1 mM GBP, as well as being replicated in DRGs. The reduction in current density was not observed using 1 mM GBP when it was applied acutely.

5.2.2 Control experiments

Having observed a significant inhibition of calcium currents using GBP, it was necessary to demonstrate this as a function of $\alpha_2\delta$ binding and subsequent interference of $\alpha_2\delta$ function.

The protocol used for transfection of the cells, and subsequent application of GBP 1 h later, meant it was feasible that GBP application could interfere with the incorporation of plasmids into the tsA-201 cells. It was necessary to determine whether or not this was the case.

The hypothesis proposed that GBP acts via binding to $\alpha_2\delta$ proteins. Therefore several experiments were carried out, all using co-expressed $\alpha_2\delta$ proteins that have been shown not to bind GBP: $\alpha_2\delta$-1 R217A (Bian et al., 2006); $\alpha_2\delta$-2 R282A (Davies et al., 2006); and $\alpha_2\delta$-3 (Marais et al., 2001), in order to show that GBP binding is necessary for the inhibitory effects observed.

5.2.2.1 $\alpha_2\delta$-1 R217A

Chronic application of 1 mM GBP was found not to inhibit currents produced by co-expressed $Ca_v2.2$, β1b and $\alpha_2\delta$-1 R217A (Figure 5.11 A). The mean peak current density observed in the presence of 1 mM GBP (-100.3 ± 18.4 pA/pF) was similar to that observed in control (-91.7 ± 25.7 pA/pF), as shown in Figure 5.11 B. Furthermore, no significant change (at $P<0.05$) in whole-cell conductance (3.8 ± 1.1 nS/pF in the absence, 3.5 ± 0.9 nS/pF, in the presence of 1 mM GBP) was detected (Figure 5.11 C), as was the case for $V_{50,\,act}$ (Figure 5.11 D).

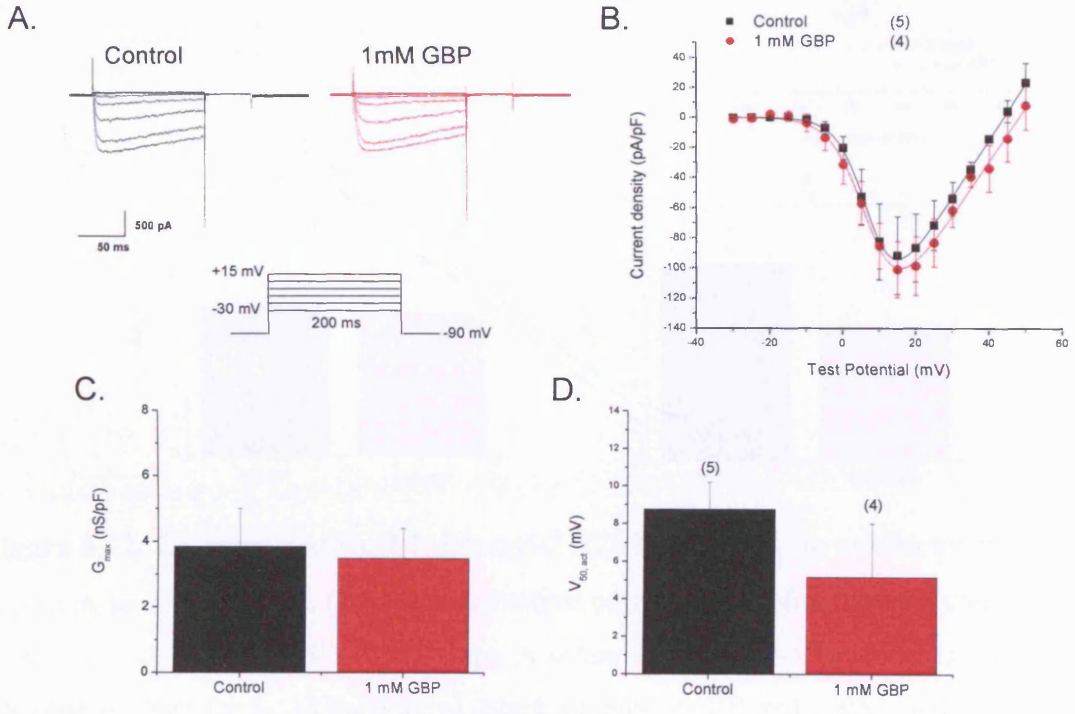

Figure 5.11. Co-expressed $Ca_v2.2$, β1b, $\alpha_2\delta$-1 R217A currents were unaffected by chronic exposure to 1 mM GBP. (**A**), Representative current traces for the two conditions in response to -30 to +15 mV voltage steps. A schematic of the I-V protocol is shown. (**B**), I-V relationships for I_{Ba} in the control (black squares, n=5) and 1 mM GBP (red circles, n=4) conditions. Current amplitude was normalised to whole-cell capacitance and plotted against membrane potential. Holding potential was -90 mV.

Mean values for G_{max} (**C**) and $V_{50,\ act}$ (**D**) were obtained from fits of individual I-V relationships using the IVFIT function. No significant difference in mean values for G_{max} or $V_{50,\ act}$ were observed.

5.2.2.2 $\alpha_2\delta$-2 R282A

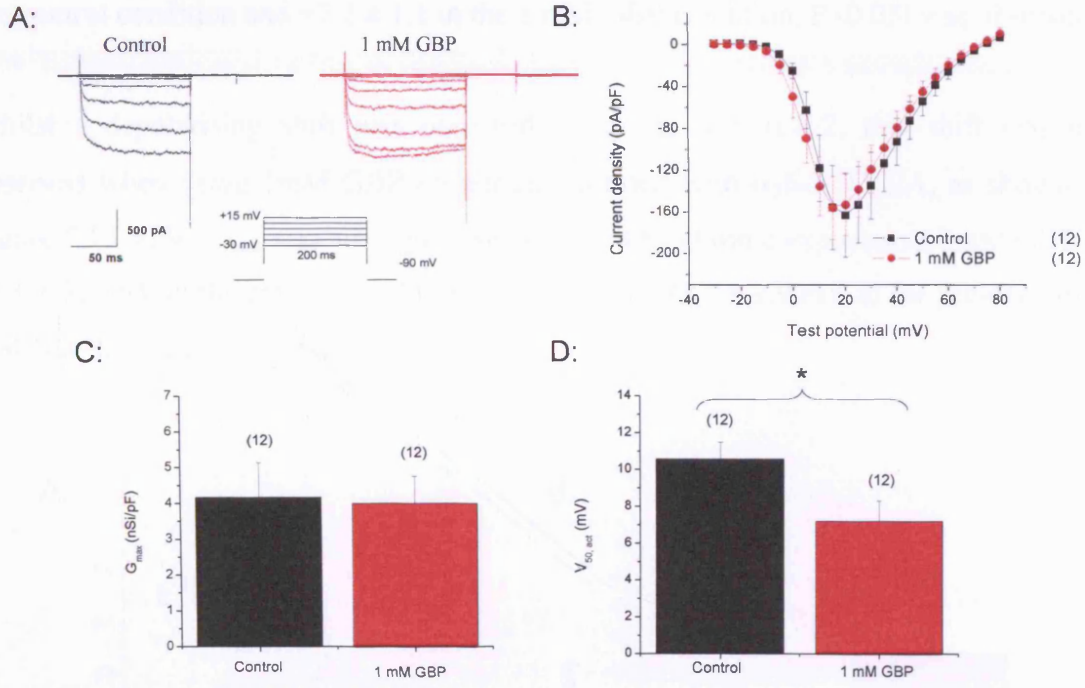

Figure 5.12. Co-expressed $Ca_v2.1$, β4, $\alpha_2\delta$-2 R282A currents are unaffected by chronic exposure to 1 mM GBP. (**A**), Representative current traces for the two conditions in response to -30 to +15 mV voltage steps. A schematic of the I-V protocol is shown. (**B**), I-V relationships for I_{Ba} in the control (black squares, n=12) and 1 mM GBP (red circles, n=12) conditions. Current amplitude was normalised to whole-cell capacitance and plotted against membrane potential. Holding potential was -90 mV. Mean values for G_{max} (**C**) and $V_{50,\ act}$ (**D**) were obtained from fits of individual I-V relationships using the IVFIT function. No significant difference in mean values for G_{max} were observed.

1 mM GBP was applied chronically to cells co-expressing the $Ca_v2.1$, β4 and $\alpha_2\delta$-2 R282A subunit combination. The currents obtained were unaffected by chronic exposure to 1 mM GBP (Figure 5.12 A). Mean peak-current densities obtained in the presence (-156.3 ± 29.5 pA/pF) and absence (-163.0 ± 40.3 pA/pF) of 1 mM GBP were similar (Figure 5.12 B). G_{max} (4.1 ± 1.0 nS/pF in the control condition and 4.0 ± 0.8 nS/pF in the 1 mM GBP condition) remained unaffected by chronic application of 1 mM GBP (Figure 5.12 C). However, a significant hyperpolarisation of $V_{50,\,act}$ (+10.5 ± 0.9 mV in the control condition and +7.2 ± 1.1 in the 1 mM GBP condition, $P<0.05$) was observed.

Whilst a depolarising shift was observed using the WT $\alpha_2\delta$-2, this shift was not observed when using 1mM GBP on currents formed with $\alpha_2\delta$-2 R282A, as shown in Figure 5.13 A. $V_{50,\,inact}$ was not significantly altered by chronic exposure to 1mM GBP (-30.1 ± 3.2 mV in the control condition, compared to -33.1 ± 2.9 mV in the presence of 1 mM GBP), as shown in Figure 5.13 B.

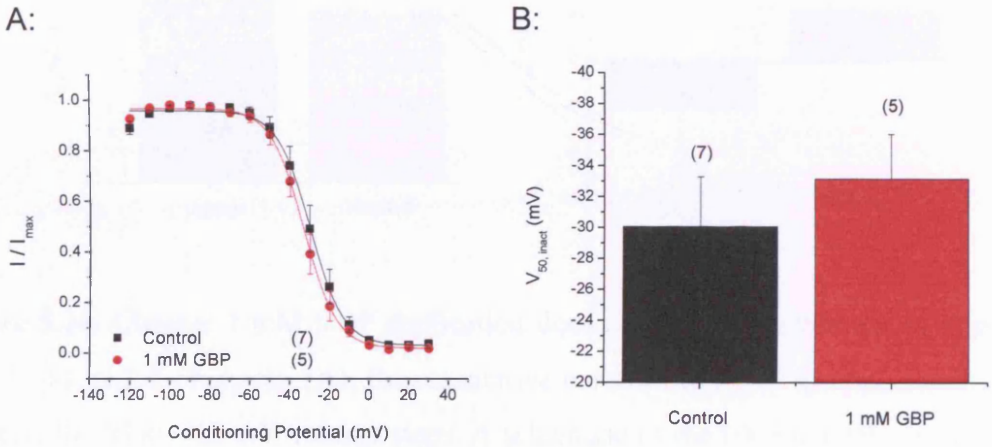

Figure 5.13. Steady-state inactivation of co-expressed $Ca_v2.1$, β4, $\alpha_2\delta$-2 R282A channels remains unaffected by chronic exposure to 1 mM GBP. (**A**), Steady-state inactivation curves for control (black squares, n=7) and 1 mM GBP (red circles, n=5) conditions. Curves are Boltzmann fits to the mean data. (**B**), Mean $V_{50,\,inact}$ data were obtained by fitting a Boltzmann function to individual steady-state inactivation curves, and were not statistically different.

5.2.2.3 $\alpha_2\delta$-3

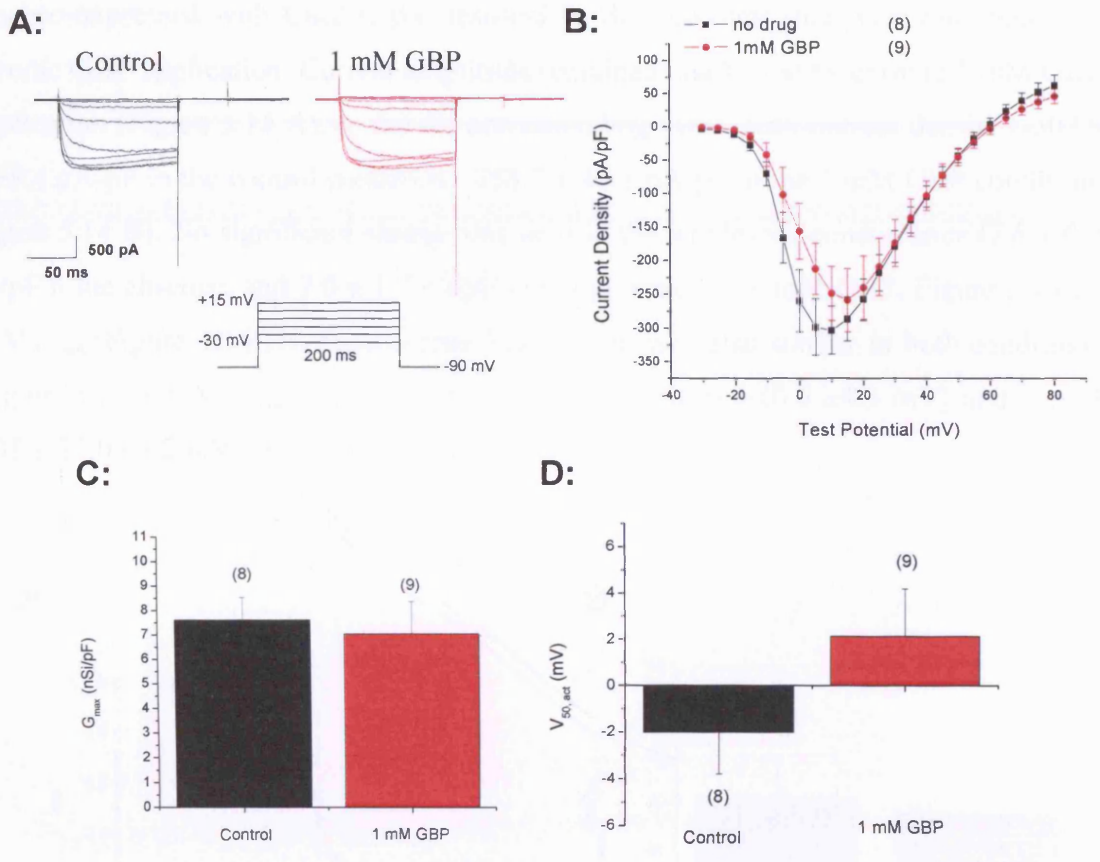

Figure 5.14. Chronic 1 mM GBP application does not inhibit I_{Ba} through co-expressed $Ca_v2.1$, β4, $\alpha_2\delta$-3 channels. (**A**), Representative current traces for the two conditions in response to -30 to +15 mV voltage steps. A schematic of the I-V protocol is shown. (**B**), I-V relationships for I_{Ba} in the control (black squares, n=8) and 1 mM GBP (red circles, n=9) conditions. Current amplitude was normalised to whole-cell capacitance and plotted against membrane potential. Holding potential was -90 mV. Mean values for G_{max} (**C**) and $V_{50, act}$ (**D**) were obtained from fits of individual I-V relationships using the IVFIT function. No significant difference in mean values for G_{max} or $V_{50, act}$ were observed.

The $\alpha_2\delta$ RRA proteins have impaired function, as discussed in Chapter 4. Therefore, $\alpha_2\delta$-3 was selected for use as a "fully-functional" $\alpha_2\delta$ protein that would not bind GBP. As was the case for the two RRA mutant $\alpha_2\delta$ subunits, the expression of $\alpha_2\delta$-3 (in this case co-expressed with $Ca_v2.1$, $\beta4$) resulted in Ba^{2+} currents that were unchanged by chronic GBP application. Current amplitude remained unaffected by chronic 1 mM GBP application (Figure 5.14 A), as did the corresponding mean peak-current density (-302.9 ± 35.4 pA/pF in the control condition, -258.7 ± 46.8 pA/pF in the 1 mM GBP condition, Figure 5.14 B). No significant change was seen in the whole-cell conductance (7.6 ± 0.9 nS/pF n the absence, and 7.0 ± 1.3 nS/pF in the presence of 1 mM GBP, Figure 5.14 C) or $V_{50,\ act}$ (Figure 5.14 D). Steady-state inactivation was also similar in both conditions (Figure 5.15 A). $V_{50,\ inact}$ was similar in both the control (-40.6 ±4.3 mV) and 1 mM GBP (-39.0 ±3.2 mV) conditions (Figure 5.15 B).

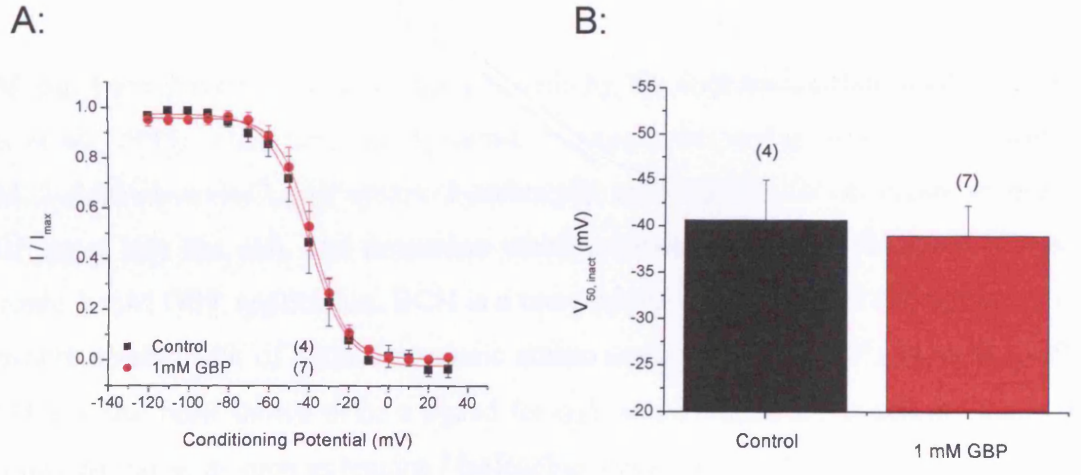

Figure 5.15. Steady state inactivation of co-expressed $Ca_v2.1$, $\beta4$, $\alpha_2\delta$-3 channels is unaffected by 1 mM GBP. (**A**), Steady-state inactivation curves for control (black squares, n=4) and 1 mM GBP (red circles, n=7) conditions. Curves are Boltzmann fits to the mean data. Holding potential was -100 mV. (**B**), Mean $V_{50,\ inact}$ data were obtained by fitting a Boltzmann function to individual steady-state inactivation curves, and were not statistically different (Student's t-test).

These control experiments therefore demonstrate that the $\alpha_2\delta$ proteins known to display negligible binding of GBP are not affected by the chronic application of GBP, thereby indicating that the inhibition of currents by GBP shown initially is mediated by $\alpha_2\delta$ subunits, and their binding to GBP.

5.2.3 Block of GBP-mediated inhibition using 2-Aminobicyclo(2,2,1)-heptane-2-carboxylic acid

If GBP were to interfere with the trafficking of calcium channels, it would need to be present in the cytoplasm, in order to bind $\alpha_2\delta$ protein before or during trafficking. Therefore GBP would elicit the inhibitory effects seen in previous experiments inside the cell, rather than at channels already expressed at the cell surface.

GBP has been shown to be taken up into cells by the System-L amino-acid transporter (Su et al., 1995). Therefore, the System-L transport mechanism was blocked with 10 mM 2-Aminobicyclo(2,2,1)heptane-2-carboxylic acid (BCH), in an effort to prevent GBP entry into the cell, and determine whether this affected the inhibitory effects of chronic 1 mM GBP application. BCH is a competitive blocking agent for System-L that prevents uptake both of neutral aromatic amino acids and also GBP (Su et al., 1995). BCH has also been shown to be a ligand for $\alpha_2\delta$, albeit with a lower affinity than GBP or other amino acids such as leucine / isoleucine (Gong et al., 2001) .

5.2.3.1 Chronic application of BCH alone

It was important to determine whether chronic application of BCH had a noticeable effect on calcium channel currents when applied at a concentration of 10 mM. BCH was applied in the same way as GBP, after transfection of VGCC subunits and for a period of ~40 h. No effect on the current amplitude (Figure 5.16 A) or mean peak-current density (Figure 5.16 B) was observed. The mean peak current density obtained in the presence of chronic BCH application was similar (-333.0 ± 73.2 pA/pF) to that obtained in its absence (-330.2 ± 84.7 pA/pF). Values for G_{max} (8.0 ± 2.1 nS/pF in the absence, and 8.4 ± 1.8 nS/pF in the presence of 10 mM BCH, as shown in Figure 5.16 C) and $V_{50,\,act}$ (+3.4 ± 1.5 mV in the absence, and +5.4 ± 0.9 mV in the presence of 10 mM BCH, as shown in Figure 5.16 D) were also similar.

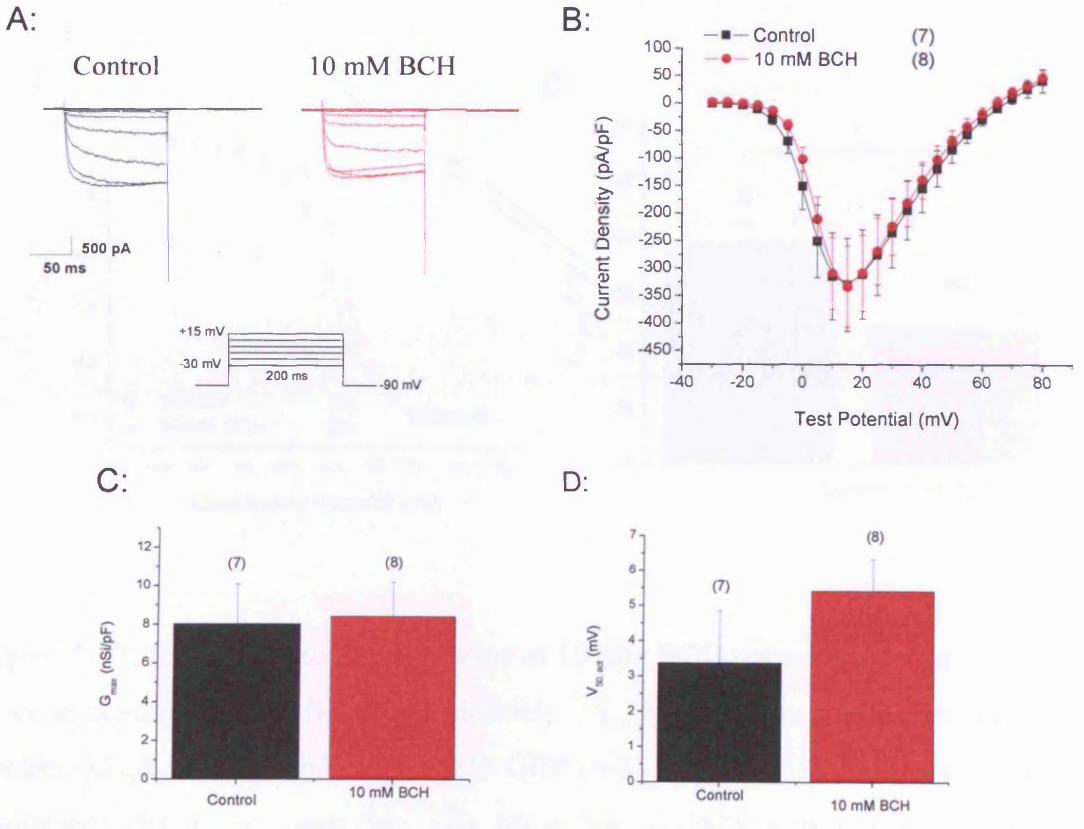

Figure 5.16. Application of 10 mM BCH has no effect on I_{Ba} through co-expressed $Ca_V2.1$, β4, $\alpha_2\delta$-2 channels. (**A**), Representative current traces for the two conditions in

response to -30 to +15 mV voltage steps. A schematic of the I-V protocol is shown. (**B**), I-V relationships for I_{Ba} in the control (black squares, n=7) and 1 mM GBP (red circles, n=8) conditions. Current amplitude was normalised to whole-cell capacitance and plotted against membrane potential. Holding potential was -90 mV. Mean values for G_{max} (**C**) and $V_{50,\ act}$ (**D**) were obtained from fits of individual I-V relationships using the IVFIT function. No significant difference in mean values for G_{max} or $V_{50,\ act}$ were observed (Student's t-test).

However, the steady-state inactivation curve obtained in the presence of 10 mM BCH was depolarised from the control curve (Figure 5.17 A). $V_{50,\ inact}$ was shifted significantly (-39.9 ± 2.0 mV in the control condition, and -32.0 ± 2.0 mV in the 10 mM BCH condition, $P<0.05$), as shown in Figure 5.17 B.

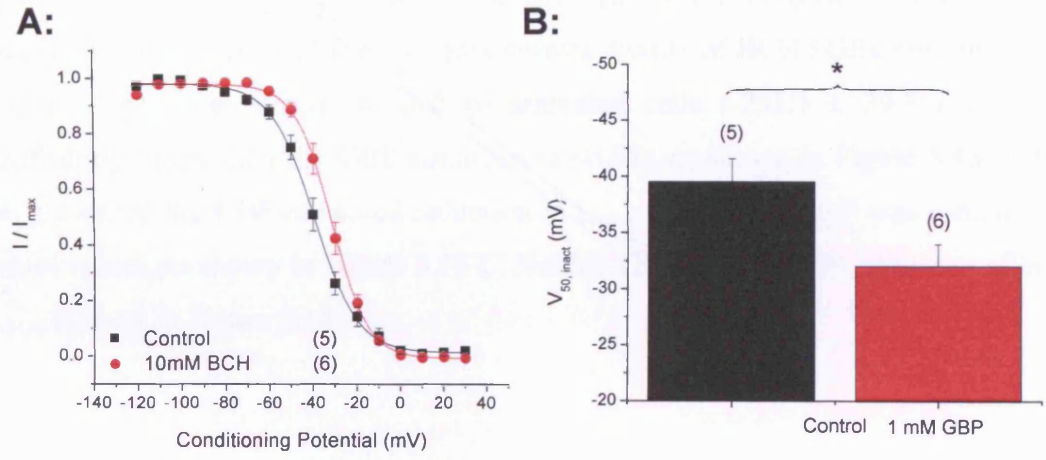

Figure 5.17. Effect of chronic application of 10 mM BCH upon steady state inactivation of co-expressed $Ca_v2.1$, β4, $\alpha_2\delta$-2 channels. (**A**), Steady-state inactivation curves for control (black squares, n=5) and 1 mM GBP (red circles, n=6) conditions. Curves are Boltzmann fits to the mean data. (**B**), Mean $V_{50,\ inact}$ data were obtained by fitting a Boltzmann function to individual steady-state inactivation curves. * denotes $P<0.05$ (Student's t-test).

Together, these results allude to a possible inhibition of $\alpha_2\delta$ biophysical effect at the channel surface, but that the ability of $\alpha_2\delta$ to enhance expression of the $Ca_v\alpha_1$ subunit remains intact.

5.2.3.2 Chronic BCH application in conjunction with 1mM GBP

10 mM BCH was applied to cells for 1 h before chronic 1 mM GBP application, and for the entire period of GBP application (see Materials and Methods). This prevented the inhibitory effect of 1 mM GBP on the currents (Figure 5.18 A). As shown in previous experiments, chronic 1 mM GBP application acted to inhibit I_{Ba} (from -251.1 ± 39.3 pA/pF to 118.6 ± 30.12 pA/pF, $P<0.05$) and reduce the G_{max} of cells (from 6.0 ± 0.8 nS/pF to 3.1 ± 0.8 nS/pF, $P<0.05$), as shown in Figures 5.18 B and C respectively. Co-application of 10 mM BCH with 1 mM GBP (BCH 1 h beforehand) prevented any observed inhibitory effect, the mean peak current density of BCH / GBP currents (-226.6 ± 43.4 pA/pF) was similar to that of untreated cells (-251.1 ± 39.3 pA/pF), and significantly larger than the GBP condition ($P<0.05$), as shown in Figure 5.18 B. BCH also prevented the GBP-mediated reduction in G_{max} (5.8 ± 1.0 nS/pF was similar to the control value), as shown in Figure 5.18 C. Neither GBP of GBP + BCH had an effect on $V_{50,\,act}$ (shown in Figure 5.18 D).

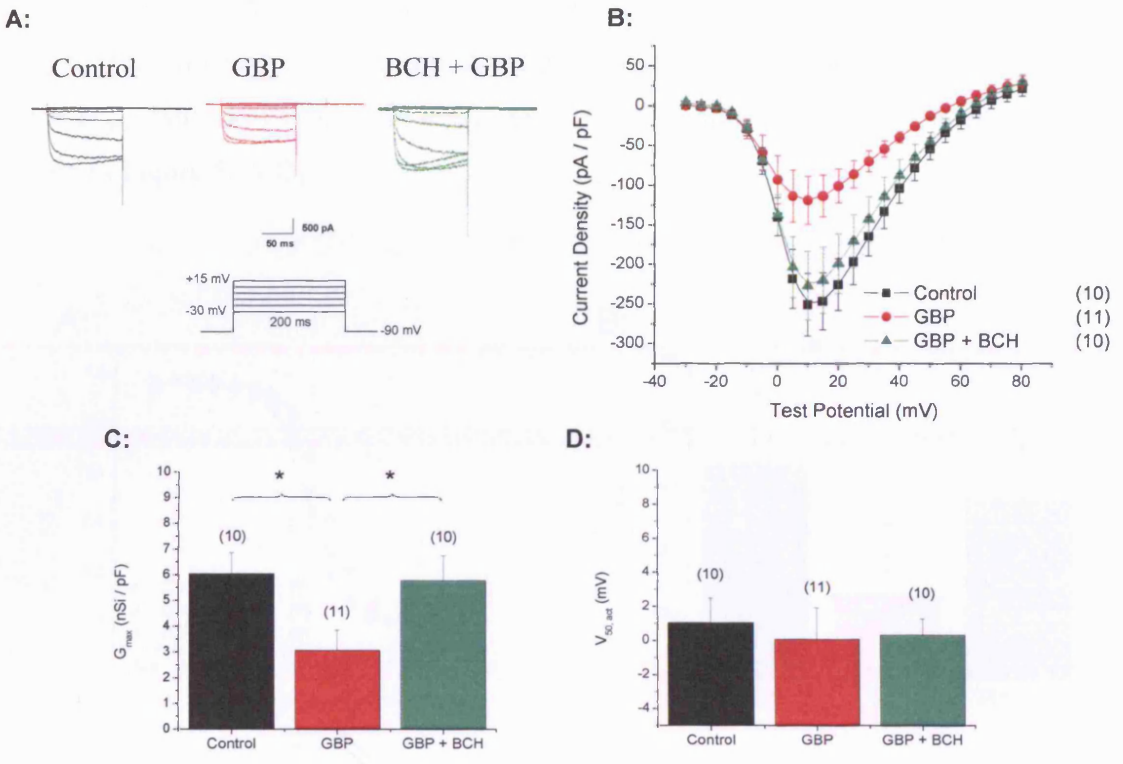

Figure 5.18. 10 mM BCH prevents the inhibitory effects of 1 mM GBP upon I_{Ba} through VGCCs composed of $Ca_v2.1$, β4, $\alpha_2\delta$-2. (**A**), Representative current traces for the three conditions in response to -30 to +15 mV voltage steps. A schematic of the I-V protocol is shown. (**B**), I-V relationships for I_{Ba} in the control (black squares, n=10), GBP (red circles, n=11) and GBP + BCH (green triangles, n=10) conditions ($P<0.05$, ANOVA). Current amplitude was normalised to whole-cell capacitance and plotted against membrane potential. Holding potential was -90 mV. Mean values for G_{max} (**C**) and $V_{50,\,act}$ (**D**) were obtained from fits of individual I-V relationships using the IVFIT function. No significant difference in mean values of $V_{50,\,act}$ was observed. * denotes $P<0.05$ (ANOVA).

1 mM GBP also failed to cause depolarising shift in the steady-state inactivation whilst in the presence of 10 mM BCH (Figure 5.19 A). The significant depolarising shift in $V_{50,\,inact}$ (-31.7 ± 3.1 mV) from the control condition (-42.0 ± 3.6 mV, $P<0.05$) was not

replicated with 1 mM GBP co-applied with 10 mM BCH, which was similar (-39.2 ± 1.7 mV) to that obtained in the control condition, although not significantly different from the $V_{50,\ inact}$ values obtained for either the control condition of the GBP condition (as shown in Figure 5.19 B).

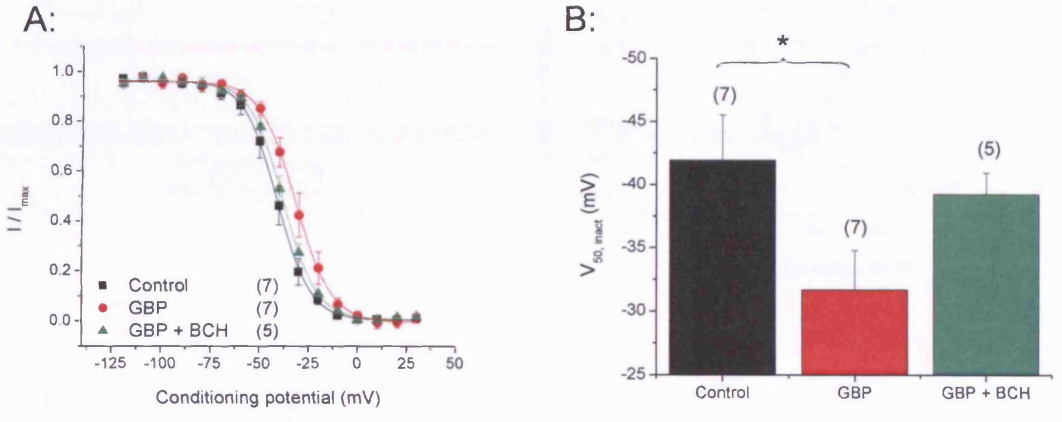

Figure 5.19. 10 mM BCH prevents the GBP-mediated depolarisation of steady-state inactivation in cells expressing $Ca_v2.1$, β4, $\alpha_2\delta$-2. (**A**), Steady-state inactivation curves for control (black squares, n=7), GBP (red circles, n=7) and GBP + BCH (green triangles, n=5) conditions ($P<0.05$, ANOVA). Curves are Boltzmann fits to the mean data. (**B**), Mean $V_{50,\ inact}$ data were obtained by fitting a Boltzmann function to individual steady-state inactivation curves. * denotes $P<0.05$ (ANOVA). No significant difference was observed between the means of the GBP and GBP + BCH conditions.

5.2.4 Effect of chronic 1 mM GBP application on calcium channel currents resulting from $Ca_v2.1$, β4, in a stable $\alpha_2\delta$-2 cell-line

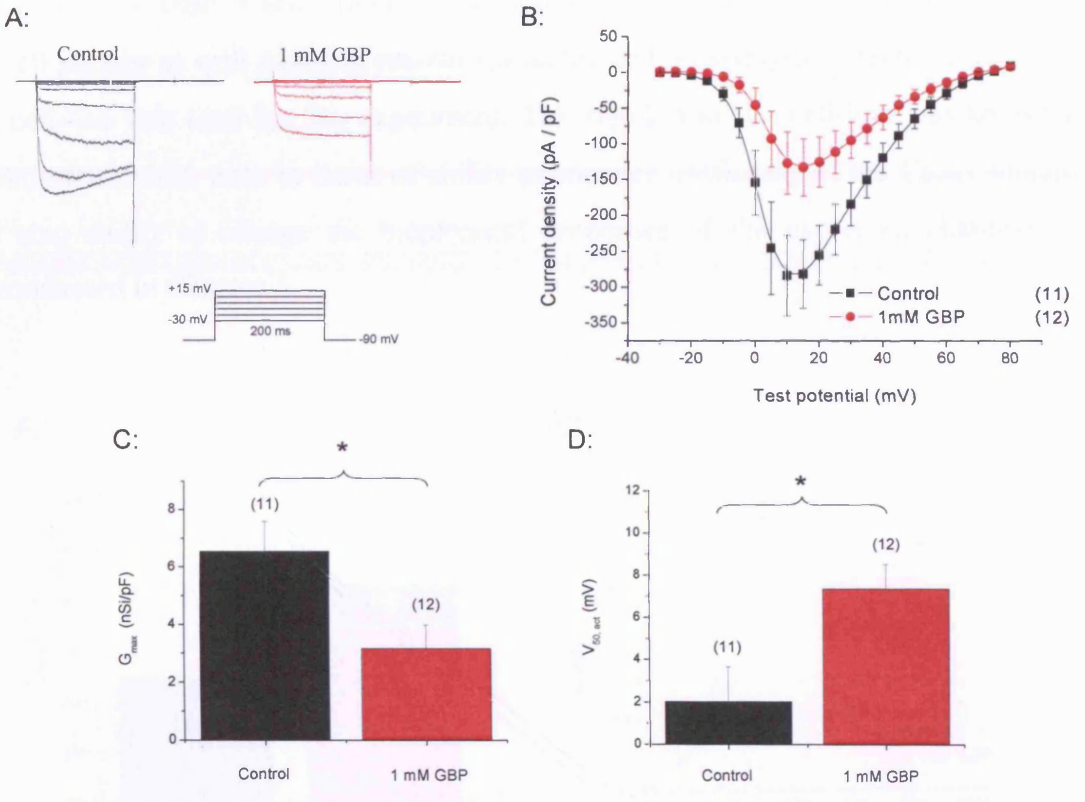

Figure 5.20. Chronic 1mM GBP inhibits currents formed by channels including stably-expressed $\alpha_2\delta$-2 co-expressed with $Ca_v2.1$ and β4. (**A**), Representative current traces for the two conditions in response to -30 to +15 mV voltage steps. A schematic of the I-V protocol is shown. (**B**), I-V relationships for control (black squares, n=11) and 1 mM GBP (red circles, n=12) conditions. Current amplitude was normalised to whole-cell capacitance and plotted against membrane potential. Holding potential was -90 mV. Mean values for G_{max} (**C**) and $V_{50,\ act}$ (**D**) were obtained from fits of individual I-V relationships using the IVFIT function. * denotes $P<0.05$ (Student's t-test).

The application of GBP to cells transiently transfected with calcium channel subunits was engineered in such a way that GBP would enter the cells and bind $\alpha_2\delta$ protein before it is functionally expressed at the cell surface. However, it was also important to determine how GBP would affect a system where functional $\alpha_2\delta$ already expressed at the cell surface as well as being present inside the cell. A stably-transfected $\alpha_2\delta$-2 mid-HA cell-line was used for this experiment. This $\alpha_2\delta$-2 mid-HA cell-line was known to be fully functional, both in terms of ability to enhance trafficking of the $Ca_v\alpha_1$ subunit, and also ability to change the biophysical properties of the expressed channels, as demonstrated in Chapter 3.

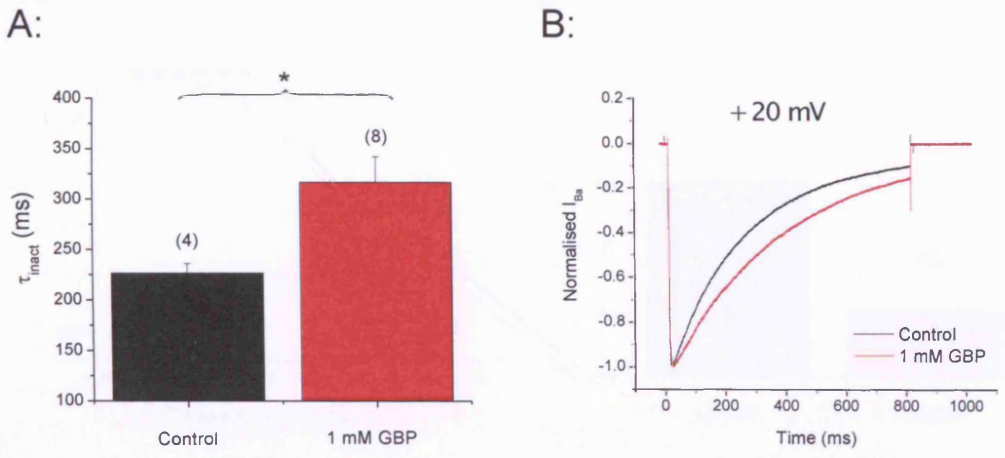

Figure 5.21. Effect of chronic exposure to 1 mM GBP upon I_{Ba} inactivation kinetics of co-expressed $Ca_v2.1$ and $\beta4$ in a stable $\alpha_2\delta$-2 mid-HA-expressing cell-line. (**A**), Mean time-constant of inactivation (τ_{inact}) data is shown for control (black, n=4) and 1 mM GBP (red, n=8) conditions (in response to a test-potential of +20 mV for 800 ms). Holding potential was -90 mV. The decay phase of individual current traces at +10 mV was fitted with a single exponential function. (**B**), Representative current traces of control and 1 mM GBP conditions in response to a long depolarising voltage step to +20 mV, traces are normalised to peak. * denotes $P<0.05$, (Student's t-test).

Application of chronic 1 mM GBP had the same inhibitory effect on stably-transfected $\alpha_2\delta$-2 subunits as was seen with transiently transfected $\alpha_2\delta$-2 subunits. Representative current traces show the reduction in current amplitude observed in the 1 mM GBP condition (Figure 5.20 A). Similar reductions in current density (-283.6 ± 56.4 pA/pF reduced to -132.2 ± 39.8 pA/pF, $P<0.05$), as shown in Figure 5.20 B. A corresponding reduction in whole-cell conductance (6.54 ± 1.0 nS/pF reduced to 3.16 nS/pF ± 0.8, $P<0.05$) was observed, as well as a shift in $V_{50,\,act}$ (shifted from +2.0 ± 1.6 mV to +7.3 ± 1.2 mV, $P<0.05$), as shown in Figures 5.20 C and D respectively.

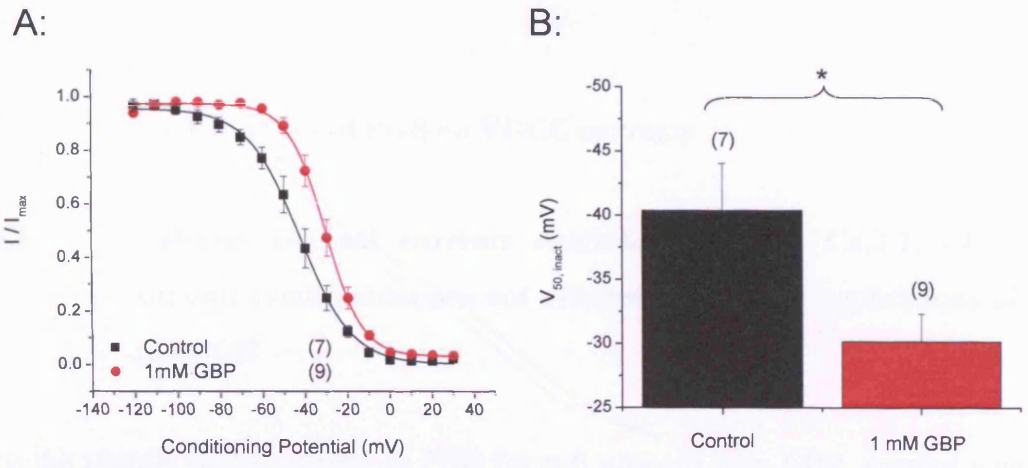

Figure 5.22. Effect of chronic exposure to 1 mM GBP upon steady-state inactivation of $Ca_v2.1$, β4, stable $\alpha_2\delta$-2-expressing cells. (**A**), Steady-state inactivation curves for control (black squares, n=7) and 1 mM GBP (red circles, n=9) conditions. Curves are Boltzmann fits to the mean data. (**B**), Mean $V_{50,\,inact}$ data were obtained by fitting a Boltzmann function to individual steady-state inactivation curves, and were not statistically different. * denotes $P<0.05$ (Student's t-test).

A reduction in the rate of channel inactivation was also observed, from 226.2 ± 9.5 ms in the control condition, to 316.4 ± 25.5 ms in the presence of chronic 1 mM GBP ($P<0.05$), as shown in Figure 5.21 A. Representative current traces are shown in Figure

5.21 B. The steady-state inactivation curve was depolarised by chronic exposure to 1 mM GBP (Figure 5.22 A), to the same extent as observed when using transiently transfected $\alpha_2\delta$-2. $V_{50,\ inact}$ was shifted from -40.4 ± 3.7 mV, to -30.1 ± 2.2 mV ($P<0.05$), as shown in Figure 5.22 B.

The similar inhibition of stably transfected $\alpha_2\delta$-2 to transiently transfected $\alpha_2\delta$-2 by GBP, coupled with its lack of inhibition on $\alpha_2\delta$-2 when applied acutely, provides evidence that GBP can interfere with $\alpha_2\delta$ function through penetrating the cell and interfering with forward trafficking of calcium channel subunits within the cell.

5.2.5 Lack of effect of PGB on VGCC currents

5.2.5.1 Calcium channel currents resulting from the $Ca_v2.1$, β4, $\alpha_2\delta$-2 subunit combination are not affected by chronic applications of 200 μM PGB

Given the slightly higher affinity of PGB for $\alpha_2\delta$ subunits over GBP, coupled with the significant inhibition seen with chronic exposure to 100 μM GBP, an initial concentration of 200 μM PGB was selected for use (see Figure 5.23 A). However, no significant inhibition of currents (through co-expressed $Ca_v2.1$, β4, $\alpha_2\delta$-2 channels) was observed. The mean peak current density for currents recorded in the presence of 200 μM PGB was reduced (-199.7 ± 38.6 pA/pF), although not significantly compared to those recorded in the absence of PGB (-241.0 ± 29.8 pA/pF).

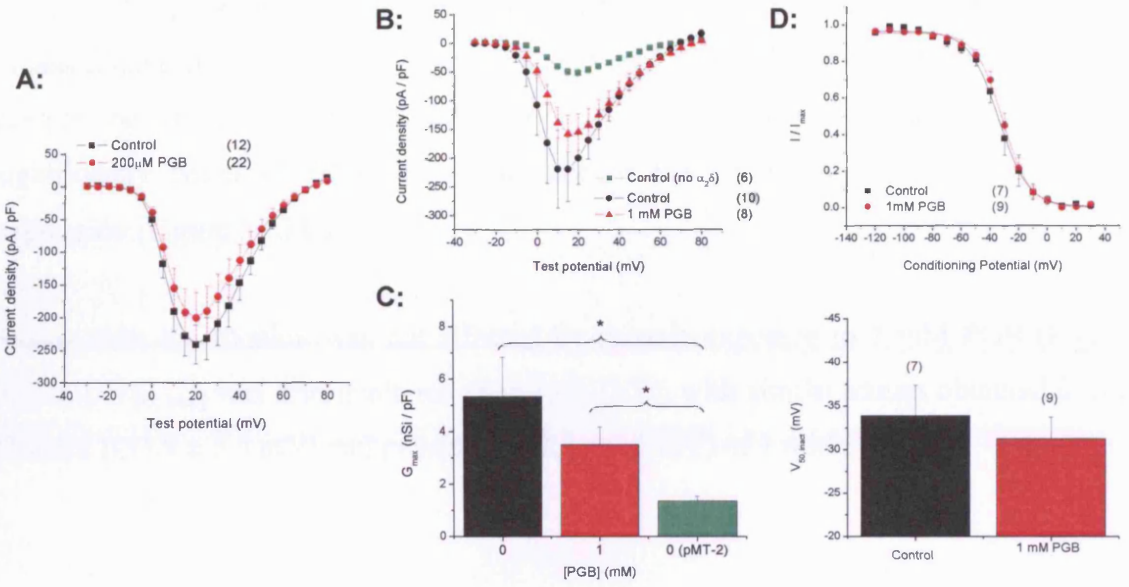

Figure 5.23. Chronic exposure to 1 mM PGB does not inhibit I_{Ba} through co-expressed $Ca_v2.1$, β4, $\alpha_2\delta$-2 channels. (**A**), I-V relationships for control (black squares, n=12) and 200 μM PGB (red circles, n=22) conditions. (**B**) I-V relationships for control (black circles, n=10) and 1 mM PGB (red triangles, n=8) conditions, as well as a control condition excluding co-expressed $\alpha_2\delta$-2 (green squares, n=6) are shown. Holding potential was -90 mV. (**C**), Corresponding mean values for G_{max} were calculated by fitting the IVFIT function to -30 to + 50 mV portions of individual I-V curves (* denotes $P<0.05$, ANOVA). (**D**), Steady-state inactivation curves for control (black squares, n=7) and 1 mM PGB (red circles, n=9) conditions. Curves are Boltzmann fits the the mean data. (**E**), No difference was observed in the mean values for $V_{50,\ inact}$ of the two conditions.

5.2.5.2 Calcium channel currents resulting from the $Ca_v2.1$, β4, $\alpha_2\delta$-2 subunit combination are affected by chronic applications of 1 mM PGB

Therefore, chronic application of a larger concentration (1 mM) of PGB was used. The reduction in mean peak current density from the control (from -219.3 ± 56.0 pA/pF to -

154.6 ± 31.4 pA/pF) was larger, but still statistically non-significant, suggesting a lack of perceivable effect of chronic application of 1 mM PGB (Figure 5.23 B). This was also seen in the similar G_{max} values obtained for the two conditions, both of which were significantly larger ($P<0.05$) than that seen in the condition excluding $\alpha_2\delta$-2 co-expression (Figure 5.23 C).

Steady-state inactivation was not affected by chronic exposure to 1 mM PGB (Figure 5.23 D). $V_{50,\ inact}$ was also unaltered (Figure 5.23 E), with similar values obtained in the absence (-33.9 ± 3.5 mV) and presence (-31.3 ± 2.5 mV) of 1 mM PGB.

5.3 Discussion

Since the discovery that GBP binds the calcium channel $\alpha_2\delta$ subunit (Gee et al., 1996), many studies have examined whether GBP has an inhibitory effect on calcium channel currents. The concept of GBP acting to reduce calcium channel function, and by extension, reduce neurotransmitter release, has long been a proposed mechanism of action (Taylor et al., 1998). A number of studies have demonstrated small or state-dependent reductions in neurotransmitter release when GBP has been applied (see Introduction).

The inhibitory effect of GBP is mediated through the $\alpha_2\delta$ subunit

GBP remains a ligand known to bind only to the $\alpha_2\delta$-1 and $\alpha_2\delta$-2 subunits, and this has been shown to be important for its action (Field et al., 2006). Therefore the link between GBP and a reduction in neurotransmitter release most probably lies in its binding to the $\alpha_2\delta$ subunit (Taylor et al., 1998). Non-GBP-binding $\alpha_2\delta$ protein was used in this study as a means of implicating $\alpha_2\delta$ as the site of action of GBP. GBP binding to $\alpha_2\delta$ has been shown to be mediated through an RRR motif in the α_2 subunit (Wang et al., 1999). This study used the RRA mutant $\alpha_2\delta$ proteins that do not bind GBP (Field et al., 2006; Davies

et al., 2006). Use of either RRA mutant $\alpha_2\delta$, co-expressed with $Ca_v\alpha_1$ and β subunits resulted in a lack of inhibition when applying GBP. In addition, use of the non GBP-binding $\alpha_2\delta$-3 subunit (Marais et al., 2001) also resulted in a lack of inhibition of current amplitude by chronic 1mM GBP.

As no inhibitory effects of 1 mM GBP were observed when using $\alpha_2\delta$ subunits that do not bind GBP, it can be concluded that the inhibitory effects of GBP seen in this study are mediated through binding to the $\alpha_2\delta$ subunit.

GBP affects calcium channel currents chronically rather than acutely

Despite reducing the neurotransmitter release associated with P/Q type calcium channel function (Fink et al., 2000; Fink et al., 2002; van Hooft et al., 2002), a direct acute inhibition of calcium channel currents has not been conclusively demonstrated. This study has confirmed a lack of acute inhibition when using 1 mM GBP (applied for 10 min). However, the effects of chronic GBP application suggest the time-course of action is more long-term.

The ability of GBP to inhibit currents on a longer-term time-scale suggests that GBP does not bind to $\alpha_2\delta$ subunits in such a way as to result in channel block. GBP uptake studies (Su et al., 1995) suggest GBP is taken up into cells by amino-acid transporter mechanisms. This intracellular location then becomes a likely site of action for GBP to have a chronic effect. The uptake of GBP would imply that it acts either on immature $\alpha_2\delta$ protein in the processing and trafficking process on the way to being expressed at the membrane, or $\alpha_2\delta$ that has entered the degradation / recycling pathway, having been expressed at the membrane.

The co-application of BCH and GBP results in a prevention of the otherwise inhibitory effects of GBP (see Section 5.2.3). BCH application alone, however, does not cause an inhibition of the currents, suggesting it acts by blocking l-type amino acid transporters.

BCH binds $\alpha_2\delta$ subunits (Gong et al., 2001), and presumably will bind $\alpha_2\delta$ at the cell surface. However this does not result in an inhibition of current density, whole-cell conductance or voltage-dependence of current activation.

When applied alone, BCH does appear to shift the steady-state inactivation curve, as seen in Figure 5.17. When co-applied with GBP, BCH prevents full depolarisation of the steady-state curve (Figure 5.19), resulting in a $V_{50,\ inact}$ intermediate to those of the control and GBP conditions (and not statistically different to either). It could be argued that both BCH and GBP act as ligands for $\alpha_2\delta$, but that BCH binding has a relatively neutral, or less inhibitory effect.

There are several ligands for $\alpha_2\delta$, many which have a similar action to GBP (tested in neuropathic pain models), but also those that have no effect (Lynch, III et al., 2006). There are also proposed positive modulators of $\alpha_2\delta$, amino acids such as leucine and isoleucine (Cunningham et al., 2004) that may be important in the production and function of $\alpha_2\delta$ (Davies et al., 2006), and whose ability to bind and positively modulate $\alpha_2\delta$ might be prevent by ligands such as GBP.

Dose-dependence of GBP and the need for high concentrations to see inhibitory effects

100 μM GBP has only marginal (if any) effects on the channel biophysics, whereas 1 mM GBP results in Ba^{2+} currents that appear to imply the absence of $\alpha_2\delta$. Given the hypothesis that individual GBP molecules bind individual $\alpha_2\delta$ proteins to impair their function, it is feasible the biophysical change from full $\alpha_2\delta$ functionality to no functionality may be graded with GBP concentration. These might be difficult to determine by electrophysiology, hence the apparent lack of effects of 100 μM GBP on channel biophysics, yet the slowing of inactivation kinetics.

A previous study has demonstrated that GBP inhibits I_{Ba} of calcium channels in DRGs in a transgenic mouse line which up-regulates production of $\alpha_2\delta$-1 (Li et al., 2006). There was no inhibition of the I_{Ba} reported in the normal mice. The electrophysiological characteristics of DRGs with up-regulated $\alpha_2\delta$-1 included significant increases in the currents and conductance of the cells, as well as a hyperpolarised voltage-dependence of current activation. This correlates with the data shown in this study if the over-expression of $\alpha_2\delta$ in a cell-line can be said to compare with up-regulated $\alpha_2\delta$-1 in a transgenic mouse. GBP application affected currents in the opposite way, currents and whole-cell conductances were smaller, and the voltage-dependence of current activation was depolarised. In addition, many of these effects were not observed when applying 100 μM GBP.

Therefore, it is plausible that the application of fairly high concentrations of GBP is necessary, in order to enable individual molecules of GBP to bind individual $\alpha_2\delta$ proteins intracellularly and prevent them from carrying out their normal regulatory function on the $Ca_v\alpha_1$ subunit. Coupled with the need to be taken up into cells, and to compete with other ligands of the $\alpha_2\delta$ subunit, such as (L)-leucine (Thurlow et al., 1993), this may explain the need for high concentrations of GBP. Relatively large (compared to other drugs) dose of GBP are given, with maximal daily doses of 1500 mg not uncommon (see Section 1.8.5). A dose of 1424 mg/day equated to a plasma concentration of 8.31 μg/ml (Bialer et al., 2007). This is roughly a 50 μM concentration. Significant differences in current amplitude were found in this study using concentration from 100 μM (lower concentrations were not used). Therefore it is feasible that the effect seen when using 100 μM in an over-expression system may equate to the therapeutic dose seen in patients, although there are many factors ($\alpha_2\delta$ expression levels, cell uptake and subsequent intracellular GBP concentration) that need to be taken into account.

The effect of GBP in different $Ca_v\alpha_1$ subunits

Inhibitory effects of GBP have been demonstrated in DRGs (Li et al., 2006; Sutton et al., 2002). These results are useful in linking binding of GBP to $\alpha_2\delta$–1 subunits to therapeutic use, especially in neuropathic pain conditions- many of which are due to an underlying over-activity of primary afferent neurons. Both $Ca_v2.1$ and $Ca_v2.2$ channels are expressed in DRGs (Varadi et al., 1999), and implicated (although in different phases) of the formalin response in which these neurons are responsible (Diaz and Dickenson, 1997).

Mutations in the CACNA1A gene can underlie conditions such as SCA-6 (See Introduction). Both GBP and PGB show efficacy in cortical cerebellar atrophy (a condition sharing neuropathological similarities to SCA-6. This effect is hypothesised to be due to reducing inactivation rate in Cav2.1 channels (increased in SCA-6, Gazulla and Tintore, 2007).

The importance of $\alpha_2\delta$ over-expression in the action of GBP

One deciding factor in the inhibitory effects of GBP may be its action in the sensitised or "$\alpha_2\delta$-1 up-regulated" state. In the experiment comparing the transgenic mouse DRGs which over-produce $\alpha_2\delta$-1 to those of normal mice (Li et al., 2006), control DRGs were subjected to electrophysiology no later than 8 h after culturing. The DRGs used in the present study were cultured 2-4 days before patching. There is evidence to suggest that cell culture may be responsible for an up-regulation of $\alpha_2\delta$ (and other proteins) in these cells, as the cutting of axons and dendrites during the culture procedure effectively constitutes nerve injury.

This study found an inhibition of peak current density of around 45% when using 1 mM GBP chronically applied to DRGs for 48 h. This compares to an EC_{50} of 2 μM GBP when applied acutely to transgenic mouse DRGs which over-produce $\alpha_2\delta$-1 (Li et al.,

2006). Whilst it is not possible to compare the two experiments directly due to the different culture conditions and the inability to quantify $\alpha_2\delta$ up-regulation in either case, it shows the importance that up-regulation of $\alpha_2\delta$ might have when it comes to the action of GBP.

Comparison of observed effects with those described in the literature

The literature surrounding GBP action at calcium channels is expansive and often contradictory. The main consensus of its mechanism of action is that having bound to $\alpha_2\delta$ protein, GBP elicits a reduction in neurotransmitter release, most probably by an inhibitory effect upon calcium channel function (Taylor et al., 1998; Gee et al., 1996). However, the exact site, time-course and mechanism of this inhibition are not yet fully understood.

The hypothesis of this study was that GBP binds to either $\alpha_2\delta$-1 or $\alpha_2\delta$-2 subunits of calcium channels intracellularly and interferes with either their functional ability to enhance forward trafficking of co-expressed calcium channel complexes to the membrane, or their ability to maintain functional channels at the cell-surface. This contrasts with other studies that find no direct inhibition of calcium currents, but instead describe a reduction in ESPC amplitude or neurotransmitter release, often at much lower doses of GBP and on a more short-term timescale (Cunningham et al., 2004; Dooley et al., 2000a; Dooley et al., 2000b). Therefore it is feasible that GBP acts upon $\alpha_2\delta$ in more than one way.

Activation of calcium channels results in an influx of calcium ions, however this calcium does not diffuse far into the cell before it has bound sequestering proteins which maintain the low intracellular free calcium concentration. Therefore pre-synaptic calcium channels are closely localised with the vesicle-release machinery (Spafford and Zamponi, 2003). It may be the case that the $\alpha_2\delta$ subunit facilitates some interaction with the vesicle release machinery to bring about an increase in neurotransmitter release,

rather than just increasing the number of calcium channels in a pre-synaptic zone. The importance of $\alpha_2\delta$ in enhancing trafficking and expression at the cell surface (and therefore pre-synaptic membrane) is well established (Canti et al., 2005). $\alpha_2\delta$ also elicits biophysical effects on expressed channels, such as the hyperpolarising shift in voltage-dependence inactivation (Singer et al., 1991), mediated through the delta subunit (Felix et al., 1997). An interaction between $\alpha_2\delta$ and structures involved in vesicle release may explain the increase in sensitivity in pain-states arising from $\alpha_2\delta$ up-regulation (Li et al., 2006), and may also be blocked by the action of drugs such as GBP. It is worth noting that the function of VGCCs extends beyond allowing calcium into cells, as a study points to the importance of an interaction between Ca_v2 α_1 subunits and laminin β2 subunits as a means of maintaining active zones in the synaptic cleft (Nishimune et al., 2004).

The calcium channel $\alpha_2\delta$ subunit is fairly unique (Hess, 1990a), with perhaps the only molecular homologue being the sodium channel beta subunit. Whist its intracellular role in enhancement of trafficking is known, its role at the cell surface as a component of the calcium channel complex is less well-defined. As a component of all Cav2.x channels, it is likely to have additional functions not yet discovered, which may shed more light on the link between $\alpha_2\delta$ and neurotransmitter release, and also the inhibitory actions of select $\alpha_2\delta$ ligands.

Conclusion

This study presents evidence for the inhibition of GBP upon calcium channel currents. This inhibition is likely to be mediated by GBP acting intracellularly to bind and obstruct the normal function of calcium channel $\alpha_2\delta$ subunits, namely the enhancement of calcium channel trafficking. This results in an expression of calcium channels with similar characteristics to those expressed without $\alpha_2\delta$ subunits. This inhibitory action of

GBP may be different to the acute effects on EPSC and neurotransmitter release shown in other studies.

Chapter 6: Concluding Discussion

Summary of results

The three results chapters detail studies carried out to explore additional roles of the $\alpha_2\delta$ subunit, other than those biophysical effects on channel properties and trafficking effects already described in previous work.

The role of the VGCC $\alpha_2\delta$-2 VWA domain so far appears limited to being intracellular, as a mechanism by which $\alpha_2\delta$-2 subunits cause the enhanced expression of $Ca_v\alpha_1$ subunits when co-expressed (Canti et al., 2005). Chapter 3 explored the possibility that $\alpha_2\delta$ might be involved in physical interactions linking it (and possibly associated calcium channels) to extracellular proteins. The μMIDAS mutant $\alpha_2\delta$-2 protein failed to elicit any of the changes normally associated with $\alpha_2\delta$-2 co-expression. These included an increase in current amplitude, as well as depolarising shifts in $V_{50,\ act}$ and $V_{50,\ inact}$. Therefore the VWA domain in the $\alpha_2\delta$-2 subunit plays an intracellular role. The same was found for the $\alpha_2\delta$-1 subunit (Canti et al., 2005). Co-cultures of tsA-201 cells expressing VGCC complexes and GC cells were employed to examine a possible extracellular role of the $\alpha_2\delta$-2 VWA domain. For this, a stable-HA-tagged $\alpha_2\delta$-2 cell-line was produced, which was found to be fully functional when expressed with $Ca_v2.1$ and β1b subunits (and compared to transiently-transfected $\alpha_2\delta$-2). The presence of GCs was hypothesised to lead to binding of extracellular protein (from GCs) to the $\alpha_2\delta$-2 VWA domain. The study failed to identify a direct interaction between $\alpha_2\delta$-2 and a protein ligand, However, at least one protein from GC cultures was found to bind $\alpha_2\delta$ in the $\alpha_2\delta$-2 stable-HA cell-line (in co-cultured tsA-201 cells). Unfortunately, this could not be attributed to VWA domain-binding, as a stable μMIDAS $\alpha_2\delta$-2 construct was not produced.

Chapter 4 examined the importance of a 3 amino acid (RRR) motif essential for GBP binding to both $\alpha_2\delta$-1 (R217A) and $\alpha_2\delta$-2 (R282A) subunits. Co-expression of these subunits with $Ca_v\alpha_1$ and β subunits resulted in a submaximal enhancement of current size, compared to co-expression of WT $\alpha_2\delta$-1 or WT $\alpha_2\delta$-2 (Field et al., 2006; Davies et

al., 2007). Where tested, no differences in $V_{50, act}$ or $V_{50, inact}$ between mutant and WT $\alpha_2\delta$ subunits were observed, suggesting the $\alpha_2\delta$ subunits lacking a functional GBP binding-site maintained their ability to elicit certain biophysical effects on co-expressed channels. Binding studies were carried out, to confirm that the $\alpha_2\delta$-1 R217A subunit did not bind GBP. This had been established for $\alpha_2\delta$-1 R217A membrane preparations (Wang et al., 1999) and $\alpha_2\delta$-2 R282A membrane / lipid raft preparations (Davies et al., 2006) already. As with $\alpha_2\delta$-2 R282A, an increase in affinity for GBP was seen in $\alpha_2\delta$-1 R217A lipid raft preparations compared to membrane preparations. This has been observed previously in WT $\alpha_2\delta$-1, and attributed to the removal of an endogenous ligand bound to $\alpha_2\delta$-1 in membranes, but removed upon further purification to $\alpha_2\delta$-1 in lipid rafts (Dissanayake et al., 1997).

The implication of lipid raft localisation of $\alpha_2\delta$-2 upon its function was tested, by disrupting lipid rafts. Using the cholesterol acceptor MBCD, lipid rafts were disrupted in cells expressing $Ca_v2.1$, β4 and stable $\alpha_2\delta$-2-mid HA. This caused a small but significant increase in current density compared to non-treated cells. The reverse experiment involved introducing extra cholesterol into the cell membrane. This caused a corresponding significant reduction in current density. Taken together, the results indicated that cell membrane cholesterol plays an important role in regulating the activity of VGCCs. The mechanism of this action has not as yet been determined.

The direct effects of GBP application upon VGCCs were examined in Chapter 5. Acute application of 1 mM GBP (up to 10 min) was found not to inhibit current density (tsA-201 cells expressing $Ca_v2.1$, β4, $\alpha_2\delta$-2 subunits. Chronic application (40 h) of 100 μM and 1 mM GBP however was found to cause a significant inhibition of current density, as well as preventing shifts in $V_{50, act}$ and $V_{50, inact}$ normally seen with $\alpha_2\delta$-2 co-expression. Similar observations were made when $Ca_v2.2$, β1b, $\alpha_2\delta$-1 subunits were co-expressed into tsA-201 cells. These results implied that the action of $\alpha_2\delta$ were prevented by GBP when applied chronically. No such effects were seen when non-GBP binding $\alpha_2\delta$ subunits were used ($\alpha_2\delta$-1 R217A, $\alpha_2\delta$-2 R282A and $\alpha_2\delta$-3), implicating GBP

binidng to $\alpha_2\delta$ subunits as a mechanism of action. The system-L amino acid trasport system has previously been shown to be responsible for GBP uptake into cells (Su et al., 1995). Blocking this transport system (using 10 mM BCH preincubated before GBP application) prevented the inhibitory effects of chronic 1 mM GBP application, implying GBP acted upon uptake into cells.

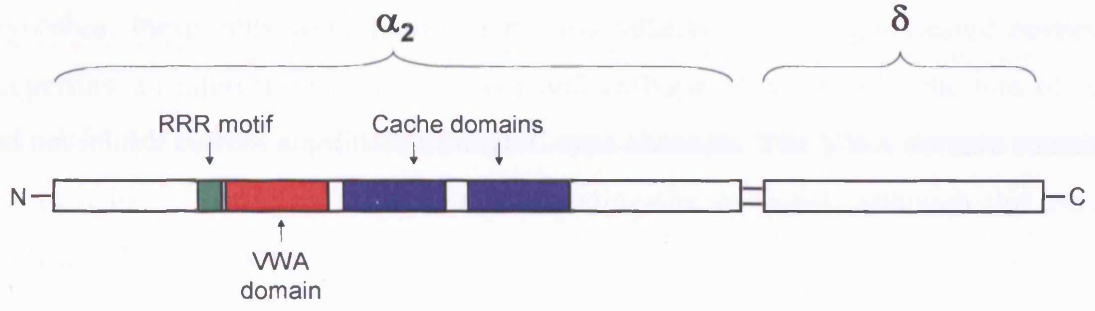

Figure 6.1. Schematic representation of $\alpha_2\delta$-1 / $\alpha_2\delta$-2 structure, with binding domains marked. Shown are the approximate relative positions of: the RRR motif necessary for GBP binding (green); the (MIDAS motif-containing) VWA domain (red) and the two cache domains (blue).

$\alpha_2\delta$ as a ligand-binding subunit

It is therefore clear that $\alpha_2\delta$ contains a number of potential interaction domains, and that their respective physiological functions are not yet fully clear.

The cache domains are predicted to be involved in binding small extracellular molecules (such as amino acids) as they are also found in prokaryotic chemotaxis receptors (Anantharaman and Aravind, 2000). Deletion mutations introduced into regions within the first cache domain (of porcine $\alpha_2\delta$-1) also prevent GBP binding (Wang et al., 1999).

It is possible GBP could bind as a ligand of the cache domains, although the importance of the RRR motif in GBP binding suggests other sites are more important.

By virtue of its structural similarity to integrin VWA domains, the $\alpha_2\delta$ VWA domain may well bind extracellular protein ligands, such as extracellular matrix proteins. Whether this would fulfil a signalling role or merely an adhesion role is not clear. A recent study (Garcia et al., 2007) explored the possible role of $\alpha_2\delta$-1 in adhesion, in the context of EC coupling in skeletal myotubes. Using siRNA to deplete $\alpha_2\delta$-1 in myotubes, these cells were found to be less adherent to collagen-coated coverslips, suggesting an interaction between $\alpha_2\delta$-1 and collagen. Additionally, the loss of $\alpha_2\delta$-1 did not inhibit current amplitude through L-type channels. The VWA domain constitutes the most likely candidate for a collagen binding-site on $\alpha_2\delta$-1, although this was not confirmed by the study.

The same study (Garcia et al., 2007) also investigated the localization of $\alpha_2\delta$-1 and $Ca_v1.1$ subunits over time. After two days in culture, little co-localisation between $\alpha_2\delta$-1 and $Ca_v1.1$ subunits was observed, with the $\alpha_2\delta$-1 expressed strongly at the extremities of the myotubes. The lack of initial association between $\alpha_2\delta$-1 and $Ca_v1.1$, in addition to the observation that $\alpha_2\delta$-1 is expressed before $Ca_v1.1$ in skeletal myotubes, suggests that $\alpha_2\delta$-1 functions in an additional role rather than merely associating with the $Ca_v\alpha_1$ subunit (and enhancing cell-surface expression).

Many of the experiments performed have focused on the $Ca_v2.1$ subunit, and the results therefore have implications for $Ca_v2.1$ subunit-containing VGCCs in their primary physiological role of neurotransmitter release.

First of all, the importance of the VWA domain in $Ca_v\alpha_1$ subunit trafficking has been demonstrated, both from work detailed in Chapter 3 as well as work carried out in the lab (Canti et al., 2005). The $\alpha_2\delta$ VWA domain is responsible for the increase in cell-surface expression (and subsequent increase in current amplitude) of the VGCC

complex. Therefore, the VWA plays a vital role in providing an intitial control over the number of $Ca_v2.1$ channels at the presynaptic membrane, for their role in neurotransmission. It would be interesting to compare the phenotype of a knock-in mouse containing the $\alpha_2\delta$-2 μMIDAS mutation with those of other $\alpha_2\delta$-2 mutants (such as *ducky* and *du*^{2J}) to examine whether this process would lead to impaired neurotransmission *in vivo*.

The proposed mechanism of action of GBP (Chapter 5) has implications for $Ca_v2.1$ and $Ca_v2.2$ synaptic pharmacology. The ability of GBP to be taken into neurons and prevent the $\alpha_2\delta$-mediated enhancement of VGCC channel trafficking would have an impact on neurotransmitter release. The mechanism demonstrated in this study would agree with other studies detailing an inhibition in neurotransmitter release (Dooley et al., 2002; Bayer et al., 2004; Cunningham et al., 2004) as a result of action at $Ca_v2.1$ channels. The implications of a drug affecting neurotransmission at central synapses are far-reaching. Reductions in neurotransmitter release by GBP (and PGB) have been demonstrated in a variety of tissues, and for a range of neurotransmitters (see Section 1.8.5). This would be liable to cause an array of unwanted side-effects. However, in many animal models, GBP has an effect on neurotransmitter release in hypersensitive neurons, rather than in normal neurons (Li et al., 2006; Patel et al., 2000), as well as having a subtle, sub-maximal influence on neurotransmission (reviewed in Dooley et al., 2007). It is perhaps these distinctions that allow the side-effect profile of GBP/PGB to be fairly limited.

Additional roles of the $\alpha_2\delta$ subunit

The $\alpha_2\delta$ subunit subtypes (1-4) all have similar effects when co-expressed with $Ca_v\alpha_1$ subunits (and β subunits), such as enhancing cell-surface expression of $Ca_v\alpha_1$ subunits, as well as having minor influences upon electrophysiological properties of the expressed channels (see Introduction). However, the differences between the VWA domains of the $\alpha_2\delta$ subunit subtypes suggest they may perhaps have evolved to carry out different

functions. All $\alpha_2\delta$ subunits contain VWA domains, however these are only completed by intact MIDAS motifs in $\alpha_2\delta$-1 and $\alpha_2\delta$-2 (Whittaker and Hynes, 2002). It is not known whether the VWA domains in $\alpha_2\delta$-3 and $\alpha_2\delta$-4 are functional, as they have not been tested (by disrupting sites within the VWA domain to see if this is necessary for an interaction with $Ca_v\alpha_1$ subunits. However, as they do not contain intact MIDAS motifs, it could be suggested they cannot transition into the active state and bind the putative ligand. This may suggest that functional VWA domains were once present in these structures, but have become redundant or unnecessary. In addition, localisation of the $\alpha_2\delta$-2 subunit in the tumour suppression region of chromosome 3 may again suggest an additional function.

Therefore, the conclusion of this body of work is that the $\alpha_2\delta$ subunit is involved in multiple interactions via adhesion domains. These interactions are important for the physiological function of $\alpha_2\delta$ as a VGCC auxiliary subunit, although additional functions not involving the VGCC complex are also possible.

Appendices

Appendix I: Buffers for lipid raft preparation

Solution	Compound
Buffer 1 50 ml w/ water	25 mM MES
	150 mM NaCl
	2x Protease inhibitor tablets
Buffer 2 50 ml w/ water	25 mM MES
	150 mM NaCl
	2x Protease inhibitor tablets
	2% Triton (v/v)

Appendix II: Base biochemical reagent compositions

Solution	Compound	Quantity
(4X) Loading sample buffer (LSB), 10 ml	Glycerol	4.00 g
	Tris Base	0.682 g
	Tris HCl	0.666 g
	Lithium dodecyl-sulfate	0.800 g
	EDTA	0.006 g
	Serva Blue G250	0.75 ml of 1% solution
	Phenol Red	0.25 ml of 1% solution
	DTT	200 μM
(20X) NuPage Tris-acetate	Tricine	89.5 g (1M)

running buffer, 500 ml		
	Tris Base	60.6 g (1M)
	SDS	10 g (69.3 mM)
(20X) NuPage MOPS running buffer, 500 ml	MOPS	104.6 g (1M)
	Tris Base	60.6 g (1M)
	SDS	10 g (69.3 mM)
	EDTA	3 g (20.5 mM)
(20X) Nupage transfer buffer, 125 ml	Bicine	10.2 g (500 mM)
	Bis-Tris	13.08 g (500 mM)
	EDTA	0.75 g (20.5 mM)

Appendix III: Composition of antibody diluent (pH 7.4)

Goat serum	10% (v/v)
Bovine serum albumin	3 % (w/v)
Ovalbumin	0.5% (w/v)
NaCl	500 mM
Tris-HCl	50 mM
Igepal	0.1% (v/v)

Acknowledgements

First of all, I would like to express my thanks to my supervisor Professor Annette Dolphin, who has provided excellent support in guiding and directing me through the PhD process, and has also been tremendously patient in reading my work and making corrections.

A number of people made my transformation from electrophysiology novice to less-of-an electrophysiology novice possible. I am indebted to Carles and Jérôme for starting me off. Thanks also to Fay for taking over the role and providing invaluable assistance, not to mention making the DRG experiments possible. Thanks also to Andriy, Laurent, Patricia and Jean-Sebastien for all the productive advice.

The members of the lab made it a pleasure to carry out my work. Thanks to Tony, Leon, Jack for helping me find my biochemical feet, as well as preventing too many accidents with the ultracentrifuge. Thank you to Manuela for help with the imaging experiments, and to Wendy for molecular biology assistance. Cheers Stuart for safe-guarding the equipment from me, as well as regaling me with seemingly endless boating / sequencing stories. A special mention must go to Kanchan, for helping make tissue-culture a painless and efficient process.

My fellow students have helped in the arena of work, in addition to shifting things to a more relaxed pace. Thanks primarily to Dom for aiding in all the adventures, as well as providing many hours of idle chit-chat / ground-breaking scientific theories. Many thanks also to PhD students in the lab, past (Adrian & Lola) and present (Alex & Anita). Cheers also to the PhD students from the Pharmacology Dept, particularly Rugina and Qionger who were instrumental in the ritual of the afternoon break.

My housemates have helped provide to provide a sanctuary to retreat to after a hard day. I thank Dom, Imran, Lucy and Jack for that. Thank you to Imran for being a light when

all other lights go out, and to Dom for the electronica. Where work was forgotten, there was ample time for plenty of other activities such as boxing, bowling and Bomberman.

Of course, I must thank my family: Mum; Papa; Kirsten (and Maddy), who have helped provide a helpful family atmosphere, not to mention a good roast dinner every now and again. Thanks also to Lucy, for everything really.... all the support, good times, teas and Pikmin!

References

Adams, B.A. and K.G.Beam. 1990. Muscular dysgenesis in mice: a model system for studying excitation-contraction coupling. *FASEB J.* 4:2809-2816.

Aggarwal, S.K. and R.MacKinnon. 1996. Contribution of the S4 segment to gating charge in the Shaker K+ channel. *Neuron* 16:1169-1177.

Ahern, C.A., J.Arikkath, P.Vallejo, C.A.Gurnett, P.A.Powers, K.P.Campbell, and R.Coronado. 2001. Intramembrane charge movements and excitation- contraction coupling expressed by two-domain fragments of the Ca2+ channel. *Proc. Natl. Acad. Sci. U. S. A* 98:6935-6940.

Alden, K.J. and J.Garcia. 2001. Differential effect of gabapentin on neuronal and muscle calcium currents. *J. Pharmacol. Exp. Ther.* 297:727-735.

Altier, C., C.S.Dale, A.E.Kisilevsky, K.Chapman, A.J.Castiglioni, E.A.Matthews, R.M.Evans, A.H.Dickenson, D.Lipscombe, N.Vergnolle, and G.W.Zamponi. 2007. Differential role of N-type calcium channel splice isoforms in pain. *J. Neurosci.* 27:6363-6373.

Anantharaman, V. and L.Aravind. 2000. Cache - a signaling domain common to animal Ca(2+)-channel subunits and a class of prokaryotic chemotaxis receptors. *Trends Biochem. Sci.* 25:535-537.

Andrade, A., A.Sandoval, N.Oviedo, M.De Waard, D.Elias, and R.Felix. 2007. Proteolytic cleavage of the voltage-gated Ca2+ channel alpha2delta subunit: structural and functional features. *Eur. J. Neurosci.* 25:1705-1710.

Angelotti, T. and F.Hofmann. 1996. Tissue-specific expression of splice variants of the mouse voltage-gated calcium channel alpha2/delta subunit. *FEBS Lett.* 397:331-337.

Arikkath, J. and K.P.Campbell. 2003. Auxiliary subunits: essential components of the voltage-gated calcium channel complex. *Curr. Opin. Neurobiol.* 13:298-307.

Arikkath, J., R.Felix, C.Ahern, C.C.Chen, Y.Mori, I.Song, H.S.Shin, R.Coronado, and K.P.Campbell. 2002. Molecular characterization of a two-domain form of the neuronal voltage-gated P/Q-type calcium channel alpha(1)2.1 subunit. *FEBS Lett.* 532:300-308.

Armstrong, C.M. and F.Bezanilla. 1974. Charge movement associated with the opening and closing of the activation gates of the Na channels. *J. Gen. Physiol* 63:533-552.

Arnaout, M.A., B.Mahalingam, and J.P.Xiong. 2005. Integrin structure, allostery, and bidirectional signaling. *Annu. Rev. Cell Dev. Biol.* 21:381-410.

Augustine, G.J. and E.Neher. 1992. Neuronal Ca2+ signalling takes the local route. *Curr. Opin. Neurobiol.* 2:302-307.

Avila, G. and R.T.Dirksen. 2000. Functional impact of the ryanodine receptor on the skeletal muscle L-type Ca(2+) channel. *J. Gen. Physiol* 115:467-480.

Backonja, M.M. 2000. Anticonvulsants (antineuropathics) for neuropathic pain syndromes. *Clin. J Pain* 16:S67-S72.

Bangalore, R., G.Mehrke, K.Gingrich, F.Hofmann, and R.S.Kass. 1996. Influence of L-type Ca channel alpha 2/delta-subunit on ionic and gating current in transiently transfected HEK 293 cells. *Am. J. Physiol* 270:H1521-H1528.

Barclay, J., N.Balaguero, M.Mione, S.L.Ackerman, V.A.Letts, J.Brodbeck, C.Canti, A.Meir, K.M.Page, K.Kusumi, E.Perez-Reyes, E.S.Lander, W.N.Frankel, R.M.Gardiner, A.C.Dolphin, and M.Rees. 2001. Ducky mouse phenotype of epilepsy and ataxia is associated with mutations in the Cacna2d2 gene and decreased calcium channel current in cerebellar Purkinje cells. *J. Neurosci.* 21:6095-6104.

Barclay, J. and M.Rees. 2000. Genomic organization of the mouse and human alpha2delta2 voltage-dependent calcium channel subunit genes. *Mamm. Genome* 11:1142-1144.

Bats, C., L.Groc, and D.Choquet. 2007. The interaction between Stargazin and PSD-95 regulates AMPA receptor surface trafficking. *Neuron* 53:719-734.

Bayer, K., S.Ahmadi, and H.U.Zeilhofer. 2004. Gabapentin may inhibit synaptic transmission in the mouse spinal cord dorsal horn through a preferential block of P/Q-type Ca2+ channels. *Neuropharmacology* 46:743-749.

Bean, B.P. 1989. Neurotransmitter inhibition of neuronal calcium currents by changes in channel voltage dependence. *Nature* 340:153-156.

Bean, B.P. 2007. The action potential in mammalian central neurons. *Nat. Rev. Neurosci.* 8:451-465.

Bell, D.C., A.J.Butcher, N.S.Berrow, K.M.Page, P.F.Brust, A.Nesterova, K.A.Stauderman, G.R.Seabrook, B.Nurnberg, and A.C.Dolphin. 2001. Biophysical properties, pharmacology, and modulation of human, neuronal L-type (alpha(1D), Ca(V)1.3) voltage-dependent calcium currents. *J. Neurophysiol.* 85:816-827.

Belliotti, T.R., T.Capiris, I.V.Ekhato, J.J.Kinsora, M.J.Field, T.G.Heffner, L.T.Meltzer, J.B.Schwarz, C.P.Taylor, A.J.Thorpe, M.G.Vartanian, L.D.Wise, T.Zhi-Su, M.L.Weber, and D.J.Wustrow. 2005. Structure-activity relationships of pregabalin and analogues that target the alpha(2)-delta protein. *J. Med. Chem.* 48:2294-2307.

Bernstein, G.M. and O.T.Jones. 2007. Kinetics of internalization and degradation of N-type voltage-gated calcium channels: role of the alpha2/delta subunit. *Cell Calcium* 41:27-40.

Berridge, M.J. 2006. Calcium microdomains: organization and function. *Cell Calcium* 40:405-412.

Berridge, M.J., P.Lipp, and M.D.Bootman. 2000. The versatility and universality of calcium signalling. *Nat. Rev. Mol. Cell Biol.* 1:11-21.

Berrou, L., H.Klein, G.Bernatchez, and L.Parent. 2002. A specific tryptophan in the I-II linker is a key determinant of beta-subunit binding and modulation in Ca(V)2.3 calcium channels. *Biophys. J.* 83:1429-1442.

Bezprozvanny, I., P.Zhong, R.H.Scheller, and R.W.Tsien. 2000. Molecular determinants of the functional interaction between syntaxin and N-type Ca2+ channel gating. *Proc. Natl. Acad. Sci. U. S. A* 97:13943-13948.

Bialer, M., S.I.Johannessen, H.J.Kupferberg, R.H.Levy, E.Perucca, and T.Tomson. 2007. Progress report on new antiepileptic drugs: a summary of the Eigth Eilat Conference (EILAT VIII). *Epilepsy Res.* 73:1-52.

Bian, F., Z.Li, J.Offord, M.D.Davis, J.McCormick, C.P.Taylor, and L.C.Walker. 2006. Calcium channel alpha2-delta type 1 subunit is the major binding protein for pregabalin

in neocortex, hippocampus, amygdala, and spinal cord: an ex vivo autoradiographic study in alpha2-delta type 1 genetically modified mice. *Brain Res.* 1075:68-80.

Bichet, D., V.Cornet, S.Geib, E.Carlier, S.Volsen, T.Hoshi, Y.Mori, and M.De Waard. 2000. The I-II loop of the Ca2+ channel alpha1 subunit contains an endoplasmic reticulum retention signal antagonized by the beta subunit. *Neuron* 25:177-190.

Birnbaumer, L., N.Qin, R.Olcese, E.Tareilus, D.Platano, J.Costantin, and E.Stefani. 1998. Structures and functions of calcium channel beta subunits. *J. Bioenerg. Biomembr.* 30:357-375.

Black, J.L., III. 2003. The voltage-gated calcium channel gamma subunits: a review of the literature. *J. Bioenerg. Biomembr.* 35:649-660.

Bork, P. and K.Rohde. 1991. More von Willebrand factor type A domains? Sequence similarities with malaria thrombospondin-related anonymous protein, dihydropyridine-sensitive calcium channel and inter-alpha-trypsin inhibitor. *Biochem. J.* 279 (Pt 3):908-910.

Borsotto, M., J.Barhanin, M.Fosset, and M.Lazdunski. 1985. The 1,4-dihydropyridine receptor associated with the skeletal muscle voltage-dependent Ca2+ channel. Purification and subunit composition. *J. Biol. Chem.* 260:14255-14263.

Bourinet, E., T.W.Soong, K.Sutton, S.Slaymaker, E.Mathews, A.Monteil, G.W.Zamponi, J.Nargeot, and T.P.Snutch. 1999. Splicing of alpha 1A subunit gene generates phenotypic variants of P- and Q-type calcium channels. *Nat. Neurosci.* 2:407-415.

Bourinet, E., S.C.Stotz, R.L.Spaetgens, G.Dayanithi, J.Lemos, J.Nargeot, and G.W.Zamponi. 2001. Interaction of SNX482 with domains III and IV inhibits activation gating of alpha(1E) (Ca(V)2.3) calcium channels. *Biophys. J.* 81:79-88.

Bregestovski, P. and N.Spitzer. 2005. Calcium in the function of the nervous system: new implications. *Cell Calcium* 37:371-374.

Brice, N.L., N.S.Berrow, V.Campbell, K.M.Page, K.Brickley, I.Tedder, and A.C.Dolphin. 1997. Importance of the different beta subunits in the membrane expression of the alpha1A and alpha2 calcium channel subunits: studies using a depolarization-sensitive alpha1A antibody. *Eur. J. Neurosci.* 9:749-759.

Brickley, K., V.Campbell, N.Berrow, R.Leach, R.I.Norman, D.Wray, A.C.Dolphin, and S.A.Baldwin. 1995. Use of site-directed antibodies to probe the topography of the alpha 2 subunit of voltage-gated Ca2+ channels. *FEBS Lett.* 364:129-133.

Brill, J., R.Klocke, D.Paul, D.Boison, N.Gouder, N.Klugbauer, F.Hofmann, C.M.Becker, and K.Becker. 2004. entla, a novel epileptic and ataxic Cacna2d2 mutant of the mouse. *J. Biol. Chem.* 279:7322-7330.

Brown, D.A. 2006. Lipid rafts, detergent-resistant membranes, and raft targeting signals. *Physiology. (Bethesda.)* 21:430-439.

Brown, D.A. and J.K.Rose. 1992. Sorting of GPI-anchored proteins to glycolipid-enriched membrane subdomains during transport to the apical cell surface. *Cell* 68:533-544.

Brown, J.P., V.U.Dissanayake, A.R.Briggs, M.R.Milic, and N.S.Gee. 1998. Isolation of the [3H]gabapentin-binding protein/alpha 2 delta Ca2+ channel subunit from porcine brain: development of a radioligand binding assay for alpha 2 delta subunits using [3H]leucine. *Anal. Biochem.* 255:236-243.

Brown, J.P. and N.S.Gee. 1998. Cloning and deletion mutagenesis of the alpha2 delta calcium channel subunit from porcine cerebral cortex. Expression of a soluble form of the protein that retains [3H]gabapentin binding activity. *J. Biol. Chem.* 273:25458-25465.

Brown, J.T. and A.Randall. 2005. Gabapentin fails to alter P/Q-type Ca2+ channel-mediated synaptic transmission in the hippocampus in vitro. *Synapse* 55:262-269.

Campbell, V., N.S.Berrow, E.M.Fitzgerald, K.Brickley, and A.C.Dolphin. 1995. Inhibition of the interaction of G protein G(o) with calcium channels by the calcium channel beta-subunit in rat neurones. *J. Physiol* 485 (Pt 2):365-372.

Canti, C., Y.Bogdanov, and A.C.Dolphin. 2000. Interaction between G proteins and accessory subunits in the regulation of 1B calcium channels in Xenopus oocytes. *J Physiol* 527 Pt 3:419-432.

Canti, C., M.Nieto-Rostro, I.Foucault, F.Heblich, J.Wratten, M.W.Richards, J.Hendrich, L.Douglas, K.M.Page, A.Davies, and A.C.Dolphin. 2005. The metal-ion-dependent adhesion site in the Von Willebrand factor-A domain of alpha2delta subunits is key to trafficking voltage-gated Ca2+ channels. *Proc. Natl. Acad. Sci. U. S. A* 102:11230-11235.

Carbone, E. and H.D.Lux. 1984. A low voltage-activated, fully inactivating Ca channel in vertebrate sensory neurones. *Nature* 310:501-502.

Castellano, A., X.Wei, L.Birnbaumer, and E.Perez-Reyes. 1993a. Cloning and expression of a neuronal calcium channel beta subunit. *J. Biol. Chem.* 268:12359-12366.

Castellano, A., X.Wei, L.Birnbaumer, and E.Perez-Reyes. 1993b. Cloning and expression of a third calcium channel beta subunit. *J. Biol. Chem.* 268:3450-3455.

Catterall, W.A. 1988. Structure and function of voltage-sensitive ion channels. *Science* 242:50-61.

Catterall, W.A. 1999. Interactions of presynaptic Ca2+ channels and snare proteins in neurotransmitter release. *Ann. N. Y. Acad. Sci.* 868:144-159.

Catterall, W.A. 2000. Structure and regulation of voltage-gated Ca2+ channels. *Annu. Rev. Cell Dev. Biol.* 16:521-555.

Catterall, W.A., S.Cestele, V.Yarov-Yarovoy, F.H.Yu, K.Konoki, and T.Scheuer. 2007. Voltage-gated ion channels and gating modifier toxins. *Toxicon* 49:124-141.

Catterall, W.A., E.Perez-Reyes, T.P.Snutch, and J.Striessnig. 2005. International Union of Pharmacology. XLVIII. Nomenclature and structure-function relationships of voltage-gated calcium channels. *Pharmacol. Rev.* 57:411-425.

Chang, F.C. and M.M.Hosey. 1988. Dihydropyridine and phenylalkylamine receptors associated with cardiac and skeletal muscle calcium channels are structurally different. *J. Biol. Chem.* 263:18929-18937.

Christian, A.E., M.P.Haynes, M.C.Phillips, and G.H.Rothblat. 1997. Use of cyclodextrins for manipulating cellular cholesterol content. *J. Lipid Res.* 38:2264-2272.

Chu, P.J., H.M.Robertson, and P.M.Best. 2001. Calcium channel gamma subunits provide insights into the evolution of this gene family. *Gene* 280:37-48.

Chuang, R.S., H.Jaffe, L.Cribbs, E.Perez-Reyes, and K.J.Swartz. 1998. Inhibition of T-type voltage-gated calcium channels by a new scorpion toxin. *Nat. Neurosci.* 1:668-674.

Cooper, C.L., S.Vandaele, J.Barhanin, M.Fosset, M.Lazdunski, and M.M.Hosey. 1987. Purification and characterization of the dihydropyridine-sensitive voltage-dependent calcium channel from cardiac tissue. *J. Biol. Chem.* 262:509-512.

Cormack, B.P., R.H.Valdivia, and S.Falkow. 1996. FACS-optimized mutants of the green fluorescent protein (GFP). *Gene* 173:33-38.

Cuello, L.G., D.M.Cortes, and E.Perozo. 2004. Molecular architecture of the KvAP voltage-dependent K+ channel in a lipid bilayer. *Science* 306:491-495.

Cunningham, M.O., G.L.Woodhall, S.E.Thompson, D.J.Dooley, and R.S.Jones. 2004. Dual effects of gabapentin and pregabalin on glutamate release at rat entorhinal synapses in vitro. *Eur. J. Neurosci.* 20:1566-1576.

Curtis, B.M. and W.A.Catterall. 1984. Purification of the calcium antagonist receptor of the voltage-sensitive calcium channel from skeletal muscle transverse tubules. *Biochemistry* 23:2113-2118.

Davies, A., L.Douglas, J.Hendrich, J.Wratten, V.M.Tran, I.Foucault, D.Koch, W.S.Pratt, H.R.Saibil, and A.C.Dolphin. 2006. The calcium channel alpha2delta-2 subunit partitions with CaV2.1 into lipid rafts in cerebellum: implications for localization and function. *J. Neurosci.* 26:8748-8757.

Davies, A., J.Hendrich, A.T.Van Minh, J.Wratten, L.Douglas, and A.C.Dolphin. 2007. Functional biology of the alpha(2)delta subunits of voltage-gated calcium channels. *Trends Pharmacol. Sci.* 28:220-228.

De Jongh, K.S., C.Warner, and W.A.Catterall. 1990. Subunits of purified calcium channels. Alpha 2 and delta are encoded by the same gene. *J. Biol. Chem.* 265:14738-14741.

De Waard, M. and K.P.Campbell. 1995. Subunit regulation of the neuronal alpha 1A Ca2+ channel expressed in Xenopus oocytes. *J. Physiol* 485 (Pt 3):619-634.

Deutsch, C. 2003. The birth of a channel. *Neuron* 40:265-276.

Diaz, A. and A.H.Dickenson. 1997. Blockade of spinal N- and P-type, but not L-type, calcium channels inhibits the excitability of rat dorsal horn neurones produced by subcutaneous formalin inflammation. *Pain* 69:93-100.

Dissanayake, V.U., N.S.Gee, J.P.Brown, and G.N.Woodruff. 1997. Spermine modulation of specific [3H]-gabapentin binding to the detergent-solubilized porcine cerebral cortex alpha 2 delta calcium channel subunit. *Br. J. Pharmacol.* 120:833-840.

Dodge, F.A., Jr. and R.Rahamimoff. 1967. Co-operative action a calcium ions in transmitter release at the neuromuscular junction. *J. Physiol* 193:419-432.

Doering, C.J. and G.W.Zamponi. 2003. Molecular pharmacology of high voltage-activated calcium channels. *J. Bioenerg. Biomembr.* 35:491-505.

Dolphin, A.C. 2003a. Beta subunits of voltage-gated calcium channels. *J. Bioenerg. Biomembr.* 35:599-620.

Dolphin, A.C. 2003b. G protein modulation of voltage-gated calcium channels. *Pharmacol. Rev.* 55:607-627.

Dooley, D.J., C.M.Donovan, W.P.Meder, and S.Z.Whetzel. 2002. Preferential action of gabapentin and pregabalin at P/Q-type voltage-sensitive calcium channels: inhibition of K+-evoked [3H]-norepinephrine release from rat neocortical slices. *Synapse* 45:171-190.

Dooley, D.J., C.M.Donovan, and T.A.Pugsley. 2000a. Stimulus-dependent modulation of [(3)H]norepinephrine release from rat neocortical slices by gabapentin and pregabalin. *J. Pharmacol. Exp. Ther.* 295:1086-1093.

Dooley, D.J., C.A.Mieske, and S.A.Borosky. 2000b. Inhibition of K(+)-evoked glutamate release from rat neocortical and hippocampal slices by gabapentin. *Neurosci. Lett.* 280:107-110.

Dooley, D.J., C.P.Taylor, S.Donevan, and D.Feltner. 2007. Ca2+ channel alpha2delta ligands: novel modulators of neurotransmission. *Trends Pharmacol. Sci.* 28:75-82.

Douglas, L., A.Davies, J.Wratten, and A.C.Dolphin. 2006. Do voltage-gated calcium channel alpha2delta subunits require proteolytic processing into alpha2 and delta to be functional? *Biochem. Soc. Trans.* 34:894-898.

Doyle, D.A., C.J.Morais, R.A.Pfuetzner, A.Kuo, J.M.Gulbis, S.L.Cohen, B.T.Chait, and R.MacKinnon. 1998. The structure of the potassium channel: molecular basis of K+ conduction and selectivity. *Science* 280:69-77.

Dubel, S.J., T.V.Starr, J.Hell, M.K.Ahlijanian, J.J.Enyeart, W.A.Catterall, and T.P.Snutch. 1992. Molecular cloning of the alpha-1 subunit of an omega-conotoxin-sensitive calcium channel. *Proc. Natl. Acad. Sci. U. S. A* 89:5058-5062.

Ducros, A., C.Denier, A.Joutel, K.Vahedi, A.Michel, F.Darcel, M.Madigand, D.Guerouaou, F.Tison, J.Julien, E.Hirsch, F.Chedru, C.Bisgard, G.Lucotte, P.Despres, C.Billard, M.A.Barthez, G.Ponsot, M.G.Bousser, and E.Tournier-Lasserve. 1999. Recurrence of the T666M calcium channel CACNA1A gene mutation in familial hemiplegic migraine with progressive cerebellar ataxia. *Am. J. Hum. Genet.* 64:89-98.

Dunlap, K., J.I.Luebke, and T.J.Turner. 1995. Exocytotic Ca2+ channels in mammalian central neurons. *Trends Neurosci.* 18:89-98.

Ellinor, P.T., J.F.Zhang, W.A.Horne, and R.W.Tsien. 1994. Structural determinants of the blockade of N-type calcium channels by a peptide neurotoxin. *Nature* 372:272-275.

Ellinor, P.T., J.F.Zhang, A.D.Randall, M.Zhou, T.L.Schwarz, R.W.Tsien, and W.A.Horne. 1993. Functional expression of a rapidly inactivating neuronal calcium channel. *Nature* 363:455-458.

Ellis, S.B., M.E.Williams, N.R.Ways, R.Brenner, A.H.Sharp, A.T.Leung, K.P.Campbell, E.McKenna, W.J.Koch, A.Hui, and . 1988. Sequence and expression of mRNAs encoding the alpha 1 and alpha 2 subunits of a DHP-sensitive calcium channel. *Science* 241:1661-1664.

Ertel, E.A., K.P.Campbell, M.M.Harpold, F.Hofmann, Y.Mori, E.Perez-Reyes, A.Schwartz, T.P.Snutch, T.Tanabe, L.Birnbaumer, R.W.Tsien, and W.A.Catterall. 2000. Nomenclature of voltage-gated calcium channels. *Neuron* 25:533-535.

Fatt, P. and B.L.Ginsborg. 1958. The ionic requirements for the production of action potentials in crustacean muscle fibres. *J. Physiol* 142:516-543.

Fatt, P. and B.Katz. 1953. The electrical properties of crustacean muscle fibres. *J. Physiol* 120:171-204.

Fehrenbacher, J.C., C.P.Taylor, and M.R.Vasko. 2003. Pregabalin and gabapentin reduce release of substance P and CGRP from rat spinal tissues only after inflammation or activation of protein kinase C. *Pain* 105:133-141.

Felix, R., C.A.Gurnett, M.De Waard, and K.P.Campbell. 1997. Dissection of functional domains of the voltage-dependent Ca2+ channel alpha2delta subunit. *J. Neurosci.* 17:6884-6891.

Feng, Z.P., J.Hamid, C.Doering, S.E.Jarvis, G.M.Bosey, E.Bourinet, T.P.Snutch, and G.W.Zamponi. 2001. Amino acid residues outside of the pore region contribute to N-type calcium channel permeation. *J. Biol. Chem.* 276:5726-5730.

Field, M.J., P.J.Cox, E.Stott, H.Melrose, J.Offord, T.Z.Su, S.Bramwell, L.Corradini, S.England, J.Winks, R.A.Kinloch, J.Hendrich, A.C.Dolphin, T.Webb, and D.Williams. 2006. Identification of the alpha2-delta-1 subunit of voltage-dependent calcium channels as a molecular target for pain mediating the analgesic actions of pregabalin. *Proc. Natl. Acad. Sci. U. S. A* 103:17537-17542.

Fink, K., D.J.Dooley, W.P.Meder, N.Suman-Chauhan, S.Duffy, H.Clusmann, and M.Gothert. 2002. Inhibition of neuronal Ca(2+) influx by gabapentin and pregabalin in the human neocortex. *Neuropharmacology* 42:229-236.

Fink, K., W.Meder, D.J.Dooley, and M.Gothert. 2000. Inhibition of neuronal Ca(2+) influx by gabapentin and subsequent reduction of neurotransmitter release from rat neocortical slices. *Br. J. Pharmacol.* 130:900-906.

Fletcher, C.F., A.Tottene, V.A.Lennon, S.M.Wilson, S.J.Dubel, R.Paylor, D.A.Hosford, L.Tessarollo, M.W.McEnery, D.Pietrobon, N.G.Copeland, and N.A.Jenkins. 2001.

Dystonia and cerebellar atrophy in Cacna1a null mice lacking P/Q calcium channel activity. *FASEB J* 15:1288-1290.

Flockerzi, V., H.J.Oeken, F.Hofmann, D.Pelzer, A.Cavalie, and W.Trautwein. 1986. Purified dihydropyridine-binding site from skeletal muscle t-tubules is a functional calcium channel. *Nature* 323:66-68.

Fox, A., C.Gentry, S.Patel, A.Kesingland, and S.Bevan. 2003. Comparative activity of the anti-convulsants oxcarbazepine, carbamazepine, lamotrigine and gabapentin in a model of neuropathic pain in the rat and guinea-pig. *Pain* 105:355-362.

Fox, A.P., M.C.Nowycky, and R.W.Tsien. 1987. Kinetic and pharmacological properties distinguishing three types of calcium currents in chick sensory neurones. *J. Physiol* 394:149-172.

Gao, B., Y.Sekido, A.Maximov, M.Saad, E.Forgacs, F.Latif, M.H.Wei, M.Lerman, J.H.Lee, E.Perez-Reyes, I.Bezprozvanny, and J.D.Minna. 2000. Functional properties of a new voltage-dependent calcium channel alpha(2)delta auxiliary subunit gene (CACNA2D2). *J Biol. Chem.* 275:12237-12242.

Garcia, K., T.Nabhani, and J.Garcia. 2007. The calcium channel alpha-2-delta 1 subunit is involved in extracellular signaling. *J. Physiol.*

Gazulla, J. and M.A.Tintore. 2007. The P/Q-type voltage-dependent calcium channel as pharmacological target in spinocerebellar ataxia type 6: gabapentin and pregabalin may be of therapeutic benefit. *Med. Hypotheses* 68:131-136.

Gee, N.S., J.P.Brown, V.U.Dissanayake, J.Offord, R.Thurlow, and G.N.Woodruff. 1996. The novel anticonvulsant drug, gabapentin (Neurontin), binds to the alpha2delta subunit of a calcium channel. *J. Biol. Chem.* 271:5768-5776.

Gong, H.C., J.Hang, W.Kohler, L.Li, and T.Z.Su. 2001. Tissue-specific expression and gabapentin-binding properties of calcium channel alpha2delta subunit subtypes. *J. Membr. Biol.* 184:35-43.

Gray, A.C., J.Raingo, and D.Lipscombe. 2007. Neuronal calcium channels: splicing for optimal performance. *Cell Calcium* 42:409-417.

Gurnett, C.A., M.De Waard, and K.P.Campbell. 1996. Dual function of the voltage-dependent Ca2+ channel alpha 2 delta subunit in current stimulation and subunit interaction. *Neuron* 16:431-440.

Gurnett, C.A., R.Felix, and K.P.Campbell. 1997. Extracellular interaction of the voltage-dependent Ca2+ channel alpha2delta and alpha1 subunits. *J. Biol. Chem.* 272:18508-18512.

Hagiwara, S. and L.Byerly. 1981. Calcium channel. *Annu. Rev. Neurosci.* 4:69-125.

Hagiwara, S., S.Ozawa, and O.Sand. 1975. Voltage clamp analysis of two inward current mechanisms in the egg cell membrane of a starfish. *J. Gen. Physiol* 65:617-644.

Hamill, O.P., A.Marty, E.Neher, B.Sakmann, and F.J.Sigworth. 1981. Improved patch-clamp techniques for high-resolution current recording from cells and cell-free membrane patches. *Pflugers Arch.* 391:85-100.

Hanlon, M.R., N.S.Berrow, A.C.Dolphin, and B.A.Wallace. 1999. Modelling of a voltage-dependent Ca2+ channel beta subunit as a basis for understanding its functional properties. *FEBS Lett.* 445:366-370.

Hans, M., A.Urrutia, C.Deal, P.F.Brust, K.Stauderman, S.B.Ellis, M.M.Harpold, E.C.Johnson, and M.E.Williams. 1999. Structural elements in domain IV that influence biophysical and pharmacological properties of human alpha1A-containing high-voltage-activated calcium channels. *Biophys. J.* 76:1384-1400.

Helton, T.D. and W.A.Horne. 2002. Alternative splicing of the beta 4 subunit has alpha1 subunit subtype-specific effects on Ca2+ channel gating. *J. Neurosci.* 22:1573-1582.

Hering, S., S.Berjukow, S.Sokolov, R.Marksteiner, R.G.Weiss, R.Kraus, and E.N.Timin. 2000. Molecular determinants of inactivation in voltage-gated Ca2+ channels. *J. Physiol* 528 Pt 2:237-249.

Herlitze, S., D.E.Garcia, K.Mackie, B.Hille, T.Scheuer, and W.A.Catterall. 1996. Modulation of Ca2+ channels by G-protein beta gamma subunits. *Nature* 380:258-262.

Herlitze, S., G.H.Hockerman, T.Scheuer, and W.A.Catterall. 1997. Molecular determinants of inactivation and G protein modulation in the intracellular loop connecting domains I and II of the calcium channel alpha1A subunit. *Proc. Natl. Acad. Sci. U. S. A* 94:1512-1516.

Hess, P. 1990b. Calcium channels in vertebrate cells. *Annu. Rev. Neurosci.* 13:337-356.

Hess, P. 1990a. Calcium channels in vertebrate cells. *Annu. Rev. Neurosci.* 13:337-356.

Hess, P., J.B.Lansman, and R.W.Tsien. 1984. Different modes of Ca channel gating behaviour favoured by dihydropyridine Ca agonists and antagonists. *Nature* 311:538-544.

Hille, B. 2001. Ion Channels of Excitable Membranes (Third Edition). Sinauer Associates Inc, Massachusetts..

Hillman, D., S.Chen, T.T.Aung, B.Cherksey, M.Sugimori, and R.R.Llinas. 1991. Localization of P-type calcium channels in the central nervous system. *Proc. Natl. Acad. Sci. U. S. A* 88:7076-7080.

Hillyard, D.R., V.D.Monje, I.M.Mintz, B.P.Bean, L.Nadasdi, J.Ramachandran, G.Miljanich, A.Azimi-Zoonooz, J.M.McIntosh, L.J.Cruz, and . 1992. A new Conus peptide ligand for mammalian presynaptic Ca2+ channels. *Neuron* 9:69-77.

Hobom, M., S.Dai, E.Marais, L.Lacinova, F.Hofmann, and N.Klugbauer. 2000. Neuronal distribution and functional characterization of the calcium channel alpha2delta-2 subunit. *Eur. J. Neurosci.* 12:1217-1226.

Hodgkin, A.L. and A.F.Huxley. 1952. A quantitative description of membrane current and its application to conduction and excitation in nerve. *J Physiol* 117:500-544.

Hodgkin, A.L. and R.D.Keynes. 1957. Movements of labelled calcium in squid giant axons. *J. Physiol* 138:253-281.

Hullin, R., D.Singer-Lahat, M.Freichel, M.Biel, N.Dascal, F.Hofmann, and V.Flockerzi. 1992. Calcium channel beta subunit heterogeneity: functional expression of cloned cDNA from heart, aorta and brain. *EMBO J.* 11:885-890.

Hynes, R.O. 2002. Integrins: bidirectional, allosteric signaling machines. *Cell* 110:673-687.

Ikeda, S.R. 1991. Double-pulse calcium channel current facilitation in adult rat sympathetic neurones. *J. Physiol* 439:181-214.

Ivanov, S.V., J.M.Ward, L.Tessarollo, D.McAreavey, V.Sachdev, L.Fananapazir, M.K.Banks, N.Morris, D.Djurickovic, D.E.Devor-Henneman, M.H.Wei, G.W.Alvord, B.Gao, J.A.Richardson, J.D.Minna, M.A.Rogawski, and M.I.Lerman. 2004. Cerebellar ataxia, seizures, premature death, and cardiac abnormalities in mice with targeted disruption of the Cacna2d2 gene. *Am. J. Pathol.* 165:1007-1018.

Jacobson, K., O.G.Mouritsen, and R.G.Anderson. 2007. Lipid rafts: at a crossroad between cell biology and physics. *Nat. Cell Biol.* 9:7-14.

Jarvis, S.E., J.M.Magga, A.M.Beedle, J.E.Braun, and G.W.Zamponi. 2000. G protein modulation of N-type calcium channels is facilitated by physical interactions between syntaxin 1A and Gbetagamma. *J. Biol. Chem.* 275:6388-6394.

Jarvis, S.E. and G.W.Zamponi. 2005. Masters or slaves? Vesicle release machinery and the regulation of presynaptic calcium channels. *Cell Calcium* 37:483-488.

Jay, S.D., S.B.Ellis, A.F.McCue, M.E.Williams, T.S.Vedvick, M.M.Harpold, and K.P.Campbell. 1990. Primary structure of the gamma subunit of the DHP-sensitive calcium channel from skeletal muscle. *Science* 248:490-492.

Jay, S.D., A.H.Sharp, S.D.Kahl, T.S.Vedvick, M.M.Harpold, and K.P.Campbell. 1991. Structural characterization of the dihydropyridine-sensitive calcium channel alpha 2-subunit and the associated delta peptides. *J. Biol. Chem.* 266:3287-3293.

Jennings, L.J., Q.W.Xu, T.A.Firth, M.T.Nelson, and G.M.Mawe. 1999. Cholesterol inhibits spontaneous action potentials and calcium currents in guinea pig gallbladder smooth muscle. *Am. J. Physiol* 277:G1017-G1026.

Jiang, Y., V.Ruta, J.Chen, A.Lee, and R.MacKinnon. 2003. The principle of gating charge movement in a voltage-dependent K+ channel. *Nature* 423:42-48.

Jones, L.P., S.K.Wei, and D.T.Yue. 1998. Mechanism of auxiliary subunit modulation of neuronal alpha1E calcium channels. *J. Gen. Physiol* 112:125-143.

Joshi, I. and C.P.Taylor. 2006. Pregabalin action at a model synapse: binding to presynaptic calcium channel alpha2-delta subunit reduces neurotransmission in mice. *Eur. J. Pharmacol.* 553:82-88.

Jun, K., E.S.Piedras-Renteria, S.M.Smith, D.B.Wheeler, S.B.Lee, T.G.Lee, H.Chin, M.E.Adams, R.H.Scheller, R.W.Tsien, and H.S.Shin. 1999. Ablation of P/Q-type Ca(2+) channel currents, altered synaptic transmission, and progressive ataxia in mice lacking the alpha(1A)-subunit. *Proc. Natl. Acad. Sci. U. S. A* 96:15245-15250.

Kamp, T.J. and J.W.Hell. 2000. Regulation of cardiac L-type calcium channels by protein kinase A and protein kinase C. *Circ. Res.* 87:1095-1102.

Kiyonaka, S., M.Wakamori, T.Miki, Y.Uriu, M.Nonaka, H.Bito, A.M.Beedle, E.Mori, Y.Hara, M.De Waard, M.Kanagawa, M.Itakura, M.Takahashi, K.P.Campbell, and

Y.Mori. 2007. RIM1 confers sustained activity and neurotransmitter vesicle anchoring to presynaptic Ca2+ channels. *Nat. Neurosci.* 10:691-701.

Klugbauer, N., S.Dai, V.Specht, L.Lacinova, E.Marais, G.Bohn, and F.Hofmann. 2000. A family of gamma-like calcium channel subunits. *FEBS Lett.* 470:189-197.

Klugbauer, N., L.Lacinova, E.Marais, M.Hobom, and F.Hofmann. 1999. Molecular diversity of the calcium channel alpha2delta subunit. *J. Neurosci.* 19:684-691.

Kraus, R.L., M.J.Sinnegger, H.Glossmann, S.Hering, and J.Striessnig. 1998. Familial hemiplegic migraine mutations change alpha1A Ca2+ channel kinetics. *J. Biol. Chem.* 273:5586-5590.

Kraus, R.L., M.J.Sinnegger, A.Koschak, H.Glossmann, S.Stenirri, P.Carrera, and J.Striessnig. 2000. Three new familial hemiplegic migraine mutants affect P/Q-type Ca(2+) channel kinetics. *J. Biol. Chem.* 275:9239-9243.

Lacinova, L. 2005. Voltage-dependent calcium channels. *Gen. Physiol Biophys.* 24 Suppl 1:1-78.

Lee, A., S.T.Wong, D.Gallagher, B.Li, D.R.Storm, T.Scheuer, and W.A.Catterall. 1999. Ca2+/calmodulin binds to and modulates P/Q-type calcium channels. *Nature* 399:155-159.

Lee, K.S., E.Marban, and R.W.Tsien. 1985. Inactivation of calcium channels in mammalian heart cells: joint dependence on membrane potential and intracellular calcium. *J. Physiol* 364:395-411.

Leroy, J., M.W.Richards, A.J.Butcher, M.Nieto-Rostro, W.S.Pratt, A.Davies, and A.C.Dolphin. 2005. Interaction via a key tryptophan in the I-II linker of N-type calcium channels is required for beta1 but not for palmitoylated beta2, implicating an additional binding site in the regulation of channel voltage-dependent properties. *J. Neurosci.* 25:6984-6996.

Letts, V.A., R.Felix, G.H.Biddlecome, J.Arikkath, C.L.Mahaffey, A.Valenzuela, F.S.Bartlett, Y.Mori, K.P.Campbell, and W.N.Frankel. 1998. The mouse stargazer gene encodes a neuronal Ca2+-channel gamma subunit. *Nat. Genet.* 19:340-347.

Leung, A.T., T.Imagawa, and K.P.Campbell. 1987. Structural characterization of the 1,4-dihydropyridine receptor of the voltage-dependent Ca2+ channel from rabbit skeletal muscle. Evidence for two distinct high molecular weight subunits. *J. Biol. Chem.* 262:7943-7946.

Li, C.Y., X.L.Zhang, E.A.Matthews, K.W.Li, A.Kurwa, A.Boroujerdi, J.Gross, M.S.Gold, A.H.Dickenson, G.Feng, and Z.D.Luo. 2006. Calcium channel alpha2delta1 subunit mediates spinal hyperexcitability in pain modulation. *Pain* 125:20-34.

Llinas, R., M.Sugimori, J.W.Lin, and B.Cherksey. 1989. Blocking and isolation of a calcium channel from neurons in mammals and cephalopods utilizing a toxin fraction (FTX) from funnel-web spider poison. *Proc. Natl. Acad. Sci. U. S. A* 86:1689-1693.

Ludwig, A., V.Flockerzi, and F.Hofmann. 1997. Regional expression and cellular localization of the alpha1 and beta subunit of high voltage-activated calcium channels in rat brain. *J. Neurosci.* 17:1339-1349.

Luo, Z.D., N.A.Calcutt, E.S.Higuera, C.R.Valder, Y.H.Song, C.I.Svensson, and R.R.Myers. 2002. Injury type-specific calcium channel alpha 2 delta-1 subunit up-regulation in rat neuropathic pain models correlates with antiallodynic effects of gabapentin. *J. Pharmacol. Exp. Ther.* 303:1199-1205.

Luo, Z.D., S.R.Chaplan, E.S.Higuera, L.S.Sorkin, K.A.Stauderman, M.E.Williams, and T.L.Yaksh. 2001. Upregulation of dorsal root ganglion (alpha)2(delta) calcium channel subunit and its correlation with allodynia in spinal nerve-injured rats. *J. Neurosci.* 21:1868-1875.

Lynch, J.J., III, P.Honore, D.J.Anderson, W.H.Bunnelle, K.H.Mortell, C.Zhong, C.L.Wade, C.Z.Zhu, H.Xu, K.C.Marsh, C.H.Lee, M.F.Jarvis, and M.Gopalakrishnan. 2006. (L)-Phenylglycine, but not necessarily other alpha2delta subunit voltage-gated calcium channel ligands, attenuates neuropathic pain in rats. *Pain* 125:136-142.

Maneuf, Y.P., M.I.Gonzalez, K.S.Sutton, F.Z.Chung, R.D.Pinnock, and K.Lee. 2003. Cellular and molecular action of the putative GABA-mimetic, gabapentin. *Cell Mol. Life Sci.* 60:742-750.

Marais, E., N.Klugbauer, and F.Hofmann. 2001. Calcium channel alpha(2)delta subunits-structure and Gabapentin binding. *Mol. Pharmacol.* 59:1243-1248.

Martin, D.J., D.McClelland, M.B.Herd, K.G.Sutton, M.D.Hall, K.Lee, R.D.Pinnock, and R.H.Scott. 2002. Gabapentin-mediated inhibition of voltage-activated Ca2+ channel currents in cultured sensory neurones is dependent on culture conditions and channel subunit expression. *Neuropharmacology* 42:353-366.

Maximov, A., T.C.Sudhof, and I.Bezprozvanny. 1999. Association of neuronal calcium channels with modular adaptor proteins. *J Biol. Chem.* 274:24453-24456.

McDonough, S.I., L.M.Boland, I.M.Mintz, and B.P.Bean. 2002. Interactions among toxins that inhibit N-type and P-type calcium channels. *J Gen. Physiol* 119:313-328.

McDonough, S.I., K.J.Swartz, I.M.Mintz, L.M.Boland, and B.P.Bean. 1996. Inhibition of calcium channels in rat central and peripheral neurons by omega-conotoxin MVIIC. *J Neurosci.* 16:2612-2623.

McEnery, M.W., A.M.Snowman, A.H.Sharp, M.E.Adams, and S.H.Snyder. 1991. Purified omega-conotoxin GVIA receptor of rat brain resembles a dihydropyridine-sensitive L-type calcium channel. *Proc. Natl. Acad. Sci. U. S. A* 88:11095-11099.

Meir, A., D.C.Bell, G.J.Stephens, K.M.Page, and A.C.Dolphin. 2000. Calcium channel beta subunit promotes voltage-dependent modulation of alpha 1 B by G beta gamma. *Biophys. J* 79:731-746.

Mintz, I.M., M.E.Adams, and B.P.Bean. 1992. P-type calcium channels in rat central and peripheral neurons. *Neuron* 9:85-95.

Missler, M., W.Zhang, A.Rohlmann, G.Kattenstroth, R.E.Hammer, K.Gottmann, and T.C.Sudhof. 2003. Alpha-neurexins couple Ca2+ channels to synaptic vesicle exocytosis. *Nature* 423:939-948.

Mori, Y., T.Friedrich, M.S.Kim, A.Mikami, J.Nakai, P.Ruth, E.Bosse, F.Hofmann, V.Flockerzi, T.Furuichi, and . 1991. Primary structure and functional expression from complementary DNA of a brain calcium channel. *Nature* 350:398-402.

Moss, F.J., A.C.Dolphin, and J.J.Clare. 2003. Human neuronal stargazin-like proteins, gamma2, gamma3 and gamma4; an investigation of their specific localization in human brain and their influence on CaV2.1 voltage-dependent calcium channels expressed in Xenopus oocytes. *BMC. Neurosci.* 4:23.

Moss, F.J., P.Viard, A.Davies, F.Bertaso, K.M.Page, A.Graham, C.Canti, M.Plumpton, C.Plumpton, J.J.Clare, and A.C.Dolphin. 2002. The novel product of a five-exon stargazin-related gene abolishes Ca(V)2.2 calcium channel expression. *EMBO J.* 21:1514-1523.

Newcomb, R., B.Szoke, A.Palma, G.Wang, X.Chen, W.Hopkins, R.Cong, J.Miller, L.Urge, K.Tarczy-Hornoch, J.A.Loo, D.J.Dooley, L.Nadasdi, R.W.Tsien, J.Lemos, and G.Miljanich. 1998. Selective peptide antagonist of the class E calcium channel from the venom of the tarantula Hysterocrates gigas. *Biochemistry* 37:15353-15362.

Nilius, B., K.Talavera, and A.Verkhratsky. 2006. T-type calcium channels: the never ending story. *Cell Calcium* 40:81-88.

Nishimune, H., J.R.Sanes, and S.S.Carlson. 2004. A synaptic laminin-calcium channel interaction organizes active zones in motor nerve terminals. *Nature* 432:580-587.

Noda, M., S.Shimizu, T.Tanabe, T.Takai, T.Kayano, T.Ikeda, H.Takahashi, H.Nakayama, Y.Kanaoka, N.Minamino, and . 1984. Primary structure of Electrophorus electricus sodium channel deduced from cDNA sequence. *Nature* 312:121-127.

Noda, M., H.Takahashi, T.Tanabe, M.Toyosato, Y.Furutani, T.Hirose, M.Asai, S.Inayama, T.Miyata, and S.Numa. 1982. Primary structure of alpha-subunit precursor of Torpedo californica acetylcholine receptor deduced from cDNA sequence. *Nature* 299:793-797.

Nowycky, M.C., A.P.Fox, and R.W.Tsien. 1985. Three types of neuronal calcium channel with different calcium agonist sensitivity. *Nature* 316:440-443.

Obermair, G.J., Z.Szabo, E.Bourinet, and B.E.Flucher. 2004. Differential targeting of the L-type Ca2+ channel alpha 1C (CaV1.2) to synaptic and extrasynaptic compartments in hippocampal neurons. *Eur. J. Neurosci.* 19:2109-2122.

Ogden,D.C. Microelectrode Techniques. The Plymouth Workshop Handbook, Second Edition. 1994. The Company of Biologists Limited, Cambridge.
Ref Type: Generic

Patel, M.K., M.I.Gonzalez, S.Bramwell, R.D.Pinnock, and K.Lee. 2000. Gabapentin inhibits excitatory synaptic transmission in the hyperalgesic spinal cord. *Br. J Pharmacol.* 130:1731-1734.

Perez-Reyes, E., A.Castellano, H.S.Kim, P.Bertrand, E.Baggstrom, A.E.Lacerda, X.Y.Wei, and L.Birnbaumer. 1992. Cloning and expression of a cardiac/brain beta subunit of the L-type calcium channel. *J. Biol. Chem.* 267:1792-1797.

Perez-Reyes, E., X.Y.Wei, A.Castellano, and L.Birnbaumer. 1990. Molecular diversity of L-type calcium channels. Evidence for alternative splicing of the transcripts of three non-allelic genes. *J. Biol. Chem.* 265:20430-20436.

Pietrobon, D. 2002. Calcium channels and channelopathies of the central nervous system. *Mol. Neurobiol.* 25:31-50.

Platzer, J., J.Engel, A.Schrott-Fischer, K.Stephan, S.Bova, H.Chen, H.Zheng, and J.Striessnig. 2000. Congenital deafness and sinoatrial node dysfunction in mice lacking class D L-type Ca2+ channels. *Cell* 102:89-97.

Pozzi, D., S.Condliffe, Y.Bozzi, M.Chikhladze, C.Grumelli, V.Proux-Gillardeaux, M.Takahashi, S.Franceschetti, C.Verderio, and M.Matteoli. 2007. Activity-dependent phosphorylation of Ser187 is required for SNAP-25-negative modulation of neuronal voltage-gated calcium channels. *Proc. Natl. Acad. Sci. U. S. A.*

Pragnell, M., M.De Waard, Y.Mori, T.Tanabe, T.P.Snutch, and K.P.Campbell. 1994. Calcium channel beta-subunit binds to a conserved motif in the I-II cytoplasmic linker of the alpha 1-subunit. *Nature* 368:67-70.

Qin, N., R.Olcese, E.Stefani, and L.Birnbaumer. 1998. Modulation of human neuronal alpha 1E-type calcium channel by alpha 2 delta-subunit. *Am. J. Physiol* 274:C1324-C1331.

Qin, N., S.Yagel, M.L.Momplaisir, E.E.Codd, and M.R.D'Andrea. 2002. Molecular cloning and characterization of the human voltage-gated calcium channel alpha(2)delta-4 subunit. *Mol. Pharmacol.* 62:485-496.

Raingo, J., A.J.Castiglioni, and D.Lipscombe. 2007. Alternative splicing controls G protein-dependent inhibition of N-type calcium channels in nociceptors. *Nat. Neurosci.* 10:285-292.

Randall, A. and R.W.Tsien. 1995. Pharmacological dissection of multiple types of Ca2+ channel currents in rat cerebellar granule neurons. *J. Neurosci.* 15:2995-3012.

Randall, A.D. and R.W.Tsien. 1997. Contrasting biophysical and pharmacological properties of T-type and R-type calcium channels. *Neuropharmacology* 36:879-893.

Reimann, W. 1983. Inhibition by GABA, baclofen and gabapentin of dopamine release from rabbit caudate nucleus: are there common or different sites of action? *Eur. J. Pharmacol.* 94:341-344.

Rettig, J., Z.H.Sheng, D.K.Kim, C.D.Hodson, T.P.Snutch, and W.A.Catterall. 1996. Isoform-specific interaction of the alpha1A subunits of brain Ca2+ channels with the presynaptic proteins syntaxin and SNAP-25. *Proc. Natl. Acad. Sci. U. S. A* 93:7363-7368.

Reuter, H. 1967. The dependence of slow inward current in Purkinje fibres on the extracellular calcium-concentration. *J. Physiol* 192:479-492.

Reuter, H. 1973. Divalent cations as charge carriers in excitable membranes. *Prog. Biophys. Mol. Biol.* 26:1-43.

Richards, M.W., A.J.Butcher, and A.C.Dolphin. 2004. Ca2+ channel beta-subunits: structural insights AID our understanding. *Trends Pharmacol. Sci.* 25:626-632.

Richards, M.W., J.Leroy, W.S.Pratt, and A.C.Dolphin. 2007. The HOOK-Domain Between the SH3- and the GK-Domains of CaV? Subunits Contains Key Determinants Controlling Calcium Channel Inactivation. *Channels* 1:92-101.

Ringer, S. 1883. A further Contribution regarding the influence of the different Constituents of the Blood on the Contraction of the Heart. *J. Physiol* 4:29-42.

Rios, E. and G.Brum. 1987. Involvement of dihydropyridine receptors in excitation-contraction coupling in skeletal muscle. *Nature* 325:717-720.

Rock, D.M., K.M.Kelly, and R.L.Macdonald. 1993. Gabapentin actions on ligand- and voltage-gated responses in cultured rodent neurons. *Epilepsy Res.* 16:89-98.

Ruth, P., A.Rohrkasten, M.Biel, E.Bosse, S.Regulla, H.E.Meyer, V.Flockerzi, and F.Hofmann. 1989. Primary structure of the beta subunit of the DHP-sensitive calcium channel from skeletal muscle. *Science* 245:1115-1118.

Sandoval, A., N.Oviedo, A.Andrade, and R.Felix. 2004. Glycosylation of asparagines 136 and 184 is necessary for the alpha2delta subunit-mediated regulation of voltage-gated Ca2+ channels. *FEBS Lett.* 576:21-26.

Sather, W.A., T.Tanabe, J.F.Zhang, Y.Mori, M.E.Adams, and R.W.Tsien. 1993. Distinctive biophysical and pharmacological properties of class A (BI) calcium channel alpha 1 subunits. *Neuron* 11:291-303.

Schlicker, E., W.Reimann, and M.Gothert. 1985. Gabapentin decreases monoamine release without affecting acetylcholine release in the brain. *Arzneimittelforschung.* 35:1347-1349.

Schmid, A., J.Barhanin, T.Coppola, M.Borsotto, and M.Lazdunski. 1986. Immunochemical analysis of subunit structures of 1,4-dihydropyridine receptors associated with voltage-dependent Ca2+ channels in skeletal, cardiac, and smooth muscles. *Biochemistry* 25:3492-3495.

Schredelseker, J., B.Di, V, G.J.Obermair, E.T.Felder, B.E.Flucher, C.Franzini-Armstrong, and M.Grabner. 2005. The beta 1a subunit is essential for the assembly of dihydropyridine-receptor arrays in skeletal muscle. *Proc. Natl. Acad. Sci. U. S. A* 102:17219-17224.

Scott, R.H. and A.C.Dolphin. 1986. Regulation of calcium currents by a GTP analogue: potentiation of (-)-baclofen-mediated inhibition. *Neurosci. Lett.* 69:59-64.

Scott, V.E., M.De Waard, H.Liu, C.A.Gurnett, D.P.Venzke, V.A.Lennon, and K.P.Campbell. 1996. Beta subunit heterogeneity in N-type Ca2+ channels. *J. Biol. Chem.* 271:3207-3212.

Scott, V.E., R.Felix, J.Arikkath, and K.P.Campbell. 1998. Evidence for a 95 kDa short form of the alpha1A subunit associated with the omega-conotoxin MVIIC receptor of the P/Q-type Ca2+ channels. *J. Neurosci.* 18:641-647.

Seino, S., L.Chen, M.Seino, O.Blondel, J.Takeda, J.H.Johnson, and G.I.Bell. 1992. Cloning of the alpha 1 subunit of a voltage-dependent calcium channel expressed in pancreatic beta cells. *Proc. Natl. Acad. Sci. U. S. A* 89:584-588.

Sheng, Z.H., J.Rettig, M.Takahashi, and W.A.Catterall. 1994. Identification of a syntaxin-binding site on N-type calcium channels. *Neuron* 13:1303-1313.

Sheng, Z.H., C.T.Yokoyama, and W.A.Catterall. 1997. Interaction of the synprint site of N-type Ca2+ channels with the C2B domain of synaptotagmin I. *Proc. Natl. Acad. Sci. U. S. A* 94:5405-5410.

Sher, E. and F.Clementi. 1991. Omega-conotoxin-sensitive voltage-operated calcium channels in vertebrate cells. *Neuroscience* 42:301-307.

Shirokov, R., G.Ferreira, J.Yi, and E.Rios. 1998. Inactivation of gating currents of L-type calcium channels. Specific role of the alpha 2 delta subunit. *J. Gen. Physiol* 111:807-823.

Shistik, E., T.Ivanina, T.Puri, M.Hosey, and N.Dascal. 1995. Ca2+ current enhancement by alpha 2/delta and beta subunits in Xenopus oocytes: contribution of changes in channel gating and alpha 1 protein level. *J. Physiol* 489 (Pt 1):55-62.

Singer, D., M.Biel, I.Lotan, V.Flockerzi, F.Hofmann, and N.Dascal. 1991. The roles of the subunits in the function of the calcium channel. *Science* 253:1553-1557.

Snutch, T.P., W.J.Tomlinson, J.P.Leonard, and M.M.Gilbert. 1991. Distinct calcium channels are generated by alternative splicing and are differentially expressed in the mammalian CNS. *Neuron* 7:45-57.

Sokolov, S., R.G.Weiss, B.Kurka, F.Gapp, and S.Hering. 1999. Inactivation determinant in the I-II loop of the Ca2+ channel alpha1-subunit and beta-subunit interaction affect sensitivity for the phenylalkylamine (-)gallopamil. *J. Physiol* 519 Pt 2:315-322.

Soong, T.W., A.Stea, C.D.Hodson, S.J.Dubel, S.R.Vincent, and T.P.Snutch. 1993. Structure and functional expression of a member of the low voltage-activated calcium channel family. *Science* 260:1133-1136.

Spafford, J.D. and G.W.Zamponi. 2003. Functional interactions between presynaptic calcium channels and the neurotransmitter release machinery. *Curr. Opin. Neurobiol.* 13:308-314.

Springer, T.A. 2006. Complement and the multifaceted functions of VWA and integrin I domains. *Structure.* 14:1611-1616.

Starr, T.V., W.Prystay, and T.P.Snutch. 1991. Primary structure of a calcium channel that is highly expressed in the rat cerebellum. *Proc. Natl. Acad. Sci. U. S. A* 88:5621-5625.

Stea, A., S.J.Dubel, and T.P.Snutch. 1999. alpha 1B N-type calcium channel isoforms with distinct biophysical properties. *Ann. N. Y. Acad. Sci.* 868:118-130.

Stefani, A., F.Spadoni, and G.Bernardi. 1998. Gabapentin inhibits calcium currents in isolated rat brain neurons. *Neuropharmacology* 37:83-91.

Stephens, G.J., K.M.Page, J.R.Burley, N.S.Berrow, and A.C.Dolphin. 1997. Functional expression of rat brain cloned alpha1E calcium channels in COS-7 cells. *Pflugers Arch.* 433:523-532.

Stewart, B.H., A.R.Kugler, P.R.Thompson, and H.N.Bockbrader. 1993. A saturable transport mechanism in the intestinal absorption of gabapentin is the underlying cause of the lack of proportionality between increasing dose and drug levels in plasma. *Pharm. Res.* 10:276-281.

Strom, T.M., G.Nyakatura, E.Apfelstedt-Sylla, H.Hellebrand, B.Lorenz, B.H.Weber, K.Wutz, N.Gutwillinger, K.Ruther, B.Drescher, C.Sauer, E.Zrenner, T.Meitinger,

A.Rosenthal, and A.Meindl. 1998. An L-type calcium-channel gene mutated in incomplete X-linked congenital stationary night blindness. *Nat. Genet.* 19:260-263.

Su, T.Z., E.Lunney, G.Campbell, and D.L.Oxender. 1995. Transport of gabapentin, a gamma-amino acid drug, by system l alpha-amino acid transporters: a comparative study in astrocytes, synaptosomes, and CHO cells. *J. Neurochem.* 64:2125-2131.

Sutton, K.G., D.J.Martin, R.D.Pinnock, K.Lee, and R.H.Scott. 2002. Gabapentin inhibits high-threshold calcium channel currents in cultured rat dorsal root ganglion neurones. *Br. J. Pharmacol.* 135:257-265.

Sutton, K.G., J.E.McRory, H.Guthrie, T.H.Murphy, and T.P.Snutch. 1999. P/Q-type calcium channels mediate the activity-dependent feedback of syntaxin-1A. *Nature* 401:800-804.

Swartz, K.J. 1993. Modulation of Ca2+ channels by protein kinase C in rat central and peripheral neurons: disruption of G protein-mediated inhibition. *Neuron* 11:305-320.

Swick, A.G., M.Janicot, T.Cheneval-Kastelic, J.C.McLenithan, and M.D.Lane. 1992. Promoter-cDNA-directed heterologous protein expression in Xenopus laevis oocytes. *Proc. Natl. Acad. Sci. U. S. A* 89:1812-1816.

Takahashi, M., M.J.Seagar, J.F.Jones, B.F.Reber, and W.A.Catterall. 1987. Subunit structure of dihydropyridine-sensitive calcium channels from skeletal muscle. *Proc. Natl. Acad. Sci. U. S. A* 84:5478-5482.

Takahashi, T. and A.Momiyama. 1993. Different types of calcium channels mediate central synaptic transmission. *Nature* 366:156-158.

Tanabe, T., H.Takeshima, A.Mikami, V.Flockerzi, H.Takahashi, K.Kangawa, M.Kojima, H.Matsuo, T.Hirose, and S.Numa. 1987. Primary structure of the receptor for calcium channel blockers from skeletal muscle. *Nature* 328:313-318.

Taverna, E., E.Saba, J.Rowe, M.Francolini, F.Clementi, and P.Rosa. 2004. Role of lipid microdomains in P/Q-type calcium channel (Cav2.1) clustering and function in presynaptic membranes. *J. Biol. Chem.* 279:5127-5134.

Taylor, C.P., T.Angelotti, and E.Fauman. 2007. Pharmacology and mechanism of action of pregabalin: the calcium channel alpha2-delta (alpha2-delta) subunit as a target for antiepileptic drug discovery. *Epilepsy Res.* 73:137-150.

Taylor, C.P., N.S.Gee, T.Z.Su, J.D.Kocsis, D.F.Welty, J.P.Brown, D.J.Dooley, P.Boden, and L.Singh. 1998. A summary of mechanistic hypotheses of gabapentin pharmacology. *Epilepsy Res.* 29:233-249.

Thurlow, R.J., J.P.Brown, N.S.Gee, D.R.Hill, and G.N.Woodruff. 1993. [3H]gabapentin may label a system-L-like neutral amino acid carrier in brain. *Eur. J. Pharmacol.* 247:341-345.

Tomita, S., A.Shenoy, Y.Fukata, R.A.Nicoll, and D.S.Bredt. 2007. Stargazin interacts functionally with the AMPA receptor glutamate-binding module. *Neuropharmacology* 52:87-91.

Tomlinson, W.J., A.Stea, E.Bourinet, P.Charnet, J.Nargeot, and T.P.Snutch. 1993. Functional properties of a neuronal class C L-type calcium channel. *Neuropharmacology* 32:1117-1126.

Toselli, M., G.Biella, V.Taglietti, E.Cazzaniga, and M.Parenti. 2005. Caveolin-1 expression and membrane cholesterol content modulate N-type calcium channel activity in NG108-15 cells. *Biophys. J.* 89:2443-2457.

Tottene, A., S.Volsen, and D.Pietrobon. 2000. alpha(1E) subunits form the pore of three cerebellar R-type calcium channels with different pharmacological and permeation properties. *J. Neurosci.* 20:171-178.

Turner, T.J., M.E.Adams, and K.Dunlap. 1992. Calcium channels coupled to glutamate release identified by omega-Aga-IVA. *Science* 258:310-313.

Uchitel, O.D., D.A.Protti, V.Sanchez, B.D.Cherksey, M.Sugimori, and R.Llinas. 1992. P-type voltage-dependent calcium channel mediates presynaptic calcium influx and transmitter release in mammalian synapses. *Proc. Natl. Acad. Sci. U. S. A* 89:3330-3333.

Urbano, F.J., E.S.Piedras-Renteria, K.Jun, H.S.Shin, O.D.Uchitel, and R.W.Tsien. 2003. Altered properties of quantal neurotransmitter release at endplates of mice lacking P/Q-type Ca2+ channels. *Proc. Natl. Acad. Sci. U. S. A* 100:3491-3496.

Usowicz, M.M., M.Sugimori, B.Cherksey, and R.Llinas. 1992. P-type calcium channels in the somata and dendrites of adult cerebellar Purkinje cells. *Neuron* 9:1185-1199.

Vaghy, P.L., J.Striessnig, K.Miwa, H.G.Knaus, K.Itagaki, E.McKenna, H.Glossmann, and A.Schwartz. 1987. Identification of a novel 1,4-dihydropyridine- and phenylalkylamine-binding polypeptide in calcium channel preparations. *J. Biol. Chem.* 262:14337-14342.

van Hooft, J.A., J.J.Dougherty, D.Endeman, R.A.Nichols, and W.J.Wadman. 2002. Gabapentin inhibits presynaptic Ca(2+) influx and synaptic transmission in rat hippocampus and neocortex. *Eur. J. Pharmacol.* 449:221-228.

Varadi, G., M.Strobeck, S.Koch, L.Caglioti, C.Zucchi, and G.Palyi. 1999. Molecular elements of ion permeation and selectivity within calcium channels. *Crit Rev. Biochem. Mol. Biol.* 34:181-214.

Venter, J.C., C.M.Fraser, J.S.Schaber, C.Y.Jung, G.Bolger, and D.J.Triggle. 1983. Molecular properties of the slow inward calcium channel. Molecular weight determinations by radiation inactivation and covalent affinity labeling. *J. Biol. Chem.* 258:9344-9348.

Wagner, J.J. and B.E.Alger. 1994. GTP modulates run-up of whole-cell Ca2+ channel current in a Ca(2+)-dependent manner. *J. Neurophysiol.* 71:814-816.

Walker, D. and M.De Waard. 1998. Subunit interaction sites in voltage-dependent Ca2+ channels: role in channel function. *Trends Neurosci.* 21:148-154.

Wang, M., J.Offord, D.L.Oxender, and T.Z.Su. 1999. Structural requirement of the calcium-channel subunit alpha2delta for gabapentin binding. *Biochem. J.* 342 (Pt 2):313-320.

Wang, M.C., A.Dolphin, and A.Kitmitto. 2004. L-type voltage-gated calcium channels: understanding function through structure. *FEBS Lett.* 564:245-250.

Wang, P.W. and T.A.Ketter. 2002. Pharmacokinetics of mood stabilizers and new anticonvulsants. *Psychopharmacol. Bull.* 36:44-66.

Welling, A., E.Bosse, A.Cavalie, R.Bottlender, A.Ludwig, W.Nastainczyk, V.Flockerzi, and F.Hofmann. 1993. Stable co-expression of calcium channel alpha 1, beta and alpha 2/delta subunits in a somatic cell line. *J. Physiol* 471:749-765.

Westenbroek, R.E., T.Sakurai, E.M.Elliott, J.W.Hell, T.V.Starr, T.P.Snutch, and W.A.Catterall. 1995. Immunochemical identification and subcellular distribution of the alpha 1A subunits of brain calcium channels. *J. Neurosci.* 15:6403-6418.

Whittaker, C.A. and R.O.Hynes. 2002. Distribution and evolution of von Willebrand/integrin A domains: widely dispersed domains with roles in cell adhesion and elsewhere. *Mol. Biol. Cell* 13:3369-3387.

Wilson, S.M., P.T.Toth, S.B.Oh, S.E.Gillard, S.Volsen, D.Ren, L.H.Philipson, E.C.Lee, C.F.Fletcher, L.Tessarollo, N.G.Copeland, N.A.Jenkins, and R.J.Miller. 2000. The status of voltage-dependent calcium channels in alpha 1E knock-out mice. *J. Neurosci.* 20:8566-8571.

Wiser, O., M.K.Bennett, and D.Atlas. 1996a. Functional interaction of syntaxin and SNAP-25 with voltage-sensitive L- and N-type Ca2+ channels. *EMBO J.* 15:4100-4110.

Wiser, O., M.Trus, A.Hernandez, E.Renstrom, S.Barg, P.Rorsman, and D.Atlas. 1999. The voltage sensitive Lc-type Ca2+ channel is functionally coupled to the exocytotic machinery. *Proc. Natl. Acad. Sci. U. S. A* 96:248-253.

Wiser, O., M.Trus, D.Tobi, S.Halevi, E.Giladi, and D.Atlas. 1996b. The alpha 2/delta subunit of voltage sensitive Ca2+ channels is a single transmembrane extracellular protein which is involved in regulated secretion. *FEBS Lett.* 379:15-20.

Wycisk, K.A., B.Budde, S.Feil, S.Skosyrski, F.Buzzi, J.Neidhardt, E.Glaus, P.Nurnberg, K.Ruether, and W.Berger. 2006a. Structural and functional abnormalities of retinal ribbon synapses due to Cacna2d4 mutation. *Invest Ophthalmol. Vis. Sci.* 47:3523-3530.

Wycisk, K.A., C.Zeitz, S.Feil, M.Wittmer, U.Forster, J.Neidhardt, B.Wissinger, E.Zrenner, R.Wilke, S.Kohl, and W.Berger. 2006b. Mutation in the auxiliary calcium-channel subunit CACNA2D4 causes autosomal recessive cone dystrophy. *Am. J Hum. Genet.* 79:973-977.

Xiao, R.P., H.Cheng, W.J.Lederer, T.Suzuki, and E.G.Lakatta. 1994. Dual regulation of Ca2+/calmodulin-dependent kinase II activity by membrane voltage and by calcium influx. *Proc. Natl. Acad. Sci. U. S. A* 91:9659-9663.

Xiao, W., A.Boroujerdi, G.J.Bennett, and Z.D.Luo. 2007. Chemotherapy-evoked painful peripheral neuropathy: analgesic effects of gabapentin and effects on expression of the alpha-2-delta type-1 calcium channel subunit. *Neuroscience* 144:714-720.

Yang, J., P.T.Ellinor, W.A.Sather, J.F.Zhang, and R.W.Tsien. 1993. Molecular determinants of Ca2+ selectivity and ion permeation in L-type Ca2+ channels. *Nature* 366:158-161.

Yellen, G. 1998. The moving parts of voltage-gated ion channels. *Q. Rev. Biophys.* 31:239-295.

Yellen, G., M.E.Jurman, T.Abramson, and R.MacKinnon. 1991. Mutations affecting internal TEA blockade identify the probable pore-forming region of a K+ channel. *Science* 251:939-942.

Yu, S.P. and G.A.Kerchner. 1998. Endogenous voltage-gated potassium channels in human embryonic kidney (HEK293) cells. *J. Neurosci. Res.* 52:612-617.

Zhang, J.F., P.T.Ellinor, R.W.Aldrich, and R.W.Tsien. 1994. Molecular determinants of voltage-dependent inactivation in calcium channels. *Nature* 372:97-100.

Zuhlke, R.D., G.S.Pitt, R.W.Tsien, and H.Reuter. 2000a. Ca2+-sensitive inactivation and facilitation of L-type Ca2+ channels both depend on specific amino acid residues in a consensus calmodulin-binding motif in the(alpha)1C subunit. *J. Biol. Chem.* 275:21121-21129.

Zuhlke, R.D., G.S.Pitt, R.W.Tsien, and H.Reuter. 2000b. Ca2+-sensitive inactivation and facilitation of L-type Ca2+ channels both depend on specific amino acid residues in a consensus calmodulin-binding motif in the(alpha)1C subunit. *J. Biol. Chem.* 275:21121-21129.

Zuhlke, R.D. and H.Reuter. 1998. Ca2+-sensitive inactivation of L-type Ca2+ channels depends on multiple cytoplasmic amino acid sequences of the alpha1C subunit. *Proc. Natl. Acad. Sci. U. S. A* 95:3287-3294.

Zwingman, T.A., P.E.Neumann, J.L.Noebels, and K.Herrup. 2001. Rocker is a new variant of the voltage-dependent calcium channel gene Cacna1a. *J Neurosci.* 21:1169-1178.